

**Investigations on Manufacturing of High Quality  
Meso-sized Bevel and Helical Gears by Wire  
Spark Erosion Machining Process**

**Ph.D. Thesis**

*By*

**Sujeet Kumar Chaubey**



**Discipline of Mechanical Engineering  
Indian Institute of Technology Indore**

**April 2018**



**Investigations on Manufacturing of High Quality  
Meso-sized Bevel and Helical Gears by Wire Spark  
Erosion Machining Process**

**A Thesis**

*Submitted in partial fulfillment of the  
requirements for the award of the degree*

*of*

**Doctor of Philosophy**

*By*

**Sujeet Kumar Chaubey**



**Discipline of Mechanical Engineering  
Indian Institute of Technology Indore**

**April 2018**





# Indian Institute of Technology Indore

## Candidate's Declaration

I hereby certify that the work which is being presented in the thesis entitled **Investigations on Manufacturing of High Quality Meso-sized Bevel and Helical Gears by Wire Spark Erosion Machining Process**, in the partial fulfillment of the requirements for the award of the degree of **DOCTOR OF PHILOSOPHY** and submitted in the **Discipline of Mechanical Engineering, Indian Institute of Technology Indore**, is an authentic record of my own work carried out during the time period from **Jan 2014 to April 2018** under the supervision of **Prof. Neelesh Kumar Jain** of Discipline of Mechanical Engineering.

The matter contained in this thesis has not been submitted by me for the award of any degree from any other institute.

(**Sujeet Kumar Chaubey**)

-----  
This is to certify that the above statement made by the candidate is correct to the best of my knowledge.

(**Prof. Neelesh Kumar Jain**)

-----  
**Sujeet Kumar Chaubey** has successfully completed his Ph.D. Oral Examination held on  
.....

**Signature of Thesis Supervisor**  
**Date:**

**Signature of Convener, DPGC**  
**Date:**

**Signature of PSPC Members**  
**Date:**

**Signature of External Examiner**  
**Date:**

**Signature (with date) of Chairman of PhD Oral Examination Board**



## Acknowledgements

First and Foremost, I would like to thank my supervisor **Prof. N. K. Jain** for providing me with the opportunity to complete my PhD thesis at **Indian Institute of Technology, Indore**. As my supervisors, he has constantly forced me to remain focused towards achieving my goal. His observations and comments helped me to establish the overall direction of the research and to move forward with investigation in depth. I am very grateful for his patience, motivation, enthusiasm, and immense knowledge in advanced machining processes and especially in gear engineering and manufacturing that taken together, make him a great mentor.

I am extremely happy to express my gratitude towards my PSPC members **Prof. Anand Parey** and **Dr. Amod C. Umarikar** for their valuable suggestion, guidance and cooperation. I am grateful to the **Prof. Pradeep Mathur, Director, IIT Indore** and **faculty members** of Discipline of **Mechanical Engineering** for providing the essential facilities and guidance.

I would like to express my gratitude to my M.Tech thesis supervisor **Prof. Shankar Singh, (SLIET Longowal, Punjab)** for his motivation, support, help and cooperation throughout my PhD research work.

I also express my sincere thanks to **Mr. Ram Mehar (M/S Shriram Industries, Ghaziabad, UP)**, **Mr. Vijay Tevatiya (M/S Alliance tooling Pvt. Ltd., Ghaziabad)**, **Mr. Ram Singh (CNC Programmer and WSEM Operator)**, **Mr. Surendra Gupta (Operator CNC Gear Metrology Machine, AVTEC Limited, Indore)** for their help and support during my research work.

I want to express my special thanks to **Mr. Anand C Petare, Dr. Devendra Gurjar, Mr. Abhijeet Vishnu, Mr. Sanjeev Sharma, Mr. Mayur Sawant, and Mr. Sagar H. Nikam**, for their help and support during my research work.

Cooperation and use of facilities extended by **AVTEC Limited, Pithampur, MP (India)** are highly acknowledged. Research scholar is also very thankful to **Advanced Manufacturing Processes (AMP) Lab, Gear Research Lab, Tribology Lab, Central Workshop** and **Sophisticated Instrumentation Center (SIC)** of IIT Indore for allowing me to use their facilities in successful completion of my PhD thesis work.

I am also thankful to staff members of **AMP lab, Gear Research Lab** and **Central Workshop, Solid Mechanics Lab** and **Tribology Lab** for their help and cooperation during my research work.

I acknowledge and thankful to **Ministry of Human Resource and Development (MHRD), Govt. of India** for providing fellowship to pursue my doctoral studies.

I would like to thanks my parents and my younger uncle **Shri C.N. Chaubey** for their love, care, support, encouragement and cooperation in each step of my life without which this journey would not have been possible.

Last, but not the least, I would like to dedicate my thesis to GOD and my Grandparents.

**Sujeet Kumar Chaubey**



**Dedicated**  
**to**  
**My Grandparents**



## Extended Abstract

Miniaturization of products, equipment and devices has become an essential requirement globally due to increasing costs of the materials and manufacturing processes and emphasis on making the products smaller, lightweight, and compact. Gears having addendum or tip diameter in a range from 1 to 10 mm are referred as meso-gears. Different types of meso-gears such as meso-spur gear (MSG), meso-helical gear (MHG), and meso-bevel gear (MBG) are primarily used for the purpose of actuation, positioning, and motion transmission at very high speed in the miniaturized products, equipment and devices, and micro electro-mechanical systems (MEMS). MSG and MHG are used between the two parallel shafts and MBG between two intersecting shafts. They offer many worth-mentioning advantages such as compactness due to smaller size, lightweight, higher dimensional accuracy, zero backlash, lower energy consumption, efficient transmission, superior operating performance and ability to perform under extreme environmental conditions. Their typical applications include meso-sized gearboxes, pumps and motors, actuating devices, scientific instruments, precision tools, smart watches, digital camera, tail and main rotors of meso-sized unmanned aerial vehicles (UAV), medical and dental instruments, precision instruments, prototype models, and domestic appliances (Gupta and Jain, 2014a). Most of these applications require quieter and smoother operating performance, more efficient and accurate transmission of motion, higher wear and corrosion resistance, increased fatigue strength, and longer service life. These characteristics are governed by overall quality of the meso-gears which is determined by their microgeometry, macrogeometry, surface roughness, surface integrity, and noise, vibration and wear related characteristics. These aspects in turn depend on material, manufacturing, finishing, and surface treatment of the meso-gears. Material of the meso-gears should have higher yield and fatigue strength, higher resistance to friction, wear and corrosion, better manufacturability (i.e. machinability, formability, and liquidity), less cost and easier availability. Brass, bronze, copper, aluminum, stainless steel, low alloy steel, and polymers are commonly used materials. Stainless steel has higher resistance to wear and corrosion and performs satisfactorily for longer period in a corrosive environment (Gupta and Jain 2016). Traditional manufacturing processes of meso-gears can be classified into three categories: (i) subtractive processes namely hobbing and milling; (ii) formative processes such as injection molding die casting, powder metallurgy, and lithography; and (iii) deformative processes which include extrusion, cold rolling, forging, stamping, and hot

embossing. Unfortunately, meso-gear manufactured by these processes have poor quality ranging from 9-12 in *Deutsches Institut für Normung (DIN)* standard, tool marks on their flank surfaces, sharp edges, burrs, poor edge definition and high geometrical and dimensional inaccuracy. These processes also have certain manufacturing limitations with regards to shape, size and materials of the meso-gears. This necessitates subsequent finishing process such as grinding, lapping, honing, shaving, skiving and burnishing to achieve the desired quality of the meso-gears and surface hardening, work hardening and appropriate coating processes to enhance their wear resistance, corrosion resistance, and fatigue strength (Gupta *et al.*, 2017).

All these factors have motivated the researchers to explore technically superior, economically viable, material and energy efficient manufacturing process for the meso-gears. Wire spark erosion machining process (WSEM) has potential to overcome the limitations of traditional manufacturing processes of the meso-gears. It is an electro-thermal type advanced machining process which uses a very thin wire as tool, deionized or distilled water as dielectric and very high pulse frequency (in the order of MHz). Despite of many advantages of WSEM process for manufacturing of meso-gears, very limited work has been reported in this area. Moreover, most of the past work only focused on manufacturing of external MSG analysing their surface finish (Ali and Mohammad, 2008), microgeometry, macrogeometry, and cutting rate (Gupta and Jain, 2014a and 2014b). Very limited work has been reported on using  $\mu$ -WSEM process to manufacture meso-ratchet wheel (Benavides *et al.*, 2002) and internal dies and micro-gears (Di *et al.*, 2006), and multi-response optimization for manufacturing meso-gears by WSEM process (Gupta and Jain, 2014a and 2014b). Bouquet *et al.* (2014) have concluded that manufacturing of helical gears and correction in their profile are very difficult by WSEM process. Consequently, present research work was undertaken with following objectives to bridge the identified research gaps using experimental investigation depicted in Fig. 1:

- To establish WSEM process to manufacture high quality MBG and MHG.
- To study the effects of WSEM process parameters on microgeometry parameters, average and maximum surface roughness and volumetric gear cutting rate of MBG and MHG so as to identify optimum values of WSEM process parameters.
- To study microstructure and microhardness of the best quality MBG and MHG manufactured using the identified optimum parameters of WSEM process.
- To develop models of the considered responses for the MBG and MHG.

- Multi-response optimization of the WSEM parameters to simultaneously optimize the conflicting responses of MBG and MHG.
- Experimental validation of the optimized results.
- Comparative evaluation of WSEM with milling process for manufacturing MBG and with hobbing process for manufacturing MHG to prove technical superiority and economic viability of WSEM process over them.

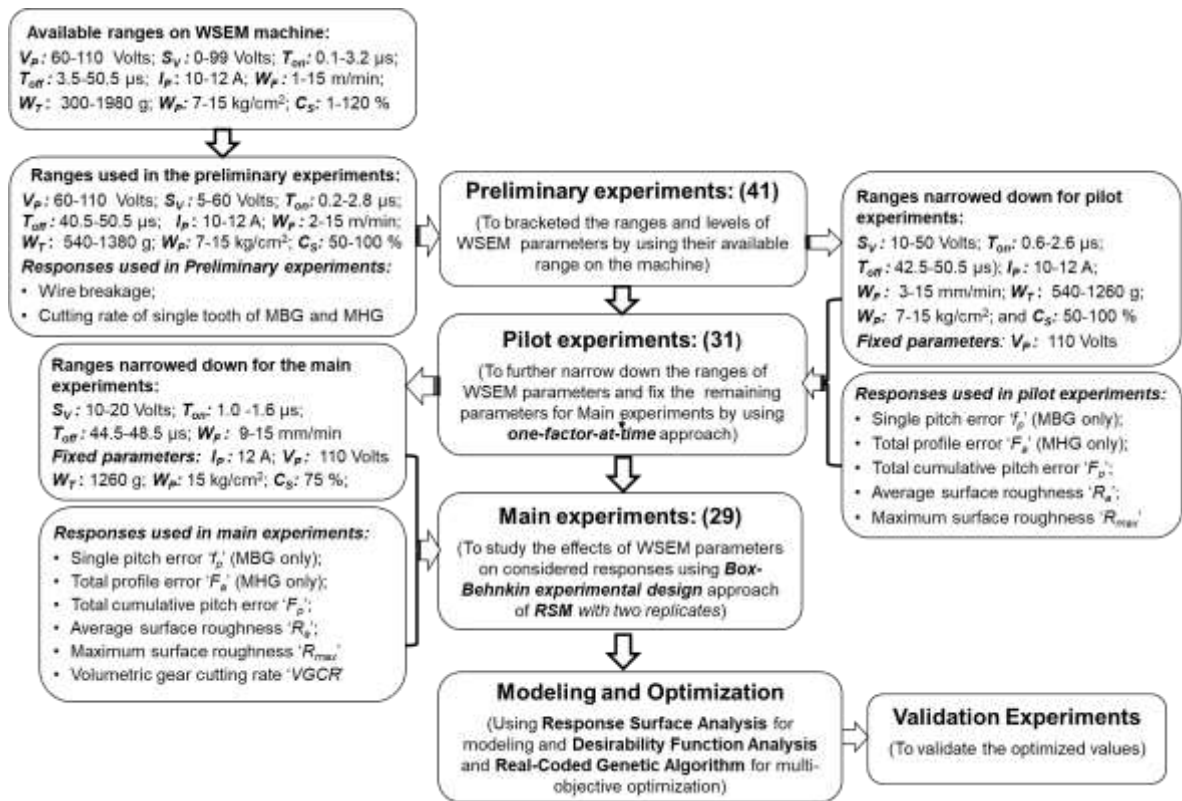


**Fig. 1:** Research methodology used in in the present work.

## 1. Materials, Specifications and Manufacturing of MBG and MHG

Austenitic stainless steel (SS 304 grade) was selected as material for MBG and MHG due to its higher resistance to corrosive environment, very good strength, non-magnetic nature and its widespread use in equipment and machines used in food processing, chemical plants, pharmaceutical, biomedical, surgical, and domestic applications. Figure 2 presents detailed specifications of the MBG and MHG used in the present work having involute profile with 20° pressure angle and 0.7 mm and 0.66 mm as module respectively.

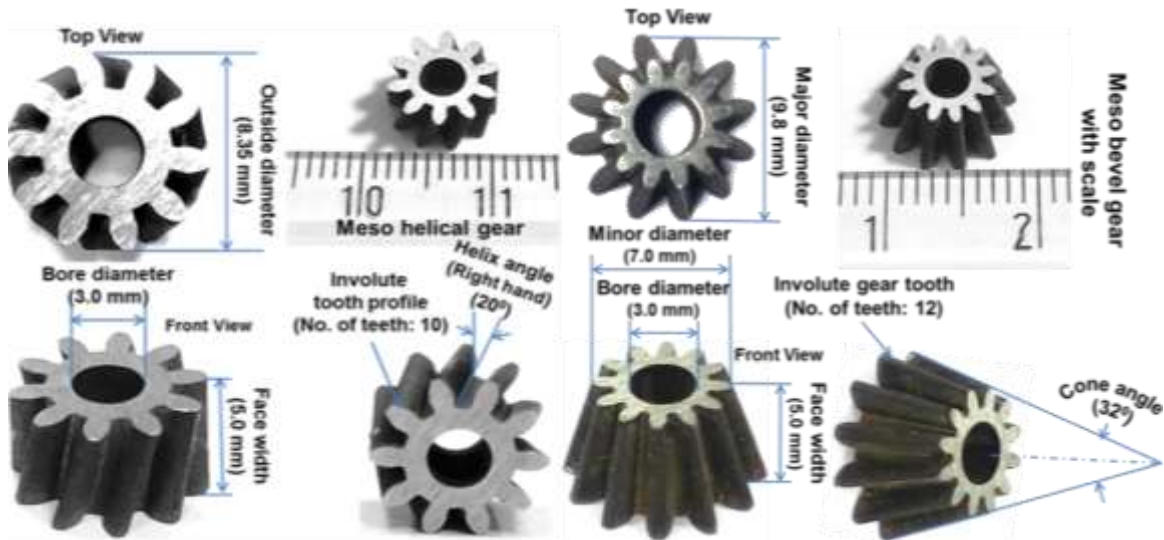


**Fig. 2:** Specifications of MHG and MBG used in the present work.

Four-axes (X, Y, U and V) computer numerical controlled (CNC) WSEM machine was used to manufacture MBG and MHG (having 3mm bore diameter) from a rectangular plate made of SS 304 using deionized water as dielectric and 250  $\mu\text{m}$  diameter soft plain brass wire having tensile strength in the range of 470-510  $\text{N}/\text{mm}^2$ . Following steps (as shown in Fig. 3) were involved in manufacturing of MBG and MHG by WSEM process: (i) preparation of 5 mm thick; 100 mm long; 50 mm wide SS 304 plate by grinding and buffing its top and bottom faces to make them perfectly flat, (ii) drilling an array of 800  $\mu\text{m}$  diameter microholes by micro spark-erosion drilling ( $\mu$ -SED). These microholes serve as passage for the wire during manufacturing of bore and meso-gears, (iii) clamping of the prepared plate on the WSEM machine worktable in perfectly horizontal position using a dial gauge, (iv) preparing layout of MBG (or MHG) by AutoCAD and importing its data exchange format (DXF) file in the ELCAM software for making part programs of MBG (or MHG) as per its specifications, (v) trepanning each microhole by WSEM process to enlarge its diameter from 0.8 mm to 3 mm so as to serve as bore of a MBG (or MHG), (vi) cutting the brass wire and running the WSEM machine in dry-mode to move the wire to an adjacent microhole, (vii) cutting a MBG (or MHG) by WSEM punching it out from the prepared plate leaving corresponding hole in the plate, (viii) repeating steps (v) to (vii) to manufacture next MBG or MHG, and (ix) measurements of microgeometry and surface roughness parameters of MBG and MHG, and analyses of microstructure, microhardness and flank surface topography of the best quality MBG and MHG.



**Fig. 3:** Sequences of different activities used in manufacturing of MBG and MHG and measurements of their responses.

## 2. Measurement of Responses

Form errors (profile and lead or helix) and location errors (pitch and runout) are two components of microgeometry of a gear as shown in Fig. 4 along with their constituents.

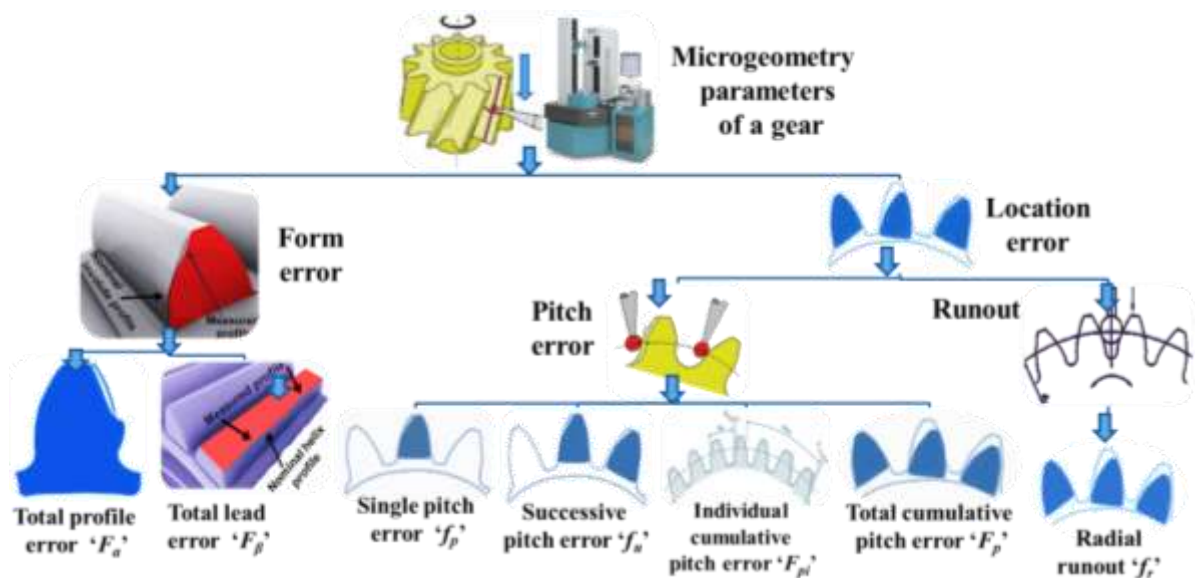


**Fig. 4:** Errors in microgeometry of a gear and their components.

Both form and location errors are relevant to the cylindrical (i.e. spur and helical) gears but only location errors are relevant to the conical (i.e. bevel) gears. Form errors indicate

deviations from the nominal shape of gear teeth. Total profile error ' $F_a$ ' and total lead error ' $F_\beta$ ' are its two components and they govern the noise generation, efficient transmission and load carrying capability of the gears. Location errors indicate inaccuracy in positioning of the gear teeth on its circumference along the pitch circle. Pitch error (or index error) and runout are its two components. They affect transmission efficiency, motion transfer characteristics, uniformity in gear motion (i.e wobbling) and noise behaviour (Gupta and Jain, 2014a). Flank surface topography is a 3D graphical representation which depicts combined effect of errors in profile and lead by showing differences between actual and theoretical flank surfaces in the form of peaks and valleys (Gupta and Jain, 2014b). Surface roughness consists of fine irregularities having short-wavelength and high-frequency, which generally results from inherent action of a manufacturing process. It significantly affects service life and operating performance of the gears. Average and maximum surface roughness ( $R_a$  and  $R_{max}$ ) are two important parameters. Volumetric gear cutting rate (VGCR) is the amount of the material removed per unit time during manufacturing of meso-gears. It is a measure of the productivity of WSEM process.

Four axes (X, Y, Z, and W axes) CNC gear metrology machine was used to measure the considered parameters of microgeometry and topography of flank surfaces of MBG and MHG using 500  $\mu\text{m}$  diameter ruby ball probe. The MBG and MHG were inspected using DIN 8 and DIN 9 corresponding to DIN 3965/86 and DIN 3961/62 standard, respectively. Average and maximum surface roughness ( $R_a$  and  $R_{max}$ ) values of the MBG and MHG were measured on 3D surface roughness measuring cum contour tracing machine by tracing 10  $\mu\text{m}$  tip diameter probe on their flank surfaces along the profile of gear tooth i.e. across direction of wire path. Vicker's microhardness was measured on Zwick Roell microhardness machine from UK using indentation force of 500 and 1000 g; 15 seconds dwell time; and 25  $\mu\text{m/s}$  indentation speed. Profile and bore of the best quality MBG and MHG and microstructures of their flank surfaces were studied using scanning electron microscope (SEM). Volumetric gear cutting rate was computed using following equation:

$$VGCR = \frac{w}{\rho t} \left( \frac{\text{mm}^3}{\text{min}} \right) \quad (1)$$

Where, ' $w$ ' is an amount of material spark eroded during manufacturing of meso-gears and calculated by subtracting sum of weight of meso-gear ( $W_{gear}$ ) and gear plate ( $W_{after}$ ) from the total weight of gear plate before machining ( $W_{before}$ ) i.e.  $W_{before} - (W_{after} + W_{gear})$ ; ' $\rho$ ' is the density of gear material; and ' $t$ ' is total manufacturing time of MBG (or MHG).

### 3. Experimentation Details, Significant Results and Brief Discussion

The experimental investigation was designed in four stages namely preliminary, pilot, main and validation experiments using appropriate design of experiments approach in each stage. Names, ranges and values of the variable and fixed parameters, and details of the responses used in each experimentation stage are shown in Fig. 1.

#### 3.1 Preliminary Experiments

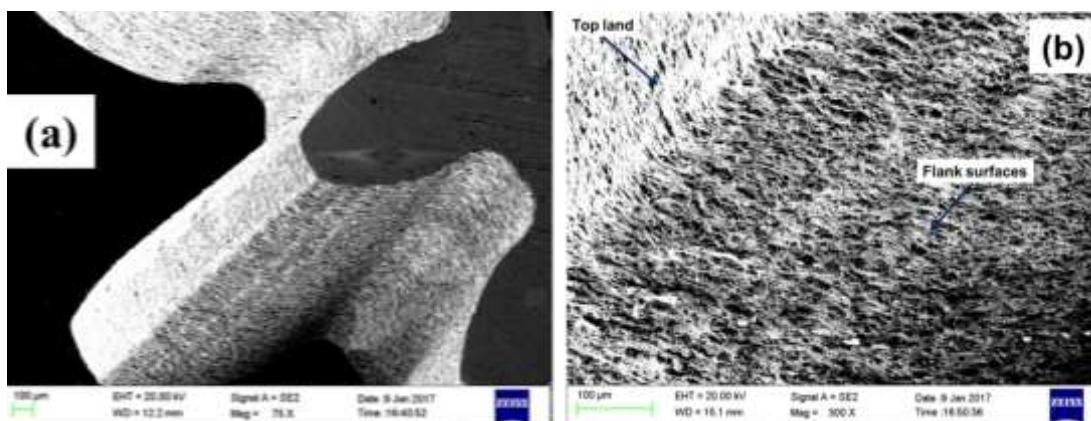
During the 1<sup>st</sup> stage, 41 *preliminary experiments* were conducted for MBG and MHG separately (i.e. 41 for MBG and 41 for MHG) by cutting only one tooth from each meso-gear and varying nine parameters of WSEM in the ranges available on WSEM machine (see in Fig. 1) using one-factor-at-time experimental design. Since, wire breakage in WSEM process significantly affects the quality, surface finish and total manufacturing time of the meso-gears, therefore, objective was to identify those ranges and levels of the considered parameters of WSEM for the pilot experiments which will avoid wire breakage and at the same time maximizes the WSEM productivity. These experiments fixed the value of pulse peak voltage ' $V_p$ ' as 110 volts and narrowed down ranges of remaining eight parameters, as presented in Fig. 1, for the pilot experiments.

#### 3.2 Pilot Experiments

Thirty one *pilot experiments* were conducted separately for MBG and MHG in the 2<sup>nd</sup> stage using one-factor-at-time (OFAT) approach to identify optimum ranges and/or values of the eight parameters of WSEM to fulfil the following objectives: (i) to further narrow down ranges of WSEM parameters and fix the other parameters for main experiments by focussing on microgeometry parameters, average and maximum surface roughness values of MBG and MHG with an objective to improve their overall quality. In case different parametric combinations yield minimum values of microgeometry and surface roughness parameters then preference was given to microgeometry, (ii) to study the effects of WSEM parameters on microgeometry and surface roughness of MBG and MHG so as to identify causes of errors in their microgeometry and surface roughness. This would help in identifying the ranges and/or values of WSEM parameters which manufacture the best quality MBG and MHG, and (iii) analyse the microstructure and flank surface topography of the best quality MBG and MHG. These experiments further narrowed down ranges of servo voltage ' $S_V$ ', pulse-on time ' $T_{on}$ ', pulse-off time ' $T_{off}$ ' and wire feed rate ' $W_F$ ' and fixed the values of peak current ' $I_P$ ', wire tension ' $W_T$ ', dielectric pressure ' $W_P$ ', and % of cutting speed ' $C_s$ ' as shown in Fig. 1. Some significant results are mentioned below:

### 3.2.1 Some Significant Results

- Irregular shaped craters, sparks having higher discharge energy, non-uniform sparks, wire-lag, recast layer, non-flatness of the gear plate, and error in its positioning with respect to wire feed are main factors which affect microgeometry and surface roughness parameters of MBG and MHG.
- Better quality and surface finish of MBG and MHG can be achieved using lower servo voltage, shorter pulse-on-time, longer pulse-off time, higher wire feed rate, wire tension and dielectric pressure.
- Higher values of pulse-on time and servo voltage should be avoided for stable sparking to improve the gear quality and surface finish of MBG and MHG.
- The better quality MBG had *DIN* quality 7 (having single pitch error as 10.75  $\mu\text{m}$  and total cumulative pitch error as 24.75  $\mu\text{m}$ ) whereas, the better quality MHG had *DIN* quality 7 for total profile error (9.15  $\mu\text{m}$ ) and *DIN* quality 6 for total cumulative pitch error (12.05  $\mu\text{m}$ ). These gears had 1.24 and 1.33  $\mu\text{m}$  as average surface roughness and 7.56 and 7.67  $\mu\text{m}$  for maximum surface roughness, respectively.
- Flank surfaces topography of the better quality MBG and MHG revealed small amount of variation in the measured flank surfaces from its theoretical form.
- Microhardness of flank surfaces of these gears is higher than parent materials due to formation of very thin recast layers and it does not induce any micro-cracks and heat affected zone to such an extent that it adversely affects fatigue strength of meso-gears.
- SEM images of the better quality MBG [Fig. 5(a)] and MHG [Fig. 5(c)] revealed their tooth profile to be burr-free, uniform, accurate, no undercutting at the root, no sharp edges on both end faces of the gears.
- Microstructural examination of flank surfaces of the better quality MBG [Fig. 5(b)] and MHG [Fig. 5(d)] had shown smoother surface free from cracks, nicks and asperities.



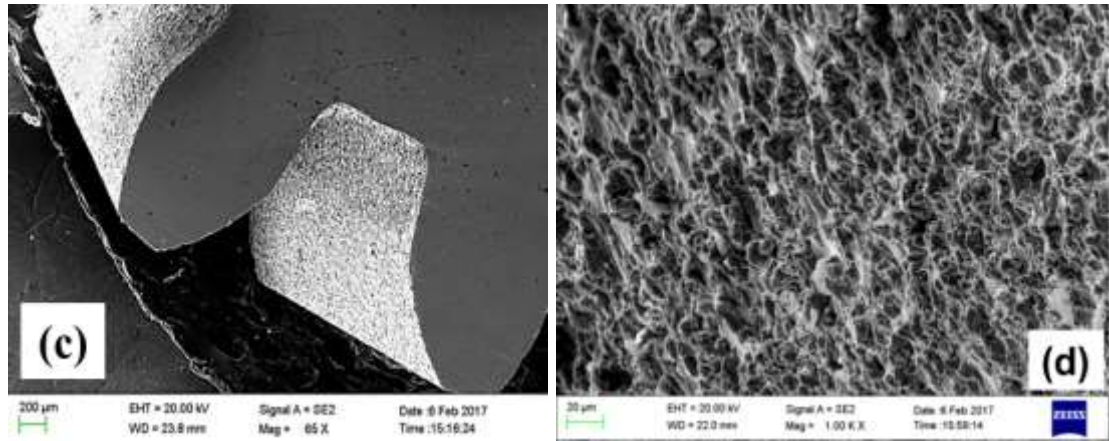


**Fig. 5.** SEM images depicting tooth profile and microstructure of tooth flank surfaces of the better quality (a), (b) MBG; and (c) (d) MHG.

### 3.3 Main Experiments

Twenty nine *main experiments* with two replicate each (thus manufacturing total 58 MHG and 58 MBG) were conducted in the 3<sup>rd</sup> stage using Box–Behnken experimental design of response surface methodology (RSM) by varying four WSEM parameters namely servo voltage ( $S_V$ ), pulse-on time ( $T_{on}$ ), pulse-off time ( $T_{off}$ ) and wire feed rate ( $W_F$ ) at three levels each in their further narrowed down ranges while, constant values of peak current ' $I_p$ ', wire tension ' $W_T$ ', dielectric pressure ' $W_P$ ', % of cutting speed ' $C_s$ ', and pulse peak voltage ' $V_p$ ' were used as presented in Fig. 1. These values were selected on the basis of the results and observations of the preliminary and the pilot experiments. Following are some significant results of the main experiments.

#### 3.3.1 Some Significant Results

- Servo voltage ( $S_V$ ), pulse-on time ( $T_{on}$ ), pulse-off time ( $T_{off}$ ) and wire feed rate ( $W_F$ ) were found to significantly affect the microgeometry parameters, maximum surface roughness, and volumetric gear cutting rate.
- Microgeometry parameters, maximum surface roughness, and volumetric gear cutting rate of MBG and MHG increase with increase in servo-voltage and pulse-on time, and decrease with pulse-off time and decrease with increase in wire feed rate but volumetric gear cutting rate slightly increases with it.
- Considered WSEM parameters had insignificant effect on average surface roughness.

### 4. Modelling and Optimization

The results of main experiments were analysed using *Design Expert* software (i) to develop modelling equations for the considered responses using regression analysis; (ii) to identify significance of the developed equations, variable parameters and their interactions

involved in these models using 95% confidence interval in analysis of variance (ANOVA); and (iii) to analyse the experimental data through graphs for the main effects and surface plots for interaction effects.

#### 4.1 Some Significant Results

- Servo voltage ( $S_V$ ), pulse-on time ( $T_{on}$ ), pulse-off time ( $T_{off}$ ) and wire feed rate ( $W_F$ ), and their squared terms were found to be significant for the considered parameters of microgeometry and surface roughness, and volumetric gear cutting rate of MBG and MHG.
- Interactions between  $T_{on}$  and  $T_{off}$ ,  $T_{on}$  and  $S_V$ ,  $T_{on}$  and  $W_F$ ,  $T_{off}$  and  $S_V$ , and  $S_V$  and  $W_F$  (except  $T_{on}$  and  $W_F$  for  $R_a$  of MHG) were found to be significant for the considered parameters of microgeometry and surface roughness of MBG and MHG.
- Interactions between  $T_{on}$  and  $T_{off}$ ,  $T_{on}$  and  $S_V$ , and  $T_{off}$  and  $S_V$  were found to be significant for volumetric gear cutting rate of MBG and MHG.

Desirability function analysis (DFA) was used to identify that combination of  $S_V$ ,  $T_{on}$ ,  $T_{off}$ , and  $W_F$  which will minimize the microgeometry and surface roughness parameters and maximize the volumetric gear cutting rate of MBG (or MHG) simultaneously. Overall desirability ' $D_j$ ' for  $j^{th}$  experimental observation was computed using following equation:

$$D_j = \left( \prod_{i=1}^m d_i \right)^{\frac{1}{\sum_{i=1}^m w_i}} \quad (2)$$

where,  $m$  is total number of the responses;  $w_i$  is relative weightage assigned to  $i^{th}$  response; and  $d_i$  is desirability of  $i^{th}$  responses which is computed using equation 3 for minimization and equation 4 for maximization of responses:

$$d_i = \left( \frac{U_i - y_{ij}}{U_i - T_i} \right)^{w_i} \quad (3)$$

$$d_i = \left( \frac{y_{ij} - L_i}{T_i - L_i} \right)^{w_i} \quad (4)$$

Where,  $T_i$  is the target value of the  $i^{th}$  response;  $U_i$  is permissible upper value the  $i^{th}$  response;  $L_i$  is permissible lower value the  $i^{th}$  response; and  $y_{ij}$  is the value of  $i^{th}$  response in  $j^{th}$  experimental observation. Responses can be classified into following three categories according to their nature: (i) smaller-the-better, (ii) larger-the-better, and (iii) nominal-the-best. Use of DFA yielded optimized values of pulse-on time as 1.41 and 1.44  $\mu$ s, pulse-off time as 48.5 and 47.3  $\mu$ s, servo voltage as 14.92 and 11.3 volts, and wire feed rate as 15 and 15 m/min for MBG and MHG respectively. These optimum values gave 8.94  $\mu$ m as single

pitch error for MBG, 8.32 as total profile error for MHG, 18.73 and 14.91  $\mu\text{m}$  as total cumulative pitch error, 1.16 and 1.19  $\mu\text{m}$  as average surface roughness, 6.53 and 7.1  $\mu\text{m}$  as maximum surface roughness, and 4.1 and 4.7  $\text{mm}^3/\text{min}$  as volumetric gear cutting rate for MBG and MHG respectively.

Real-coded genetic algorithm (RCGA) were also used to identify optimum values of  $T_{on}$ ,  $T_{off}$ ,  $S_V$ , and  $W_F$  through simultaneous optimization of the conflicting objectives of minimizing the microgeometry and surface roughness parameters and maximizing the volumetric gear cutting rate of MBG (or MHG) using their corresponding regression equations as objective functions and ranges of  $T_{on}$ ,  $T_{off}$ ,  $S_V$ , and  $W_F$  used in the main experiments as their variable bounds. Use of GA yielded optimized values of pulse-on time as 1.21 and 1.23  $\mu\text{s}$ , pulse-off time as 47.15 and 46.31  $\mu\text{s}$ , servo voltage as 10.86 and 11.41 volts, and wire feed rate as 11.24 and 11.68  $\text{m}/\text{min}$  for MBG and MHG respectively. These values gave 9.39  $\mu\text{m}$  as single pitch error for MBG, 9.46 as total profile error for MHG, 16.66 and 15.37  $\mu\text{m}$  as total cumulative pitch error, 1.04 and 1.09  $\mu\text{m}$  as average surface roughness, 6.43 and 7.65  $\mu\text{m}$  as maximum surface roughness, 3.02 and 3.33  $\text{mm}^3/\text{min}$  as volumetric gear cutting rate for MBG and MHG respectively.

Results of optimization by DFA and GA were confirmed by conducting validation experiments using those standard values available on the WSEM machine which were nearest to the optimized values of WSEM parameters. Fig. 6 presents SEM images of MBG and MHG manufactured during the validation experiments.

#### **4.2 Significant Results**

- There is very good agreement between the experimental results and optimization results given by DFA and GA.
- SEM images show that the MBG and MHG manufactured during validation experiments have burr-free, accurate and uniform teeth profile and smooth flank surfaces free from the crack, voids and asperities.
- WSEM attained quality up to DIN 6 in microgeometry of MBG and MHG.

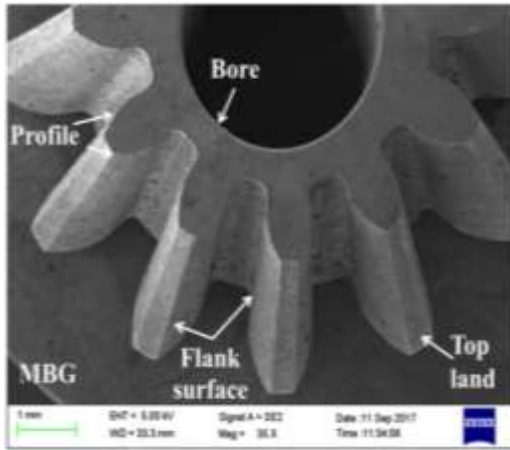


**Fig. 6(a)**

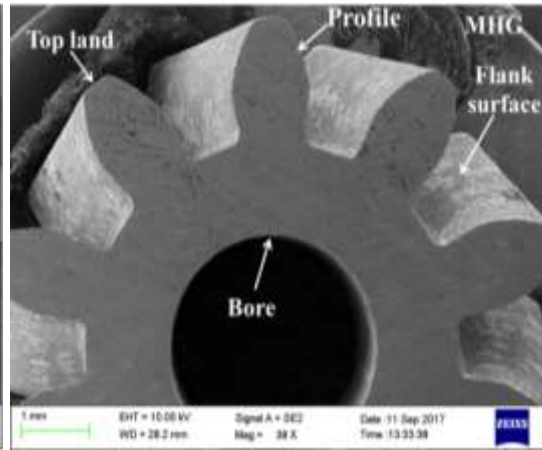


**Fig. 6(b)**

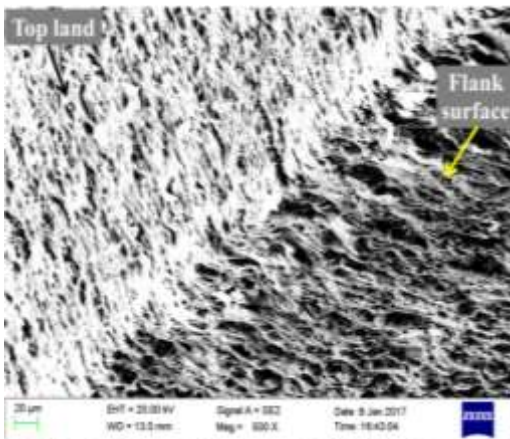


**Fig. 6(c)**

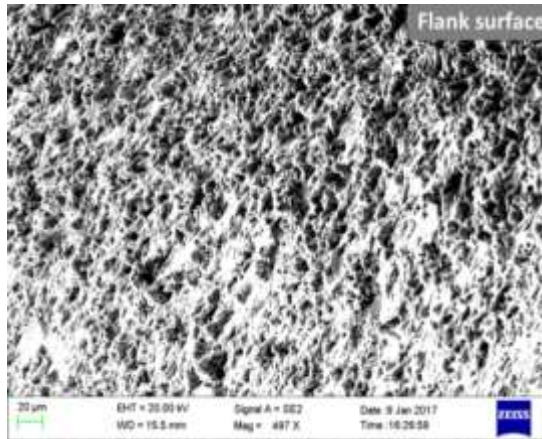


**Fig. 6(d)**

**Fig. 6:** SEM images showing bore, tooth profile, and flank surfaces of the best quality meso-gears manufactured by WSEM (a) MBG; (b) MHG; microstructures of the flank surfaces of the best quality; (c) MBG; and (d) MHG.

## 5. Comparative Study of WSEM, Milling and Hobbing

Comparison of capabilities of WSEM process with milling for manufacturing MBG and with hobbing for manufacturing MHG was done in terms parameters of microgeometry, macrogeometry, flank surface topography, surface roughness, microstructure, microhardness, manufacturing time and cost, and loss of gear material to prove technical superiority and economic viability of WSEM process over them. Its results are presented in Table 1 while Fig. 7 presents SEM images of WSEMed and milled MBG, and WSEMed and hobbed MHG.

### 5.1 Significant Results

- Microgeometry and macrogeometry of WSEM manufactured MBG and MHG is better than milled MBG and hobbed MHG. But, surface finish of milled MBG and hobbed MHG is better than the WSEM manufactured MBG and MHG.

- Flank surface topography of WSEM manufactured MBG and MHG revealed very less deviation of actual flank surface from the theoretical surface as compared to milled MBG and hobbed MHG.
- WSEM manufactured MBG and MHG exhibit smoother, crack-free and burr-free tooth flank surfaces whereas the milled MBG and hobbed MHG have presence of chip particles, burrs and cutter marks on its flank surfaces.
- WSEM manufactured MBG and MHG have accurate and uniform tooth profile than milled MBG and hobbed MHG.
- Total manufacturing time, total manufacturing cost, tooling cost and cost of the machining medium of milled MBG and hobbed MHG are very high as compared to the WSEM manufactured MBG and MHG. But, capital cost of WSEM machine is higher than that of milling and hobbing machine.
- Loss of meso-gear material is very less in WSEM process.

**Table 1.** Comparative evaluation of WSEM with milling and hobbing processes.

Criterion for comparison	Best quality MHG manufactured by		Best quality MBG manufactured by	
	<i>WSEM</i>	<i>Hobbing</i>	<i>WSEM</i>	<i>Milling</i>
<b><i>Value of the considered parameters of microgeometry and corresponding quality DIN system</i></b>				
Total profile error ( $\mu\text{m}$ )	8.8 (DIN 6)	30.9 (DIN 10)	Not applicable	
Single pitch error ( $\mu\text{m}$ )	7.2 (DIN 7)	8.8 (DIN 8)	6.9 (DIN 6)	63.2 (DIN 11)
Adjacent pitch error ( $\mu\text{m}$ )	12.3 (DIN 7)	9.2 (DIN 7)	11.5 (DIN 7)	47.2 (DIN 10)
Total pitch error ( $\mu\text{m}$ )	8.7 (DIN 5)	18.5 (DIN 7)	17.5 (DIN 6)	163.2 (DIN 12)
Radial runout ( $\mu\text{m}$ )	10.3 (DIN 6)	14.9 (DIN 7)	12.3 (DIN 6)	151.8 (>DIN 12)
<b><i>Value of the considered parameters of macrogeometry</i></b>				
Deviation in span ( $\mu\text{m}$ )	29	373	Not applicable	
Deviation in tooth thickness ( $\mu\text{m}$ )	33	351	Not applicable	
Deviation in outside dia. ( $\mu\text{m}$ )	46	250	Not applicable	
<b><i>Value of considered parameters of surface roughness</i></b>				
Average roughness ( $\mu\text{m}$ )	1.07	0.48	1.04	0.45
Maximum roughness ( $\mu\text{m}$ )	6.60	4.11	6.16	3.77
Skewness	-0.19	-0.188	-0.05	-0.56
Kurtosis	2.77	2.56	2.70	2.98
<b><i>Economic aspect for comparison (per meso-gear)</i></b>				
Total manufacturing time gears (minutes)	35	190	40	240
Total manufacturing cost (US \$)	4	8	4	10
Loss of gear material per meso-gear	0.75 g	1.29 g	0.7 g	1.18 g



Fig. 7(a)

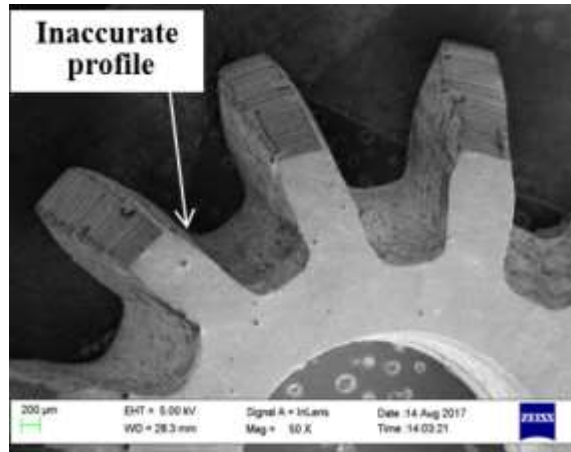


Fig. 7(b)

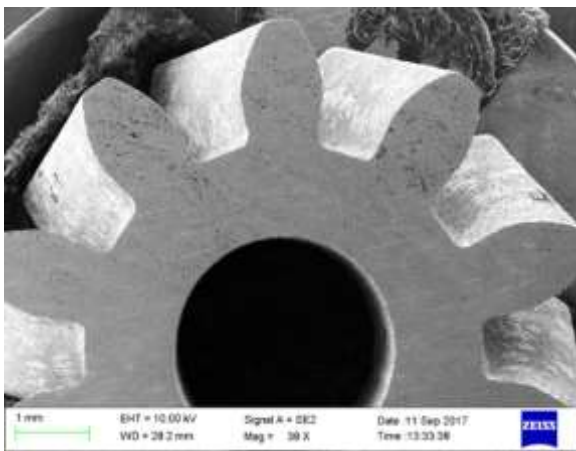


Fig. 7(c)

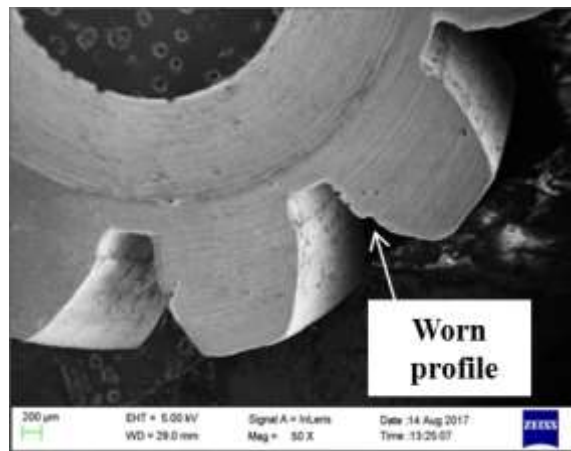


Fig. 7(d)

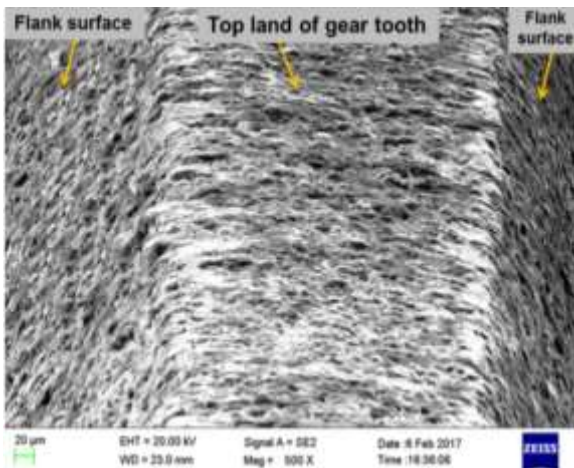


Fig. 7(e)

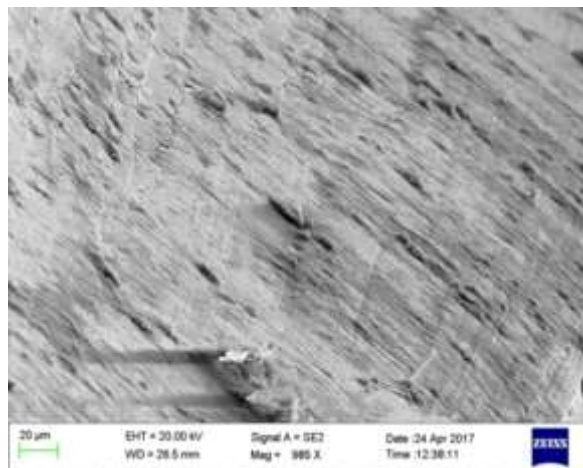
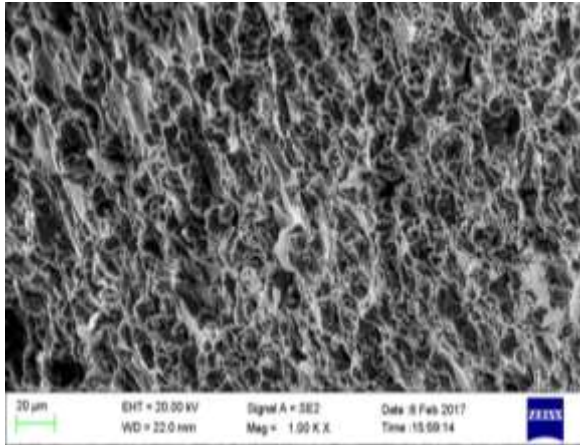
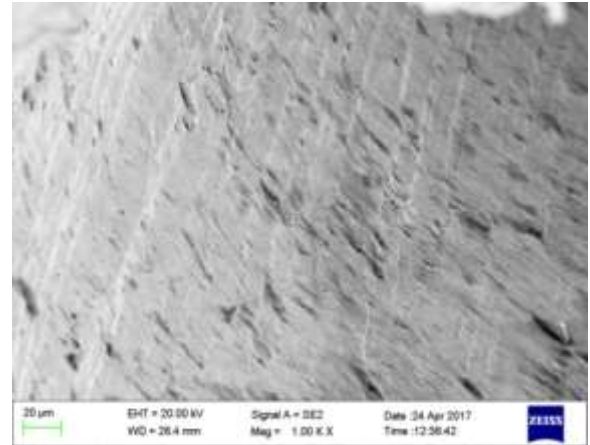


Fig. 7(f)



**Fig. 7(g)**



**Fig. 7(h)**

**Fig. 7:** SEM images showing tooth profile, flank surface and bore of (a) WSEM manufactured MBG; (b) milled MBG; (c) WSEM manufactured MHG; (d) hobbed MHG; microstructure of tooth flank surface of (e) WSEM manufactured MBG; (f) milled MBG; (g) WSEM manufactured MHG; and (h) hobbed MHG.

## 6. Some Significant Conclusions

- WSEM found capable to manufacture high quality MBG and MHG which are close to net-shape thus eliminating subsequent finishing and heat treatment processes.
- WSEM can manufacture MBG and MHG having gear quality up to DIN 6 which is much better than the quality of the meso-gears manufactured by any other process.
- WSEM gave  $0.95\ \mu\text{m}$  and  $1.0\ \mu\text{m}$  as average surface roughness and  $6.1\ \mu\text{m}$  and  $7.04\ \mu\text{m}$  as maximum surface roughness for the optimized MBG and MHG respectively.
- WSEM manufactured MBG and MHG exhibited higher wear resistance at tooth flank.
- SEM images of MBG and MHG revealed uniform tooth profile, free from burrs, sharp edge definition and no undercut at root.
- Microstructure studies revealed smooth and crack-free tooth flank surfaces of WSEM manufactured MBG and MHG.
- Comparative study of WSEM and traditional manufacturing processes proved that WSEM is a superior, economical, material efficient, and environment friendly process to manufacture high quality MBG and MHG.
- The results of present work can be very useful for industrial users and researchers working in manufacturing and use of meso-gears.



## List of Publications

### [A] Papers Published in Refereed Journals from the PhD Work

1. **Sujeet K Chaubey, N.K. Jain (2018)** “Capabilities evaluation of WSEM, milling and hobbing for meso-gear manufacturing” **Materials and Manufacturing Processes**, DOI: 10.1080/10426914.2018.1453156 (**Impact Factor: 2.27**)
2. **Sujeet K Chaubey, N.K. Jain (2018)** “State-of-art review of past research on manufacturing of meso and micro cylindrical gears” **Precision Engineering**, 51, 702-728, DOI: 10.1016/j.precisioneng.2017.07.014 (**Impact factor: 2.24**) (Jan. 2018)
3. **Sujeet K Chaubey, N.K. Jain (2018)** “Investigations on surface quality of WEDM manufactured meso bevel and helical gears” **Materials and Manufacturing Processes**, DOI: 10.1080/10426914.2017.1415440 (**Impact Factor: 2.27**)
4. **Sujeet K Chaubey, N.K. Jain (2017)** “Investigations on microgeometry of meso bevel and meso helical gears manufactured by WEDM process” **International Journal of Advanced Manufacturing Technology**, 93(9), 4217-4231, DOI: 10.1007/s00170-017-0884-y (**Impact factor: 2.21**) (Dec 2017)
5. **Sujeet K Chaubey, N.K. Jain (2018)** “Analysis and multi-response optimization of gear quality and surface finish of meso-sized helical and bevel gears manufactured by WSEM process” **Precision Engineering** (under review in since Feb. 2018) (manuscript ID: PRE\_2018\_65) (**Impact Factor: 2.24**).
6. **Sujeet K Chaubey, N.K. Jain (2018)** “Optimization of WSEM Parameters for Manufacturing Meso-sized Bevel and Helical Gears” to be submitted to **Journal of Intelligent Manufacturing** in Feb 2018 (**Impact factor: 3.035**).
7. **Sujeet K Chaubey, N.K. Jain (2018)** “Exploring WSEM process for manufacturing meso helical and bevel gears” accepted for publication in **Materials Today: Proceedings**.
8. **Sujeet K Chaubey, N.K. Jain (2018)** “On productivity of WSEM process for manufacturing meso-sized helical and bevel gears” ” **IOP Conference Series: Materials Science and Engineering** 389 (2018) 012007, DOI:10.1088/1757-899X/389/1/012007

### **[B] Book Chapter Published from PhD Work**

9. Jain, N.K., and **Chaubey, Sujeet Kumar (2016)**, Review of Miniature Gear Manufacturing, In: *Comprehensive Materials Finishing*-Vol. 1 (Ed. Hashmi, M.S.J.) pp. 504–538, Elsevier, Oxford (UK), DOI: 10.1016/B978-0-12-803581-8.09159-1, (ISBN: 978-0-12-803581-8)

### **[C] Other Publications**

10. Deepak Raj, R. Tyagi, **S. K. Chaubey**, A. D'Souza, I. A. Palani, N. K. Jain (**2015**), “Investigation on Solid State Nd-YAG Nano-second Laser Assisted Shock Peening of Miniature Gears” **Materials Today: Proceedings**, 2(4-5), 1755–1762 (DOI: 10.1016/j.matpr.2015.07.012).
11. Kapil Gupta, **S.K. Chaubey**, N.K. Jain (**2014**), “Exploring Wire-EDM for Manufacturing the High Quality Meso-gears” **Procedia Materials Science**, 5, 1755-1760 (DOI: 10.1016/j.mspro.2014.07.365).

# Table of Contents

<b>List of Figures</b>	<b>xxix</b>
<b>List of Tables</b>	<b>xxxv</b>
<b>Nomenclature</b>	<b>xxxvii</b>
<b>Abbreviations</b>	<b>xxxix</b>
<b>Chapter 1: Introduction</b>	<b>1-30</b>
1.1 Introduction to Meso-Gears	3
1.2 Materials for Meso-Gears	3
1.3 Advantages and Applications of Meso-Gears	5
1.4 Manufacturing of Meso-Gears	6
1.4.1 Traditional Manufacturing Processes	6
1.4.1.1 Subtractive Processes	8
1.4.1.2 Formative Processes	8
1.4.1.3 Deformative Processes	9
1.4.2 Advanced Machining Processes	9
1.4.2.1 Controlled Spark Erosion Machining	10
1.4.2.2 Thermo-Electric Vaporization	10
1.4.2.3 Mechanical Erosion	10
1.4.2.4 Chemical Ablation	11
1.5 Quality Aspects of Gears	11
1.5.1 Gear Quality and its Standards	12
1.5.1.1 Errors in Gear Microgeometry	13
1.5.1.2 Errors in Gear Macrogeometry	16
1.5.2 Surface Quality of Gears	17
1.5.2.1 Flank Surface Topography	17
1.5.2.2 Surface Roughness	18
1.5.2.3 Wear Characteristics	19

1.5.3 Surface Integrity Aspects of Gears	19
1.5.3.1 Microhardness	20
1.5.3.2 Microstructure	20
1.5.3.3 Residual Stresses	21
1.6 Use of WSEM for Meso-Gear Manufacturing	21
1.7 Introduction to WSEM Process	22
1.7.1 Working Principle	23
1.7.2 Mechanism of Material Removal	24
1.7.3 Process Parameters	25
1.7.4 Advantages and Limitations	27
1.7.5 Applications	28
1.8 Organization of the Thesis	29
<b>Chapter 2: Review of Past Work and Research</b>	<b>31-52</b>
<b>Objectives</b>	
2.1 Past Work on Manufacturing of Micro and Meso-Gears	31
2.1.1 Manufacturing of Meso and Micro-Spur Gears using Spark Erosion based Processes	31
2.1.1.1 Manufacturing of Micro-Spur Gears by SEM and $\mu$ -SEM	32
2.1.1.2 Manufacturing of Meso and Micro-Spur Gears by WSEM and $\mu$ -WSEM	36
2.1.2 Manufacturing of Meso and Micro-Spur Gears by other Advanced Machining Processes	46
2.2 Past Work on other Aspects of WSEM	49
2.3 Identified Research Gaps	50
2.4 Objectives of the Present Work	51
2.5 Research Methodology	51
<b>Chapter 3: Details of Experimentation</b>	<b>53-68</b>
3.1 Material Selection for the Meso-Gears	53
3.2 Design Specifications of the Meso-Gears	53
3.3 Planning and Designs of Experiments	54

3.3.1 Preliminary Experiments	56
3.3.2 Pilot Experiments	56
3.3.3 Main Experiments	57
3.3.4 Validation Experiments	59
3.4 Procedure of Experimentation	60
3.4.1 Details of the WSEM Machine	60
3.4.2 Details of Manufacturing of MBG and MHG	61
3.5 Evaluation of the Responses	63
3.5.1 Measurements of Microgeometry and Macrogeometry	63
3.5.2 Measurements of Flank Surface Topography	64
3.5.3 Measurements of Surface Roughness	65
3.5.4 Characterization of Surface Integrity	66
3.5.4.1 Microstructure Examination	66
3.5.4.2 Microhardness Testing	66
3.5.5 Evaluation of Volumetric Gear Cutting Rate	67
3.6 Analysis of the Experimental Results	67
<b>Chapter 4: Results and Analysis</b>	<b>69-114</b>
4.1 Observations and Conclusions of the Preliminary Experiments	69
4.2 Results and Analysis of the Pilot Experiments	70
4.2.1 Influence of WSEM Parameters on MBG and MHG Microgeometry	72
4.2.2 Influence of WSEM Parameters on MBG and MHG Surface Roughness	78
4.2.3 Analysis of MBG and MHG having Minimum Microgeometry Errors	84
4.2.3.1 Microgeometry	84
4.2.3.2 Flank Surface Topography	88
4.2.3.3 Surface Roughness	89
4.2.3.4 Microhardness	89
4.2.3.5 Microstructure	91

4.2.4 Conclusions of the Pilot Experiments	92
4.3 Results and Analysis of the Main Experiments	93
4.3.1 Development of Response Surface Models	96
4.3.1.1 For Microgeometry Errors of MBG and MHG	96
4.3.1.2 For Surface Roughness of MBG and MHG	98
4.3.1.3 For Volumetric Gear Cutting Rate of MBG and MHG	100
4.3.2 Influence of WSEM Parameters	100
4.3.2.1 On Microgeometry and Surface Roughness	101
4.3.2.2 On Volumetric Gear Cutting Rate	106
4.3.3 Influence of Significant Interactions of WSEM Parameters	107
4.3.4 Conclusions of the Main Experiments	113
<b>Chapter 5: Modeling and Optimization</b>	<b>115-132</b>
5.1 Modeling using Artificial Neural Network (ANN)	115
5.2 Comparison of the Response Surface and ANN Models	117
5.3 Optimization Using Desirability Function Analysis	120
5.3.1 Minimization of Microgeometry Errors and Surface Roughness	121
5.3.2 Maximization of Volumetric Gear Cutting Rate	122
5.4 Multi-Objective Optimization	122
5.4.1 Using Desirability Functional Analysis	123
5.4.2 Using Real-Coded Genetic Algorithm	124
5.5 Validation of the Optimization Results	125
5.6 Investigations on the Best Quality MBG and MHG	128
5.6.1 Microgeometry	128
5.6.2 Flank Surface Topography	131
5.6.3 Surface Roughness	131
5.6.4 Microstructure	131

<b>Chapter 6: Comparison of WSEM with Traditional Processes</b>	<b>133-142</b>
6.1 Details of Experimentation	133
6.2 Comparison of WSEMed, Milled and Hobbed Gears	135
6.2.1 Microgeometry	135
6.2.2 Macrogeometry	136
6.2.3 Flank Surface Topography	137
6.2.4 Surface Roughness	137
6.2.5 Microhardness	137
6.2.6 Economic Aspects	138
6.2.7 Microstructure	139
6.3 Conclusions from the Comparative Study	141
<b>Chapter 7: Conclusions and Scope for the Future Work</b>	<b>143-147</b>
7.1 Significant Achievements	143
7.2 Conclusions	143
7.3 Scope for the Future Work	147
<b>References</b>	<b>149-155</b>
<b>Appendix-A: Chemical Composition of Meso Gears Material</b>	<b>157</b>
<b>Appendix-B: Details of the Measuring Instruments Used</b>	<b>158</b>
<b>Appendix-C: Gear Part Program</b>	<b>163</b>
<b>Appendix-D: Process Parameters and their Available Ranges on WSEM Machine Used</b>	<b>171</b>
<b>Appendix-E: ANOVA Table</b>	<b>172</b>



# List of Figures

<b>Figure Number and its Caption</b>	<b>Page No.</b>
<b>Fig. 1.1:</b> Different types of gears.	1
<b>Fig. 1.2:</b> Different types of materials used for meso-gears (Jain and Chaubey, 2016).	4
<b>Fig. 1.3:</b> Typical applications of different types of meso-gears (Chaubey and Jain, 2018).	6
<b>Fig. 1.4:</b> Different components of microgeometry of a gear.	13
<b>Fig. 1.5:</b> Macrogeometry parameters of a gear.	16
<b>Fig. 1.6:</b> Graphical representation of tooth flank surface topography.	17
<b>Fig. 1.7:</b> Representation of surface roughness parameters.	19
<b>Fig. 1.8:</b> Schematic diagram showing working principle of WSEM process.	24
<b>Fig. 1.9:</b> Different phases and concepts of spark generation in WSEM process.	25
<b>Fig. 1.10:</b> Different electrical parameters in a spark-erosion based process.	26
<b>Fig. 1.11:</b> Some typical complicated parts manufactured by WSEM processes.	29
<b>Fig. 2.1:</b> Mold for micro-gear made of 30CrMo6 by SEM process by Schulz et al. (2012).	32
<b>Fig. 2.2:</b> SEM images showing external micro- spur gear manufactured by $\mu$ -SEM process by Takahata et al. (2000).	33
<b>Fig. 2.3:</b> SEM images showing (a) external micro-spur gear manufactured by $\mu$ -SEM process; and (b) LIGA manufactured hollow internal micro-spur gear used as tool by Takahata and Gianchandani (2002).	33
<b>Fig. 2.4:</b> SEM images showing (a) internal micro-spur gear of steel manufactured by vibration-assisted $\mu$ -SEM process; and (b) external micro-spur gear of copper used as tool by Tong et al. (2008).	34
<b>Fig. 2.5:</b> Micrographs of external micro-spur gears manufactured by by Hsue et al. (2007) using WSEM process having worktable driven by: (a) CRM; and (b) LSM.	37
<b>Fig. 2.6:</b> Photographs of (a) stepped mold of internal MSG of copper manufactured by WSEM and thermal diffusion welding process; and (b) external stepped MSG of plastic materials manufactured using this mold by Zhong et al. (2015).	39
<b>Fig. 2.7:</b> Meso-ratchet wheel manufactured by $\mu$ -WSEM process by Benavides et	39

al. (2002): (a) photograph of beryllium copper meso-ratchet wheel; and (b) SEM image of teeth of Nitronic 60 stainless steel meso-ratchet wheel.	
<b>Fig. 2.8:</b> SEM images of X38CrMoVS_1 steel micro-spur gears manufactured by Schoth et al. (2005) by $\mu$ -WSEM using tungsten wire of diameter (a) 20 $\mu\text{m}$ ; (b) 30 $\mu\text{m}$ ; and (c) made of ceramic (SiSiC) using 30 $\mu\text{m}$ diameter tungsten wire.	41
<b>Fig. 2.9:</b> SEM image of MSG with shaft manufactured by Schoth et al. (2005) using by $\mu$ -WSEM.	41
<b>Fig. 2.10:</b> SEM images of SKD11 tool steel micro-spur gear manufactured by Yan and Chiang (2009) using $\mu$ -WSEM and 70 $\mu\text{m}$ diameter copper wire.	42
<b>Fig. 2.11:</b> SEM images of MSG of beryllium copper manufactured by Ali et al. (2010) using: (a) WSEM process; and (b) $\mu$ -WSEM process.	43
<b>Fig. 2.12:</b> SEM images of micro-spur gears manufactured by Youn et al. (2007): (a) 50 $\mu\text{m}$ deep mold of micro-spur gear from glassy carbon by laser ablation process; and (b) hot-embossed micro-spur gear of Pyrex glass.	47
<b>Fig. 2.13:</b> Research methodology used in the present work.	52
<b>Fig. 3.1:</b> Three-dimensional views and of MBG and MHG made of SS 304.	54
<b>Fig. 3.2:</b> Geometric representation of BBD of RSM for three factors having three levels.	58
<b>Fig. 3.3:</b> Photograph of the WSEM used in the present work.	60
<b>Fig. 3.4:</b> Different activities and their sequence used in the experimental investigations of the present work.	62
<b>Fig. 3.5:</b> Movement of the wire during trepanning of the bore and manufacturing of the meso-gears by WSEM process for (a) MBG; and (b) MHG.	63
<b>Fig. 3.6:</b> Measurements of microgeometry parameters by WenzelTec SmartGear 500 CNC gear metrology machine for: (a) MBG; and (b) MHG.	64
<b>Fig. 3.7:</b> Concept of the measurement of microgeometry, macrogeometry and flank surface topography of the meso-gears by CNC gear metrology machine.	65
<b>Fig. 3.8:</b> Measurements of surface roughness of WSEM manufactured meso-gears by LD130 surface roughness cum contour tracer for: (a) MBG; and (b) MHG.	66
<b>Fig. 4.1:</b> Variation of single pitch error ' $f_p$ ' and total cumulative pitch error ' $F_p$ ' for MBG, and total profile error ' $F_a$ ' and total cumulative pitch error ' $F_p$ ' for MHG with: (a) peak current; (b) servo voltage; (c) pulse-on time; (d) pulse-off time; (e) wire feed rate; (f) wire tension; (g) dielectric pressure; (h) % cutting	78

speed.

**Fig. 4.2:** SEM images showing irregular shaped deep craters on tooth flank surface of the meso-gears manufactured by WSEM process: (a) MBG; and (b) MHG. 78

**Fig. 4.3:** Variation in average surface roughness and maximum surface roughness with WSEM process parameters for MBG and MHG: (a) peak current; (b) servo voltage; (c) pulse-on time; (d) pulse-off time; (e) wire feed rate; (f) wire tension; (g) dielectric pressure; and (h) % cutting speed. 83

**Fig. 4.4:** Microgeometry investigation graphs showing DIN quality number for both left and right hand flanks of better quality MBG: (a) single pitch error ' $f_p$ ', adjacent pitch error ' $f_u$ '; and (b) total cumulative pitch error ' $F_p$ ' and radial runout ' $F_r$ '. 85

**Fig. 4.5:** Microgeometry investigation graphs showing DIN quality number for both left and right hand flanks of better quality MHG: (a) total profile error ' $F_a$ '; (b) single pitch error ' $f_p$ ' and adjacent pitch error ' $f_u$ ' and (c) total cumulative pitch error ' $F_p$ ' and radial runout ' $F_r$ '. 87

**Fig. 4.6:** Flank surface topography of the better quality (a) MBG; and (b) MHG. 89

**Fig. 4.7:** Microhardness of the better quality MBG and MHG manufactured by WSEM process and their material SS 304 at different applied load. 90

**Fig. 4.8:** Microscopic image of the recast layer and heat affected zone (HAZ) on tooth flank surface of the better quality (a) MBG; and (b) MHG. 90

**Fig. 4.9:** SEM images showing tooth profile and microstructure of tooth flank surface of the better quality (a), (b) MBG; and (c), (d) MHG, respectively. 91

**Fig. 4.10:** Normal plot of residuals for (a) single pitch error ' $f_p$ '; and (b) total cumulative pitch error ' $F_p$ ' of MBG; and (c) total profile error ' $F_a$ '; and (d) total cumulative pitch error ' $F_p$ ' of MHG. 97

**Fig. 4.11:** Normal plot of residuals for average and maximum surface roughness of (a); (b) MBG; and (c) and (d) MHG, respectively. 99

**Fig. 4.12:** Normal plot of residuals for volumetric gear cutting rate VGCR of (a) MBG; and (b) MHG. 100

**Fig. 4.13:** Variation of surface roughness parameters and microgeometry errors of MBG with (a) servo voltage; (b) pulse-on time; (c) pulse-off time; and (d) wire feed rate. 103

**Fig. 4.14:** Variation of surface roughness parameters and microgeometry errors of 105

MHG with (a) servo voltage; (b) pulse-on time; (c) pulse-off time; and (d) wire feed rate.	
<b>Fig. 4.15:</b> Variation of volumetric gear cutting rate with WSEM parameters for: (a) MBG; and (b) MHG.	107
<b>Fig. 4.16:</b> Surface plots showing effects of the identified significant interactions on the considered responses of MBG.	110
<b>Fig. 4.17:</b> Surface plots showing effects of the identified significant interactions on the considered responses of MHG.	113
<b>Fig. 5.1:</b> Architecture of the ANN models for the considered responses of MBG and MHG.	116
<b>Fig. 5.2:</b> Flowchart of the real-coded genetic algorithm used in multi-objective optimization	125
<b>Fig. 5.3:</b> Reports of metrological investigation for the best quality MBG manufactured using the optimized WSEM parameters: (a) single pitch error ' $f_p$ ' and adjacent pitch error ' $f_u$ '; (b) total cumulative pitch error ' $F_p$ '; and (c) radial runout ' $F_r$ '.	129
<b>Fig. 5.4:</b> Reports of metrological investigation for the best quality MHG manufactured using optimized WSEM parameters: (a) single pitch error ' $f_p$ ' and adjacent pitch error ' $f_u$ '; (b) total cumulative pitch error ' $F_p$ '; (c) radial runout ' $F_r$ '; and (d) total profile error ' $F_a$ '.	130
<b>Fig. 5.5:</b> SEM images showing bore, tooth profile, and flank surfaces of the best quality meso-gears manufactured by WSEM (a) MBG; (b) MHG; microstructures of the flank surfaces of the best quality; (c) MBG; and (d) MHG.	132
<b>Fig. 6.1:</b> Concepts of manufacturing: (a) MHG by hobbing; and (b) MBG by milling process.	134
<b>Fig. 6.2:</b> Photographs showing 3D views of (a) WSEM manufactured MBG; (b) WSEM manufactured MHG; (c) milled MBG; and (d) hobbed MHG.	135
<b>Fig. 6.3:</b> Microhardness values of the hobbed MHG, milling MBG and WSEM manufactured MHG and MBG at different values of indentation load.	138
<b>Fig. 6.4:</b> SEM micrographs showing tooth profile, flank surface and bore of (a) WSEM manufactured MBG; (b) milled MBG, microstructure of tooth flank surface of (c) WSEM manufactured MBG; and (d) milled MBG.	140
<b>Fig. 6.5:</b> SEM images showing tooth profile, flank surface and bore of (a) WSEM	141

manufactured MHG; (b) hobbed MHG, microstructure of tooth flank surface of (c) WSEM manufactured MHG; and (d) hobbed MHG.



# List of Tables

<b>Table Number and its Caption</b>	<b>Page No.</b>
<b>Table 1.1:</b> Classification of gears according to different criteria (Townsend, 2011; Radzevich, 2012; Davis, 2005; Bralla, 1998).	2
<b>Table 1.2:</b> Summary of different meso-gear materials, their characteristics, features and applications (Radzevich, 2012; Jain and Chaubey, 2016).	4
<b>Table 1.3:</b> Commonly used process for manufacturing micro-gears and meso-gears (Radzevich, 2012; Gupta and Jain, 2014b; Jain and Chaubey, 2016).	7
<b>Table 1.4:</b> Traditional processes for manufacturing the meso-gears and the gear quality achieved by them (Davis, 2005; Brala, 1998; Gupta and Jain, 2014c).	7
<b>Table 1.5:</b> Details of most commonly used gear standards.	13
<b>Table 2.1:</b> Summary of past research works on manufacturing of micro-spur gears by SEM and $\mu$ -SEM processes.	35
<b>Table 2.2:</b> Summary of past research works on manufacturing of meso and micro-spur gears by WSEM.	40
<b>Table 2.3:</b> Summary of past research works on manufacturing of meso and micro-spur gears by $\mu$ -WSEM.	44
<b>Table 2.4:</b> Summary of past research works on manufacturing of meso and micro-spur gears by other advanced machining processes.	48
<b>Table 3.1:</b> Specifications of the MBG and MHG used in the present work.	54
<b>Table 3.2:</b> Details of ranges and values of parameters of WSEM process, responses, and approach of experimental design used in each stage of experimental investigation.	55
<b>Table 3.3:</b> Comparison of different experimental design approaches on the basis of number of experimental runs required for three level factors.	58
<b>Table 3.4:</b> Actual and coded values of WSEM parameters for 29 experimental runs designed using BBD approach of RSM for main experiments.	59
<b>Table 3.5:</b> Specifications of CNC WSEM machine used in the present work.	60
<b>Table 4.1:</b> Values of WSEM process parameters and the considered microgeometry parameters of MBG and MHG for the pilot experiments.	71
<b>Table 4.2:</b> Values of WSEM process parameters and corresponding values of average and maximum surface roughness of MBG and MHG for the pilot	72

experiments.

<b>Table 4.3:</b> Summary of microgeometry errors for better quality MBG and MHG.	84
<b>Table 4.4:</b> Values of microgeometry errors, average and maximum surface roughness values and volumetric gear cutting rate of MBG for two replicates ( <i>R1</i> and <i>R2</i> ) of the main experiments with along with corresponding variable parameters of WSEM process.	94
<b>Table 4.5:</b> Values of microgeometry errors, average and maximum surface roughness values and volumetric gear cutting rate of MHG for two replicates ( <i>R1</i> and <i>R2</i> ) of the main experiments with along with corresponding variable parameters of WSEM process.	95
<b>Table 5.1:</b> Details of the ANN models for the considered responses of MBG and MHG.	117
<b>Table 5.2:</b> Response surface and ANN model predicted values of the considered responses of MBG.	118
<b>Table 5.3:</b> Response surface and ANN model predicted values of the considered responses of MHG.	119
<b>Table 5.4:</b> Variable bounds of the WSEM parameters and RCGA parameters used in multi-objective optimization	124
<b>Table 5.5:</b> Optimized values of four parameters of WSEM given by DFA and RCGA along with corresponding values of considered responses of MBG and MHG.	126
<b>Table 5.6:</b> Optimized values of WSEM parameters and responses along with their corresponding values from the experimental validation.	127
<b>Table 6.1:</b> Details of the processes used to manufacture MBG and MHG along with their specifications.	134
<b>Table 6.2:</b> Microgeometry, flank surface topography, macrogeometry, and surface roughness parameters for the meso-gears manufactured by WSEM, milling and hobbing.	136

## Nomenclature

$C_S$	Cutting Speed
$F_a$	Total Profile Error
$ff_a$	Profile Form Error
$ff_\beta$	Lead Form Error
$fh_a$	Profile Angle Error
$fh_\beta$	Lead Angle (Slope) Error
$f_p$	Single Pitch Error
$F_p$	Total Cumulative Pitch Error
$F_r$	Radial Runout
$f_u$	Adjacent Pitch Error
$F_\beta$	Total Lead Error
$I_P$	Peak Current
$R_a$	Average Surface Roughness
$R_{max}$	Maximum Surface Roughness
$S_V$	Servo Voltage
$T_{off}$	Pulse-off Time
$T_{on}$	Pulse-on Time
$V_P$	Pulse Peak Voltage
$W_F$	Wire Feed Rate
$W_P$	Dielectric Pressure
$W_T$	Wire Tension



## Abbreviations

<i>AGMA</i>	American Gear Manufacturers Association
<i>AMP</i>	Advanced Machining Processes
<i>ANN</i>	Artificial Neural Network
<i>ANOVA</i>	Analysis of Variance
<i>BBD</i>	Box-Behnken Design
<i>FF-BPNN</i>	Feed Forward Back Propagation Neural Network
<i>CNC</i>	Computer Numeral Control
<i>DFA</i>	Desirability Function Analysis
<i>DIN</i>	Deutsches Institut für Normung (German Institute for Standardization)
<i>DOE</i>	Design of Experiments
<i>DOF</i>	Degree of Freedom
<i>FE-SEM</i>	Field Emission Scanning Electron Microscope
<i>RCGA</i>	Real-Coded Genetic Algorithm
<i>HV</i>	Vicker's Hardness Number
<i>LHF</i>	Left Hand Flank
<i>MBG</i>	Meso-Bevel Gear
<i>MHG</i>	Meso-Helical Gear
<i>MRR</i>	Material Removal Rate
<i>MSG</i>	Meso-Spur Gear
<i>RHF</i>	Right Hand Flank
<i>RSM</i>	Response Surface Methodology
<i>SEM</i>	Spark Erosion Machining
<i>SS</i>	Sum of Square
<i>SS 304</i>	Stainless Steel 300 Series (Grade 304)
<i>SST</i>	Total Sum of Square
<i>VGCR</i>	Volumetric Gear Cutting Rate
<i>WSEM</i>	Wire Spark Erosion Machining



# Chapter 1

## Introduction

Gear is a modified form of a wheel having teeth uniformly placed around its circumference. It is one of most important and widely used mechanical element to transmit power and/or motion from one shaft to another through successive engagement of teeth without slipping i.e. positive drive (Townsend, 2011). Noiseless, accurate and efficient transmission of motion and/or power transmission, higher torque transfer capability, better operating performance without wear and tear, and longer service life are basis requirements of a gear. These can be fulfilled if a gear has accurate dimension and form, better surface finish, and wear resistance at its tooth flank surfaces. Various types of gears are used in different industrial, commercial, domestic, scientific, entertainment, and other applications. Figure 1.1 depicts different types of gears. Table 1.1 presents different classifications of the gears according to different criteria.



**Fig. 1.1:** Different types of gears.

**Table 1.1:** Classification of gears according to different criteria (Townsend, 2011; Radzevich, 2012; Davis, 2005; Bralla, 1998).

Criteria of classification	Type of gears
According to the position of axes of the shafts	<ul style="list-style-type: none"> <li>• Parallel shaft <ul style="list-style-type: none"> <li>✓ Spur gear</li> <li>✓ Helical gear</li> </ul> </li> </ul>
	<ul style="list-style-type: none"> <li>• Intersecting shaft <ul style="list-style-type: none"> <li>✓ Miter gear</li> <li>✓ Straight bevel gear</li> <li>✓ Spiral bevel gear</li> </ul> </li> </ul>
	<ul style="list-style-type: none"> <li>• Non-parallel and non-intersecting shafts <ul style="list-style-type: none"> <li>✓ Worm and worm wheel</li> <li>✓ Screw gear</li> </ul> </li> </ul>
According to the peripheral velocity of gears	<ul style="list-style-type: none"> <li>• Low velocity (&lt; 3 m/s)</li> <li>• Medium velocity (3 to 15 m/s)</li> <li>• High velocity (&gt; 15 m/s)</li> </ul>
According to the type of gearing	<ul style="list-style-type: none"> <li>• External gearing</li> <li>• Internal gearing</li> <li>• Rack and Pinion</li> </ul>
According to the position of the shaft on gear surface	<ul style="list-style-type: none"> <li>• Straight</li> <li>• Inclined</li> <li>• Curved</li> </ul>
According to the form of tooth profile	<ul style="list-style-type: none"> <li>• Standard gear</li> <li>• Profile shifted gear <ul style="list-style-type: none"> <li>(a) Positive profile shifted gear</li> <li>(b) Negative profile shifted gear</li> </ul> </li> </ul>
According to gear teeth	<ul style="list-style-type: none"> <li>• Straight</li> <li>• Inclined</li> <li>• Curved</li> </ul>
According to profile of gear teeth	<ul style="list-style-type: none"> <li>• Involute</li> <li>• Non-involute</li> </ul>
According symmetry of gear blank	<ul style="list-style-type: none"> <li>• Circular gear</li> <li>• Non-circular gear</li> </ul>
According to pressure angle	<ul style="list-style-type: none"> <li>• Constant pressure angle</li> <li>• Variable pressure angle i.e. asymmetric gears</li> </ul>
According to the function	<ul style="list-style-type: none"> <li>• Motion transfer gear</li> <li>• Power transfer gear</li> <li>• Precision gear (<i>used in scientific instruments</i>)</li> </ul>
According to outside diameter	<ul style="list-style-type: none"> <li>• Micro-gear (0.1-1 mm)</li> <li>• Meso-gear (1-10 mm)</li> <li>• Macro-gear (&gt;10 mm)</li> </ul>

## 1.1 Introduction to Meso-Gears

Though there is no universally adopted standard for classifying gears according of their size. But, generally gears are classified into three categories namely according to their size i.e. micro-gears, meso-gears and macro-gears. Gears having addendum or tip diameter (in case of external gears) or root circle diameter (in case of internal gear) or crown circle diameter (in case of bevel gears) up to 1 mm are known as *micro-gears*, those having more than 1 mm and up to 10 mm are called *meso-gears*, and those having more than 10 mm are refereed as *macro-gears*. Meso-gears are fine-pitched gears and primarily used for very high speed (up to 50,000 rpm) and low torque applications (Jain and Gupta, 2016; Hsu, 2008, Qin, 2010).

Miniaturization of products, equipment and devices has become an essential requirement globally due to increasing costs of the materials and manufacturing processes and emphasis on making the products smaller, lightweight, and compact. Different types of meso-gears such as meso-spur gear (MSG), meso-helical gear (MHG), and meso-bevel gear (MBG) are primarily used for the purpose of actuation, positioning, and motion transmission at very high speed in the miniaturized products, equipment and devices, and micro electro-mechanical systems (MEMS). MSG and MHG are used between the two parallel shafts and MBG between two intersecting shafts. The functional characteristics and operating performance of MEMS, microsystems, micro-products and micro-devices mainly depend on the overall quality of the meso-gears used by them. Consequently, minimum running noise, accurate motion transfer, high wear and fatigue resistance on flank surface, and longer service life are the desirable characteristics for these gears (Jain and Chaubey, 2016; Gupta and Jain, 2014a).

## 1.2 Materials for Meso-Gears

Material of the meso-gears should have higher yield and fatigue strength, higher resistance to friction, wear and corrosion, better manufacturability (i.e. machinability, formability, and liquidity), less cost and easier availability. Selection of material for meso-gears mainly depends on their application, material characteristics, strength, cost, type of gear and manufacturing process (Bell, 1971; Davis, 2005; Townsend, 2011; Radzevich, 2012). Different materials used for manufacturing the meso-gears can be broadly classified as non-metallic and metallic materials. Non-metallic gear materials mainly include different types of plastics, mostly used for *smooth* and *silent* operation at *high speed* and *no-load* applications. Metallic materials are further classified as ferrous and

non-ferrous materials. Ferrous materials are used for *low speed* and *high load* applications whereas non-ferrous materials are preferred for *high speed* and *no-load* to *low-load* applications. Figure 1.2 shows classification of the different materials used in manufacturing of the meso-gears while Table 1.2 presents their characteristics, features, and specific applications.

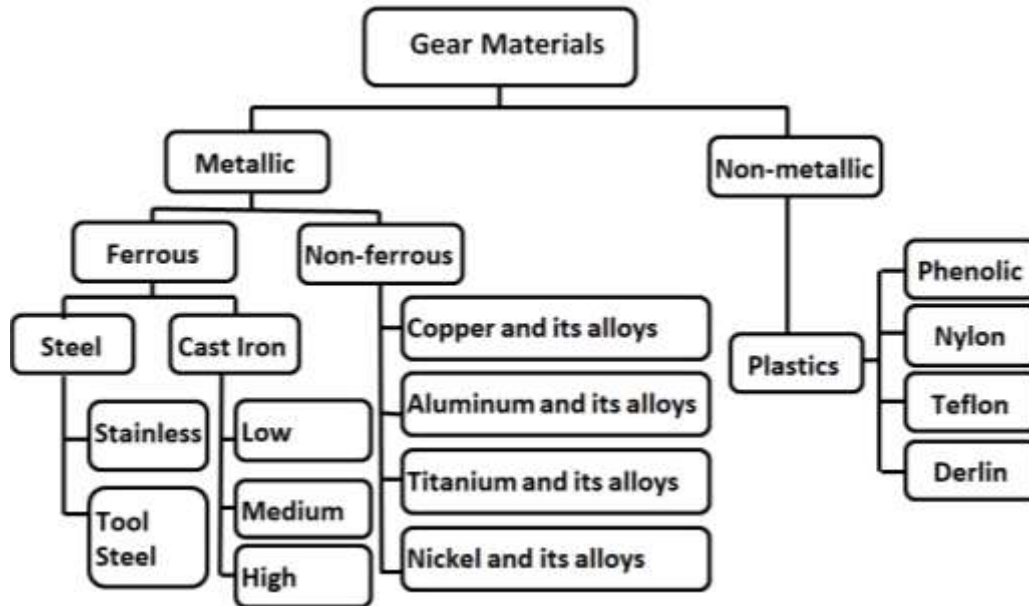


**Fig. 1.2:** Different types of materials used for meso-gears (Jain and Chaubey, 2016).

**Table 1.2:** Summary of different meso-gear materials, their characteristics, features and applications (Radzevich, 2012; Jain and Chaubey, 2016).

Material type	Characteristics	Features and applications
<b>(A1) Ferrous materials</b>		
Cast irons	Low cost, good machinability, high internal damping	For large-sized gears, moderate power rating, for commercial applications
Cast steels	Low cost, high strength	For power gears, medium power rating, for commercial applications
Plain-carbon steels	Good machinability, heat treatable	For power gears, medium power rating, for commercial to medium precision applications
Alloy steels	Very high strength, heat treatable, durability	For very high power requirement, For precision and high precision applications
Stainless steel (300 series)	High corrosion resistance, non-magnetic, non-hardenable	Low power rating, for precision applications
Stainless steel (400 series)	Moderate corrosion resistance, magnetic, hardenable,	Low to medium power rating, for high precision applications
<b>(A2) Non-ferrous materials</b>		
Aluminum alloys	Light weight, non-corrosive, excellent machinability	For extremely light-duty instrument gears, for high precision applications
Brass alloys	Low cost, non-corrosive, excellent machinability	For low-cost commercial equipment, for medium precision applications
Bronze alloys	Excellent machinability, low friction, good compatibility with steel gears	Mating gears for steel power gears, for high precision applications

Magnesium alloys	Extreme light weight, poor corrosion resistance	For low load applications, for medium precision applications
Nickel alloys	Low thermal expansion coefficient, poor machinability	For special thermal applications, for commercial applications
Titanium alloys	Higher strength to weight ratio, corrosion resistant	For lightweight strength applications, for medium precision applications
Die-Cast alloys	Low cost, low precision, low strength	Higher production rate, low quality, for low-grade commercial applications
Sintered powdered alloys	Low cost, low quality, moderate strength	Higher production rate, low quality, for commercial applications
<b>(B) Non-metallic materials</b>		
Delrin	Wear resistant, longer life, low water absorption	Less noise, low loads, for commercial applications
Phenolic laminates	Quiet operation, highest strength plastic	Medium loads, for commercial applications
Nylons	Low friction, less noise, no lubricant	Longer life, for low load commercial applications
Teflon	Low friction, no lubricant	For low friction commercial applications

### 1.3 Advantages and Applications of Meso-Gears

Meso-gears offer many worth-mentioning advantages such as compactness due to smaller size, lightweight, higher dimensional accuracy, zero backlash, lower energy consumption, efficient transmission, superior operating performance and ability to perform under extreme environmental conditions. Their typical applications include meso-sized gearboxes, pumps and motors, actuating devices, scientific instruments, precision tools, smart watches, digital camera, tail and main rotors of the meso-sized unmanned aerial vehicles (UAV), medical and dental instruments, precision instruments, prototype models, and domestic appliances (Gupta and Jain, 2014b). Figure 1.3 depicts some typical applications of different types of the meso-gears.

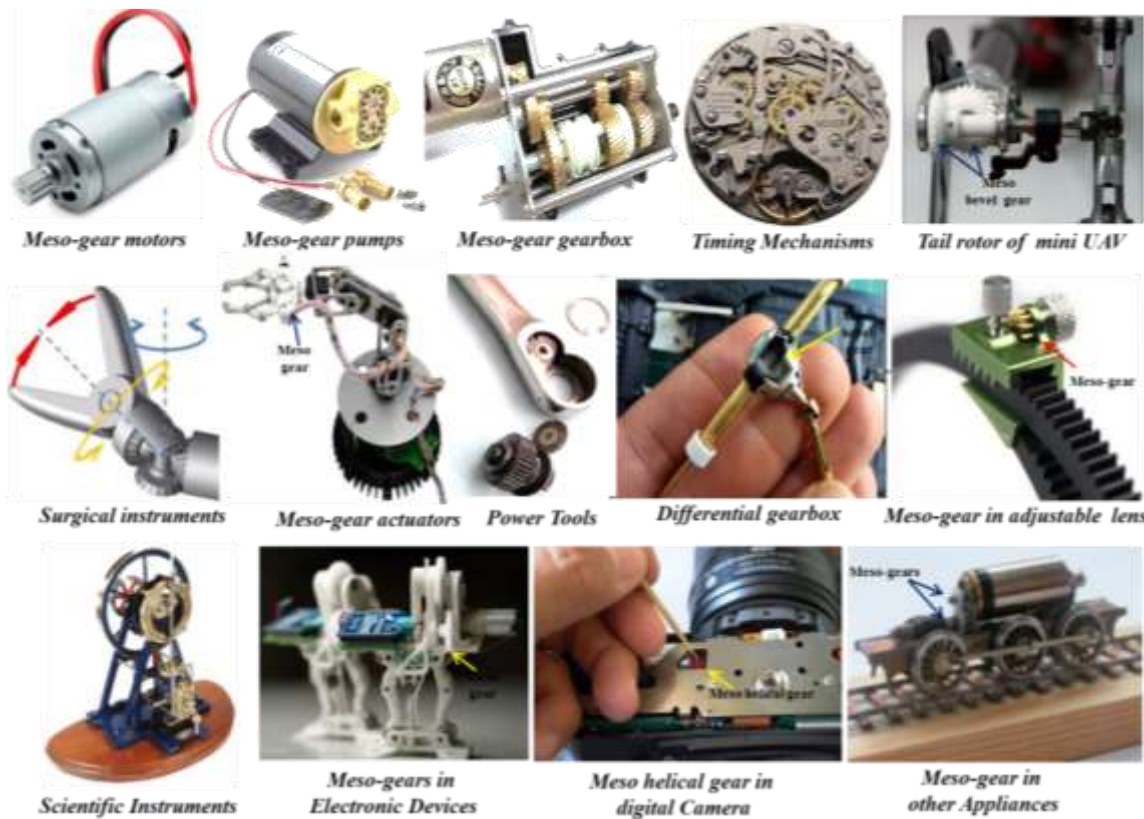


**Fig. 1.3:** Typical applications of different types of meso-gears (Chaubey and Jain, 2018).

## 1.4 Manufacturing of Meso-Gears

Since, meso-gears are key elements of the actuating and transmitting devices widely used in the MEMS, micro-systems, and micro-products therefore, their tooth profile and flank surfaces should be accurate in form and burr-free to ensure their satisfactory, smooth, and noiseless operation. Quality of a gear significantly affects its performance and service life which is primarily determined by its manufacturing, finishing, and surface property enhancing processes. Therefore, manufacturing of the meso-gears should be highly precise and accurate. Table 1.3 presents different traditional, non-traditional or advanced machining processes and their micro-versions used to manufacture the micro-gears and meso-gears. Selection of a particular process mainly depends up on the type of the gear, its material and applications.

### 1.4.1 Traditional Manufacturing Processes

Traditional manufacturing processes of metallic and non-metallic micro-gears and meso-gears can be classified into three categories: (i) **subtractive processes** namely hobbing and milling; (ii) **formative processes** such as injection molding die casting, powder metallurgy, and lithography; and (iii) **deformative processes** which include extrusion, cold rolling, forging, stamping, and hot embossing. Unfortunately, these

processes suffer from certain limitations such as poor quality of the manufactured meso-gear (i.e. ranging from 9-12 in *Deutsches Institut für Normung (DIN)* standard as shown in Table 1.4), tool marks on their flank surfaces, sharp edges, burrs, poor edge definition and high geometrical and dimensional inaccuracy. This necessitates subsequent finishing process such as grinding, lapping, honing, shaving, skiving and burnishing to achieve the desired quality of the meso-gears and surface hardening, work hardening and appropriate coating processes to enhance their wear resistance, corrosion resistance, and fatigue strength (Gupta *et al.*, 2017). These manufacturing processes are briefly described in the following subsections.

**Table 1.3:** Commonly used process for manufacturing micro-gears and meso-gears (Radzevich, 2012; Gupta and Jain, 2014b; Jain and Chaubey, 2016).

Type	Mechanism	Manufacturing process
Traditional and micro manufacturing processes	Subtractive	<ul style="list-style-type: none"> <li>• Hobbing</li> <li>• Milling</li> </ul>
	Formative	<ul style="list-style-type: none"> <li>• Powder metallurgy (PM)</li> <li>• Die casting</li> <li>• Micro-metal injection molding (<math>\mu</math>-MIM)</li> <li>• Injection compression molding (ICM)</li> <li>• Micro-powder injection molding (<math>\mu</math>-PIM)</li> <li>• Lithography, electroplating, and molding (LIGA)</li> </ul>
	Deformative	<ul style="list-style-type: none"> <li>• Extrusion</li> <li>• Forging</li> <li>• Stamping</li> <li>• Hot Embossing</li> <li>• Cold rolling</li> </ul>
Non-traditional or advanced machining processes and their micro-versions	Controlled spark erosion	<ul style="list-style-type: none"> <li>• SEM and micro-SEM (<math>\mu</math>-SEM)</li> <li>• WSEM and micro-WSEM (<math>\mu</math>-WSEM)</li> </ul>
	Thermo-electric	<ul style="list-style-type: none"> <li>• Laser ablation</li> </ul>
	Mechanical erosion	<ul style="list-style-type: none"> <li>• Micro-abrasive water jet machining (<math>\mu</math>-AWJM)</li> </ul>
	Chemical ablation	<ul style="list-style-type: none"> <li>• Bio-etching</li> </ul>

**Table 1.4:** Traditional processes for manufacturing the meso-gears and the gear quality achieved by them (Davis, 2005; Brala, 1998; Gupta and Jain, 2014c).

Process	Materials	Gear quality number <i>DIN standard</i>
Hobbing	Ferrous and non-ferrous	9
Milling	Ferrous and non-ferrous	10
Powder metallurgy	Metallic and non-metallic	10
Die casting	Non-ferrous	11
Injection molding	Plastic	12
Compression molding	Plastic	12
Extrusion	Non-ferrous	12
Forging	Ferrous	10-11
Stamping	Sheet metal	10

#### **1.4.1.1 Subtractive Processes**

Subtractive processes remove the excess material from the raw stock in chip form to achieve the desired shape and size of a product. They are also referred as machining processes and can manufacture all types of gears in all sizes. Gear machining still is unsurpassed for those gears which require very high accuracy. It can be divided broadly into (i) form cutting, and (ii) generating processes. In the **gear form cutting**, the gear tooth profile is obtained by using a formed cutting tool which may be a multiple-point cutting tool as used in a *gear milling* and *gear broaching* process or a single-point cutting tool as used in *gear shaping* process. In **gear generating process**, the gear tooth profile is obtained by a tool that simulates one or more teeth of an imaginary generating gear. A relative rolling motion of the tool with the gear blank generates the gear tooth surface. This method is used in *gear hobbing*, *gear milling* and *gear shaping* processes for manufacturing cylindrical gears. Out of different gear machining processes, only *hobbing* and *milling* processes are most commonly used for manufacturing micro and meso-gears. *Hobbing* is a continuous process and faster than *milling* process but, bevel and internal gears cannot be machined by this process. Both, hobbing and milling can be used to manufacture gears made of both ferrous and non-ferrous materials and most economical for medium to high volume production.

#### **1.4.1.2 Formative Processes**

Formative processes involve deposition of the material in bulk to make the desired component in a single step using its mold. These processes are suitable for both metallic and non-metallic materials. Formative and additive or accretion type processes for manufacturing the micro and meso-gears include: powder metallurgy (P/M) process, die casting, micro-metal injection molding ( $\mu$ -MIM), injection compression molding (ICM), micro-powder injection molding ( $\mu$ -PIM), and Lithography, electroforming and molding (LIGA). *Powder metallurgy* manufactures net-shaped micro and meso-gears having porosity which requires repressing or coining after sintering. *Die casting* process has capability to manufacture any type of gears but only for light load applications. The  $\mu$ -*MIM* process manufactures precise and net shape or near net-shaped micro and meso-gears with minimum material loss but it results in shrinkage during sintering and incurs higher manufacturing time and tooling costs. The *ICM* process has capability to manufacture micro and meso-gears requiring higher dimensional accuracy but it is very slow process and causes wastage of the gear material due to overfilling. The  $\mu$ -*PIM* process can

manufacture micro-gears from different metallic materials and ceramics but it requires use of a micro-mold and vacuum before the injection and also has possibility of the feeding stock being frozen during the injection. The *LIGA* process (abbreviation of German words Lithographie, Galvanoformung, Abformung. It is combination of lithography, electroplating, and molding process) is capable of manufacturing micro-gears with high aspect ratio having superior dimensional accuracy ( $< 1 \mu\text{m}$ ) and excellent surface finish ( $< 50 \text{ nm}$ ). But, this process is very complicated and expensive due to requirement of X-ray source for X-ray LIGA or ultra-violet (UV) light source for UV-LIGA process.

#### **1.4.1.3 Deformative Processes**

The processes transform the material into the desired shape and size by plastic deformation using dies of corresponding shape and size. Deformative processes used to manufacture meso-gear include: extrusion, stamping, forging, and hot embossing. *Extrusion* process can be used to manufacture high strength micro and meso-gears having good surface finish and dense structure with clean and porosity-free edges from the non-ferrous materials only. But, it can result in surface cracking and requires some post-machining processes to attain the desired gear quality. *Stamping* process manufactures micro and meso-gears from different metallic materials with uniform dimensional accuracy at a faster rate but this process is best suited for the gears having thickness up to 3 mm only. Near net-shape or net-shape micro and meso-gears having higher load carrying capacity can be manufactured by the *forging* process. But, wear rate of forging die is higher due to requirement of high forging force. *Hot embossing* process can manufacture more dimensionally accurate micro-gears from the polymers at lower cost but at a slower rate. *Cold rolling* process can manufacture net-shape gear with higher accuracy and surface integrity but it is most suitable for external spur and helical gears only and relatively high initial setup cost.

#### **1.4.2 Advanced Machining Processes**

To overcome the limitations of the traditional processes of manufacturing meso-gears, advanced machining processes have been explored to manufacture high quality micro and meso-gears with better dimensional accuracy and surface quality. These processes also referred as non-traditional manufacturing processes which do not use any sharp cutting tool and remove the material from workpiece by various material removal mechanisms such as controlled spark erosion, thermo-electric vaporization, mechanical erosion, and chemical ablation by using thermal, electrical and chemical energy. Brittle and fragile

materials can be easily machined by these processes because there is no direct contact between tool and workpiece. Following sections briefly describe these processes.

#### ***1.4.2.1 Controlled Spark Erosion Machining***

Non-traditional machining processes using controlled sparks for material removal include *spark erosion machining (SEM)* process, and *wire spark erosion machining (WSEM)* processes and their micro versions namely  $\mu$ -*SEM* and  $\mu$ -*WSEM*. These processes have capability to manufacture high quality close to net-shape meso-gears from only electrically conductive materials of any hardness and thickness. *SEM* and  $\mu$ -*SEM* processes use a pre-manufactured tool electrode having its shape complementary to the gear to be manufactured while, *WSEM* and  $\mu$ -*WSEM* processes use a very fine wire made of electrically conductive material to manufacture different types of meso-gears and micro-gears respectively. It can achieve gear quality up to DIN standard 6-7. But, these processes are slow and the recast layer form on machined surfaces (Gupta and Jain, 2015).

#### ***1.4.2.2 Thermo-Electric Vaporization***

Thermo-electric vaporization process involves application of very intense heat in localized region which removes material from the workpiece by localized melting and vaporization. Laser ablation (LA), laser shock punching (LSP) and ion-beam machining (IBM) processes are micro and meso-gears manufacturing processes based on thermo-electric vaporization. Laser using gear manufacturing processes are costly and can be used for only thin gears made of metallic and non-metallic materials having low reflectivity. *IBM* process requires vacuum in which stream of charged atoms (ions) of inert gas are accelerated in the high voltage electric field and bombarded with high energy to the workpiece transferring their kinetic energy and dislodging (or sputtering) the surface atoms. It can manufacture the high precision meso-gears from all kind of materials.

#### ***1.4.2.3 Mechanical Erosion***

In mechanical erosion based non-traditional processes use focused stream of very high velocity jet of abrasive particles through a carrier liquid to remove the material from the workpiece by erosive action. The impact of abrasive water jet causes a tiny brittle fracture and the carrier liquid carries away the dislodged small workpiece particles. Each abrasive particle act as multipoint cutting tool and accelerate the material removal from workpiece. *Micro-abrasive water jet machining ( $\mu$ -AWJM)* process uses a jet of high velocity abrasive particles with water as their carrier coming out of a nozzle impinging on the work surface and eroding it. It can manufacture the meso-gears from both metallic and non-metallic

materials. It is a faster and cheaper process to manufacture the meso-gears but its initial investment cost is very high. The process is more suitable for brittle and fragile materials.

#### **1.4.2.4 Chemical Ablation**

Chemical ablation based processes remove materials from the selected or unmasked areas by controlled chemical action. *Photochemical machining* (PCM) is an extension of *chemical milling* (CHM) that uses a series of photographic and chemical etching techniques to manufacture components and devices for wide range of materials, especially stainless steel. *Bio-etching* process is used to manufacture the micro-parts. Working principle of bio-etching process is that certain micro-organisms in nature consume some metal ions from materials during their growth and propagation. No cutting force is developed during this process which results in accurate and precision manufacturing of micro-gears. It uses *thiobacillus ferrooxidans* (TF) for manufacturing the micro-gear. This process is most suitable for very thin gears only (Yude et al., 2009).

### **1.5 Quality Aspects of Gears**

Microgeometry, macrogeometry, surface finish, and surface integrity of a meso-gear determine its quality. Poor quality of a gear adversely affects its operating performance characteristics (i.e. load carrying capacity, power and motion transmission characteristics, transmission efficiency, noise and vibrations related characteristics, non-uniformity in gear motion or wobbling, and reliability) and aspects of service life (i.e. fatigue strength, friction and wear characteristics, corrosion resistance and parameters of the bearing area curve). Difference between the measured values of macrogeometry and microgeometry related parameters and their corresponding theoretical (or nominal) values lead to error in macrogeometry and microgeometry. Microgeometry errors of a gear are classified as form error (i.e. total profile error and total lead error) and location or position error (i.e. pitch error and radial runout). Both form error and location errors are relevant to the cylindrical gears (i.e. spur and helical gear) but only location errors are relevant to the conical gears (i.e. straight and spiral bevel gear). *Total profile error* leads to tooth-to-tooth composite error, generation of stress and noise, and premature failures of a gear. *Total lead error* affects the load carrying capacity of a gear. *Pitch error* affects the transmission characteristics and introduces noise and vibrations. Radial runout causes non-uniformity in gear motion i.e. wobbling (Moderow, 1992; Farago, 2007; Damir, 2012; Gupta and Jain, 2013a; Pathak, *et. al.*, 2016). Macrogeometry parameters of a gear include: span, tooth thickness, and outside diameter of a gear. Deviation in span and tooth thickness affect

transmission characteristics whereas deviation in outside diameter affects noise of a gear. Topography of tooth flank surfaces affects the transmission characteristics and service life of a gear. Surface roughness significantly affects the fatigue strength, service life and operating performance of a gear. Wear characteristics (i.e. coefficient of friction, frictional force and wear rate) affects tribological fitness and mechanical efficiency of a gear. Microhardness, microstructure and residual stresses are surface integrity parameters significantly affect the wear resistance, fatigue strength and mechanical efficiency of a gear. Several heat treatment processes are used to improve wear resistance and fatigue strength of a gear.

### **1.5.1 Gear Quality and its Standards**

Gear quality is determined by gear manufacturing, gear finishing, and surface treatment processes. Various international and national standards have been evolved to classify quality of a gear and indicate its suitability for different applications: Following is the list of available gear standards:

- American Gear Manufacturers Association (AGMA) standard
- Deutsches Institut für Normung or German institute for standardization (*DIN*) standard
- British standards institute (BSI) standard
- French gear standard
- Italian gear standard (UNI)
- Australian gear standard
- Japanese Industrial Standards (JIS)
- Japanese gear manufacturing association (JGMA) standard
- Indian standard specifications (ISS)
- International organization for standardization (ISO)

AGMA, DIN, JIS, and ISO are the most commonly used standards to indicate quality of a gear. DIN and BSI standards classify gear quality into 12 categories; AGMA standard into 13 categories; JIS standard into 9 categories; and ISO into 12 categories. Higher value in AGMA (Q3-Q15) standard and lower value in DIN (1-12) and JIS standard indicate better gear quality (Jain and Chaubey, 2016). Table 1.5 presents details of AGMA, DIN, JIS and ISO gear standards.

**Table 1.5:** Details of most commonly used gear standards.

Gear standard	Categories (Quality class)												
	Best						Worst						
AGMA	15	14	13	12	11	10	9	8	7	6	5	4	3
DIN	1	2	3	4	5	6	7	8	9	10	11	12	-
JIS	-	-	-	0	1	2	3	4	5	6	7	8	-
ISO	1	2	3	4	5	6	7	8	9	10	11	12	-

### 1.5.1.1 Errors in Gear Microgeometry

Figure 1.4 depicts constituents of *form errors* and *location errors* which are two components of the gear microgeometry while following paragraphs describe them. These errors are the measures of geometrical inaccuracy of a gear and their values are used to categorize quality of a gear in the adopted standard.

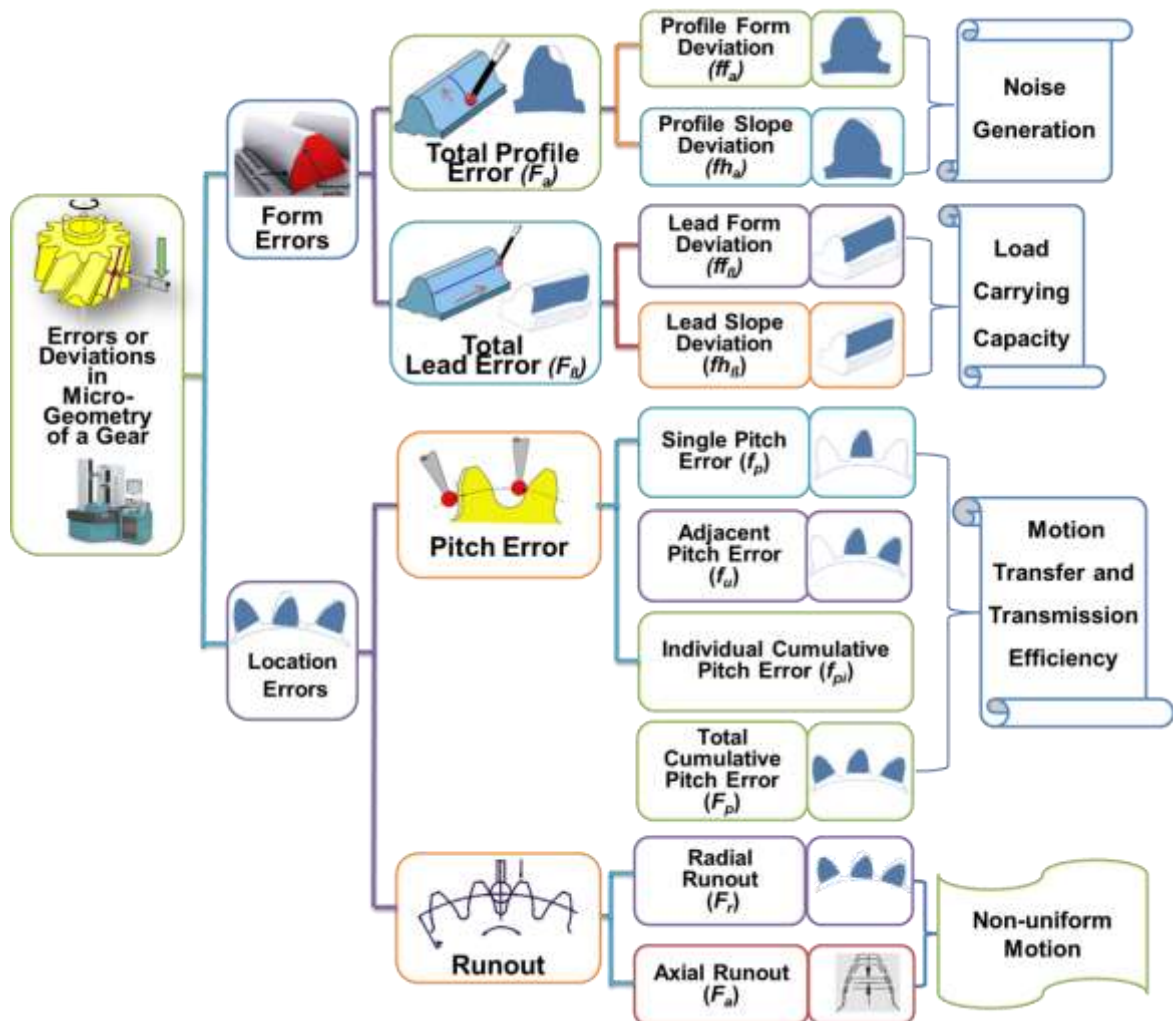


**Fig. 1.4:** Different components of microgeometry of a gear.

**(A) Form Errors:** *Form errors* indicate deviations of actual shape of gear teeth from its theoretical (or nominal) shape. *Total profile error* ' $F_a$ ' and *total lead error* ' $F_\beta$ ' are its two components.

**Total Profile Error ' $F_a$ ':** *Profile* of a gear tooth is a geometrically defined curve (i.e. involute, cycloidal, or some other curve) from start active point (SAP) to end active point (EAP). Variation in a gear tooth profile may either be positive or negative indicating presence of excess material or less material respectively at tip of the gear. *Total profile error* defines the form and location of the involute profile. It is evaluated perpendicular to the functional portion (i.e. from SAP and EAP which covers the area on the tooth flank surface between the tooth profile control diameter and the tip circle diameter) of the gear profile. It determines noise generation characteristics of a gear. It is the difference between the measured profile of a gear tooth and its corresponding theoretical profile. It has two components namely, profile form deviation and profile slope deviation. *Profile form deviation* ' $ff_a$ ' is the difference between the actual and theoretical form of gear profile. *Profile slope deviation* ' $fh_a$ ' is the difference between the actual and theoretical angle of the gear profile (ANSI/AGMA 2000-A88; Gupta and Jain, 2016).

**Total Lead Error ' $F_\beta$ ':** *Lead* is the axial advance of a gear tooth in its one revolution. Error in lead is difference between its actual and theoretical trace. It is generally measured from one end of the gear tooth to other end along face width along the pitch line. *Lead error* may either be positive or negative indicating positive and negative helix angle respectively. *Total lead error* (also known as *tooth alignment deviation* or *helix deviation*) defines the form and location of the tooth flank. It determines load carrying capacity of a gear. It is evaluated at the middle of the tooth height along the tooth width. It is the difference between the measured (or actual) and the theoretical tooth flank surface. It has two constituents namely lead form deviation and lead slope deviation. *Lead form deviation* ' $ff_\beta$ ' or *helix form deviation* the difference between the actual and theoretical lead form line. *Lead slope deviation* ' $fh_\beta$ ' or *helix angle error* is the difference between the actual and the theoretical helix angle.

**(B) Location Errors:** *Location errors* (also referred as position errors) indicate inaccuracy in positioning of the gear teeth with respect to its pitch circle. *Pitch error* (or *index error*) and *radial runout* are its two components. *Pitch* is the distance along the pitch circle between two corresponding points on flank surfaces (i.e. right or left hand side) of two

consecutive gear teeth. *Pitch error* describes the middle location of all right and left flanks with respect to each other indicating inaccurate angular positioning of the gear teeth along its pitch circle. The characteristics of pitch error are evaluated at the middle of the tooth height along the pitch circle. It has four components namely single pitch error, adjacent pitch error, individual cumulative pitch error and total cumulative pitch. *Single pitch error* ' $f_p$ ' is the maximum absolute value among all the individual single pitch deviations ' $f_{pi}$ ' i.e.  $f_p = \max |f_{pi}|$  where individual single pitch deviation ' $f_{pi}$ ' is the algebraic difference between the actual pitch and the corresponding theoretical pitch. *Adjacent or successive pitch error or pitch-to-pitch error* ' $f_u$ ' is the maximum difference between two successive single pitches measured on the specified flanks of all the teeth of a gear. It is used to identify maximum change between two adjacent pitch values. *Individual cumulative pitch error or individual index error* ' $F_{pi}$ ' is algebraic difference between the actual arc length and corresponding theoretical arc length over a sector of  $n$  number of adjacent pitches. Theoretically, it is equal to the algebraic sum of the individual single pitch deviations of  $n$  number of pitches and corresponds to displacement of any tooth flank from its theoretical position, relative to a datum tooth flank. *Total cumulative pitch error or total pitch error* ' $F_p$ ' is the largest algebraic difference between the individual cumulative pitch deviations ' $F_{pi}$ ' measured on the specified flank of all the teeth of a gear (i.e.  $F_p = \max. F_{pi} - \min. F_{pi}$ ). It can also be obtained as difference between summation of the theoretical values of pitches and summation of the actual values of the pitches over all the teeth of a gear. *Runout* results from eccentricities in both the manufacturing and the assembly of the gears. It has two components namely *radial runout* ' $F_r$ ' and *axial runout* ' $F_{ax}$ ' and it causes non-uniformity in gear motion. *Radial runout* is most common form of runout that occurs in a gear. It describes the radial location of all teeth with respect to the pitch circle and is evaluated at the middle of the tooth height along the pitch circle (Houser, 2009; AGMA/ANSI2009-B01). It is the maximum difference between the actual radial positions of all gear teeth measured with respect to their theoretical (or nominal) radial positions. *Axial runout* indicates total variation of the gear teeth along its axis in the direction of the face width. It is measured from a reference plane perpendicular to its axis. It is always accompanied by lead variation which causes noise, excessive stress and bending stress in mating gears (Moderow, 1992).

### 1.5.1.2 Errors in Gear Macrogeometry

Microgeometry parameters of a gear (namely span, chordal tooth thickness, and outside diameter) as depicted in Fig. 1.5 can be measured manually or using CNC gear metrology machine. Span ‘W’ of a gear is the distance over a number of teeth ‘k’ along a line tangent to the base circle. Generally, it is measured from the middle of the tooth profile and flank surface (Zhao *et al.*, 2018). The measured value is the sum of normal tooth thickness on the base circle and normal pitch (k-1). For external gears, the measurement is conducted on the outside of the teeth and for internal gears, the measurement is done between the inside of the tooth profiles. *Span deviation* ‘ $W_k$ ’ is the difference between its theoretical value and actual measured value. *Chordal tooth thickness* is the thickness of a gear tooth measured along a chord of the pitch circle as shown in Fig. 1.5. Deviation in chordal tooth thickness is the difference between its actually measured and theoretical values. *Outside diameter* ‘D’ is the maximum distance between two diametrically opposite tooth spaces of a gear. It can be measured by inserting two balls ( $M_{dk}$ ) or two pins ( $M_{dp}$ ) of appropriate size in the diametrically opposite tooth spaces as shown in Fig. 1.5. Deviation in outside diameter is the difference between its actual and theoretical values.

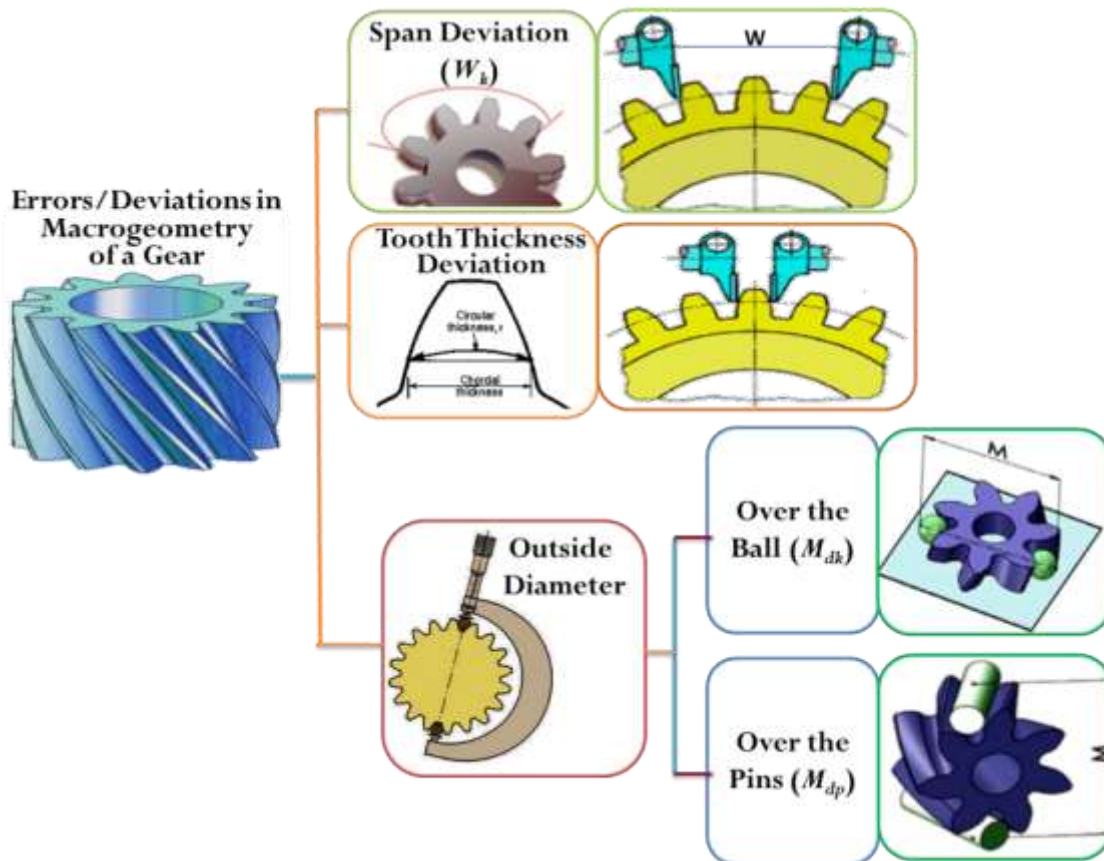


Fig. 1.5: Macrogeometry parameters of a gear.

## 1.5.2 Surface Quality of Gears

Surface quality is a term which comprises surface topography, surface finish and wear characteristic which significantly affect the operating performance, noise generation, tribological behavior, mechanical efficiency and service life of a gear. Following paragraphs describes these parameters in detail.

### 1.5.2.1 Flank Surface Topography

Flank topography is a 3D graphical representation depicting combined effect of the errors in profile and lead by showing differences between actual and theoretical flank surfaces in the form of peaks and valleys (Gupta and Jain, 2014b). It indicates the presence of nicks, burr, peaks and valley on actual flank surface of a gear tooth which can help in understanding the wear thus service life of a gear. Actual flank surface of a gear is divided into a 3D-grid by dividing the entire face width along its profile in certain number of discrete points on which measurements are taken. Then the measured points are joined with straight lines along the lead and profile directions (Goch, 2003; Pathak et al., 2016). The actual and theoretical flank surfaces are represented by different colour, while amount of deviation between the actual and theoretical flank surfaces are represented by small vertical line at each grid point. Fig. 1.6 depicts topography of the left and right hand flanks of a gear.

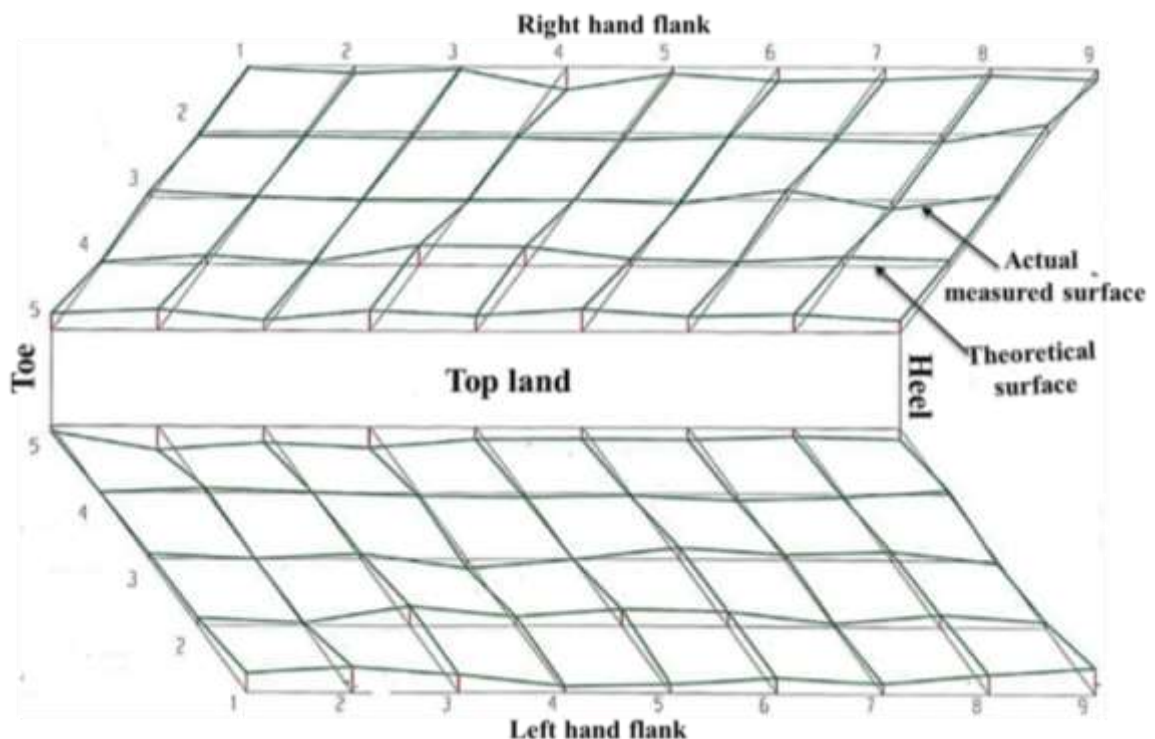


**Fig. 1.6:** Graphical representation of tooth flank surface topography.

### 1.5.2.2 Surface Roughness

Surface texture of manufactured part is the repetitive or random deviations from the nominal surface which form the 3D surface topography. It includes the small spatial deviations of a surface from the perfectly flat ideal surface. It has four components namely surface roughness, waviness, lay, and flaws. Surface roughness consists of fine irregularities having short-wavelength and high-frequency, which generally results from inherent action of a manufacturing process. It significantly affects fatigue strength, service life, and operating performance of a gear. Parameters related to surface roughness are generally classified into following categories: amplitude parameters (i.e. average surface roughness ' $R_a$ ', maximum surface roughness ' $R_{max}$ ', ten-point height ' $R_t$ ', root mean square ' $R_q$ ', skewness ' $R_{sk}$ ' and kurtosis ' $R_{ku}$ '), spacing parameters (i.e. mean spacing of profile elements ' $R_{sm}$ '), hybrid parameters (i.e. root mean square slope ' $R_{dq}$ ', peak count number ' $R_{pc}$ ') and functional parameters (i.e. material ratio ' $R_{mr}$ ') (Davim 2010, Griffith, 2001). Surface roughness parameters can be measured by 2D or 3D surface roughness tester. Recently, 3D roughness tester is being mostly preferred because it provides complete information of the measured surface including surface topography, parameters of Abbott-Firestone or bearing area curve and 2D profile along with values of different parameters of surface roughness. The present research used only amplitude parameters (average and maximum surface roughness) of flank surface of the meso bevel gear (MBG) and meso helical gear (MHG).

**Average surface roughness ' $R_a$ '** (Fig. 1.7) is also known as centerline average (CLA) or arithmetic mean deviation of the surface profile. It is the most commonly used roughness parameter for evaluation of surface finish. It is arithmetic average of the absolute values of the roughness profile ordinates from mean within the evaluation length which generally consists of five consecutive sampling lengths. It can be evaluated by following equation:

$$R_a = \frac{1}{l_s} \int_0^{l_s} |Z(x)| dx \quad (1.1)$$

**Maximum surface roughness ( $R_{max}$ )** is the largest single roughness depth (i.e. maximum peak to valley height) within the evaluation length (Fig. 1.7).

**Skewness ' $R_{sk}$ '** is asymmetry of the height distribution within the sampling length. It is an important parameter because it gives information about morphology of the surface texture. Its positive value indicates distribution of higher peaks on the flank surface and its

negative value means that tooth flank surface of a gear has good bearing strength and has pores which are very good for lubrication purposes.

**Kurtosis** ' $R_{su}$ ' is a measure of the sharpness of the height distribution within the sampling length and its value above 3 indicates good bearing strength of tooth flank surface of a gear.

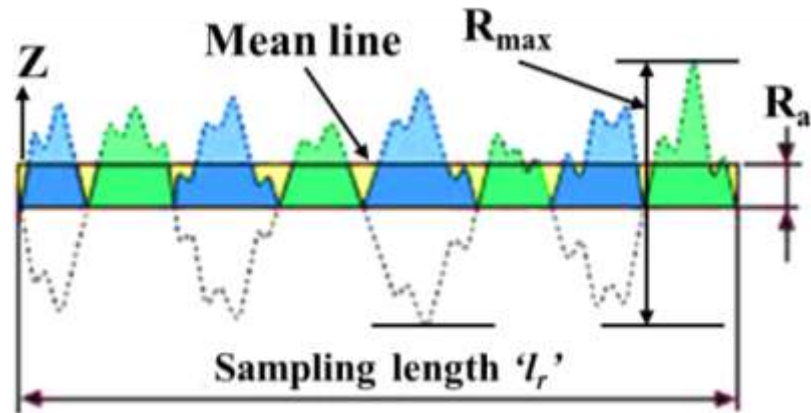


**Fig. 1.7:** Representation of surface roughness parameters.

### 1.5.2.3 Wear Characteristics

Wear is a surface phenomenon which describes gradual and non-uniform loss of the materials from the mating surfaces having relative motion thus significantly altering their dimensions. Wear of a gear generally occurs on its flank surfaces. Material loss from the gear flank surfaces increases backlash between the mating gears which cause transmission error, noise and vibrations and affect their service life, tribological fitness and mechanical efficiency. Moreover, the removed material (known as wear debris) may be adhere to the flank surface thus acting as surface contaminates which further increase the wear rate. Wear characteristics are evaluated in terms of coefficient of sliding friction, frictional force and wear rate. Lower values of coefficient of sliding friction of meshing gears increase their mechanical efficiency which can be achieved up to 99.5 % if value of coefficient of sliding friction is less than 0.05 (Moldovean *et al.*, 2011).

### 1.5.3 Surface Integrity Aspects of Gears

Surface integrity significant influences the performance of the engineered components that are heavily stressed, dynamically loaded, and operates in the severe environment. It is the description and control of many possible metallurgical and other alterations produced by the manufacturing, finishing and heat treatment processes generally below 0.5 mm of the manufactured surface including their effects on the material properties and the performance of the surface during the service. The alterations can be caused due to mechanical, metallurgical, thermal, chemical, electrical sources and they can affect both

physical and metallurgical properties of the material. They broadly depend upon the manufacturing process parameters such as variables, workpiece, cutting tool, machine tool, and the environmental conditions. These parameters can significantly affect the surface integrity of the manufactured surfaces due to (i) plastic deformation in the workpiece (residual stresses) and mechanical strain; (ii) involvement of high temperatures and temperature gradient; (iii) chemical reactions and absorption by the nascent machined surface; (iv) excessive electrical currents; (v) excessive energy densities during manufacturing. Fatigue strength, wear and corrosion resistance, and stress concentration is sensitive to surface integrity of a component. Formation of recast layer, cracks, pits, tears, heat affected zone, oxidation, recrystallization, mechanical and thermal stresses, grain growth, burr, asperities and nicks are surface defects cause premature failures of the manufactured parts. These surface defects can be minimize by selecting appropriate manufacturing processes and materials.

Surface integrity of flank surface of a gear significantly affects its operating performance, service life, wear and fatigue resistance. Microhardness, microstructure, and residual stresses are there parameters mostly used to evaluate the surface integrity of flank surface of a gear. Microhardness and microstructure affect the load carrying capably and wear resistance while residual stresses affect the fatigue strength of a gear. They are describes in the following paragraphs:

#### ***1.5.3.1 Microhardness***

Microhardness refers to the hardness determined applying very small load on the surface thus creating negligible indentation on the surface of a manufactured part. A microhardness test can measure hardness from surface to the core on a heat treated as well as manufactured parts. Microhardness studies of a gear helps in determining changes in flank surface hardness after and before manufacturing, finishing and heat treatment processes. It also helps to identifying the effect of recast layer and heat affected zone (HAZ) on the hardness of flank surfaces of a gear and in determining the thickness of recast layer. Knoop and Vickers hardness test are most commonly used microhardness measuring methods.

#### ***1.5.3.2 Microstructure***

Microstructure is micro-level structure of the prepared sample of a manufactured part which is revealed by scanning electron microscopy (SEM) or optical microscopy using magnification above 25x. Microstructure of any material significantly affects its hardness, toughness, ductility, strength, wear and corrosion resistance. These properties govern the

selection of a material for different applications. Microstructure analysis of manufactured surface helps to identify the changes in its microstructure caused by its manufacturing. Formation of recast layer, heat affected zone, and craters, surface defects (i.e. cracks, built-up edge, burr, and tool marks), plastic deformation, grain structure, grain size, and phase transformation are responsible for microstructural changes in a manufactured part.

### ***1.5.3.3 Residual Stresses***

Residual stresses depict internal stress distribution within a material in the absence of external loading. It may be compressive or tensile. Almost all manufacturing processes introduce residual stresses to a manufactured part. Fatigue failure is a common phenomenon of a gear because it is subjected to varying load. Improper gear design, gear tooth meshing, shaft alignment and selection of gear material can cause early failure of a gear. Fatigue strength and fatigue life of flank surface of a gear can be improved by inducing compressive residual stress using laser shock peening or laser punching process. This improves the load carrying capacity of a gear. Also, bending strength of gear teeth depends on hardness and compressive strength at the root of a gear (Totten *et al.*, 2002). X-ray diffraction, ultrasonic, magnetic and electronic speckle pattern interferometry method are known methods to determine the residual stresses but X-ray diffraction (XRD) analysis is the widely used method for determining residual stresses for a manufactured part.

## **1.6 Use of WSEM for Meso-Gear Manufacturing**

Sustained focus on continuous development, advancement, and automation of the non-traditional or advanced machining processes (AMP) have established them as superior processes by overcoming the limitations (as mentioned in section 1.4.1) of the traditional process. This has enabled AMP to manufacture high quality complex geometries, intricate shapes and features, micro and meso-gears, delicate parts from all kinds of materials irrespective of their hardness, brittleness and toughness. Wire spark erosion machining (WSEM) process is one of most commonly used AMP to achieve better surface finish, dimensional accuracy and quality. It offers following advantages for manufacturing high quality meso-gears.

- Ability to manufacture near net-shape meso-gears from all the electrically conductive materials of any hardness.
- Ability to manufacture meso-sized external and internal cylindrical gears, conical gears, non-circular gears, ratchet gears and splines.

- Ability to manufacture meso-gears from very thin sheet to thick plate.
- Capability to restore the worn profile and modify the flank surfaces of a gear tooth.
- Ability to produce smooth and crack-free flank surfaces without sharp edges.
- Better dimensional accuracy and surface finish.
- No mechanical stresses on flank surfaces of the meso-gears.
- Accurate and burr-free gear tooth profile and high wear resistance on flank surfaces.
- Minimum material loss during meso-gear manufacturing.
- Formation of very small craters on flank surfaces which help in oil retention and better lubrication results in minimizing the friction and wear which enhance its service life.
- Higher productivity due to lesser setup, lead time and minimum inspection because different types and sizes of meso-gears can be manufactured using the same gear plate and cutting tool i.e. brass wire.
- Less idle time due to absence of special tooling requirements.
- Easy to automate and excellent repeatability.
- Requires very little attention during manufacturing of meso-gears.

Following paragraphs describe details of WSEM process.

## **1.7 Introduction to WSEM Process**

English scientist Sir Joseph Priestly discovered the phenomenon of material removal by electrical sparks in 1768. But, this could not be used for controlled material removal purpose till 1943 when two Russians scientists B.R. Lazarenko and N.I. Lazarenko developed a circuit to supply pulse power required for material removal by the controlled spark-erosion phenomenon. WSEM is the derived process of spark erosion machining (SEM) process using very thin wire as cutting tool electrode. First WSEM machine with the limited features (i.e. limited manufacturing capabilities, extremely slow, and suitable for brass and copper wires only) was introduced by SWISS company 'AGIE' in 1969 which brought the significant evolution in manufacturing industries. Manufacturing capabilities of WSEM process have been improved significantly since then fulfilling the demands of modern manufacturing industries. Nowadays, most of the WSEM machines are computer numerically controlled (CNC) and equipped with features of machining the inclined surfaces which helps in machining complex parts and improving the efficiency, accuracy, repeatability and productivity. It has enabled this process to provide the best alternative or only alternative to manufacture those complex shapes, intricate profiles and delicate parts from the electrically conductive materials for aerospace, automotive,

healthcare, defence and tool and die making industries (speeding and Wang, 1997; Ho *et al.*, 2004) which are difficult to manufacture by other processes.

### **1.7.1 Working Principle**

SEM, WSEM and their hybrid and derived processes are thermal type AMP in which mechanism of material removal is melting and vaporization. WSEM process removes the materials from workpiece by occurrence of series of discrete spark between the cathodic thin wire and anodic workpiece in the presence of a dielectric having low break down voltage. Basic function of the dielectric is to flush away the eroded particles from the inter-electrode gap (IEG) and to avoid formation of the recast layer on the machined parts. Generally, deionized water is used as dielectric in WSEM process due to its lower dielectric strength and viscosity, higher cooling rate and material removal rate (MRR), and absence of fire hazard. Figure 1.8 shows the schematic diagram of the working principle of WSEM process. WSEM machine consist of a worktable (called as X-Y table) for holding the workpiece, an auxiliary table (called as U-V), wire feed system, dielectric supply system and pulsed DC power supply system. The workpiece is mounted and clamped on the main worktable by means of clamps. Cutting is performed by pulsed servomotor controlled and CNC programed movement of main worktable along X and Y axes. U and V axes are used for machining the tapered surfaces which is achieved by keeping fixed the lower wire guide and moving the upper wire guide in X, and Y directions with the help of pulsed servomotors. Brass, copper, molybdenum, tungsten and coated wire having diameter in the range from 100 to 300  $\mu\text{m}$  is continuously fed from the wire spool via workpiece. The used wire is collected by take-off spool. Wire is kept under certain tension by means of upper and lower guides which are placed above and below the workpiece respectively. The deionized or distilled water is supplied as dielectric through the sapphire nozzle attached to the upper and lower guides to supply it concentric with the wire to continuously flush the eroded particles from the machining zone. Its conductivity is maintained by applying resin in the dielectric supply system. A very small value (about 0.025 mm) of inter-electrode gap (IEG) is maintained between the wire and the workpiece by means of the servo-mechanism.

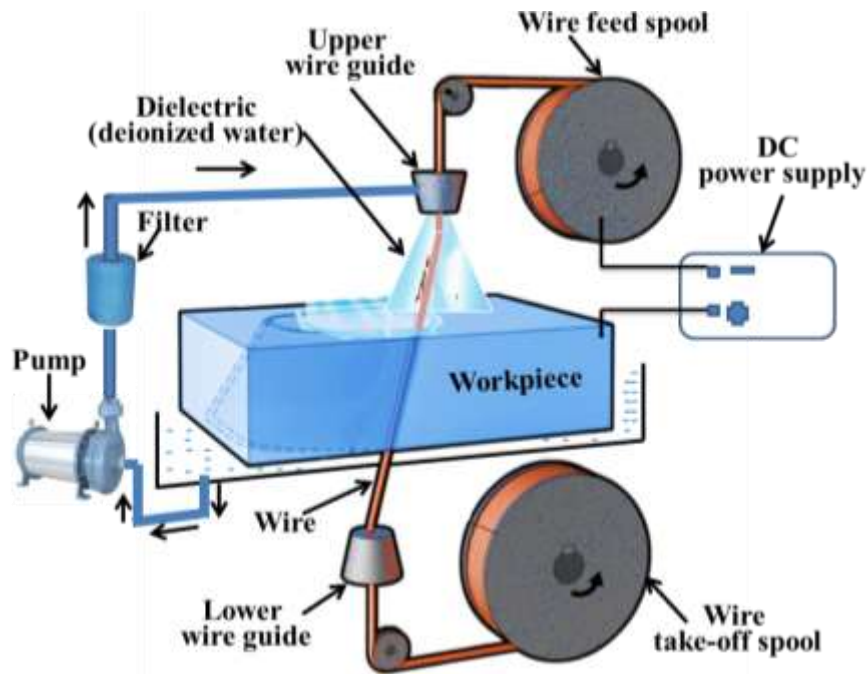


**Fig. 1.8:** Schematic diagram showing working principle of WSEM process.

### 1.7.2 Mechanism of Material Removal

Spark generation in WSEM process takes place in following three phases namely preparation phase, discharge phase and interval phase (as depicted in Fig. 1.9): (i) **Preparation phase:** when pulsed DC voltage is applied between the wire and workpiece, an intense electrical field is developed at point of minimum IEG. The microscopic contaminants suspended in the dielectric are attracted towards this electric field and accumulated where electric field has maximum value. This forms a highly conductive bridge in the IEG, (ii) **Discharge phase:** Wire and the conductive bridge get heated continuously as the applied voltage increases and some portion of the conductive bridge is ionized to initiate formation of spark channel in the IEG. Both temperature and pressure continue to increase rapidly leading to generation of sparks in the IEG for very short duration. Transformation of the kinetic energy of electrons into heat takes place which is concentrated over extremely small area causing very high energy density. This is enough to increase the instantaneous local temperature to a very high value (about 8000 to 12000 °C) which is beyond melting point of the workpiece material thus eroding a very small amount of material locally from both the workpiece and wire by melting and vaporization, (iii) **Interval phase or pulse-off duration:** no sparking and heating take place during this phase resulting in collapse of the spark channels. Continuously supplied deionized water flushes away the eroded particles (also known as debris) from the IEG leaving a very

small crater on the machined surface. Same sequence of events is repeated till the required geometry is manufactured in the workpiece (Schumacher, 2004).

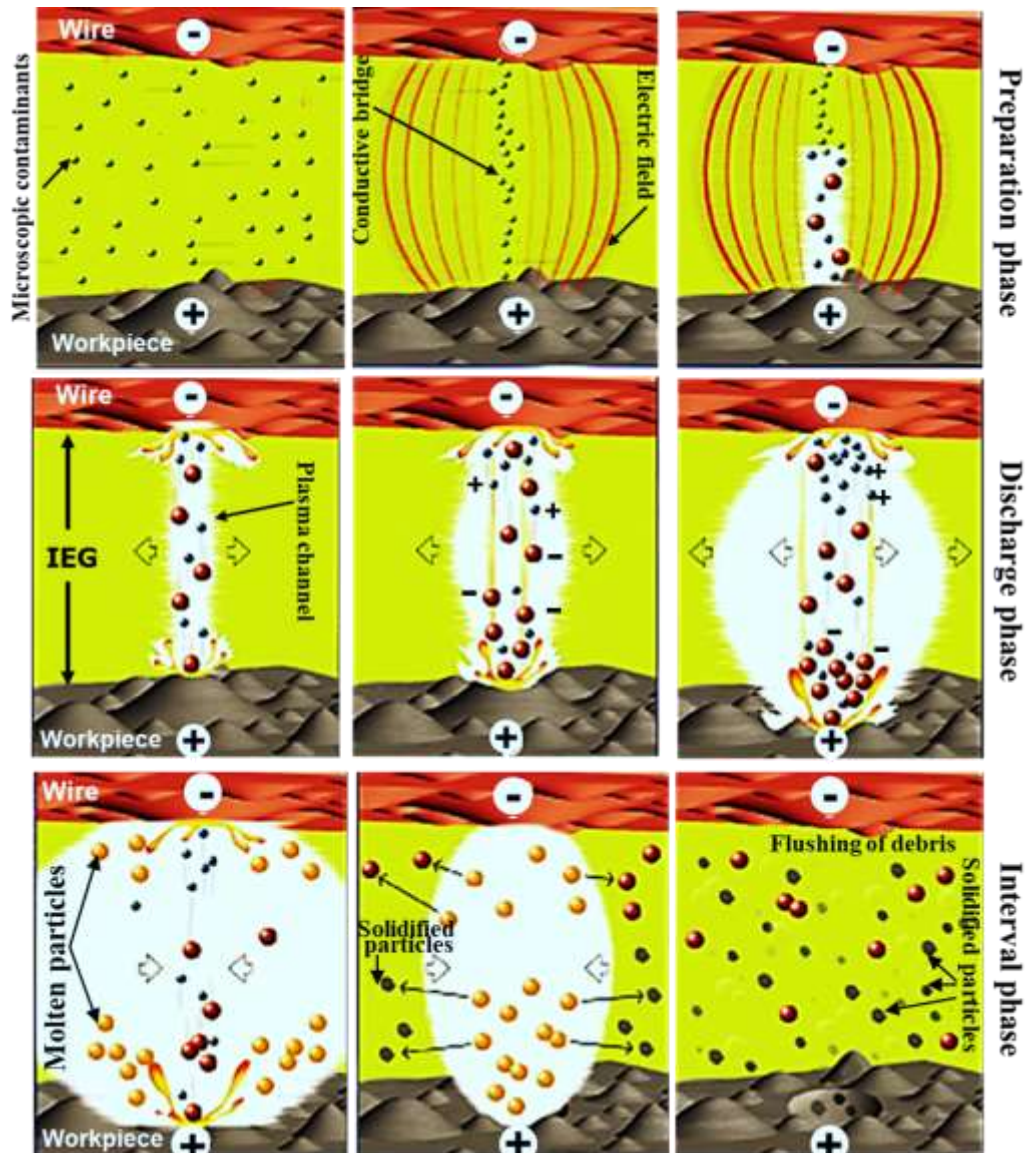


Fig. 1.9: Different phases and concepts of spark generation in WSEM process.

### 1.7.3 Process Parameters

Manufacturing components in a desired shape, size with better surface finish significantly depends on the proper selection of WSEM process parameters which can be classified into following two groups:

(i) **Electrical Parameters:** These parameters can be explained with the help of Fig. 1.10

- **Pulse peak voltage ' $V_P$ ':** It is the maximum value of voltage which occurs just before the discharge of the spark. It is also referred as open gap voltage. Its higher value will increase the discharge energy per spark resulting in higher machining rate. Its lower value causes unstable machining and slower machining rate. For the WSEM machine

used in the present work, 110 volts was selected as pulse peak voltage to ensure stable machining.

- **Gap voltage ' $V_G$ '**: It is the value of the voltage when the discharge channel between the workpiece and the wire electrode is established and the dielectric in the IEG breaks down.
- **Pulse-on time ' $T_{on}$ '**: It is the time duration during which spark occurs between the wire and workpiece resulting in controlled erosion of the workpiece material. A higher value of pulse-on time causes longer duration of spark resulting in higher material removal rate (MRR), poor surface finish, wire vibration and frequent wire breakage.
- **Pulse-off time ' $T_{off}$ '**: It represents the time duration between occurrences of two consecutive sparks. The voltage is absent during this period of cycle and no power is supplied across the electrodes and de-ionization of dielectric takes place. Deionized water flushes out the eroded particles from the IEG during this period. Using lower value of pulse-off time increases the frequency of spark in the IEG for a given time which results in increasing the machining rate. But, too short pulse-off time causes frequent wire breakage and poor surface finish due to unstable machining.
- **Peak current ' $I_p$ '**: It is the maximum value of the current passing through the electrodes for the given pulse and read directly on ammeter during the machining process. Its higher values will increase the discharge energy per spark which increases the machining rate but deteriorate the surface finish.

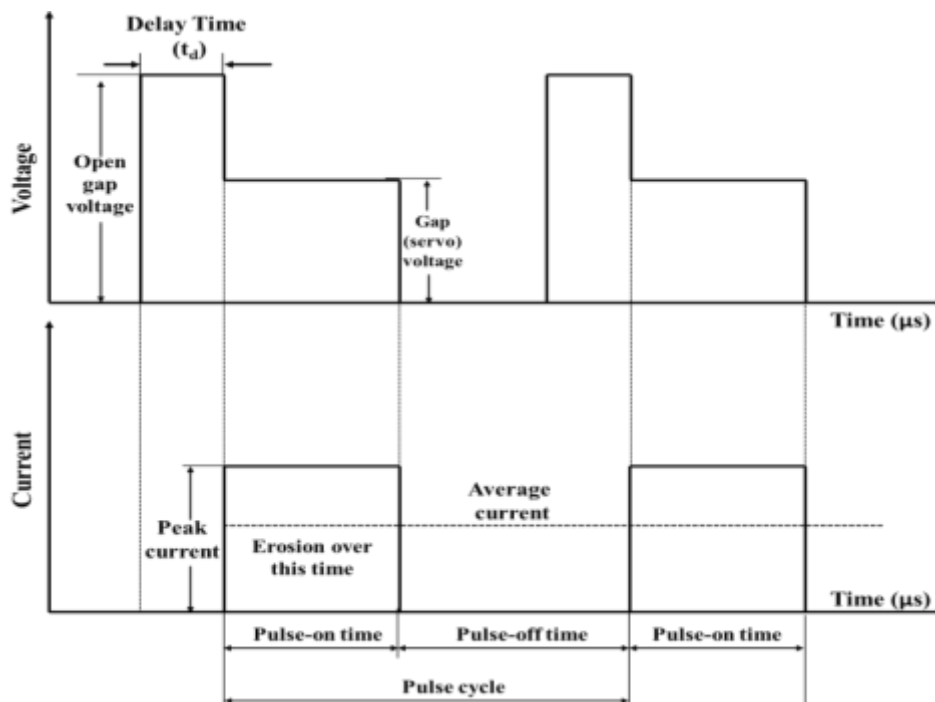


Fig: 1.10: Different electrical parameters in a spark-erosion based process.

**(ii) Non-electrical Parameters**

- **Wire feed rate ' $W_F$ '**: It is the rate at which the fresh wire travels through the wire guides and fed continuously through the IEG for sparking. It defines the continuous movement of wire per unit time (i.e. mm/min). Higher value of wire feed rate are desirable for stable machining and to avoid frequent wire breakage. Wire breakage significantly affects the machining time as well as surface finish.
- **Wire tension ' $W_T$ '**: It determines how much the wire is to be stretched between the upper and lower wire guides. It is a gram-equivalent load with which the continuously wire is fed under tension so that it remains straight and stretched between the wire guides. Higher wire tension is desirable to ensure the higher geometrical and dimension accuracy, and to avoid wire lag or wire vibrations. Wire vibrations significantly affect the dimensional accuracy of machined parts. Higher wire tension is essential for machining of thicker workpiece.
- **Dielectric flow rate ' $W_P$ '**: It is volumetric flow rate of the dielectric through IEG to flush away the eroded particles. Higher dielectric pressure is essential for machining of the thicker workpiece. However, low dielectric flow rate is used for machining of thin workpiece and trim cut. Improper selection of dielectric flow rate may cause formation of recast layer on the manufactured parts and frequent wire breakage.
- **Percentage cutting speed ' $C_S$ '**: It is primarily used to reduce the machining rate without modifying the parametric condition of WSEM process in order to avoid wire breakages during machining of the inclined surface with high inclination angle, machining of complex profile having different top and bottom profiles, and very sharp corners.

**1.7.4 Advantages and Limitations**

WSEM offers following worth-mentioning advantages:

- Performance does not depend on the mechanical properties (such as hardness, brittleness, toughness) of the workpiece material as long as the material is electrically conductive.
- Ability to achieve high degree of dimensional accuracy (up to  $\pm 7 \mu\text{m}$  and with special care  $\pm 2.5 \mu\text{m}$  over 152 mm thickness is possible) and surface finish (120 to 250 nm routinely and up to 50 nm with special care in the finishing pass).
- Requires minimum or no finishing process after WSEM.

- Ability to machine thin fragile sections and complicated shapes free from the burrs because no mechanical stresses and tool marks are introduced during machining.
- Use of generic tool in the form of wire for manufacturing any complicated geometry.
- Excellent repeatability.
- Once the setup for WSEM machine is ready and running then it can be run in unattended mode for longer period of time. Multiple workpiece setups can extend that amount of time. With WEDM the overall manufacturing time can be reduced by 37% however the attended processing time can be reduced by 66 % .

Despite several unique advantages, WSEM process suffers from following major limitations:

- Suitable for through cut of electrically conductive materials only.
- Not suitable for mass production and very large-size workpiece.
- Formation of recast layers on manufactured parts.
- Requires precision uniform wire having high tensile strength.
- Leaves marks made for initial entry of the wire in the machine part.
- Lower MRR as compared to traditional manufacturing process.
- Higher initial investment cost.

### **1.7.5 Applications**

WSEM process has become a necessity in many industries and research organization. Fig. 1.11 depicts some typical complicated parts manufactured by WSEM process. Following are its typical fields of applications:

- *Automotive industries:* Engine mountings and fuel metering valves
- *Aerospace and aircraft industries:* Turbine blades and jet engine blades
- *Healthcare industries:* Surgical and dental instruments, and ratchets
- *Tool and die making industries:* Various tools, dies, punches, fixture and gauges
- *Mechanical manufacturing industries:* Cutting tools, various shape holes, and molds
- *Electronic industries:* Slots and cavity in circuit boards and precision parts
- *Defence industries:* Complicated parts for artillery, aircraft, armored vehicles and ships
- *Other applications:* Cam wheel, precision instruments and parts of watch



**Fig. 1.11:** Some typical complicated parts manufactured by WSEM processes.

## 1.8 Organization of the Thesis

The thesis has been divided into seven chapters. Following paragraphs give the brief description of contents of each chapter:

**Chapter 2** presents the review of past work on manufacturing the micro and meso-gears by spark erosion based machining processes namely SEM, WSEM, their micro-versions ( $\mu$ -SEM and  $\mu$ -WSEM), other advanced manufacturing processes and on other aspects of WSEM manufactured process. It also presents identified research gaps and objectives of the present research work.

**Chapter 3** presents details of selection of material and specifications of MBG and MHG, planning, design and procedure of the experimental investigations for different stages namely preliminary, pilot, main and confirmation experiments. It also describes evaluation and characterization of the parameters related to microgeometry, surface roughness, microhardness, microstructure of MBG and MHG and WSEM productivity.

**Chapter 4** describes the results and discussions of different stages of experiments, their analyses and conclusions.

**Chapter 5** describes the modeling by regression analysis and artificial neural network (ANN), and optimization of WSEM process by desirability function analysis and real-coded genetic algorithm.

**Chapter 6** presents the comparative evaluation of manufacturing capabilities of WSEM with milling and hobbing processes for manufacturing MBG and MHG in terms of

microgeometry, macrogeometry, surface roughness, flank surface topography, microhardness, microstructure, manufacturing cost and time and gear material loss.

**Chapter 7** presents the significant achievements and conclusions from the present research work along with the scope for the future research.

## Chapter 2

### Review of Past Work and Research Objectives

This chapter presents review of the past research work done on manufacturing of micro and meso-gears by SEM,  $\mu$ -SEM, WSEM,  $\mu$ -WSEM, and other advanced machining processes. It also focuses on other aspects of WSEM process using different statistical and soft computing techniques. Summary of the relevant past work on micro and meso-gears manufacturing by SEM,  $\mu$ -SEM, WSEM,  $\mu$ -WSEM, other advanced machining processes and parametric optimization of WSEM are also summarized in the tabular form for easy future referencing. It also describes the identified research gaps based upon the review of past work, objectives of the present research work, and the research methodology used to achieve these objectives.

#### 2.1 Past work on Manufacturing of Micro and Meso-Gears

In last two decades considerable research works have been reported on micro and meso-spur gears manufacturing from different materials using different traditional manufacturing processes (namely hobbing, milling, die casting, extrusion, stamping, forging, metal injection molding) and as well as advanced manufacturing processes (such as micro-injection compression molding ( $\mu$ -ICM), lithography (LIGA), hot embossing). But, very little research work has been reported on manufacturing of micro and meso-gears by advanced machining processes namely SEM, WSEM, laser ablation, laser shock punching, bio-etching, micro-abrasive water jet machining ( $\mu$ -AWJM) and ion beam machining (IBM) processes. Therefore, relevant past work was critically reviewed (i) to highlight gear materials and specifications, process parameters, and responses of the relevant past works; (ii) to identify the existing research gaps; and (iii) to define directions and objectives for present research for manufacturing high quality micro-gears and meso-gears by WSEM process.

##### 2.1.1 Manufacturing of Micro and Meso-Spur Gears using Spark Erosion based Processes

Better geometrical accuracy, dimensional accuracy and surface quality, enhanced wear resistance, corrosion resistance and fatigue strength, near net-shape manufacturing, and higher gear quality of micro and meso-gears have always been the motivational factors for researchers, scientists and industrial users (Chaubey and Jain, 2016; Gupta and Jain, 2015). Researchers have found that spark erosion based processes (i.e. SEM, WSEM,  $\mu$ -SEM,  $\mu$ -WSEM and their variants) have capabilities and potential to meet these

requirements. Following paragraphs describe in detail the relevant past work done on manufacturing of micro-gears and meso-gears by these processes and other advanced machining processes. Tables 2.1–2.4 present review of the relevant past work in tabular formats for ease of concise summary and future referencing.

#### **2.1.1.1 Manufacturing of Micro-Spur Gear by SEM and $\mu$ -SEM**

Review of the past work use of SEM and  $\mu$ -SEM processes for manufacturing meso and micro-gears found following work reported in the literature which is summarized in Table 2.1 also.

**Schulz et al. (2012)** manufactured mold for 30CrMo6 micro-planetary gear having 98  $\mu\text{m}$  outside diameter and 12 teeth (as shown in Fig. 2.1) by SEM process using 100  $\mu\text{m}$  diameter external micro-spur gear made of WC-6Co as the tool. They reported that (i) at the end of 1<sup>st</sup> manufacturing step, the mold had a depth of 73  $\mu\text{m}$  against a target of 100  $\mu\text{m}$  and surface waviness as 1.5  $\mu\text{m}$ ; (ii) after the 5<sup>th</sup> manufacturing step, geometrical accuracy of the mold improved because its depth increased to 98  $\mu\text{m}$ , total surface waviness as 0.96  $\mu\text{m}$ , and maximum dimensional accuracy less than 2  $\mu\text{m}$  and; (iii) deviation at the surface of the mold occurred due to fluctuation in the SEM tool wear.

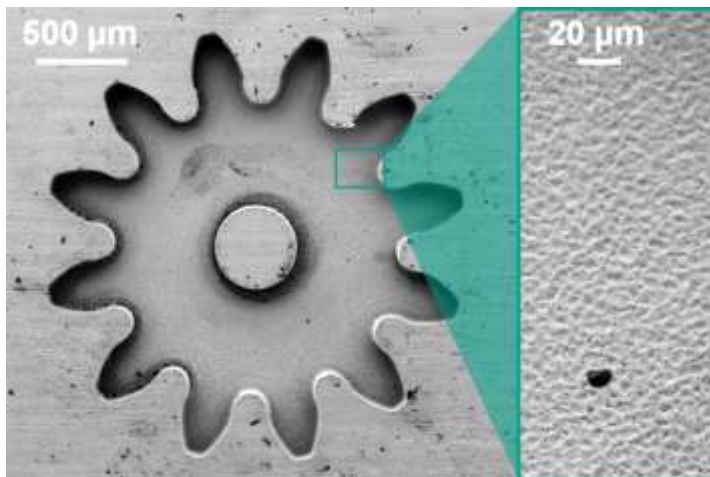


**Fig. 2.1:** Mold for micro-gear made of 30CrMo6 by SEM process by Schulz et al. (2012).

**Takeuchi et al. (2000)** manufactured 30  $\mu\text{m}$  module external micro-spur gears made of WC-Ni-Cr super alloy and SKS3 tool steel by  $\mu$ -SEM process using copper electrode. These micro-gears were part of a micro-planetary gear reduction mechanism which is used as micro-reducer in a self-propelled, chain-type machine employed in the power plants. They concluded that (i)  $\mu$ -SEM manufactured micro-gears have good torque transmission capability; (ii) dimensional variation of the micro-gears was 0.4% of outside diameter of the micro-gears; (iii) surface modification of micro-gears occurred due to formation of a recast layer; and (iv) use of the  $\mu$ -SEM manufactured micro-gears and the oil-lubricated

rolling bearing helped the developed micro-reducer to perform satisfactorily even after  $5 \times 10^6$  rotations.

**Takahata et al. (2000)** manufactured 1 mm long external micro-spur gears (having 196  $\mu\text{m}$  as outside diameter and shown in Fig. 2.2) from WC-Co super alloy by  $\mu\text{-SEM}$  process using LIGA manufactured internal micro-gears of nickel (having 200  $\mu\text{m}$  root circle diameter and 300  $\mu\text{m}$  face width) as the tool. They found that the manufactured external micro-gears had variation up to 4  $\mu\text{m}$  in their outside diameter.

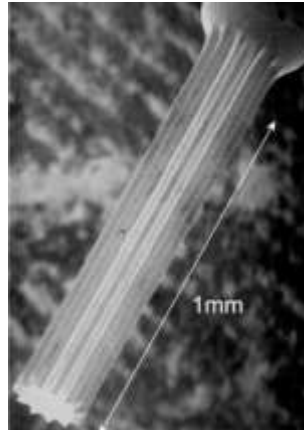


**Fig. 2.2:** SEM images showing external micro-spur gear manufactured by  $\mu\text{-SEM}$  process by Takahata et al. (2000).

**Takahata and Gianchandani (2002)** simultaneously manufactured 36 external micro-spur gears (having bore, 300  $\mu\text{m}$  outside diameter, and 70  $\mu\text{m}$  face width, and shown in Fig. 2.3(a) from WC-Co super alloy in 15 min by  $\mu\text{-SEM}$  process using an array of LIGA manufactured hollow internal micro-spur gears of nickel [having 10  $\mu\text{m}$  wall thickness and 300  $\mu\text{m}$  face width and depicted in Fig. 2.3(b)] as the tool.

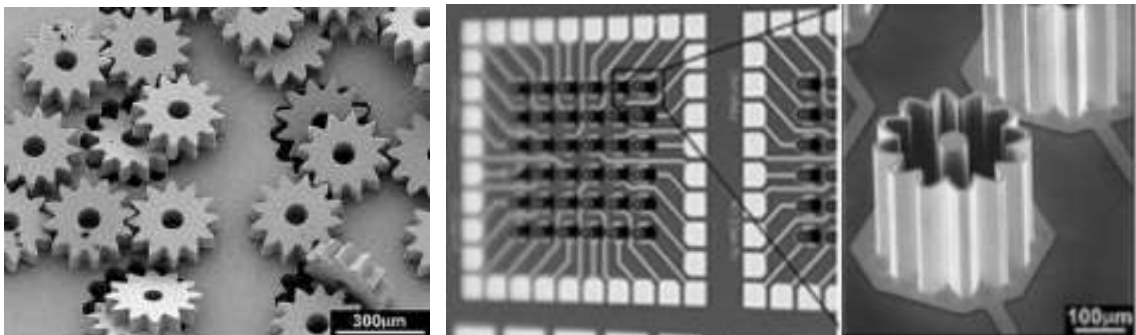


**Fig. 2.3(a)**

**Fig. 2.3(b)**

**Fig. 2.3:** SEM images showing (a) external micro-spur gear manufactured by  $\mu\text{-SEM}$  process; and (b) LIGA manufactured hollow internal micro-spur gear used as tool by Takahata and Gianchandani (2002).

**Tong et al. (2008)** used vibration-assisted  $\mu$ -SEM process for batch manufacturing of different sized internal micro-spur gears of steel using external micro-spur gears of copper (having outside diameter ranging from 300 to 600  $\mu\text{m}$  and 300  $\mu\text{m}$  face width) as the tool. These tool gears were manufactured by combination of micro-lithography and electroforming process. Fig. 2.4(a) depicts 618  $\mu\text{m}$  root circle diameter internal micro-spur gear manufactured by vibration-assisted  $\mu$ -SEM process using 600  $\mu\text{m}$  outside diameter external micro-spur gear as tool shown in Fig. 2.4(b). They reported that machining efficiency increased by 18 times and dimensional accuracy improved by 10.5  $\mu\text{m}$  by providing vibrations of 6 kHz frequency and 3  $\mu\text{m}$  amplitude to the workpiece.

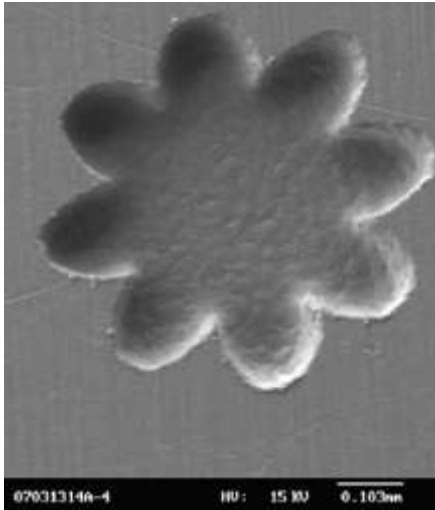


**Fig. 2.4(a)**

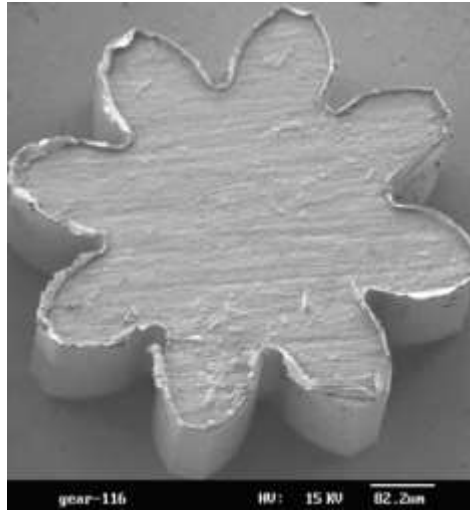


**Fig. 2.4(b)**

**Fig. 2.4:** SEM images showing (a) internal micro-spur gear of steel manufactured by vibration-assisted  $\mu$ -SEM process; and (b) external micro-spur gear of copper used as tool by Tong et al. (2008).

**Table 2.1:** Summary of past research works on manufacturing of micro-spur gears by SEM and  $\mu$ -SEM processes.

Sr. No.	Researchers (Year)	Gear specifications	Gear and tool material	Processes parameters	Responses	Remarks
<i>Micro-spur gear manufacturing using SEM process</i>						
1.	Schulz et al. (2012)	Micro-planetary gear wheel cavity OD: 98 $\mu$ m No. of teeth: 12	30CrMo6 WC-6Co of 100 $\mu$ m diameter			<ul style="list-style-type: none"> <li>• Deviation at the mold surface of the mold occurred due to fluctuation in the SEM tool wear.</li> </ul>
<i>Micro-spur gear manufacturing using <math>\mu</math>-SEM process</i>						
2.	Takeuchi <i>et al.</i> (2000)	External micro-spur gear Module: 30 $\mu$ m	SKS3 tool steel WC-Ni-Cr super alloy  Copper			Observed <ul style="list-style-type: none"> <li>• Surface modification due to recast layer formation</li> <li>• 0.4% dimensional variation</li> <li>• Good torque transmission capability</li> <li>• Sufficient performance after <math>5 \times 10^6</math> rotation</li> </ul>
3.	Takahata et al. (2000)	External micro-spur gear OD: 196 $\mu$ m Face width: 1 mm	WC-Co super alloy  LIGA manufactured internal micro-gears of nickel and having 200 $\mu$ m root circle diameter and 300 $\mu$ m face width	Discharge current	Dimensional accuracy	<ul style="list-style-type: none"> <li>• Manufactured high aspect ratio micro-gears having variation up to 4 <math>\mu</math>m in the outside diameter</li> </ul>
4.	Takahata and Gianchandani (2001)	External micro-spur gear with bore OD: 300 $\mu$ m Face width: 70 $\mu$ m	WC-Co super alloy  Array of LIGA manufactured hollow internal micro-gear of copper having wall thickness of 10 $\mu$ m and 300 $\mu$ m face width	Pulse discharge frequency	Machining rate	<ul style="list-style-type: none"> <li>• Simultaneous manufacturing of 36 external micro-spur gears in 15 minutes</li> </ul>
5.	Tong et al (2008)	Internal micro-spur gear Root circle diameter: 309 and 618 $\mu$ m	Steel  External micro-gears of copper (having outside diameter ranging from 300 to 600 $\mu$ m, and 300 $\mu$ m face width)	Open voltage Peak current Pulse-on time Pulse-off time Vibration frequency Vibration amplitude	Machining efficiency Dimensional accuracy	<ul style="list-style-type: none"> <li>• Provided high-frequency vibrations to workpiece in the <math>\mu</math>-SEM process to enhance its performance during manufacturing of micro-gear array structures</li> <li>• Machining efficiency increased by 18 times, dimensional accuracy improved by 10.5 <math>\mu</math>m by providing vibrations of 6 kHz frequency and 3 <math>\mu</math>m amplitude to the workpiece.</li> </ul>

### ***2.1.1.2 Manufacturing of Meso and Micro-Spur Gears by WSEM and $\mu$ -WSEM***

Review of the available literature indicates that comparatively more research work has been done in last two decades in using WSEM and  $\mu$ -WSEM processes for manufacturing meso and micro-gears due to their excellent capabilities for near net-shape manufacturing with higher geometrical and dimensional accuracy, better surface finish and improved quality. Following paragraphs describe review of the relevant past work and Tables 2.2 and 2.3 summarize them for WSEM and  $\mu$ -WSEM processes respectively.

**Hori and Murta (1994)** manufactured external micro-spur gears having 280  $\mu\text{m}$  outside diameter; 24  $\mu\text{m}$  module; and 9 teeth by WSEM using 25  $\mu\text{m}$  diameter of tungsten wire. They reported that WSEM process (i) has capability to manufacture high quality of micro-gear having involute profile and module less than 1 mm; and (ii) can achieve micro-gears with uniform involute tooth profile free from burrs and having error less than 1  $\mu\text{m}$  without any undercutting.

**Ali et al. (2007)** manufactured external MSG having 3.58 mm outside diameter; 17 teeth; and 0.07 mm fillet radius from 6 mm thick copper blank material by WSEM process using 100  $\mu\text{m}$  diameter of brass wire using that parametric combination which gave lower energy discharge. They studied influence of different levels of peak (or discharge) current at constant value of gap voltage and pulse-on-time on surface quality of MSG manufactured by WSEM. They concluded that WSEM can achieve average surface roughness value of 1.0  $\mu\text{m}$ ; maximum surface roughness value of 7.0  $\mu\text{m}$ ; and dimensional variation in the range of 1–2% for the MSG.

**Hsue et al. (2007)** manufactured external micro-spur gears having 400  $\mu\text{m}$  outside diameter; 285  $\mu\text{m}$  module; and 12 teeth by WSEM process using wire of 50  $\mu\text{m}$  and 70  $\mu\text{m}$  diameters to compare the performance WSEM process using worktable driven by conventional rotary motor (CRM) having ball screw and linear synchronous motor (LSM) with feed being given at submicron level. Figures 2.5(a) and 2.5(b) depict the micrographs of the external micro-gears manufactured by WSEM process using worktable driven by CRM and LSM respectively. They concluded that LSM driven rotary table achieved better dimensional accuracy ( $\pm 2.1 \mu\text{m}$ ), contouring accuracy, and uniformity in pitch than that in the CRM driven rotary table (dimensional accuracy  $\pm 3.5 \mu\text{m}$ ) in the WSEM.

**Ali and Mohammed (2008)** performed microstructural examination to determine the shape, size and distribution of the shallow craters, and irregularities on the tooth flank surface of the external MSG manufactured from 6 mm thick copper blank by WSEM process using 100  $\mu\text{m}$  diameter brass wire. Specifications of the MSG were: 3.58 mm

outside diameter; 17 teeth; and 70  $\mu\text{m}$  fillet radius. They reported that (i) better surface finish is achieved at lower values of discharge current, gap voltage, and pulse-on time; (ii) WSEM gave average surface roughness value of 1.0  $\mu\text{m}$ ; maximum surface roughness value of 7  $\mu\text{m}$ ; and dimensional variation within the range of 1-2% of outside diameter of the MSG.



**Fig. 2.5(a)**

**Fig. 2.5(b)**

**Fig. 2.5:** Micrographs of external micro-spur gears manufactured by by Hsue et al. (2007). using WSEM process having worktable driven by: (a) CRM; and (b) LSM.

**Jaster and Snyder (2010)** presented an overview on manufacturing of micro-spur gear and MSG by WSEM process. They reported that (i) extremely small gears having outside diameter as 1.27 mm and 6 teeth can be manufactured by WSEM using 25  $\mu\text{m}$  diameter wire; (ii) WSEM is superior alternative process having capability to manufacture an extremely accurate and near net-shape or net-shape micro-gear as electrode from difficult-to-machine materials for SEM process; and (iii) WSEM can yield greater dimensional accuracy and better surface quality of micro-gears.

**Tieli et al. (2011)** designed and developed program using the CAD/CAM software to manufacture external micro-spur gear by WSEM process and verified it by manufacturing one pair of micro-gears (having module of 24  $\mu\text{m}$ ) using 25  $\mu\text{m}$  diameter wire.

**Gupta and Jain (2013a, 2013b, 2014b, 2014c, 2014d)** worked extensively on manufacturing of MSG by WSEM process using 250  $\mu\text{m}$  diameter brass wire. The specifications of the MSG included: 9.8 mm outside diameter; 8.4 mm pitch circle diameter; 0.7 mm module; 5 mm face width and 12 teeth from a rectangular plate of brass. They studied the effects of WSEM process parameters such as servo or gap voltage, pulse-on time, pulse-off time and wire feed rate on microgeometry parameters (such as total profile and total pitch), surface finish, surface integrity, and gear cutting rate of MSG. The

experimental investigation was performed in three stages namely pilot experiments (conducted 23 experiments using one-factor-at-time experimental design approach), main experiments (conducted 29 experiments with two replicates each using Box-Behnken experimental design of response surface methodology) and validation experiments to verify the results of main experiments. They concluded that (i) gear quality of DIN 7 and 5 for profile and pitch with average surface roughness value of 1  $\mu\text{m}$  and maximum surface roughness values of 6.4  $\mu\text{m}$  can be achieved by WSEM process; (ii) wire deflection and non-uniform craters formed by higher discharge energy parameters (namely gap voltage and pulse-on time) are responsible for deviations in microgeometry of MSG; (iii) total profile error, total pitch error, runout and flank surface roughness increased with increase in gap voltage and pulse-on-time, and decreased with increase in pulse-off time and wire feed rate; (iv) better surface finish obtained at optimum parametric values of gap voltage 6 V, pulse-on-time 0.6  $\mu\text{s}$ , pulse-off time 160  $\mu\text{s}$  and wire feed rate 14 m/min.; (v) excellent microgeometry of MSG were achieved at servo voltage of 9 V, pulse-on time of 0.6  $\mu\text{s}$ , pulse-off time of 160  $\mu\text{s}$ , and wire feed rate of 13 m/min; and (vi) lower discharge energy parameters (i.e. lower values of gap voltage and pulse-on time), higher pulse-off-time, higher wire feed rate and maximum cutting speed (100%) are recommended for manufacturing MSG by WSEM process. They also compared WSEM with hobbing process for manufacturing MSG and found that WSEM resulted in better microgeometry, macrogeometry, surface integrity, microhardness, material efficiency, cost of manufacturing, and environment friendly manufacturing of MSG but hobbing yielded better surface finish of MSG (Gupta and Jain, 2014a).

**Zhong et al. (2015)** manufactured internal MSG of different pitch circle diameter (i.e. 3, 4, 5 mm) from 0.1 mm thick copper foil by WSEM process using 180  $\mu\text{m}$  diameter molybdenum wire. Subsequently, these internal MSG were joined together by thermal diffusion welding process to obtain the stepped (two and three step) mold of the internal micro-gear as shown in Fig. 2.6(a). This was used to manufacture the stepped external MSG from plastics by micro-ultrasonic powder molding method as shown in Fig. 2.6(b).

**Suzumori and Hori (1997)** used  $\mu$ -WSEM process to manufacture external MSG of steel having 0.063 mm module; 95 teeth; and internal MSG of steel having 0.063 mm module and 96 teeth using 25  $\mu\text{m}$  diameter tungsten wire. These MSG had newly designed composite tooth profile having combination of involute and arc, and were used to develop a prototype wobble motor. They reported that developed prototype wobble motor

maintained constant speed with full wobble motion and performed satisfactorily under high load conditions.



**Fig. 2.6(a)**

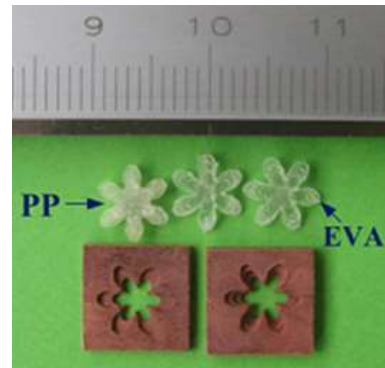


**Fig. 2.6(b)**

**Fig. 2.6:** Photographs of (a) stepped mold of internal MSG of copper manufactured by WSEM and thermal diffusion welding process; and (b) external stepped MSG of plastic materials manufactured using this mold by Zhong et al. (2015).

**Benavides et al. (2002)** manufactured meso-ratchet wheel, having 6.4 mm outside diameter and 0.88 mm face width, from four different materials namely Nitronic 60 stainless steel, 304L stainless steel, titanium alloy and beryllium copper by  $\mu$ -WSEM process using 30  $\mu$ m diameter tungsten wire. Total seven meso-ratchet wheels were manufactured: one for beryllium and two each for remaining materials. Discharge energy, pulse frequency, polarity, electrode material, dielectric, kerf and dielectric pressure were considered as input process parameters. Performance of  $\mu$ -WSEM process was compared in terms of profile tolerance, perpendicularity and repeatability for various materials. They achieved submicron level surface finish, burr-free edges, minimum formation of recast layer and uniform tooth profile of the meso-ratchet wheels. Figure 2.7 depicts  $\mu$ -WSEM manufactured meso-ratchet wheels made of beryllium copper and having hub [Fig. 2.7(a)] and teeth of Nitronic 60 stainless steel ratchet wheel [Fig. 2.7(b)].

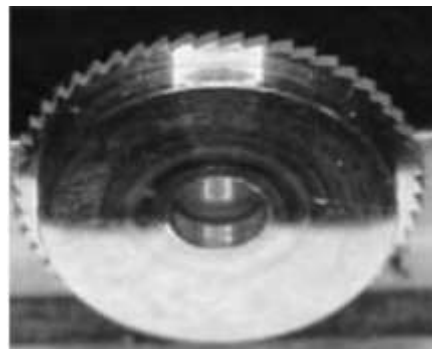


**Fig. 2.7(a)**

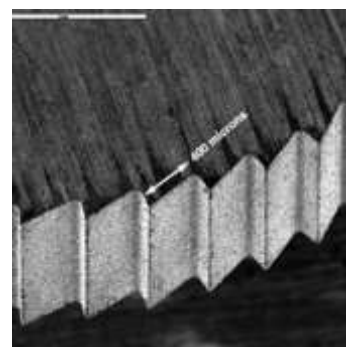


**Fig. 2.7(b)**

**Fig. 2.7:** Meso-ratchet wheel manufactured by  $\mu$ -WSEM process by Benavides et al. (2002): (a) photograph of beryllium copper meso-ratchet wheel; and (b) SEM image of teeth of Nitronic 60 stainless steel meso-ratchet wheel.

**Table 2.2:** Summary of past research works on manufacturing of meso and micro-spur gears by WSEM.

Sr. No.	Researchers (Year)	Gear specifications	Gear and tool material	Processes parameters	Responses	Remarks
1.	Hori and Murta (1994)	External micro-spur gear OD: 280 $\mu\text{m}$ Module: 24 $\mu\text{m}$ No. of teeth: 9	Tungsten wire of 25 $\mu\text{m}$ diameter			<ul style="list-style-type: none"> <li>• Tooth profile error less than 1 <math>\mu\text{m}</math></li> <li>• Achieved accurate tooth profile without undercutting at the root</li> </ul>
2.	Ali et al. (2007)	External MSG OD: 3.58 mm Face width: 6 mm Pitch: 0.66 mm No. of teeth: 17	Copper  Brass wire of 100 $\mu\text{m}$ diameter	Discharge current	Surface roughness Dimensional accuracy	<ul style="list-style-type: none"> <li>• Obtained average surface roughness as 1.0 <math>\mu\text{m}</math>, max. surface roughness as 7 <math>\mu\text{m}</math> and dimensional variation in range of 1-2% for MSG</li> </ul>
3.	Hsue et al. (2007)	External micro-spur gear OD: 400 $\mu\text{m}$ Module: 285 $\mu\text{m}$ Teeth: 12	Wire of 50 and 70 $\mu\text{m}$ diameter	Linear synchronous motor (LSM) driven worktable Conventional rotary motor (CRM) driven worktable	Geometrical accuracy	<ul style="list-style-type: none"> <li>• Achieved better dimensional accuracy, contouring accuracy, and uniform pitch of micro-gears using the LSM driven worktable than the CRM driven worktable in WSEM process.</li> </ul>
4.	Ali and Mohammad (2008)	External MSG OD: 3.58 mm Face width: 6 mm No. of teeth: 17	Copper  Brass wire of 100 $\mu\text{m}$ diameter	Peak current Pulse-on time Gap voltage	Surface roughness	<ul style="list-style-type: none"> <li>• Achieved average and maximum surface roughness as 1 <math>\mu\text{m}</math> and 7 <math>\mu\text{m}</math> respectively and dimensional variation: 1-2 %</li> </ul>
5.	Tieli et al. (2011)	External micro-spur gear Module: 24 $\mu\text{m}$	Fine wire of 25 $\mu\text{m}$ diameter			<ul style="list-style-type: none"> <li>• Developed program using the CAD/CAM software to manufacture external micro-gears by WSEM and verified it by manufacturing one pair of micro-gears having module of 24 <math>\mu\text{m}</math>.</li> </ul>
6.	Gupta and Jain (2013a; 2013b; 2014a; 2014b; 2014c; 2014d)	External MSG OD: 9.8 mm; Module: 0.7 mm Face width: 5 mm No. of teeth: 12	Brass  Brass wire of 250 $\mu\text{m}$ dia.	Servo voltage Pulse-on time Pulse-off time Wire feed rate	Surface roughness Profile error Pitch error Gear cutting rate	<ul style="list-style-type: none"> <li>• Explored WSEM for manufacturing MSG</li> <li>• Manufactured near net-shape MSG</li> <li>• Achieved gear quality up to DIN 6</li> <li>• Determined significant WSEM parameters</li> <li>• Optimized WSEM parameters</li> </ul>
7.	Zhong et. al. (2015)	Internal MSG PCD: 3; 4; 5 mm Face width: 0.1 mm No. of teeth: 6	Copper  Molybdenum wire of 180 $\mu\text{m}$ diameter	Discharge current Discharge voltage Pulse-on time Cycle time (i.e. pulse-on + pulse-off time)	Kerf size Surface roughness Dimensional accuracy	<ul style="list-style-type: none"> <li>• Manufactured different sizes of internal meso-gear from 0.1 mm thick copper foil</li> </ul>

**Schoth et al. (2005)** manufactured high aspect ratio micro-spur gears from X38CrMoVS\_1 steel [having 8 teeth; 6.0 mm face width; and outside diameter 0.5 and 1.0 mm as shown in Fig. 2.8(a) and 2.8(b)] and ceramic (SiSiC) [having outside diameter of 1.0 mm; face width of 10 mm and 8 teeth as shown in Fig. 2.7(c)] by  $\mu$ -WSEM process using 20 and 30  $\mu$ m diameter of tungsten wire. They also manufactured micro-spur gear with shaft (for ease of gear assembly) as illustrated in Fig. 2.9. They concluded that (i)  $\mu$ -WSEM has capability to manufacture high aspect ratio micro-spur gears from variety of electrically conductive materials with good geometry and surface quality; (ii) wire diameter is the most significant parameter that affects accuracy of the micro-spur gears manufactured by  $\mu$ -WSEM process; (iii) future trend in  $\mu$ -WSEM process is to use very small sized wires ( $< 20 \mu$ m) and equip the  $\mu$ -WSEM machine with the advanced wire guiding systems and sensing devices to manufacture high aspect ratio micro-components.



**Fig. 2.8(a)**

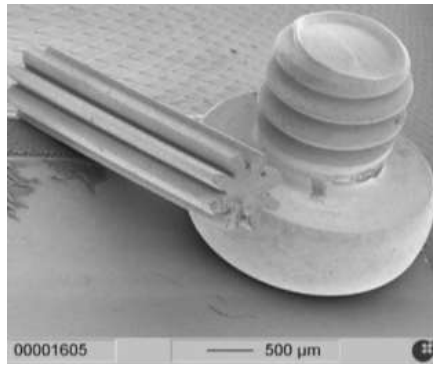


**Fig. 2.8(b)**

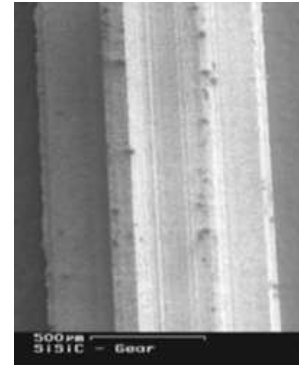


**Fig. 2.8(c)**

**Fig. 2.8:** SEM images of X38CrMoVS\_1 steel micro-spur gears manufactured by Schoth et al. (2005) by  $\mu$ -WSEM using tungsten wire of diameter (a) 20  $\mu$ m; (b) 30  $\mu$ m; and (c) made of ceramic (SiSiC) using 30  $\mu$ m diameter tungsten wire.

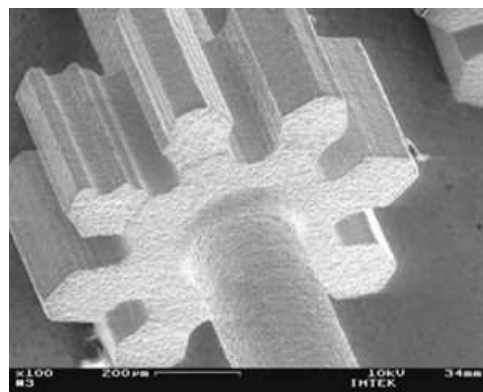


**Fig. 2.9:** SEM image of MSG with shaft manufactured by Schoth et al. (2005) using by  $\mu$ -WSEM.

**Uhlmann et al. (2005)** presented detailed overview of  $\mu$ -WSEM processes for manufacturing micro-spur gear and concluded that (i) machining accuracies of  $\pm 1 \mu\text{m}$ ; value of surface roughness  $< 0.1 \mu\text{m}$ ; and aspect ratio  $> 100$  can be attained by  $\mu$ -WSEM process; (ii) wire vibrations increase the surface roughness and variation in dimensional accuracy of micro-spur gear.

**Di et al. (2006)** manufactured internal micro-spur gears made of stainless steel having 40 and 100  $\mu\text{m}$  module; 1 mm face width; and 7 teeth by  $\mu$ -WSEM process using 30  $\mu\text{m}$  diameter tungsten wire fed at the rate of 20 m/min under tension of 500 g. They also manufactured a pair of stainless steel micro-dies having 100  $\mu\text{m}$  module; 3.5 mm face width and 10 teeth by  $\mu$ -WSEM process. These micro-dies were used for manufacturing the micro-spur gears from aluminum alloy by forming process. They claimed to have achieved dimensional accuracy  $< \pm 0.2 \mu\text{m}$ ; surface roughness  $< 0.1 \mu\text{m}$ ; and thickness of recast layer  $< 2 \mu\text{m}$ .

**Yan and Chiang (2009)** used  $\mu$ -WSEM process to manufacture 12 teeth micro-spur gears from SKD11 tool steel using 70  $\mu\text{m}$  diameter copper wire (shown in Fig. 2.10a), 50  $\mu\text{m}$  diameter brass wire, and 50  $\mu\text{m}$  diameter carbon steel wire to evaluate and verify the functionality of the newly developed transistor-controlled power supply. It was designed to provide higher pulse frequency and lower pulse energy because it will improve surface finish of the  $\mu$ -WSEM manufactured parts. They also manufactured micro-rack of pitch 320  $\mu\text{m}$  and 230  $\mu\text{m}$  using 70 and 50  $\mu\text{m}$  diameter wires respectively. They reported (i) attainment of better surface finish at lower peak current; (ii) uniform pitch of micro-spur gear teeth; and (iii) achieving 0.38  $\mu\text{m}$  average surface roughness; 0.75  $\text{mm}^2/\text{min}$  maximum cutting rate (product of cutting speed of the wire and workpiece thickness). They claimed that these results prove superiority of the developed pulse generator.



**Fig. 2.10:** SEM images of SKD11 tool steel micro-spur gear manufactured by Yan and Chiang (2009) using  $\mu$ -WSEM and 70  $\mu\text{m}$  diameter copper wire.

Ali et al. (2010) compared  $\mu$ -WSEM process with WSEM process for manufacturing MSG made of beryllium-copper alloy in terms of surface roughness and dimensional accuracy of the MSG. They used optimal parameters namely 1 A peak current; 6  $\mu$ s pulse-on time; 5  $\mu$ s pulse-off time; and 5 V gap voltage identified from the preliminary experiments. WSEM was used to manufacture MSG (Fig. 2.11a) having 3.58 mm outside diameter; 0.66 mm circular pitch; 17 teeth; 6.0 mm face width; and 0.07 mm fillet radius using 100  $\mu$ m diameter brass wire as tool and de-ionized water as dielectric.  $\mu$ -WSEM was used to manufacture MSG [Fig. 2.11(b)] having 1.2 mm outside diameter; 0.2 mm circular pitch; 17 teeth; 1.5 mm face width; and 0.04 mm fillet radius using 70  $\mu$ m diameter of zinc coated copper wire as tool and SEM-3 synthetic oil as dielectric. They reported that (i) WSEM can achieve crack-free surface having average surface roughness value of 1.8  $\mu$ m; dimensional variation in the range of 2-3  $\mu$ m; and (ii)  $\mu$ -WSEM process can achieve these values as 0.05  $\mu$ m and 0.1-1.0  $\mu$ m i.e. average surface roughness and dimensional accuracy of MSG achieved by  $\mu$ -WSEM process are much better than those achieved by WSEM. They also mentioned that (i)  $\mu$ -WSEM is slower process than WSEM; (ii) MRR increases with increase in discharge current and gap voltage at the cost of the surface quality; and (iii) low discharge energy is recommended for manufacturing meso-gears requiring better geometrical accuracy and surface finish by the WSEM process.

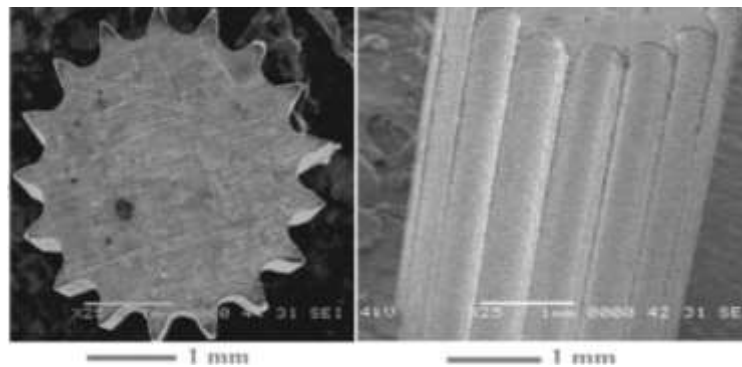


Fig. 2.11(a)

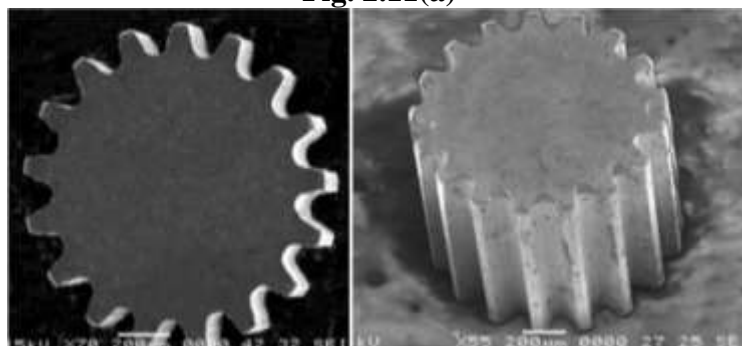


Fig. 2.11(b)

Fig. 2.11: SEM images of MSG of beryllium copper manufactured by Ali et al. (2010) using: (a) WSEM process; and (b)  $\mu$ -WSEM process.

**Table 2.3:** Summary of past research works on manufacturing of meso and micro-spur gears by  $\mu$ -WSEM.

Sr. No.	Researchers (Year)	Gear specifications	Gear and tool material	Processes parameters	Responses	Remarks
1.	Suzumori and Hori (1997)	External MSG Module: 0.063 mm No. of teeth: 95 Internal meso-gear Module: 0.063 mm No. of teeth: 96	Steel  Tungsten wire of 25 $\mu$ m diameter			<ul style="list-style-type: none"> <li>Proposed a new design for tooth profile called as 'composite profile'</li> <li>Adequate operating performance under high load conditions</li> </ul>
2.	Benavides <i>et al.</i> (2002)	Meso-ratchet wheel OD: 6.4 mm Wheel thickness: 0.88 mm	Nitronic 60 stainless steel, 304L stainless steel, Titanium alloy and Beryllium copper Tungsten wire of 30 $\mu$ m diameter	Pulse energy Pulse frequency Polarity Dielectric pressure	Profile tolerance Perpendicularity Repeatability	<ul style="list-style-type: none"> <li>Achieved submicron level surface finish, burr-free edges, minimum formation of recast layer and uniform tooth profile of meso-ratchet wheels</li> </ul>
3.	Schoth <i>et al.</i> (2005)	Micro-spur gear OD: 0.5 and 1 mm Face width: 6 and 10 mm No. of teeth: 8	X38CrMoVS_1 Steel; and ceramic (SiSiC)  Tungsten wire of 20 and 30 $\mu$ m diameter			<ul style="list-style-type: none"> <li>Manufactured high aspect ratio micro-spur gear with good geometry and surface quality</li> <li>Wire diameter is the most important parameter that significantly affect the accuracy of micro-spur gear and MSG</li> </ul>
4.	Di <i>et al.</i> (2006)	Micro-spur gears and micro-dies for their manufacturing Module: 40 and 100 $\mu$ m Face width: 1 and 3.5 mm No. of teeth: 7 and 10	Stainless steel  Tungsten wire of 30 $\mu$ m diameter	Open voltage Peak current Pulse-on time Pulse-off time	Surface roughness Dimensional accuracy Recast layer	<ul style="list-style-type: none"> <li>Achieved dimensional accuracy and surface roughness less than <math>\pm 0.2 \mu</math>m and <math>0.1 \mu</math>m respectively and thickness of recast layer less than 2 <math>\mu</math>m.</li> </ul>

**Table 2.3 Continued**

<b>Sr. No.</b>	<b>Researchers (Year)</b>	<b>Gear specifications</b>	<b>Gear and tool material</b>	<b>Processes parameters</b>	<b>Responses</b>	<b>Remarks</b>
5.	Yan and Chiang (2009)	Micro-spur gear No. of teeth: 12	SKD11 tool steel  Copper wire of 70 $\mu\text{m}$ diameter;  Carbon steel and brass wire of 50 $\mu\text{m}$ diameter	Discharge current Wire feed rate Wire tension	Machining rate Surface roughness Dimensional accuracy	<ul style="list-style-type: none"> <li>• Developed new transistor-controlled power supply</li> <li>• Achieved average roughness: 0.38 <math>\mu\text{m}</math>; and maximum cutting rate: 0.75 <math>\text{mm}^2/\text{min}</math></li> <li>• Achieved better surface finish at lower peak current</li> </ul>
6.	Ali et al. (2010)	MSG by WSEM OD: 3.58 mm Circular pitch: 0.66 mm Face width: 6 mm Fillet radius: 0.07 mm No. of teeth: 17	Beryllium copper  Brass wire of 100 $\mu\text{m}$ diameter	Discharge current	Surface roughness Dimensional accuracy	<ul style="list-style-type: none"> <li>• Achieved average roughness: 1.8 <math>\mu\text{m}</math>; maximum roughness: 7 <math>\mu\text{m}</math> and dimensional accuracy: 2-3 <math>\mu\text{m}</math></li> </ul>
		MSG by $\mu$ -WSEM OD: 1.2 mm Circular pitch: 0.2 mm Face width: 1.5 mm Fillet radius: 0.04 mm No. of teeth: 17	Beryllium copper  Zinc coated copper wire of 70 $\mu\text{m}$ diameter	Discharge current	Surface roughness Dimensional accuracy	<ul style="list-style-type: none"> <li>• Achieved average surface roughness: 50 nm and dimensional accuracy: 0.1-1 <math>\mu\text{m}</math></li> </ul>

### 2.1.2 Manufacturing of Meso and Micro-Spur Gears by other Advanced Machining Processes

Some researchers have explored some other advanced machining processes such as micro-abrasive water jet machining ( $\mu$ -AWJM), laser ablation (LA), laser shock punching (LSP) and bio-etching for manufacturing of micro-spur gears and MSG. Table 2.4 presents their summary and following sections describe them.

**Liu and Schubert (2011)** manufactured macro spur gear (19.05 mm outside diameter) and MSG (having outside diameters 9.68 mm and 3.55 mm) of stainless steel  $\mu$ -AWJM process using 254  $\mu$ m diameter nozzle. These gears were used in a micro-planetary gearing system consisting of seven gears including a sun gear having 9.68 mm outside diameter, a ring gear having 19.05 mm outside diameter and five small planetary gears having 3.55 mm outside diameter. They reported that  $\mu$ -AWJM process (i)  $\mu$ -AWJM process possess capability to manufacture MSG from variety of materials and recognized it as one of the most adaptable precision process for micro-manufacturing; (ii) is a low cost and environment friendly process; and (iii)  $\mu$ -AWJM process is the fastest growing meso and micro-gear manufacturing process.

**Youn et al. (2007)** manufactured 50  $\mu$ m deep mold of micro-spur gears made of glassy carbon [as shown in Fig. 2.12(a)] by nanosecond KrF excimer laser ablation process of 248 nm wavelength. This mold was used to manufacture micro-spur gears from Pyrex glass [Fig. 2.12(b)] having 200  $\mu$ m outside diameter by hot embossing process. They concluded that (i) sidewalls of mold of the micro-spur gear are inclined and bottom face is not perfectly flat; (ii) average surface roughness values are about 45 and 70 nm at the bottom and at sidewalls respectively; and (iii) laser ablation is a very effective process to manufacture high aspect ratio deep V-shaped channels.

**Liu et al. (2015)** manufactured MSG having 1.36 mm outside diameter; 0.1 mm module and 12 teeth from aluminum foil by Nd-YAG laser shock punching (LSP) process to investigate influence of the machining parameters such as blank-holder, soft punch properties and laser energy on quality of MSG. They explored the capability of LSP process to manufacture the meso-gears of different thickness and used heavier blank holder to improve cutting quality. They reported that (i) higher dimensional accuracy is achieved using 1690 mJ laser energy; (ii) quality of meso-gears becomes poor when higher laser energy and soft punch are used; (ii) 200  $\mu$ m thickness of silica gel is more suitable for getting improved punching impression.

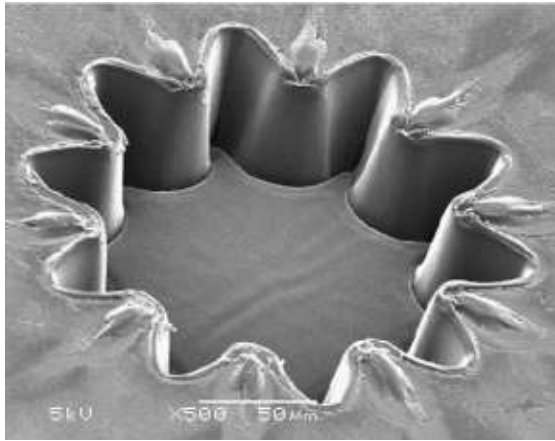


**Fig. 2.12(a)**

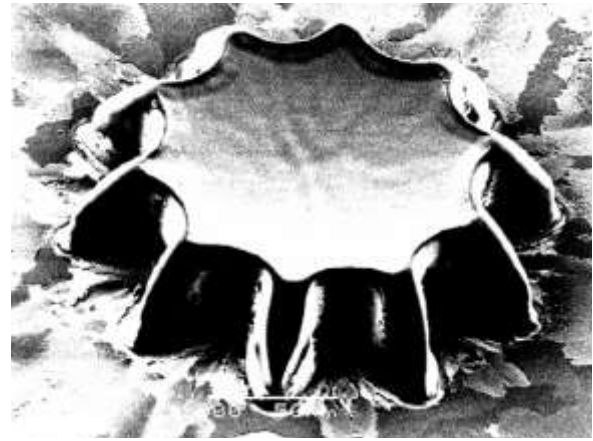


**Fig. 2.12(b)**

**Fig. 2.12:** SEM images of micro-spur gears manufactured by Youn et al. (2007): (a) 50  $\mu\text{m}$  deep mold of micro-spur gear from glassy carbon by laser ablation process; and (b) hot-embossed micro-spur gear of Pyrex glass.

**Yude et al. (2009)** manufactured the micro-spur gears from 50  $\mu\text{m}$  thick copper sheet by bio-etching process using thiobacillus ferrooxidans (TF) as a bio-etching agent. This process involves following steps: (i) cleaning of the copper thin sheet in the acid liquid to remove dirt and grease; (ii) applying mask to its surface where machining is not required; (iii) irradiation by ultraviolet light dissolving or machining the unmasked areas of the copper thin sheet; (iv) dipping the machined copper thin sheet into the TF liquid and agitating it. It took 3 hours to manufacture one micro-spur gear. They concluded that (i) micro-spur gear can be manufactured by bio-etching process; and (ii) bio-etch time significantly affects the micro-spur gear quality.

**Table 2.4:** Summary of past research works on manufacturing of meso and micro-spur gears by other advanced machining processes.

<b>Researchers (Year)</b>	<b>Gear Specifications</b>	<b>Gear material</b>	<b>Manufacturing process</b>	<b>Remarks</b>
Liu and Schubert (1998)	External MSG OD: 9.68 and 3.55 mm Macro-gear OD:19.05 mm	Stainless steel	$\mu$ -AWJM	<ul style="list-style-type: none"><li>• Capability to manufacture gears from different types of materials from micro to macro scale.</li><li>• Successfully manufactured micro-planetary gears made of stainless steel.</li><li>• <math>\mu</math>-AWJM is a low cost and environment friendly process.</li></ul>
Youn et al. (2007)	Mold of micro-spur gear having 50 $\mu$ m depth	Glassy carbon	Laser ablation	<ul style="list-style-type: none"><li>• Mold of micro-gear having 50 <math>\mu</math>m depth was manufactured by KrF excimer laser having 248 nm wavelength.</li><li>• Mold was used to manufacture micro-gear of Pyrex glass by hot embossing process.</li><li>• Achieved average surface roughness values at the bottom and at the sidewall as 45 and 70 nm respectively.</li><li>• Very effective process to manufacture high aspect ratios V-shaped deep channels.</li></ul>
Liu et al. (2015)	External MSG OD: 1.36 mm Module: 0.1 mm No. of teeth: 12	Aluminum foil	Laser shock punching	<ul style="list-style-type: none"><li>• Explored capability to produce meso-gears of different thickness using laser shock punching process.</li><li>• Used heavier blank holder to improve cutting quality.</li><li>• Achieved higher dimensional accuracy when shocked at 1690 mJ.</li><li>• Quality of meso-gears becomes poor when higher laser energy and soft punch are used.</li><li>• Observed that 200 <math>\mu</math>m thickness of silica gel is best suitable for getting significant punching impression.</li></ul>
Yude et al. (2009)	Micro-spur gear	Copper	Bio-etching	<ul style="list-style-type: none"><li>• Successfully manufactured micro-spur gears by bio-etching process using thiobacillus ferrooxidans as a bio-etching agent in 3 hours.</li><li>• Observed that bio-etch time is a significant factor which affects the quality of bio-etched micro-spur gear.</li></ul>

## 2.2 Past Work on other Aspects of WSEM

Following paragraphs describe summary of the relevant past work on other aspects of WSEM process such as wire lag phenomenon and optimization of process parameter using statistical and soft-computing techniques:

**Speeding and Wang (1995)** used response surface methodology (RSM) and artificial back propagation neural network (BPNN) to develop models for cutting speed of wire and workpiece surface roughness in WSEM process in terms of pulse-on time, pulses-off time, wire tension, and dielectric pressure. For this, they used the results obtained while machining AISI 420 steel by 250  $\mu\text{m}$  diameter brass wire. They compared the developed models for goodness of fit and confirmed them by conducting the validation experiments. They concluded that both models gave accurate results.

**Puri and Bhattacharyya (2003)** studied behavior of the wire vibrations and used analytical approach for solving the wire vibration equation considering multiple spark discharges. They investigated effects of wire vibration on MRR, surface roughness and wire wear ratio during machining of die steel by WSEM process using 250  $\mu\text{m}$  diameter brass wire. They also studied variation of wire vibration amplitude with the ratio of workpiece thickness to wire length between the upper and lower guides.

**Ramakrishnan and Karunamoorthy (2006)** identified optimum parameters of WSEM process (i.e. pulse-on time, delay time, peak current, wire tension, wire feed rate) by simultaneous optimization of MRR and surface finish and wire wear ratio. They used results obtained in experiments conducted Taguchi  $L_{16}$  orthogonal experimental design on WSEM of steel by 250  $\mu\text{m}$  diameter zinc coated brass wire. They found that pulse-on time and peak current were more influencing parameters than other WSEM parameters.

**Sarkar et al. (2006)** developed feed-forward BPNN models for cutting speed of wire, surface roughness, dimensional accuracy, and wire offset (i.e wire radius plus overcut) as the function of six WSEM parameters namely pulse-on time, pulse-off time, peak current, gap (or servo) voltage, wire tension, and dielectric flow rate. They used the experimental results obtained during WSEM of  $\gamma$ -titanium aluminide alloy using 250  $\mu\text{m}$  diameter brass wire. They found that surface roughness increases with increase in cutting speed of wire.

**Mahapatra and Patnaik (2007)** optimized six parameter of WSEM (namely pulse-on time, pulse frequency, peak current, wire feed rate, wire tension, and dielectric flow rate) by multi-objective optimization of MRR, surface roughness, and kerf width using genetic algorithms (GA). They confirmed the optimization results by conducting WSEM

of AISI D2 tool steel using 250  $\mu\text{m}$  diameter zinc coated copper wire and found that the achieved optimum combination of WSEM parameters simultaneously improved MRR, surface finish and kerf width.

**Zhang et al. (2013)** used BPNN integrated GA and RSM to develop models for surface roughness and MRR to optimize pulse-on time, pulse-off time, peak current and wire feed rate using the results of WSEM of SKD11 tool steel using 120  $\mu\text{m}$  diameter molybdenum wire. They found that BPNN integrated GA models are superior to RSM based models.

**Okada et al. (2015)** investigated the effect of dielectric flow rate on wire breakage during WSEM of chrome alloy (Cr12) using 170  $\mu\text{m}$  diameter molybdenum wire. They developed simulation model for the same and its basis they concluded that wire deflection mainly occurs due to hydrodynamic force exerted by the dielectric in the WSEM process. Higher dielectric flow rate causes maximum wire deflection resulting in accumulation of the eroded particles in IEG which leads frequent wire breakage.

### **2.3 Identified Research Gaps**

Following research gaps were identified based on the review of the relevant past work presented in the sections 2.1 and 2.2:

- Though WSEM process is a very promising near net-shape process for manufacturing micro and meso-gears. It has found to quality of MSG up to 6-7 DIN standard. Important WSEM process parameters that affect microgeometry and surface finish of MSG are pulse-on time, pulse-off time, peak current, wire tension, wire feed rate and dielectric flow rate. But, very limited work has been reported on manufacturing of micro and meso-spur gears by WSEM and  $\mu$ -WSEM processes investigating their surface roughness, dimensional accuracy and microstructure.
- Very limited work has been reported on parametric optimization of WSEM to minimize surface roughness and microgeometry errors of MSG and improving productivity of WSEM process.
- No work has been reported on manufacturing MBG and MHG by WSEM process focusing on microgeometry, surface roughness, surface integrity, and gear cutting rate of WSEM manufactured (WSEMed) MBG and MHG.
- No work has been reported on optimization of WSEM process parameters to minimizing microgeometry errors and improving the surface quality of the WSEMed MBG and MHG.

- Comparative evaluation of WSEM with traditional machining processes (i.e. hobbing and milling) to manufacture MBG and MHG has not been investigated.

## **2.5 Objectives of the Present Work**

Bouquet et al. (2014) while comparing performance of WSEM with milling and selective laser melting processes in terms of surface finish, microgeometry parameters, machining time and process flexibility of the manufactured macro-spur gears (having 76.3 mm pitch diameter; 36 teeth; and 2.12 module) from 16MnCr5 steel, have concluded that “manufacturing of helical gears and correction in their profile are not possible by WSEM process”. This served as motivation to undertake the present research work with the following research objectives:

- To establish WSEM process to manufacture high quality MBG and MHG.
- To study the effects of WSEM process parameters on microgeometry parameters, average and maximum surface roughness and volumetric gear cutting rate of MBG and MHG so as to identify optimum values of WSEM process parameters.
- To study microstructure and microhardness of the best quality MBG and MHG manufactured using the identified optimum parameters of WSEM process.
- To develop models of the considered responses for the MBG and MHG.
- Multi-response optimization of the WSEM parameters to simultaneously optimize the conflicting responses of MBG and MHG.
- Experimental validation of the optimized results.
- Comparative evaluation of WSEM with milling process for manufacturing MBG and with hobbing process for manufacturing MHG to prove technical superiority and economic viability of WSEM process over them.

## **2.6 Research Methodology**

Figure 2.13 depicts the research methodology used to fulfil the identified research objectives of the present research work.

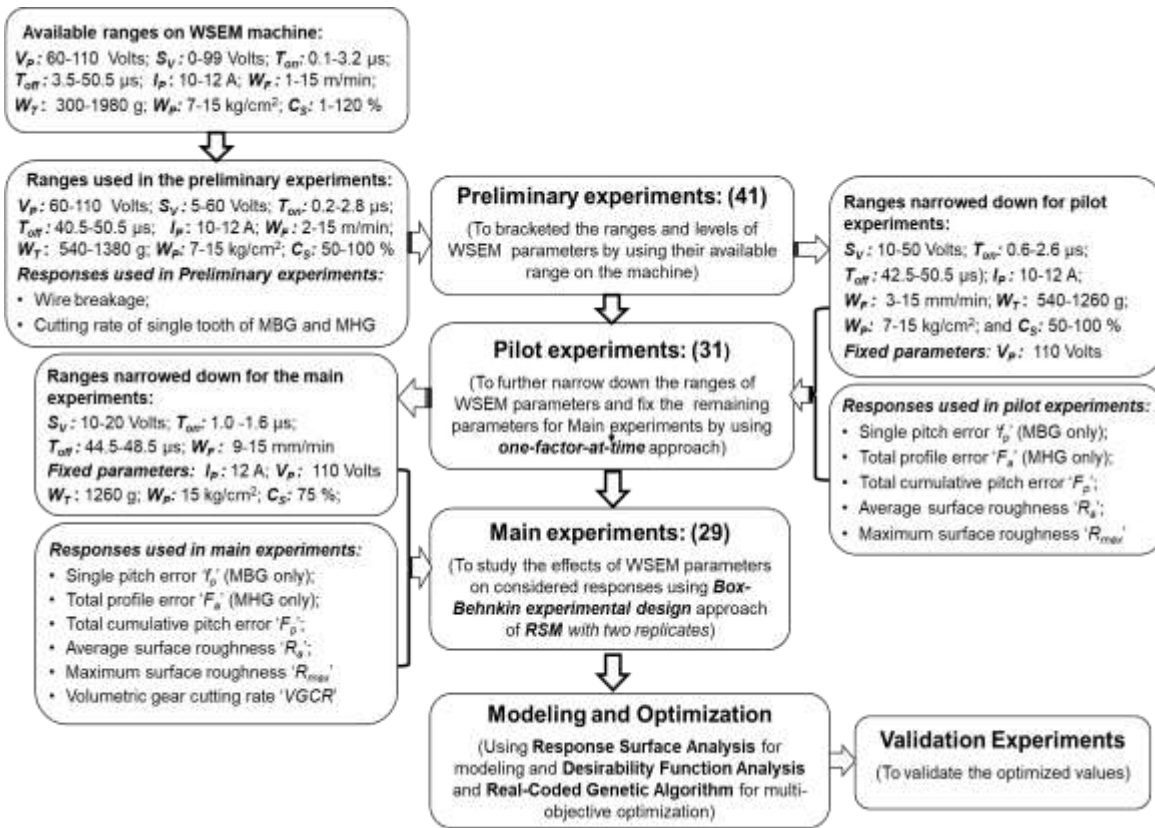


**Fig. 2.13:** Research methodology used in the present work.

The *next chapter* describes the selection of materials for MBG and MHG, and their design specifications. It also gives details about planning and design of the experiments for the different experimental stages along with details of the evaluation procedure of the performance measures, and concepts and methods used in the analyzing results of each experimental stage.

## **Chapter 3**

### **Details of Experimentation**

This chapter describes the selection of material for meso-helical gears (MHG) and meso-bevel gears (MBG), their design specifications, planning and design of experimentation in different stages, details of variable and fixed parameters and performance measures used in each experimental stage, details of experimentation and manufacturing MBG and MHG by WSEM process, details of the evaluation of the responses, and concepts and methods used in the analyzing the experimental results of the present research work.

#### **3.1 Material Selection for the Meso-Gears**

Selection of material for meso-gears mainly depends on their application, material characteristics, manufacturing process and material cost. Only metallic materials can be used for manufacturing meso-gears by WSEM process because it can cut electrically conductive materials only. Since, MBG and MHG are primarily used for low load application under corrosive environment therefore austenitic stainless steel (grade) was selected as their material to pursue research on their manufacturing by WSEM process in the present research work. This was based on higher resistance to corrosive environment, very good strength, non-magnetic nature and widespread use of SS 304 in the equipment and machines used in food processing, chemical plants, pharmaceutical, biomedical, surgical, and domestic applications. Examination of its chemical composition revealed to possess (by weight): 8.32% Ni; 18.04% Cr; 1.08% Mn; 0.053% C; 0.48% Si; 0.017% S; and balance Fe (refer Appendix-A for details).

#### **3.2 Design Specifications of the Meso-Gears**

Design specifications of a meso-gear mainly depend on its applications, material and manufacturing process, capabilities of the available measuring instruments. Table 3.1 presents detailed specifications of MBG and MHG used in the present work whereas Fig. 3.1 depicts their 3D-view along with their specifications.

**Table 3.1:** Specifications of the MBG and MHG used in the present work.

Parameter	Meso-bevel gear (MBG)	Meso-helical gear (MHG)
Material	SS 304	SS 304
Profile	Involute	Involute
Pressure angle	20°	20°
Module	0.7 mm	0.66 mm
No. of teeth	12	10
Face width	5 mm	5 mm
Bore diameter	3.0 mm	3.0 mm
Diameter	Major 9.8 mm Minor 7.0 mm	8.35 mm ---
Angle	32° (cone angle)	20° helix angle of right hand type

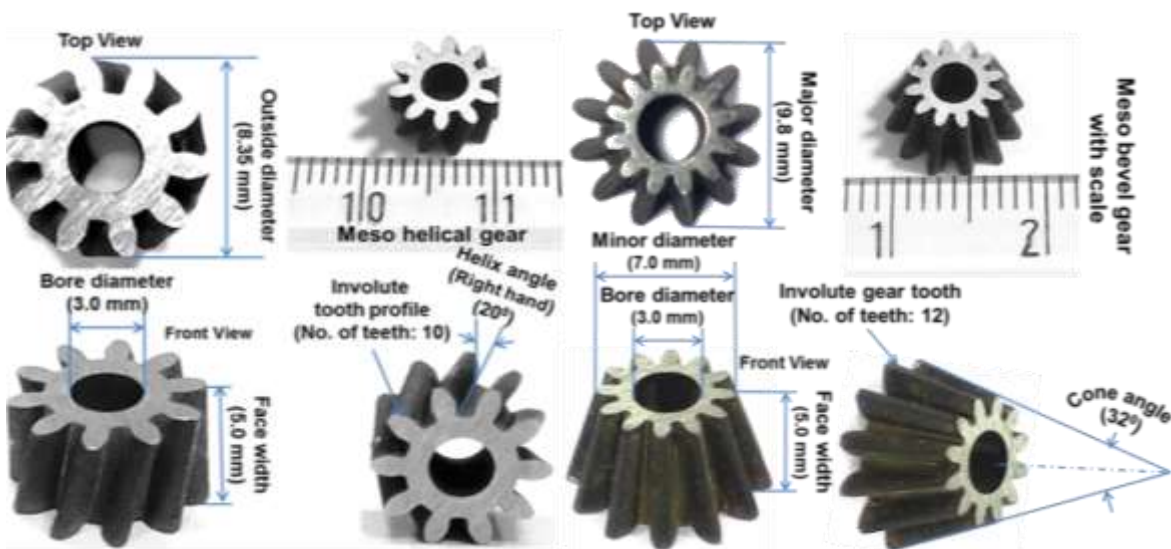


**Fig. 3.1:** Three-dimensional views of MBG and MHG made of SS 304.

### 3.3 Planning and Designs of Experiments

Experiments were planned, designed and conducted in four different stages namely: (a) preliminary experiments, (b) pilot experiments, (c) main experiments, and (d) validation experiments with objectives to (i) to study effects of the considered process parameters on the responses considered in each experimental stage; (ii) to identify the significant parameters and their interactions on the considered responses; (iii) to identify the optimum ranges or values of WSEM parameters to optimize the considered responses. Table 3.2 presents details of ranges and values of parameters of WSEM process, responses, and approach of experimental design used in each stage of experimental investigation. Approach for designing the experiments in each stage was selected keeping in view its objectives, number of variable parameters and their levels. Following subsections describe each experimental stage in detail.

**Table 3.2:** Details of ranges and values of parameters of WSEM process, responses, and approach of experimental design used in each stage of experimental investigation.

Name, symbol and unit of WSEM parameters	Ranges available on the machine	Ranges and values used in 41 preliminary experiments for MBG and MHG each	Identified ranges from preliminary experiments and the values used in 31 pilot experiments for MBG and MHG each	Identified ranges from the pilot experiments and the values used in 29 main experiments (with two replicates) for MBG and MHG each
Pulse peak voltage ' $V_p$ ' (Volts)	60-110	<b>60-110:</b> 60, 110	<i>110 volts</i>	<i>110 volts</i>
Servo voltage ' $S_v$ ' (Volts)	0-99	<b>5-60:</b> 5, 10, 20, 30, 40, 50, 60	<b>10-50:</b> 10, 20, 30, 40, 50	<b>10-20:</b> 10, 15, 20
Pulse-on time ' $T_{on}$ ' ( $\mu$ s)	0.1-3.1	<b>0.2-2.8:</b> 0.2, 0.6, 1.1, 1.6, 2.1, 2.6, 2.8	<b>0.6-2.6:</b> 0.6, 1.1, 1.6, 2.1, 2.6	<b>1-1.6:</b> 1, 1.3, 1.6
Pulse-off time ' $T_{off}$ ' ( $\mu$ s)	3.5-50.5	<b>40.5-50.5:</b> 40.5, 42.5, 44.5, 46.5, 48.5, 50.5	<b>42.5-50.5:</b> 42.5, 44.5, 46.5, 48.5, 50.5	<b>44.5-48.5:</b> 44.5, 46.5, 48.5
Peak current ' $I_p$ ' (A)	10-12	<b>10-12:</b> 10, 11, 12	<b>10-12:</b> 10, 11, 12	<i>12 A</i>
Wire feed rate ' $W_F$ ' (m/min)	1-15	<b>2-15:</b> 2, 3, 6, 9, 12, 15	<b>3-15:</b> 3, 6, 9, 12, 15	<b>9-15:</b> 9, 12, 15
Wire tension ' $W_T$ ' (g)	300-1980	<b>540-1380:</b> 540, 900, 1260, 1380	<b>540-1260:</b> 540, 900, 1260	<i>1260 g</i>
Dielectric pressure ' $W_p$ ' ( $\text{kg/cm}^2$ )	7-15	<b>7-15:</b> 7, 15	<b>7-15:</b> 7, 15	<i>15 kg/cm<sup>2</sup></i>
% Cutting speed ' $C_s$ ' (%)	1-120	<b>50-120:</b> 50, 75, 100, 120	<b>50-100:</b> 50, 75, 100	<i>75%</i>
<b>Approach for design of experiments</b>		One-factor-at-time	One-factor-at-time	Box-Behnken design (BBD) of RSM
<b>Considered Responses</b>		Wire breakage, Cutting rate of single tooth of MBG and MHG	Single pitch error ' $f_p$ ' (MBG only) Total profile error ' $F_a$ ' (MHG only) Total cumulative pitch error ' $F_p$ ', Average surface roughness ' $R_a$ ', Maximum surface roughness ' $R_{max}$ '	Single pitch error ' $f_p$ ' (MBG only), Total profile error ' $F_a$ ' (MHG only), Total cumulative pitch error ' $F_p$ ', Average surface roughness ' $R_a$ ', Maximum surface roughness ' $R_{max}$ ', Volumetric gear cutting rate ' $VGCR$ '

### 3.3.1 Preliminary Experiments

WSEM has large number of process parameters which can be varied in wide ranges by predefined increment available on the machine used (refer Appendix-D for process parameters, their available ranges on the WSEM machine used in the present work). Therefore, selection of appropriate parameters, their ranges and levels which will avoid wire deflection or wire lag, frequent wire breakage, and also achieve better surface finish, geometrical and dimensional accuracy, and higher gear cutting rate, is very challenging task. Total forty one preliminary experiments were planned and conducted for MBG and MHG separately by cutting only one tooth for each gear in each experiment. In these experiments, nine parameters of WSEM (i.e. pulse-on time ' $T_{on}$ ', pulse-off time ' $T_{off}$ ', servo voltage ' $S_v$ ', peak current ' $I_p$ ', pulse peak voltage ' $V_p$ ', wire feed rate ' $W_F$ ', wire tension ' $W_T$ ', dielectric pressure ' $W_P$ ', and cutting speed ' $C_S$ ') were varied using one-factor-at-a-time approach in which only one parameter of WSEM was varied at a time in the ranges slightly curtailed from those available on the WSEM machine (to avoid wire breakage, please refer to the Table 3.2 for details) and other parameters were kept constant at their intermediate levels (except pulse-off time). Objectives of the preliminary experiments were to narrow down ranges of the considered parameters of WSEM for the pilot experiments using wire breakage and cutting rate of single tooth as responses or criteria because they significantly affect surface finish and total manufacturing time of MBG and MHG by WSEM process.

### 3.3.2 Pilot Experiments

Total 31 experiments were designed and conducted for MBG and MHG separately (i.e. 31 MBG and 31 MHG were manufactured) using one-factor-at-a-time approach of design of experiments following objectives:

- To study influence of WSEM parameters on considered parameters of microgeometry (i.e. single pitch error ' $f_p$ ' for MBG only, total profile error ' $F_a$ ' for MHG only, and total cumulative pitch error ' $F_p$ ' for both) and surface roughness (average roughness ' $R_a$ ' and maximum roughness ' $R_{max}$ ' values) of MBG and MHG.
- To bracket the ranges of WSEM parameters and fix the remaining parameters for further experimental investigations using the considered response.
- To study microstructure, microhardness and flank surface topography of the best quality (i.e. minimum error in their microgeometry parameters) MBG and MHG.

In these experiments, eight WSEM parameters namely (i) pulse-on time ' $T_{on}$ ', pulse-off time ' $T_{off}$ ', servo voltage ' $S_v$ ', and wire feed rate ' $W_F$ ' were varied at five levels each; (ii) peak current ' $I_P$ ', wire tension ' $W_T$ ', and cutting speed ' $C_S$ ' were varied at three levels each; (iii) dielectric pressure ' $W_P$ ' was varied at two level in the ranges identified from the preliminary experiments. Pulse peak voltage ' $V_p$ ' was kept constant at 110 volts according to its value identified during the preliminary experiments.

### 3.3.3 Main Experiments

Twenty nine experiments were designed and conducted for MBG and MHG separately with two replicates of each experiment (thus manufacturing 58 MBG and 58 MHG by WSEM process) according to Box–Behnken design approach of response surface methodology (RSM) by varying four WSEM parameters namely servo voltage ( $S_v$ ), pulse-on time ( $T_{on}$ ), pulse-off time ( $T_{off}$ ) and wire feed rate ( $W_F$ ) at three levels each in the ranges narrow down by the pilot experiments. Other remaining five parameters of WSEM kept constant throughout the experiments at the values identified by the pilot experiments (refer Table 3.2 for details). Following were the main objectives of conducting main experiments:

- To study influence of WSEM parameters on the considered parameters of microgeometry and surface roughness of MBG and MHG as mentioned in Table 3.2.
- To identify the most significant WSEM parameters and their interactions on the considered responses of MBG and MHG.
- To identify optimum combinations of WSEM parameters which minimize microgeometry errors and surface roughness of MBG and MHG and maximize the volumetric gear cutting rate so as to improve their overall quality and productivity of WSEM process.

Since, one-variable-at-time approach cannot evaluate the interactions between the process parameters and optimum combinations of the process parameters therefore Box-Behnken design (BBD) approach of RSM was found suitable for designing the main experiments because it provides complete information in minimum number of experiments as compared to other fractional factorial experimental design approaches. The BBD approach was proposed by George E. P. Box and Donald Behnken in 1960. It is a class of rotatable or nearly rotatable second-order design based on three-level fractional factorial designs. Levels of each factor are usually coded as -1, 0, +1. Total number of experiments ( $N$ ) required using BBD is  $N = 2k(k-1) + C_0$ ; where  $k$  is number of factors and  $C_0$  is the

number of central points. Total number of experiments required using the central composite design (CCD) is  $N = 2^k + 2k + C_0$  (Ferreira, 2007). The BBD has limited capability for orthogonal blocking than CCD. Hence, if there is a requirement to separate experimental runs into blocks for BBD, then it allows the blocks to be used in such a manner that the calculations of the regression for variables effects are not affected by these blocks. The parametric combinations for each experiment are at the midpoints of edges of the process parameters space and at the center. Figure 3.2 depicts graphical representation of BBD for three factors three levels experiment. Table 3.3 presents comparison of number of experimental runs required for three-level factors for the factorial design, central composite design and Box-Behnken design. Table 3.4 presents actual and coded values of WSEM parameters for 29 experimental runs designed using BBD approach of RSM for main experiments.

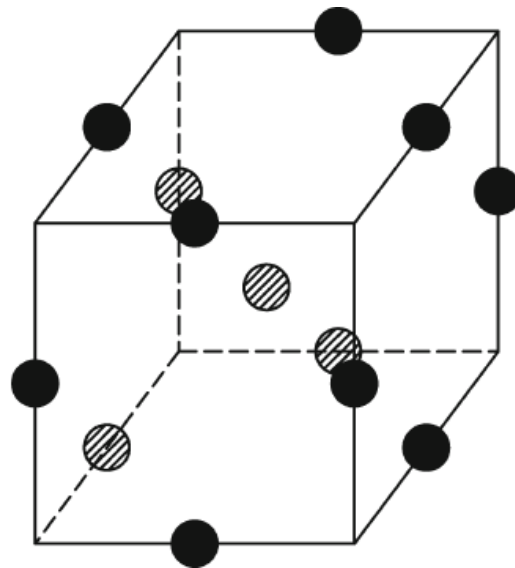


**Fig. 3.2:** Geometric representation of BBD of RSM for three factors having three levels.

**Table 3.3:** Comparison of different experimental design approaches on the basis of number of experimental runs required for three level factors.

No. of factors	Factorial design	Fractional factorial	
	No. of runs	CCD	BBD
2	9	13	NA
3	27	20	17
4	81	30	29
5	243	50	46
6	729	86	54
7	2187	152	61

**Table 3.4:** Actual and coded values of WSEM parameters for 29 experimental runs designed using BBD approach of RSM for main experiments.

Exp. Run	Variable parameters of WSEM							
	$T_{on}$ ( $\mu$ s)		$T_{off}$ ( $\mu$ s)		$S_V$ (Volts)		$W_F$ (m/min)	
	<i>Actual</i>	<i>Coded</i>	<i>Actual</i>	<i>Coded</i>	<i>Actual</i>	<i>Coded</i>	<i>Actual</i>	<i>Coded</i>
1	1.3	(0)	46.5	(0)	10	(-1)	15	(+1)
2	1.0	(-1)	44.5	(-1)	15	(0)	12	(0)
3	1.3	(0)	46.5	(0)	15	(0)	12	(0)
4	1.6	(+1)	48.5	(+1)	15	(0)	12	(0)
5	1.6	(+1)	46.5	(0)	15	(0)	15	(+1)
6	1.3	(0)	46.5	(0)	15	(0)	12	(0)
7	1.3	(0)	44.5	(-1)	20	(+1)	12	(0)
8	1.3	(0)	48.5	(+1)	15	(0)	15	(+1)
9	1.6	(+1)	46.5	(0)	10	(-1)	12	(0)
10	1.3	(0)	44.5	(-1)	15	(0)	15	(+1)
11	1.3	(0)	48.5	(+1)	20	(+1)	12	(0)
12	1.3	(0)	46.5	(0)	20	(+1)	15	(+1)
13	1.3	(0)	48.5	(+1)	10	(-1)	12	(0)
14	1.0	(-1)	46.5	(0)	15	(0)	15	(+1)
15	1.3	(0)	46.5	(0)	20	(+1)	9	(-1)
16	1.6	(+1)	46.5	(0)	15	(0)	9	(-1)
17	1.3	(0)	44.5	(-1)	15	(0)	9	(-1)
18	1.3	(0)	48.5	(+1)	15	(0)	9	(-1)
19	1.0	(-1)	46.5	(0)	20	(+1)	12	(0)
20	1.0	(-1)	46.5	(0)	15	(0)	9	(-1)
21	1.3	(0)	46.5	(0)	15	(0)	12	(0)
22	1.3	(0)	46.5	(0)	15	(0)	12	(0)
23	1.0	(-1)	46.5	(0)	10	(-1)	12	(0)
24	1.0	(-1)	48.5	(+1)	15	(0)	12	(0)
25	1.6	(+1)	44.5	(-1)	15	(0)	12	(0)
26	1.3	(0)	46.5	(0)	10	(-1)	9	(-1)
27	1.3	(0)	46.5	(0)	15	(0)	12	(0)
28	1.6	(+1)	46.5	(0)	20	(+1)	12	(0)
29	1.3	(0)	44.5	(-1)	10	(-1)	12	(0)

### 3.3.4 Validation Experiments

Total 8 validation experiments were conducted to (i) validate the results of modeling of the considered responses by regression analysis and artificial neural networks (ANN) using results of the main experiments; and (ii) results of the multi-objective optimization of the considered responses of MBG and MHG by desirability functional analysis and real-coded genetic algorithms (RCGA). In these experiments, those standard values of the WSEM parameters (i.e. available on the WSEM machine) were used which were nearest to their optimized values and corresponding values of the responses were recorded.

### 3.4 Procedure of Experimentation

#### 3.4.1 Details of the WSEM Machine

Four-axes ( $X$ ,  $Y$ ,  $U$  and  $V$ ) computer numerical controlled (CNC) WSEM machine (model: *Sprintcut win* from *Electronica India Limited Pune, India*) as shown Fig. 3.3 was used for experimental investigations on manufacturing of MBG and MHG having bores from a rectangular plate of SS 304. Table 3.5 presents specifications of this machine.

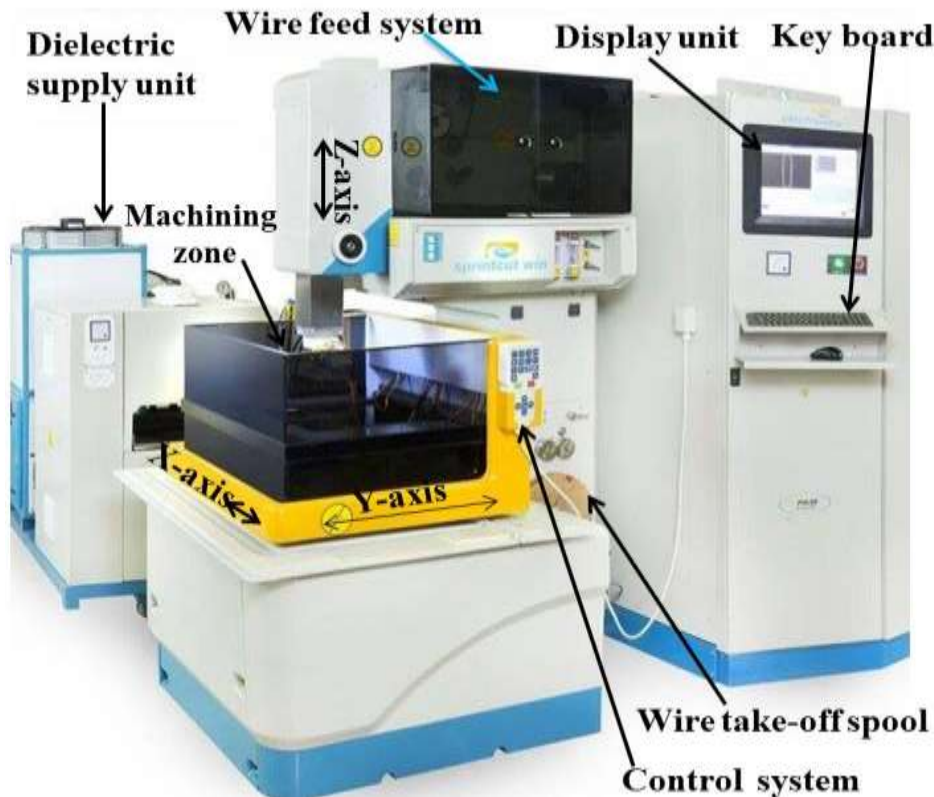


**Fig. 3.3:** Photograph of the WSEM used in the present work.

**Table 3.5:** Specifications of CNC WSEM machine used in the present work.

Make	Electronica Machine Tools Ltd, Pune, India
Model	Sprintcut Win
Design	Fixed column, Moving table
Taper cutting	$\pm 30^{\circ} / 50$ mm
Table size	440 x 650 mm
Max. height and weight of workpiece	200 mm, 500 Kg
Traverse lengths of main table (x, y)	300, 400 mm
Traverse length of auxiliary table (u, v)	80, 80 mm
Diameter of wire electrode	150; 200; and 250 $\mu$ m
Dielectric type and tank capacity	Deionized water; 350 Ltrs.
Pulse power generator	ELPULS-40 A DLX
Input power supply	3 Phase, AC 415 V, 50 HZ
Connected load	10 KVA
Average power consumption	6-7 KVA

This machine is based on closed-loop DC servo control system for  $X$ ,  $Y$ ,  $U$  and  $V$  to achieve higher repeatability. Meso-gears manufacturing capabilities of this machine include: maximum values of inclination angle as  $\pm 30^\circ$  and face width as 50 mm. Exact value of the inclination angle required for manufacturing an MHG or MBG as per its specification was achieved by the CNC program controlled movement of the upper wire guide in  $U$  and  $V$  directions with respect to the fixed lower wire guide in steps of  $0.5 \mu\text{m}$ . Cutting of the meso-gear teeth takes place due to CNC programmed movement of the worktable in  $X$  and  $Y$  directions by means of servo motors with minimum value of movement (i.e.  $1 \mu\text{m}$  as least input increment). Fresh wire is fed continuously through the gear blank from the wire feed spool by upper and lower guides which also maintains the required wire tension. The used wire is collected in the take-off spool. A constant value of inter-electrode gap (IEG) is maintained between the soft plain brass wire and gear plate by means of servo motor. Deionized water was used as dielectric and  $250 \mu\text{m}$  diameter soft plain brass wire (having tensile strength in a range from 470 to  $510 \text{ N/mm}^2$ ) as tool. Deionized water is supplied via sapphire nozzles provided in the upper and lower guides with make it to flow concentric with the wire to flush away the eroded particles from IEG.

### **3.4.2 Details of Manufacturing of MBG and MHG**

Following is sequence of the different activities used in experimental investigations of the present work and also depicted in Fig. 3.4.

- (i) Preparation of 5 mm thick; 100 mm long; 50 mm wide SS 304 plate by grinding and buffing its top and bottom faces to make it perfectly flat so that there is no deflection during its mounting on the worktable of the CNC machine. Proper clamping of the prepared plate to ensure its perfect positioning with respect to the wire on CNC WSEM machine worktable.
- (ii) Drilling an array of  $800 \mu\text{m}$  diameter microholes in the prepared plate by  $\mu$ -spark-erosion drilling ( $\mu$ -SED) process. These microholes serve as passage for the wire during manufacturing of the bore and MBG (or MHG).
- (iii) Clamping of the prepared plate on the CNC WSEM machine worktable in perfectly horizontal position using a dial gauge because even minor inclination of it with respect the wire may significantly deteriorate quality of MBG and MHG.
- (iv) Preparing layout of the MBG (or MHG) by AutoCAD software and importing its geometric information through data exchange format (DXF) file in the *ELCAM* software available on the CNC WSEM machine for making part program (in terms

of G and M codes) of MBG (or MHG) as per its specification. The wire compensation (offset) was specified separately for both bore and MBG (or MHG) in the part program. During WSEM process, the wire follows the path as defined in the part program of MBG (or MHG).

- (v) Trepanning each microhole by WSEM to enlarge its diameter from 0.8 mm to 3 mm to serve as bore of MBG (or MHG). Microhole adjacent to this bore serve as passage for the wire during manufacture of next MBG (or MHG) as depicted in Fig. 3.5(a) and 3.5(b).
- (vi) Cutting the wire and running the WSEM machine in dry-mode (i.e. without flushing and sparking) to move the wire to center of adjacent microhole [Figs. 3.5(a)-3.5(b)].
- (vii) Cutting of MBG (or MHG) by WSEM punching it out from the prepared plate leaving corresponding hole in the plate.
- (viii) Repeating steps (v) to (vii) to manufacture next MBG (or MHG).
- (ix) Measurement of microgeometry and surface roughness parameters of MBG and MHG using the procedure and equipment detailed in Section 3.5.
- (x) Analyses of microstructure, microhardness and flank surface topography of the best quality MBG and MHG.



**Fig. 3.4:** Different activities and their sequence used in the experimental investigations of the present work.

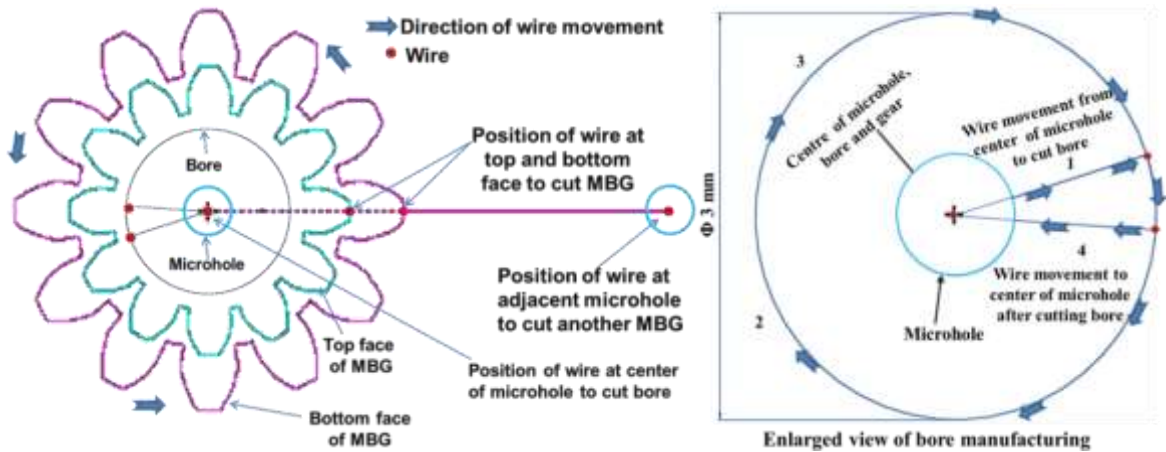


Fig. 3.5(a)

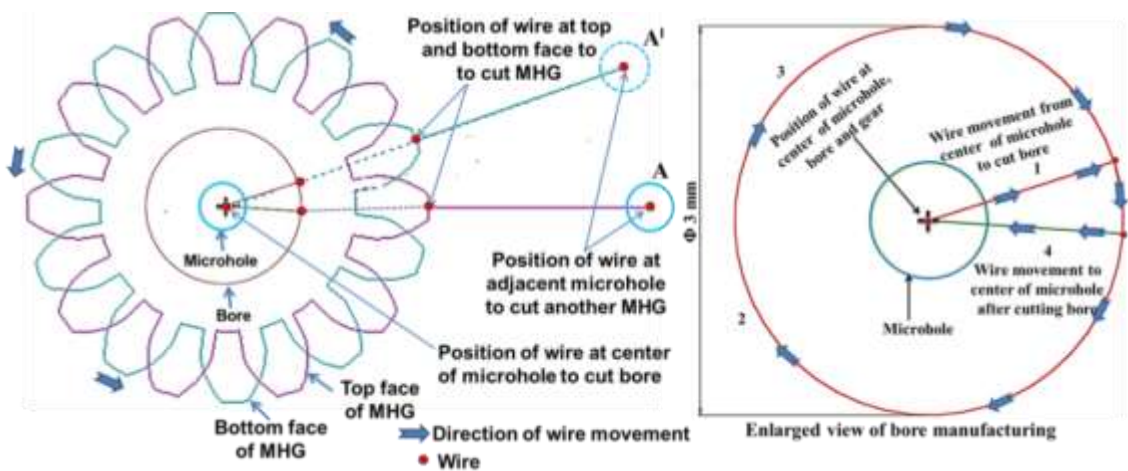


Fig. 3.5(b)

Fig. 3.5: Movement of the wire during trepanning of the bore and manufacturing of the meso-gears by WSEM process for (a) MBG; and (b) MHG.

### 3.5 Evaluation of the Responses

Following paragraphs describe details of the measurement process and equipment of the considered parameters of microgeometry, macrogeometry and surface roughness, computation of volumetric gear cutting rate, evaluation of flank surface topography, microhardness and microstructure of WSEM manufactured MBG and MHG.

#### 3.5.1 Measurements of Microgeometry and Macrogeometry

In the present work, microgeometry parameters selected to indicate the quality of meso-gears are: error in total profile ' $F_a$ ' (only for MHG), error in single pitch ' $f_a$ ' (only for MBG), and error in total cumulative pitch ' $F_p$ ', for both of MBG and MHG. Other microgeometry parameters namely single pitch error ' $f_p$ ' (for MHG only) adjacent pitch error ' $f_u$ ' and radial runout ' $F_r$ ' were also considered for the best quality WSEM manufactured MBG and MHG in pilot experiments, validation experiments and

comparative evaluation of WSEM with hobbing and milling processes. Macrogeometry parameters (i.e. span deviation, chordal tooth thickness deviation and deviation in outside diameter) are applicable for cylindrical (i.e. spur and helical) gears only. Therefore, these parameters were measured for comparative evaluation of WSEM with hobbing processes for manufacturing MHG.

Four-axes (X, Y, Z, and W axes) CNC gear metrology machine *SmartGear 500* from *Wenzel GearTech Germany* (refer Appendix-B) was used to measure the considered parameters of microgeometry, macrogeometry and topology of flank surfaces of MBG and MHG using 500  $\mu\text{m}$  diameter ruby ball probe. A specially designed stepped fixture was manufactured from mild steel for mounting MBG (Fig. 3.6a) and MHG (Fig. 3.6b) in the rotary chuck of the CNC gear metrology machine. The MBG and MHG were inspected against DIN 8 and DIN 9 standards corresponding to international standard DIN 3965/86 and DIN 3961/62 respectively. Total profile error of MHG was measured by moving the probe from start to end of involute profile at middle of the face width on left and right hand flanks of the randomly selected three teeth for the pilot and four teeth for the main experiments. Pitch errors and radial runout of MBG and MHG were measured by touching the probe on right and left hand flanks of all teeth of MBG and MHG along their pitch circles at middle of the face width.

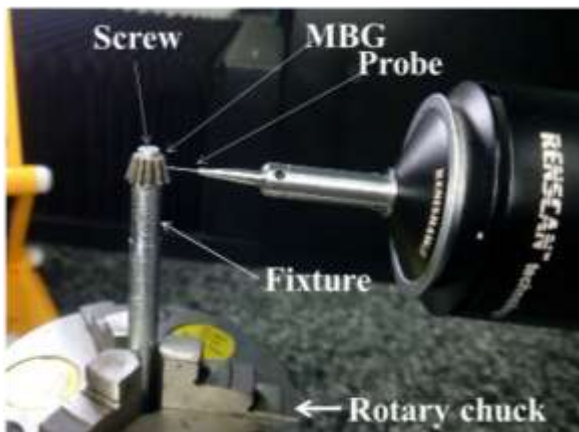


**Fig. 3.6(a)**

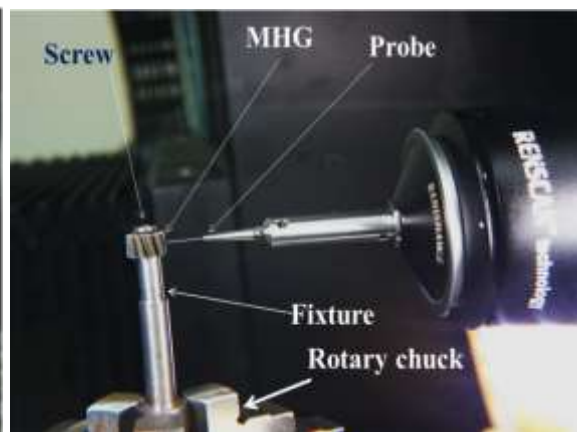


**Fig. 3.6(b)**

**Fig. 3.6:** Measurements of microgeometry parameters by WenzelTec SmartGear 500 CNC gear metrology machine for: (a) MBG; and (b) MHG.

### 3.5.2 Measurements of Flank Surface Topography

Flank surface topography was measured only for those MBG and MHG which exhibited the best quality microgeometry (i.e. minimum error in their microgeometry parameters) during pilot experiments, validation experiments and comparative evaluation

of WSEM with hobbing and milling processes by the CNC gear metrology machine. Tooth flank surface topography was measured by moving the probe from start to end of involute profile of the face width from top to bottom on left and right hand flanks of the randomly selected one tooth of MBG and MHG. In the topography graphs of MBG and MHG, theoretical flank surfaces are represented by blue grid lines and the actual flank surfaces are represented by black grid lines for MHG and by green grid lines for MBG. Amount of deviations between the actual and theoretical flank surfaces are represented by red colour vertical lines at each grid point. Figure 3.7 depicts the concept of microgeometry, macrogeometry and flank surface topography measurements by CNC gear metrology machine.

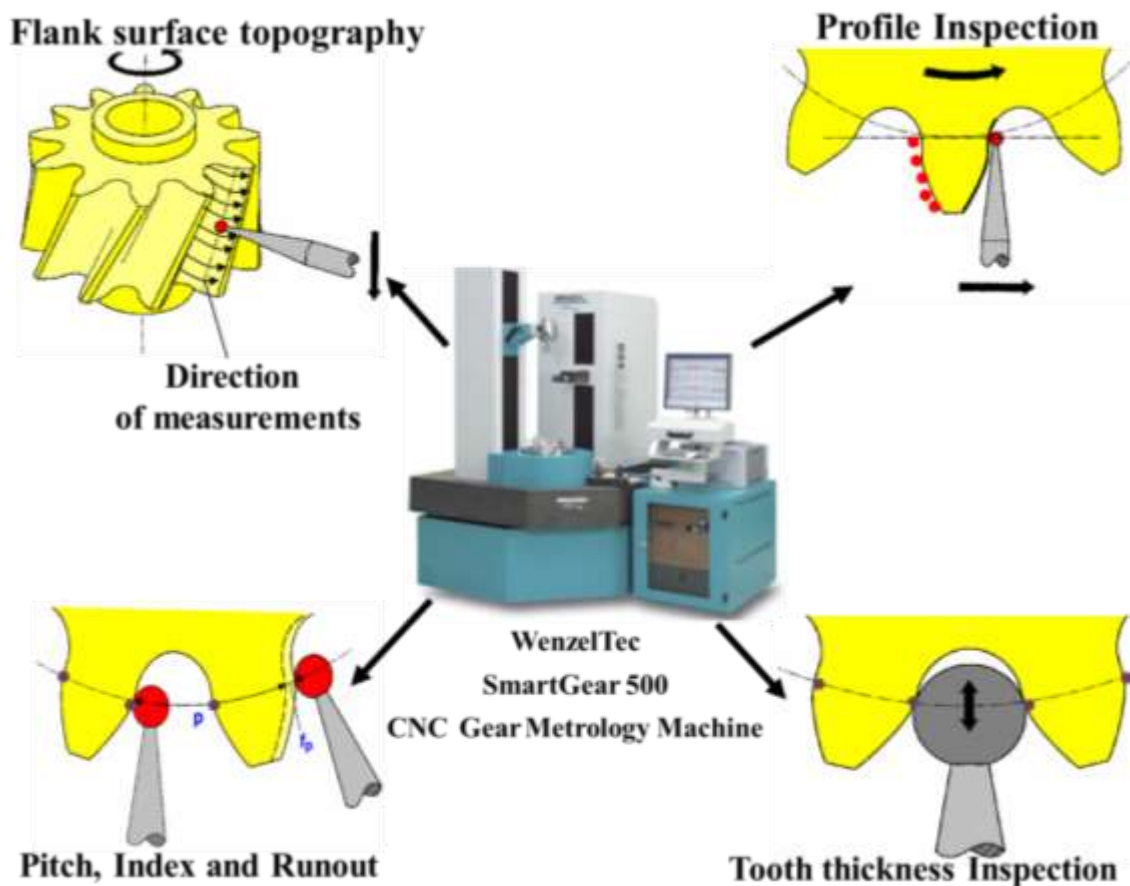
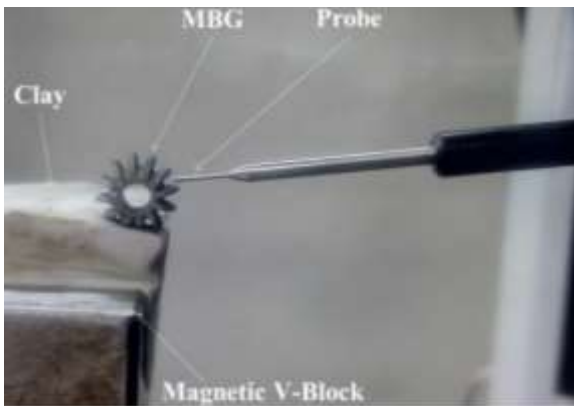


**Fig. 3.7:** Concept of the measurement of microgeometry, macrogeometry and flank surface topography of the meso-gears by CNC gear metrology machine.

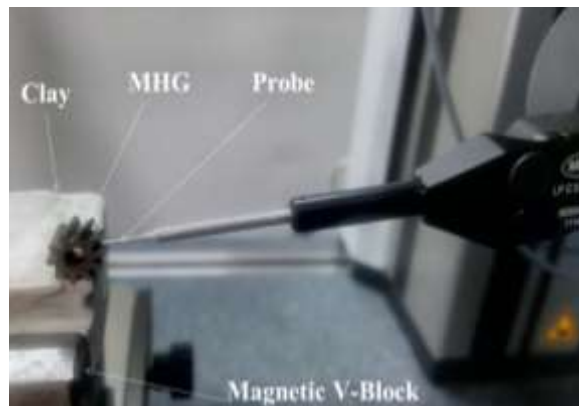
### 3.5.3 Measurements of Surface Roughness

Fig. 3.8 depicts measurement of surface roughness parameters (i.e. average surface roughness ' $R_a$ ', maximum surface roughness ' $R_{max}$ ', skewness ' $R_{sk}$ ' and kurtosis ' $R_{ku}$ ') of WSEM manufactured MBG (Fig. 3.8a) and MHG (Fig. 3.8b) by 3D-surface roughness measuring cum contour tracing equipment *LD130* from *Mahr Metrology, Germany* (refer

Appendix-B for details). This was done by tracing 10  $\mu\text{m}$  tip diameter probe at three different locations (i.e. middle and towards both the ends) on right hand flank of one tooth and left hand flank of its radially opposite gear tooth of MBG (or MHG) along the tooth profile (i.e. across the direction of wire path) for each experimental run. An evaluation length of 1.0 mm; cut-off or sampling length of 0.08 mm; and Gaussian filter (to distinguish between the roughness and waviness profiles) were used in the surface roughness measurements. Value of average surface roughness ' $R_a$ ' and maximum surface roughness ' $R_{max}$ ' for each experimental run was calculated by taking average of their corresponding six values measured.



**Fig. 3.8(a)**



**Fig. 3.8(b)**

**Fig. 3.8:** Measurements of surface roughness of WSEM manufactured meso-gears by LD130 surface roughness cum contour tracer for: (a) MBG; and (b) MHG.

### 3.5.4 Characterization of Surface Integrity

The following paragraphs present details of examination of microstructure, and evaluation of microhardness of WSEM manufactured best quality MBG and MHG.

#### 3.5.4.1 Microstructure Examination

Tooth profile, bore and microstructure of tooth flank surface of the best quality MBG and MHG were studied using field emission scanning electron microscope (FE-SEM) *SUPRA 55* from *Carl Zeiss, Germany* (refer Appendix-B for details). For this one randomly selected tooth of the best quality MBG and MHG obtained in the pilot experiments, validation experiments and comparative evaluation experiments were cut by WSEM process to prepare their samples for examination of the microstructure.

#### 3.5.4.2 Microhardness Testing

Vickers microhardness of flank surfaces of the best quality MBG and MHG and their parent material SS 304 was measured on *Zwick Roell* microhardness machine from *Zwick Testing Machines Ltd., UK* (refer Appendix-B for details). For this, one randomly

selected tooth of the best quality MBG and MHG obtained in the pilot experiments and comparative evaluation experiments were cut by WSEM process to prepare their samples. Evaluations of microhardness were done using 15 seconds as dwell time and 25  $\mu\text{m/s}$  as indentation speed for 200 g, 500 g and 1000 g of applied load. Each test was repeated three times and their average values were taken for the analysis purpose. In the present work, it helps to compare microhardness of the parent material and the recast layer formed on the flank surfaces of WSEM manufactured MBG and MHG.

### 3.5.5 Evaluation of Volumetric Gear Cutting Rate

Productivity of manufacturing process indicates speed of manufacturing a part. It helps in selecting a process for commercial purposes. In the present work, productivity of WSEM process was measured in the terms of volumetric gear cutting rate (*VGCR*). It is defined as the amount of the material removed per unit time and can be computed by the following relation equation:

$$VGCR = \frac{w}{\rho \times t} \quad \left( \frac{\text{mm}^3}{\text{min}} \right) \quad (3.1)$$

where,  $w$  is total material lost (g) during manufacturing of a MBG (or MHG) obtained by subtracting weight of meso-gear ( $W_{gear}$ ) and gear plate ( $W_{after}$ ) from the total weight of gear plate ( $W_{before}$ ) before machining i.e.  $w = W_{before} - (W_{after} + W_{gear})$ ;  $\rho$  is density of the gear material ( $\text{g/mm}^3$ ); and  $t$  is the total manufacturing time of MBG (or MHG). Weight of gear plate was measured on precision weighing machine make (model: *DS 852G*, from *Essae-Teraoka Ltd.*) having accuracy up to 0.01g. Manufacturing time of MBG and MHG was directly revealed on the monitor of WSEM or can be calculated by a digital stop watch having a least count of 0.01 seconds.

### 3.6 Analysis of the Experimental Results

Breakage of the wire was recorded through observations while cutting teeth of MBG and MHG in the preliminary experiments while the cutting rate was recorded from the display of the CNC WSEM machine. Results of the pilot experiments were analyzed by studying the influence of the selected parameters of WSEM on the considered responses. Results of the main experiments were analyzed using analysis of variance (ANOVA) to determine the significant parameters of WSEM and their significant interactions influencing the considered responses. It also evaluated the error variance for the main effects and the prediction error. The total variability in the experimental observations was divided into two components: (i) the variability among the different experiments; and (ii)

variability within a particular experiment. Based upon the ANOVA results, mathematical equations (referred as regression equations) of the considered responses were developed in terms of the significant parameters of WSEM and their interactions by regression analysis using results of the main experiments. Adequacy of the developed models was examined using  $R^2$  value and 95% confidence interval. Models of the considered responses were also developed by ANN using results of the main experiments. Optimum values of the four WSEM parameters (namely  $S_V$ ;  $T_{on}$ ;  $T_{off}$ ; and  $W_F$ ) were identified by (i) desirability function analysis using results of the main experiment; and (ii) real coded genetic algorithms (RCGA) using the developed regression equations of the considered responses as the objective functions and using the ranges of four WSEM parameters narrowed down for the main experiments as the variable bounds. Results of the optimization were confirmed by comparing values of the responses obtained from multi-objective optimization with results of the validation experiments and computing the corresponding errors.

The *next chapter* describe in details results of different stages of the experiments performed using the experimental plans described in this chapter along with their analyses, interpretations, and explanations.

## Chapter 4

### Results and Analysis

This chapter describes the observations and results of the experiments planned and conducted in different stages (i.e. preliminary, pilot, and main experiments), their analyses, interpretations, explanations, and major conclusions drawn from each stage.

#### 4.1 Observations and Conclusions of the Preliminary Experiments

Total 41 preliminary experiments were conducted for MBG and 41 for MHG cutting only one tooth for each meso-gear in each experiment and varying 9 parameters of WSEM (please refer Table 3.2 for details) using one-factor-at-a-time experimental design approach with an objective to narrow down their ranges for the pilot experiments using wire breakage and cutting rate of single tooth as responses. These experiments narrowed down ranges or value of the considered parameters of WSEM (as mentioned in Table 3.2) based upon following observations:

- ❖ No spark occurred when pulse peak voltage as 60 volts was used therefore, 110 volts was fixed as its value for further experimentation.
- ❖ Values of gap or servo voltage less than 10 volts and more than 50 volts caused unstable WSEM process due to low energy sparks (which consequently lowers the cutting rate) and due to occurrence of violent sparks respectively. Therefore, 10 to 50 volts was narrowed range for varying servo voltage during the pilot experiments.
- ❖ Pulse-on time more than 2.6  $\mu\text{s}$  caused frequent wire breakage whereas its value less than 0.6  $\mu\text{s}$  resulted in low cutting rate of meso-gear tooth. Consequently, pulse-on time was bracketed to be varied in 0.6 to 2.6  $\mu\text{s}$  during the pilot experiments.
- ❖ Pulse-off time less than 42.5  $\mu\text{s}$  caused frequent wire breakage and its maximum value on the WSEM machine used in the present work is 50.5  $\mu\text{s}$ . Therefore, 42.5 to 50.5  $\mu\text{s}$  was selected for varying pulse-off time during the pilot experiments.
- ❖ No wire breakage was observed while varying peak current in the range of 10 to 12A. Consequently, peak current was decided to be varied in this range during the pilot experiments.
- ❖ Wire feed rate less than 3 m/min caused frequent wire breakage whereas its higher value reduces duration of concentration of sparks at a particular location on the wire thus avoids frequent wire-breakage and also slightly improves the cutting rate. Therefore, wire feed rate was selected to vary in the range from 3 to 15 m/min (the

maximum value of wire feed rate available on the WSEM machine) for pilot experiments.

- ❖ Values of wire tension above 1260 g also caused frequent wire breakage whereas its value less than 540 g caused more deflection of wire and wire streak marks on the manufactured meso-gear tooth. Consequently, it was decided to vary wire tension from 540 to 1260 g during the pilot experiments.
- ❖ No wire breakage was observed using dielectric pressure as 7 or 15 kg/cm<sup>2</sup> (the only values available on the WSEM machine used in the present work) though slight increase in the meso-gear tooth cutting rate was observed using 15 kg/cm<sup>2</sup> as dielectric pressure. Therefore, it was decided to use these values during the pilot experiments.
- ❖ Using % cutting speed below 50 % caused unstable WSEM process with very slow meso-gear tooth cutting rate whereas, its value more than 100% made WSEM process unstable due to frequent wire breakage.

## 4.2 Results and Analysis of the Pilot Experiments

Total 31 *pilot experiments* were conducted separately for MBG and MHG using one-factor-at-time approach to identify optimum ranges and values of the eight parameters of WSEM for further experimentation by varying (or using) them in the ranges (or values) identified in preliminary experiments (refer Table 3.2 for details) and to fulfil the objectives as mentioned in the Subsection 3.3.2. These experiments further narrowed down ranges of servo voltage, pulse-on time, pulse-off time and wire feed rate and fixed the values of peak current, wire tension, dielectric pressure, and % cutting speed.

Tables 4.1 and 4.2 present values of the variable WSEM parameters and the considered parameters of microgeometry and surface roughness of MBG and MHG for the pilot experiments. Figures 4.1a-4.1h graphically depict the influence of the eight variable parameters of WSEM process on single pitch error ( $f_p$ ), total cumulative pitch error ( $F_p$ ) of MBG and total profile error ( $F_a$ ) and total cumulative pitch error ( $F_p$ ) of MHG whereas Figs. 4.3(a)-4.3(h) depict the same on  $R_a$  and  $R_{max}$  values of MBG and MHG. These figures depict experimental observations, best fit curves to these observations and their equations (green color graphs and equations for MBG and red color graphs and equations for MHG) obtained by regression analysis, and values of the constant parameters.

**Table 4.1:** Values of WSEM process parameters and the considered microgeometry parameters of MBG and MHG for the pilot experiments.

Exp. No.	WSEM process parameters								Microgeometry parameters of MBG						Microgeometry parameters of MHG					
	$I_P$ (A)	$T_{on}$ ( $\mu$ s)	$T_{off}$ ( $\mu$ s)	$S_V$ (V)	$W_F$ (m/min)	$W_T$ (g)	$W_P$ (kg/cm <sup>2</sup> )	$C_S$ (%)	Single pitch error ' $f_p$ ' ( $\mu$ m)			Total cumulative pitch error ' $F_p$ ' ( $\mu$ m)			Total profile error ' $F_a$ ' ( $\mu$ m)			Total cumulative pitch error ' $F_p$ ' ( $\mu$ m)		
									<i>RHF</i>	<i>LHF</i>	Avg.	<i>RHF</i>	<i>LHF</i>	Avg.	<i>RHF</i>	<i>LHF</i>	Avg.	<i>RHF</i>	<i>LHF</i>	Avg.
1	10																			
2	11	1.6	44.5	20	8	1020	15	75	24.40	21.00	22.70	78.50	76.50	76.55	30.70	22.10	26.40	32.80	30.00	31.40
3	12								16.40	25.70	21.05	63.30	67.30	65.30	24.10	27.50	25.80	31.60	20.70	26.15
4		0.6							18.50	20.30	19.40	17.80	36.80	27.30	12.10	18.50	15.30	11.00	15.40	13.20
5	12	1.1	44.5	20	8	1020	15	75	24.90	13.00	18.95	28.00	31.90	29.95	16.60	10.00	13.30	23.50	13.80	18.65
6		1.6							16.20	17.70	16.95	27.30	26.50	26.90	08.40	14.40	11.40	13.30	20.30	16.80
7		2.1							18.50	20.30	19.40	17.80	36.80	27.30	12.10	18.50	15.30	11.00	15.40	13.20
8		2.6							23.80	26.30	25.05	48.40	43.80	46.10	16.10	22.80	19.45	26.80	21.60	24.20
9			42.5						24.00	33.70	28.85	74.90	87.50	81.20	27.30	19.90	23.60	39.00	36.10	37.55
10	12	1.6	44.5	20	8	1020	15	75	26.50	29.20	27.85	68.30	39.90	54.10	30.70	22.10	26.40	32.80	30.00	31.40
11			46.5						18.50	20.30	19.40	17.80	36.80	27.30	12.10	18.50	15.30	11.00	15.40	13.20
12			48.5						16.90	12.70	14.80	21.80	45.00	33.40	12.00	14.90	13.45	08.40	16.90	12.65
13			50.5						11.10	15.10	13.10	27.30	29.80	28.55	11.60	17.00	14.30	07.30	17.30	12.30
14			44.5	10					26.10	26.60	26.35	24.10	36.50	30.30	12.20	17.40	14.80	14.50	19.00	16.75
15	12	1.6		20	8	1020	15	75	13.90	15.30	14.60	21.80	28.60	25.20	12.00	14.90	13.45	12.20	10.90	11.55
16				30					18.50	20.30	19.40	17.80	36.80	27.30	12.10	18.50	15.30	11.00	15.40	13.20
17				40					17.40	26.10	21.75	31.50	46.10	38.80	20.60	23.90	22.25	17.50	19.30	18.40
18				50					21.40	23.40	22.40	70.20	46.70	58.45	16.10	28.80	22.45	26.00	42.70	34.35
19				20	3				23.60	24.60	24.10	60.00	65.20	62.60	18.60	27.60	23.10	26.80	50.00	38.40
20	12	1.6	44.5		6	1020	15	75	26.70	29.20	27.95	71.60	93.00	82.30	22.80	31.70	27.25	21.50	24.30	22.90
21					9				19.20	23.50	21.35	53.10	49.80	51.45	13.20	13.70	13.45	16.80	22.40	19.60
22					12				17.10	21.70	19.40	31.50	38.10	34.80	09.80	12.10	10.95	12.50	23.40	17.90
23					15				11.10	16.70	13.90	26.60	38.20	32.40	11.00	09.60	10.30	12.40	18.90	15.70
24	12	1.6	44.5	20	8	540			12.20	16.60	14.40	23.90	37.10	30.50	<b>10.80</b>	<b>07.50</b>	<b>09.15</b>	<b>11.30</b>	<b>12.80</b>	<b>12.05</b>
25						900	15	75	19.90	31.80	25.85	77.60	90.00	83.80	22.30	26.10	24.20	23.00	24.70	23.85
26						1260			22.90	27.90	25.40	55.40	80.90	68.15	18.60	23.00	20.80	12.50	18.90	15.70
27	12	1.6	44.5	20	8	1020	7	75	<b>09.40</b>	<b>12.10</b>	<b>10.75</b>	<b>21.80</b>	<b>27.70</b>	<b>24.75</b>	13.90	14.70	14.30	16.10	11.70	13.90
28							15		32.20	21.50	26.85	62.00	67.10	64.55	10.70	22.70	16.70	32.50	29.60	31.05
29	12	1.6	44.5	20	8	1020	15	50	18.50	20.30	19.40	17.80	36.80	27.30	12.10	18.50	15.30	11.00	15.40	13.20
30								75	21.30	28.40	28.40	57.30	65.10	61.20	31.10	29.80	30.45	26.80	50.00	38.40
31								100	18.50	20.30	19.40	17.80	36.80	27.30	12.10	18.50	15.30	11.00	15.40	13.20
									20.00	27.90	23.95	42.30	32.20	37.25	16.10	28.80	22.45	30.40	23.80	27.10

**Table 4.2:** Values of WSEM process parameters and corresponding values of average and maximum surface roughness of MBG and MHG for the pilot experiments.

Exp. No.	WSEM process parameters									Surface roughness parameters ( $\mu\text{m}$ )			
	$I_p$ (A)	$T_{on}$ ( $\mu\text{s}$ )	$T_{off}$ ( $\mu\text{s}$ )	$S_v$ (V)	$W_F$ m/min	$W_T$ (g)	$W_P$ ( $\text{kg}/\text{cm}^2$ )	$C_S$ (%)	MBG		MHG		
									$R_a$	$R_{max}$	$R_a$	$R_{max}$	
1	10	1.6	44.5	20	8	1020	15	75	1.24	8.57	1.33	8.60	
2	11								1.41	9.39	1.53	8.93	
3	12								1.51	10.74	1.57	10.06	
4	12	0.6	44.5	20	8	1020	15	75	1.31	7.90	1.19	6.88	
5		1.1							1.36	8.69	1.24	7.75	
6		1.6							1.38	8.76	1.33	8.93	
7		2.1							1.43	9.93	1.52	9.73	
8		2.6							1.70	12.28	1.58	11.34	
9	12	1.6	42.5	20	8	1020	15	75	1.41	9.01	1.60	10.27	
10			44.5						1.38	8.83	1.44	9.80	
11			46.5						1.34	8.33	1.39	8.93	
12			48.5						1.15	7.85	1.33	8.48	
13			50.5						1.11	7.84	1.16	8.33	
14	12	1.6	44.5	10	8	1020	15	75	1.23	7.72	1.15	8.13	
15				20					1.24	7.72	1.33	8.93	
16				30					1.25	8.14	1.40	9.62	
17				40					1.33	8.57	1.43	10.31	
18				50					1.49	9.00	1.58	10.48	
19	12	1.6	44.5	20	3	1020	15	75	1.47	10.40	1.58	11.31	
20					6				1.31	8.76	1.49	10.03	
21					9				1.29	8.53	1.35	8.59	
22					12				1.24	7.56	1.34	8.09	
23					15				1.12	7.39	1.33	7.67	
24	12	1.6	44.5	20	8	540	15	75	1.46	10.40	1.45	9.75	
25						900			1.29	8.53	1.33	8.93	
26						1260			1.24	7.56	1.26	8.38	
27	12	1.6	44.5	20	8	1020	7	75	1.34	9.11	1.33	8.02	
28							15		1.24	8.57	1.30	7.90	
29	12	1.6	44.5	20	8	1020	15	50	1.24	8.57	1.32	8.77	
30								75	1.37	8.72	1.33	8.93	
31								100	1.47	9.10	1.43	9.15	

Subsections 4.2.1 and 4.2.2 describe and analyze the results and observations of the pilot experiments for microgeometry and surface roughness of MBG and MHG respectively. Subsection 4.2.3 analyzes the results for the MBG and MHG having minimum microgeometry errors.

#### 4.2.1 Influence WSEM Parameters on MBG and MHG Microgeometry

It can be seen in Fig. 4.1(a) that microgeometry errors in MBG and MHG decrease with increase in peak current and that total cumulative pitch error of MBG is more than that of MHG at any value of peak current. This can be explained by the fact that lower values of peak current causes generation of less number of sparks having lower discharge energy in the IEG which leads to improper cutting of the inclined gear teeth. However, lower peak current is more suitable for straight cutting of very thin and fragile

components. It is evident from Fig. 4.1(b) that (i) total cumulative pitch error in MBG and MHG decreases and then increase with increase in servo voltage thus showing existence of optimum range of servo voltage; and (ii) total cumulative pitch error of MBG is more than MHG whereas values of single pitch error of MBG, and total profile error of MHG are nearly same at any value of servo voltage. Figures 4.1(c) and 4.1(d) depict (i) existence of the optimum ranges of pulse-on time and pulse-off time because microgeometry errors in MBG and MHG decreases up to certain value of pulse-on and pulse-off time and then starts increasing; (ii) total cumulative pitch error of MBG varies significantly with pulse-on time and pulse-off time; and (iii) values of total cumulative pitch error for MBG are more than that of MHG at any value of pulse-on and pulse-off time. These observations can be explained by the fact that very small values of servo voltage and pulse-on time cause occurrence of sparks having insufficient discharge energy which leads to improper cutting of gear tooth which deteriorates microgeometry of MBG and MHG. Whereas, higher values of pulse-on time and servo voltage cause occurrence of higher discharge energy sparks making them violent which leads to production of irregular shaped, non-uniform, deep and wide craters and microcracks on flank surface of the MBG and MHG (as shown in Fig. 4.2) again increasing microgeometry errors along with surface roughness. Lowering values of the pulse-off time increases the frequency of the sparks causing formation of irregular shaped deeper craters on the flank surfaces of the meso-gear deteriorating their microgeometry. Increase in pulse-off time decreases frequency of sparks which causes drop in temperature due to loss of substantial amount of discharge energy of sparks to the surroundings. This makes the available discharge energy insufficient for melting and vaporization of the workpiece which leads to improper cutting of inclined gear teeth. Figures 4.1(e) and 4.1(f) depict that (i) increase in wire feed rate and wire tension non-linearly decreases the single pitch and total cumulative pitch errors in MBG and total profile and total cumulative pitch errors in MHG; and (ii) total cumulative pitch error of MBG is more than that of MHG at any value of wire feed rate and wire tension. This is due to the fact that higher wire feed rate makes availability of fresh wire at faster rate for machining by spark erosion. This reduces duration of concentration of sparks at a particular location on the wire and prevents wire-breakage frequently which otherwise adversely affects quality of WSEM manufactured meso-gears. Increased wire tension avoids wire deflection or lag, wire streaks and wire vibration marks which otherwise deteriorate quality of the flank surfaces. Also, higher wire tension leads to the easy and rapid removal of the eroded particles from the IEG. Therefore, higher wire

tension and wire feed rate are desirable during taper cutting to achieve better dimension accuracy, profile and surface finish. Figure 4.1(g) illustrates that increase in dielectric pressure significantly decreases total cumulative pitch error of MBG and MHG and slightly decreases single pitch error of MBG and total profile error of MHG. Increased dielectric pressure helps in efficient cleaning of IEG by flushing out the debris formed due to material removal by spark erosion in WSEM and prevents formation of the recast layer. Figure 4.1(h) shows existence of 75% of the cutting speed (i.e. 3.60 mm/min for MBG and 3.88 mm/min for MHG) as its optimum value because parameters of microgeometry of MBG and MHG decrease with % of the cutting speed, attain their minimum values, and then again start increasing. This can be explained by the fact that higher % cutting speed is used for machining the straight edges while medium value of % cutting speed is required for machining the sharp corners, taper and complex profiles without frequent wire breakages. Use of low values of % cutting speed increases the meso-gear manufacturing time. The operating manual of the WSEM machine used in the present work also recommends use of 75% of the cutting speed as the most suitable for manufacturing MBG and MHG using 0.25 mm diameter soft plain brass wire.

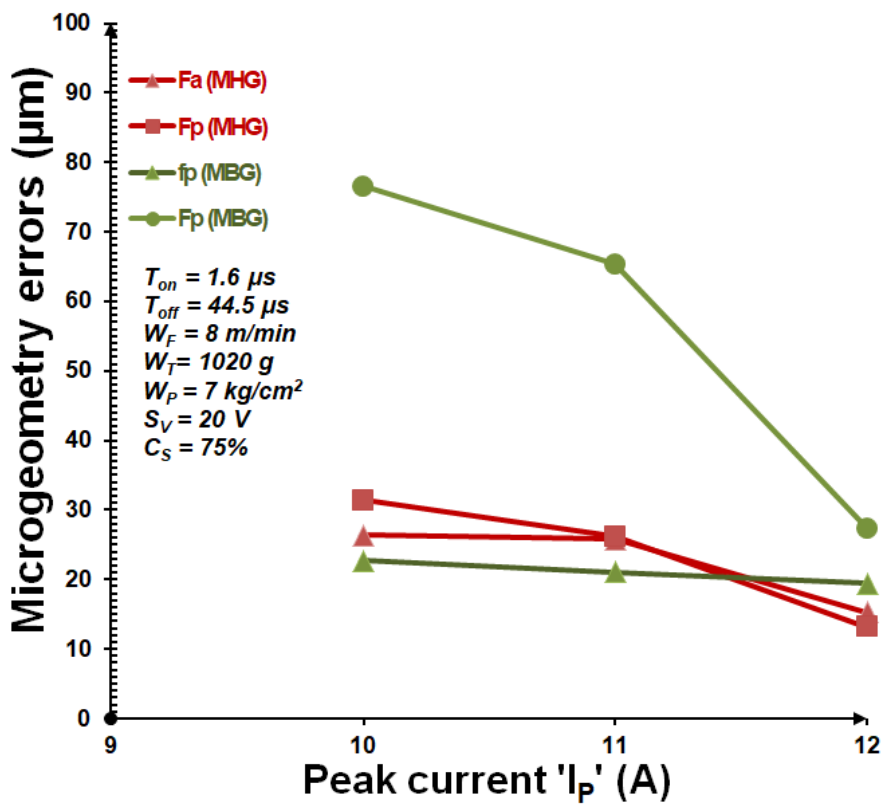


Fig. 4.1(a)

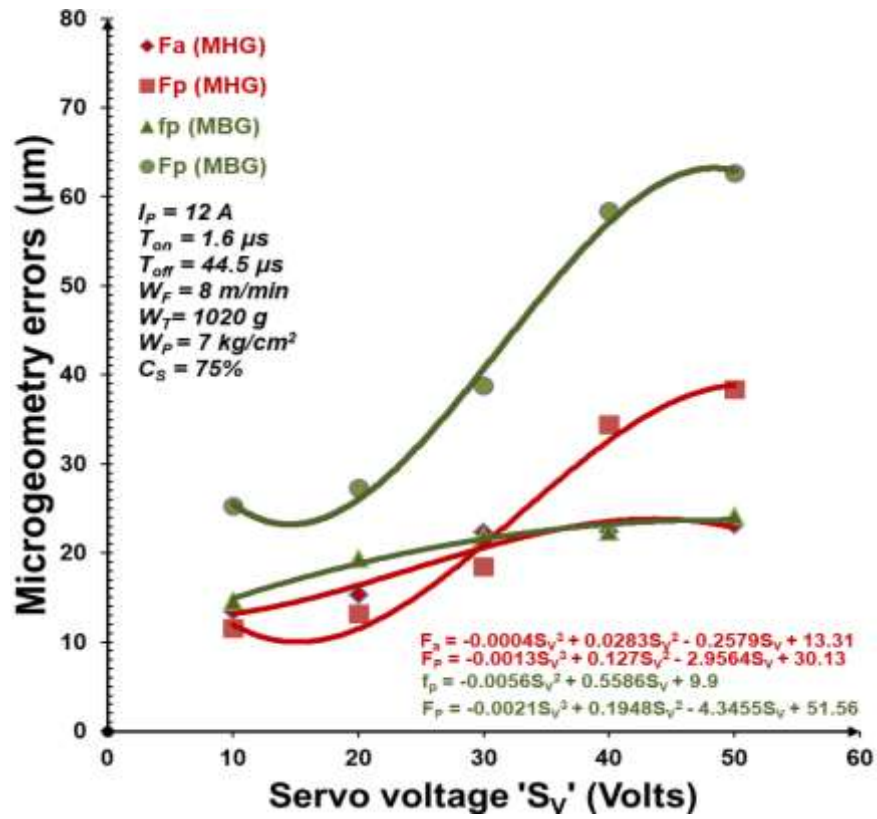


Fig. 4.1(b)

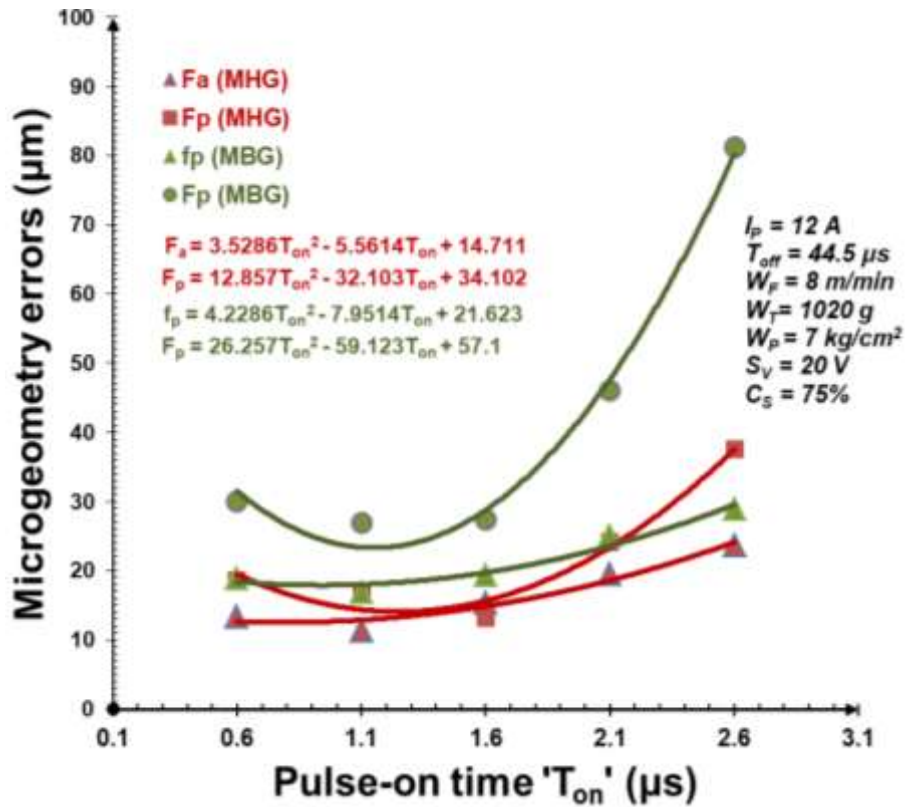


Fig. 4.1(c)

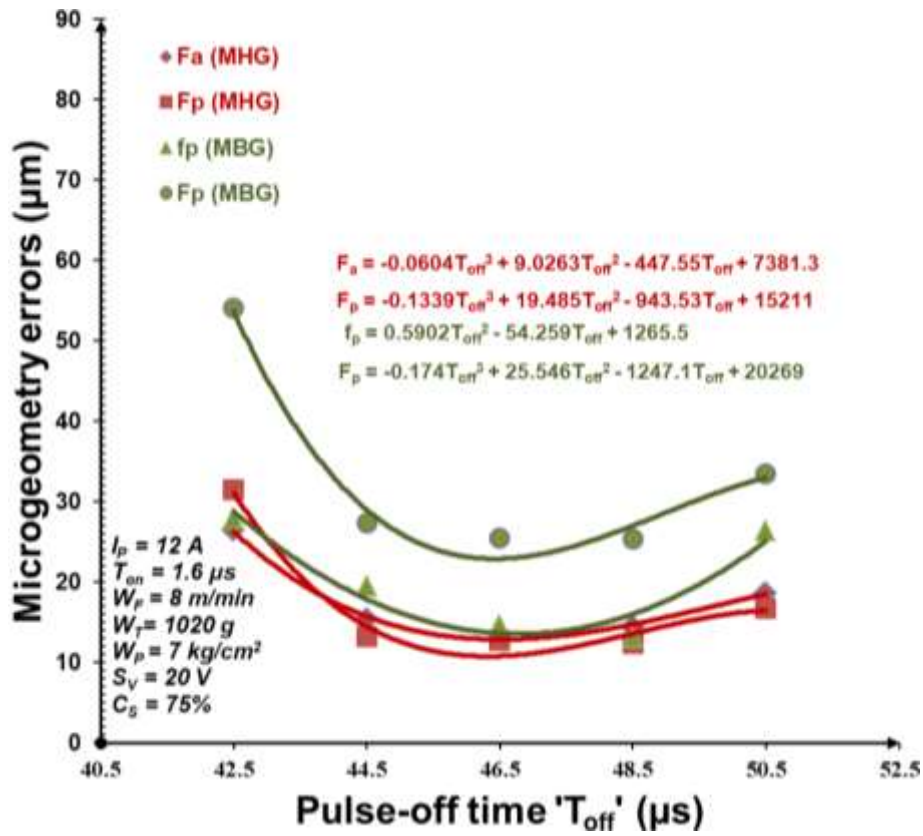


Fig. 4.1(d)

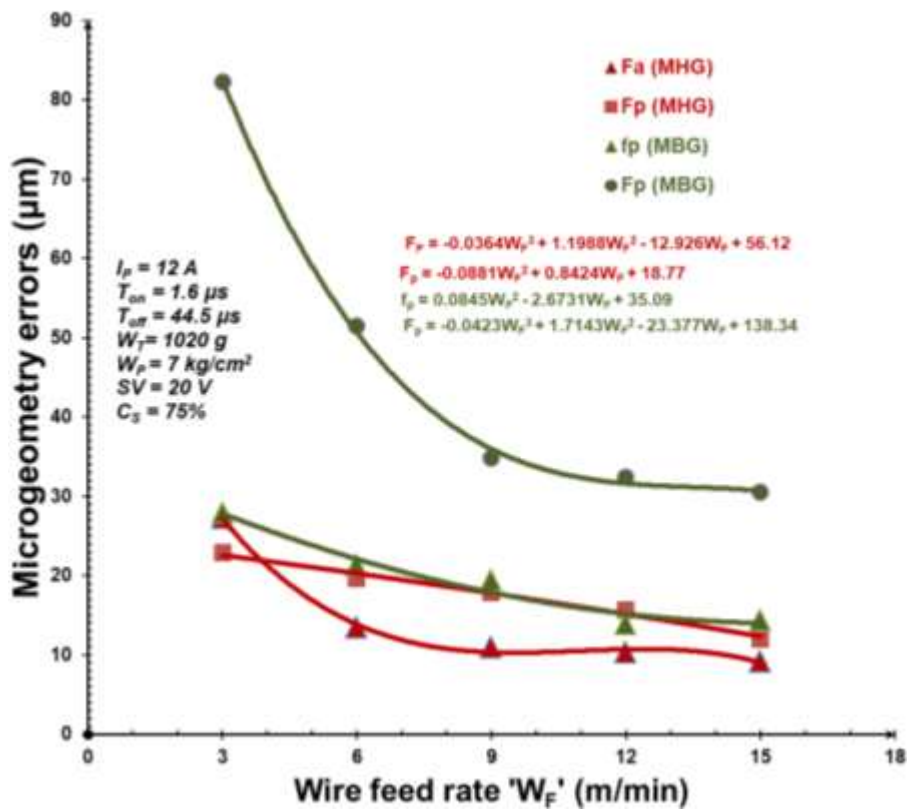


Fig. 4.1(e)

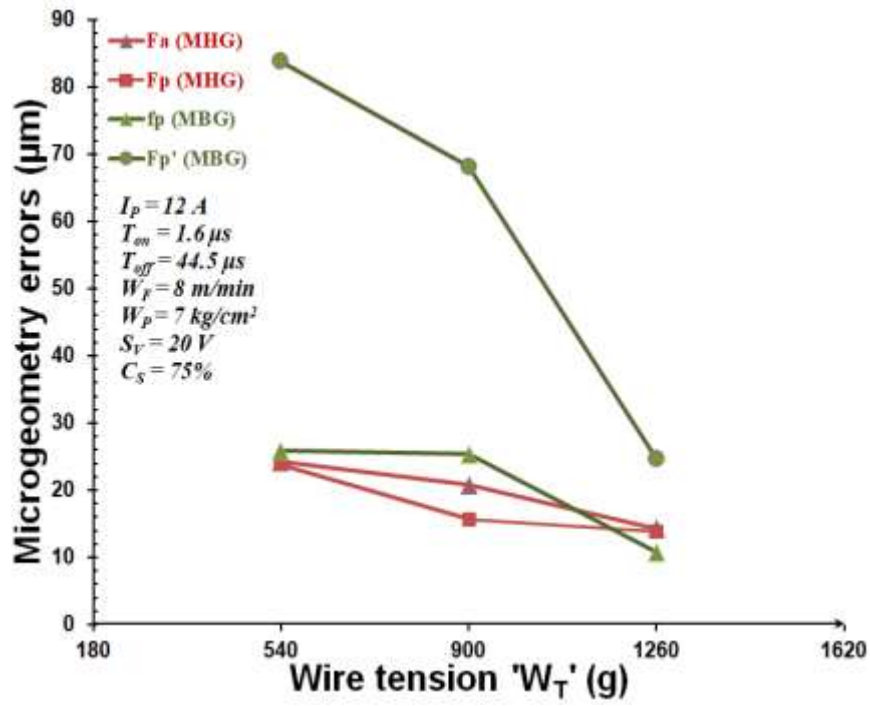


Fig. 4.1(f)

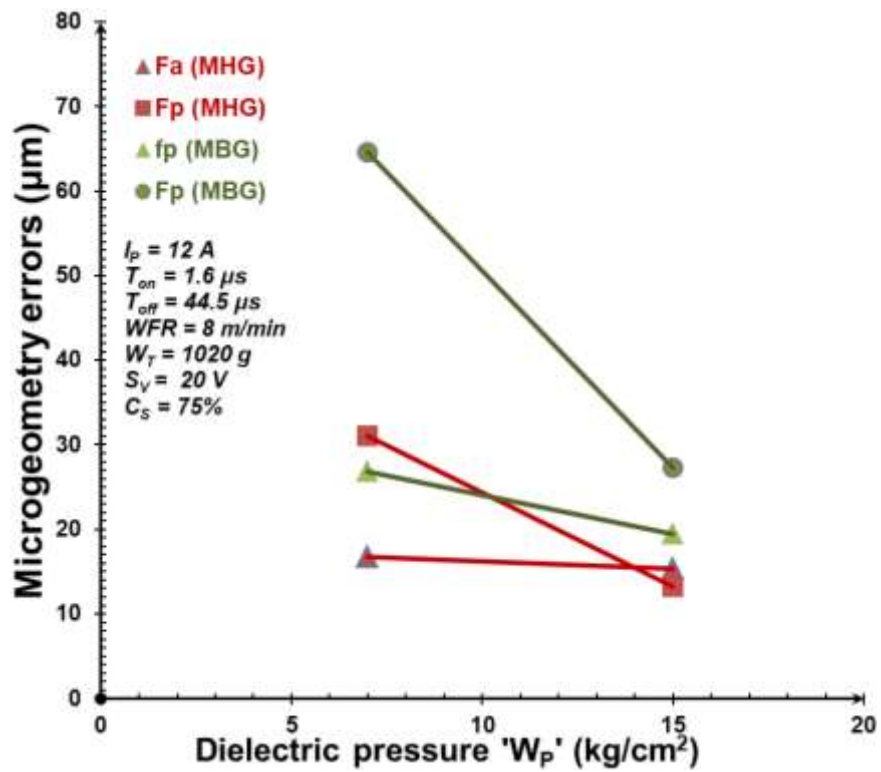


Fig. 4.1(g)

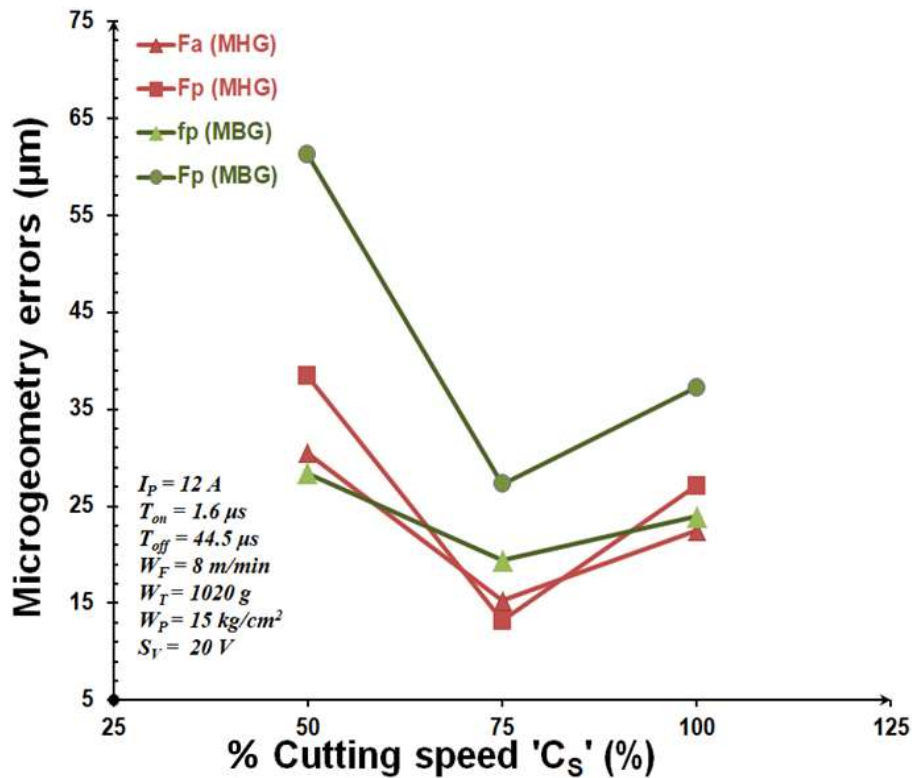


Fig. 4.1(h)

**Fig. 4.1:** Variation of single pitch error ' $f_p$ ' and total cumulative pitch error ' $F_p$ ' for MBG, and total profile error ' $F_a$ ' and total cumulative pitch error ' $F_p$ ' for MHG with: (a) peak current; (b) servo voltage; (c) pulse-on time; (d) pulse-off time; (e) wire feed rate; (f) wire tension; (g) dielectric pressure; (h) % cutting speed.

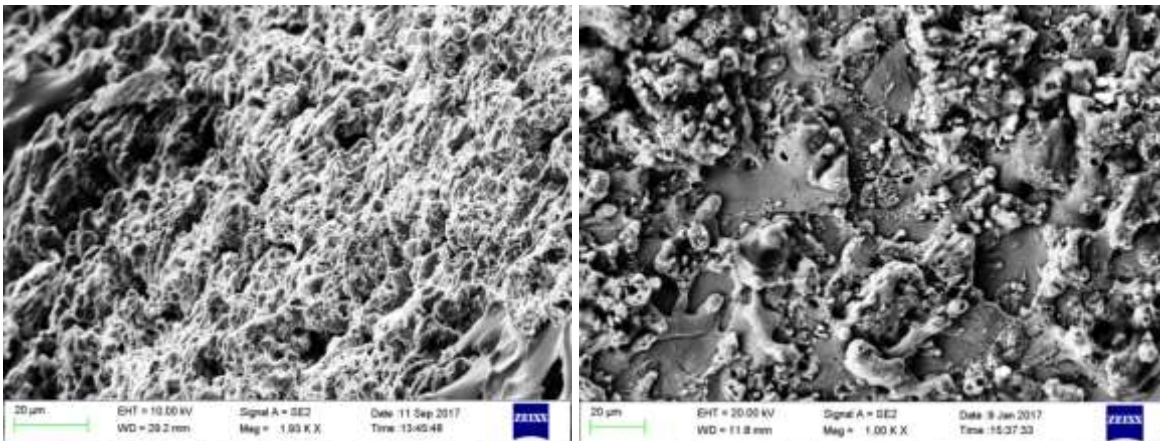


Fig. 4.2(a)

Fig. 4.2(b)

**Fig. 4.2:** SEM images showing irregular shaped deep craters on tooth flank surface of the meso-gears manufactured by WSEM process: (a) MBG; and (b) MHG.

#### 4.2.2 Influence of WSEM Parameters on MBG and MHG Surface Roughness

It can be seen in Figure 4.3(a) that  $R_a$  and  $R_{max}$  of MBG and MHG increase with increase in peak current. This can be explained by the fact that increase in peak current

increases energy released per spark making spark violent which causes production of non-uniform, irregular shaped deep and wide craters on flank surfaces of the MBG and MHG which increase both surface roughness and MRR. It can also be observed from Fig. 4.3(a) that  $R_{max}$  of MBG is more than that of MHG whereas  $R_a$  of MBG is less than that of MHG. This is due to complicated conical geometry of MBG teeth which obstructs smooth movement of wire resulting in presence of more surface peaks on its flank surfaces than that of MHG. It is evident from Fig. 4.3(b) that  $R_{max}$  values of MBG and MHG increase linearly while their  $R_a$  values increase non-linearly with the servo voltage. Higher value of servo voltage increases discharge energy of the sparks making them violent and causes deflection and vibrations of the wire. This leads to the formation of irregular shaped deeper craters as shown Fig. 4.2, wire streaks and vibration marks on flank surfaces of the MBG and MHG deteriorating their surface finish. Fig. 4.3(c) shows that  $R_a$  and  $R_{max}$  increase linearly for MHG and non-linearly for MBG with pulse-on time. Higher pulse-on time increases duration of transfer of discharge energy of a spark to the wire and the meso-gear blank. This increases chances of wire deflection, wire breakage and melting and deposition of wire on flank surfaces of the meso-gears deteriorating their surface finish. Fig. 4.3(d) depicts that  $R_a$  of MBG and MHG decreases linearly while their  $R_{max}$  show non-linearly decreasing trend with increase in pulse-off time. This is due to decreased occurrence of frequency of the sparks with increase in pulse-off-time which reduces numbers of craters formed thus decreasing surface roughness and MRR. Increase in wire feed rate [Fig. 4.3(e)] decreases  $R_a$  and  $R_{max}$  of MBG and MHG. This is due to the fact that higher wire feed rate makes fresh wire available for machining by spark erosion at a faster rate thus reducing duration of spark concentration at a particular location on the wire which decreases wire-breakage and wire deflection. This improves surface finish of the WSEMed meso-gears. Increase in wire tension [Fig. 4.3(f)] decreases  $R_a$  and  $R_{max}$  of MBG and MHG because increased wire tension avoids wire deflection, taper, wire streaks and vibration marks thus reducing their surface roughness. Fig. 4.3(g) depicts that increase in dielectric pressure does not affect significantly  $R_a$  and  $R_{max}$  of MHG whereas  $R_a$  and  $R_{max}$  of MBG decrease slightly. Increased dielectric pressure helps in efficient cleaning of IEG by flushing out the debris formed due to spark erosion and prevents formation of the recast layer. It can be seen from Fig. 4.3(h) that  $R_a$  and  $R_{max}$  of MBG and  $R_{max}$  of MHG continuously increase with increase in % of the cutting speed (base values are 3.60 mm/min for MBG and 3.88 mm/min for MHG) while  $R_a$  of MHG show existence of optimum value of % cutting speed.

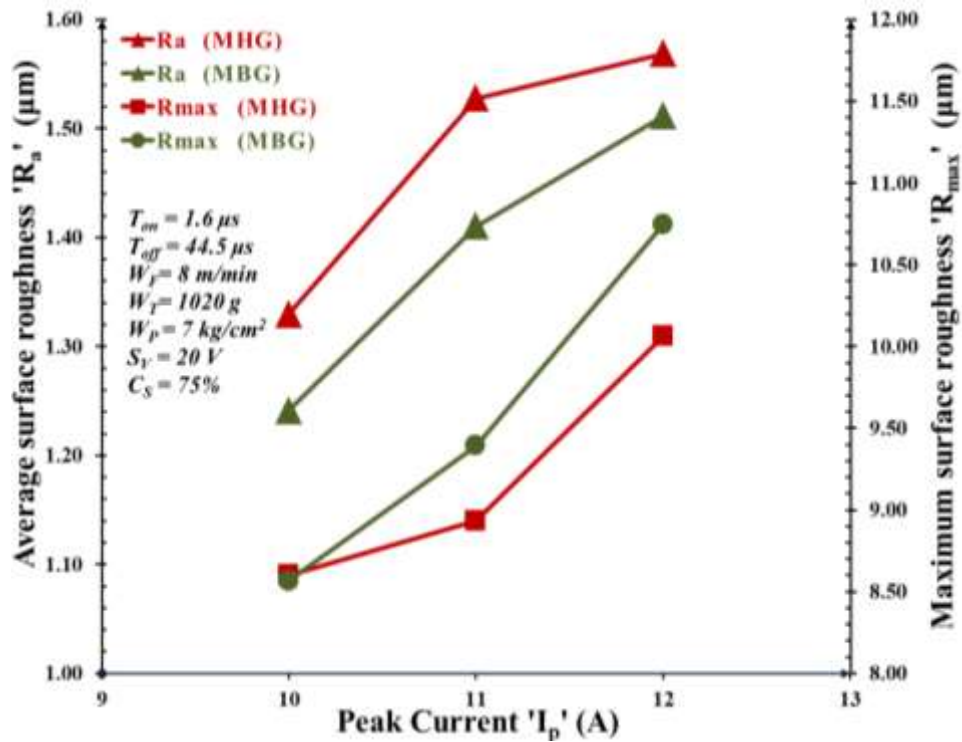


Fig. 4.3(a)

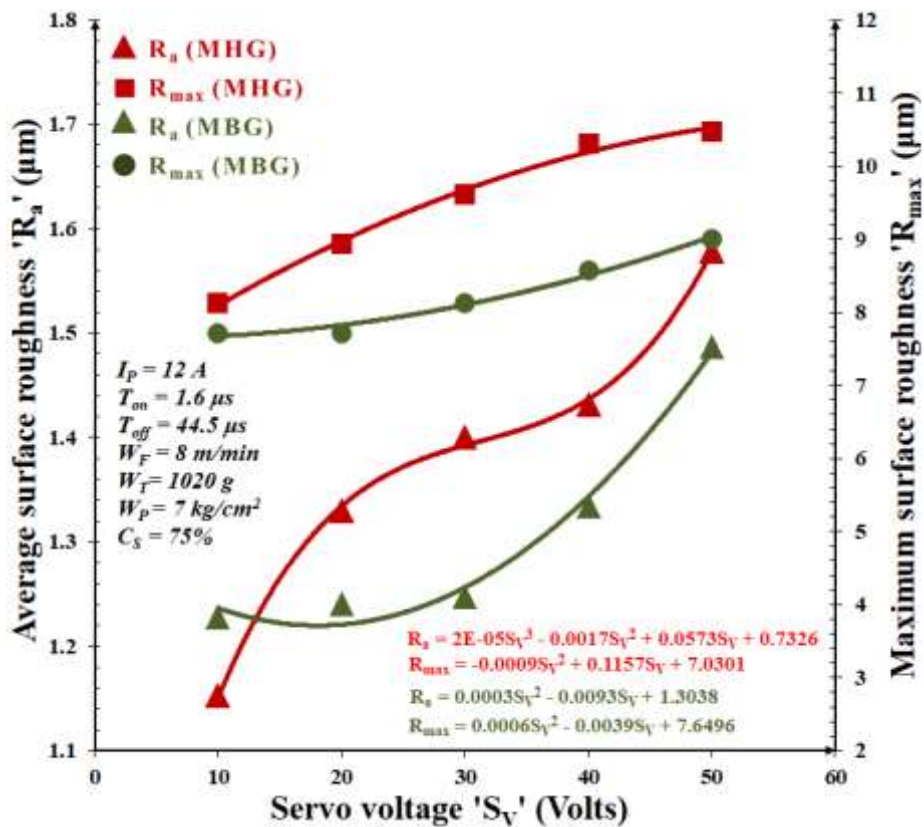


Fig. 4.3(b)

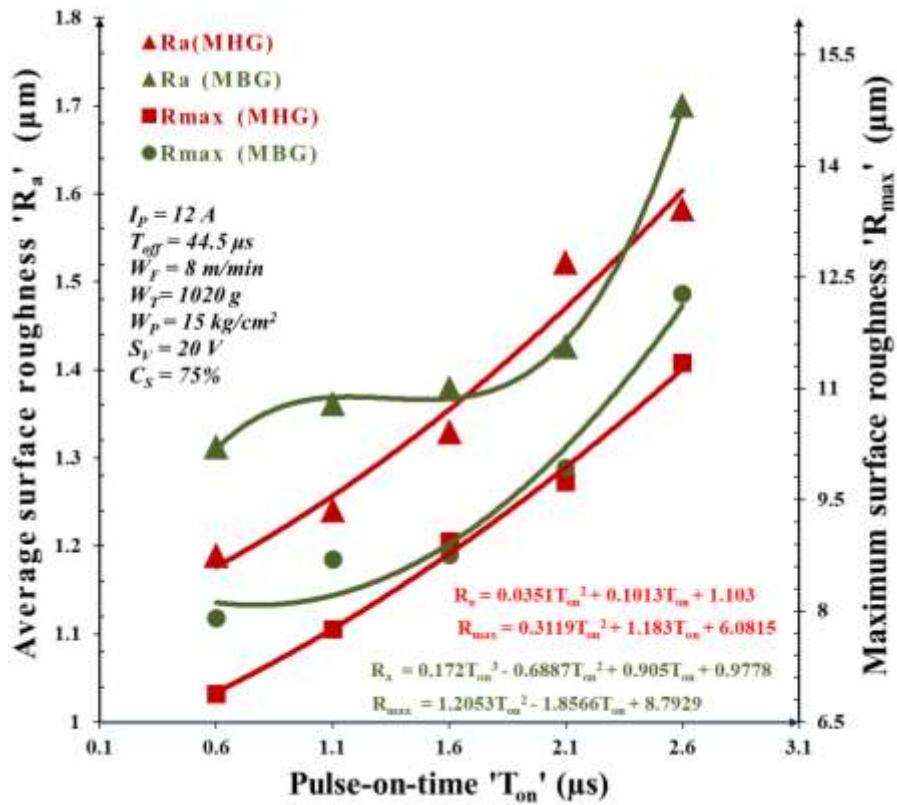


Fig. 4.3(c)

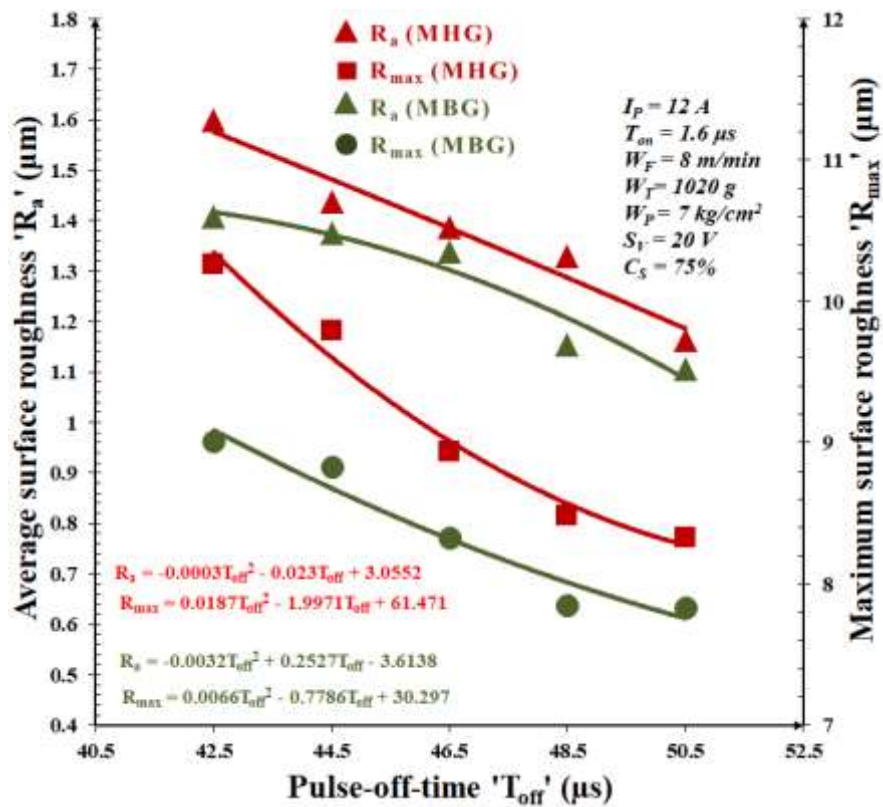


Fig. 4.3(d)

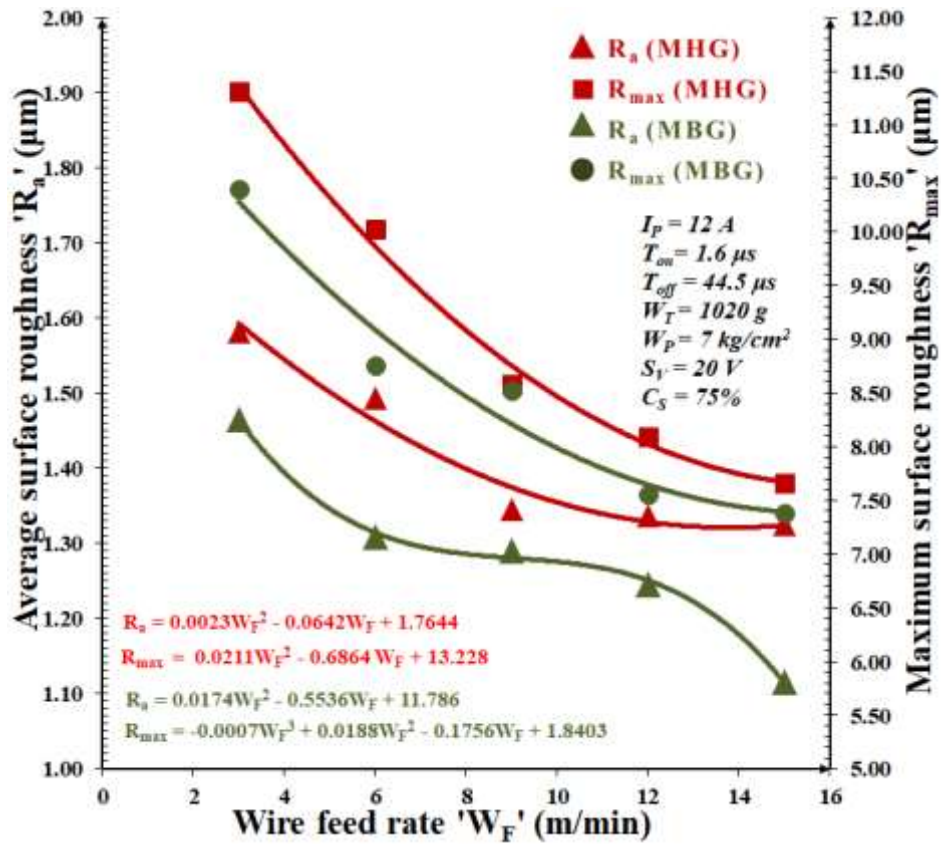


Fig. 4.3(e)

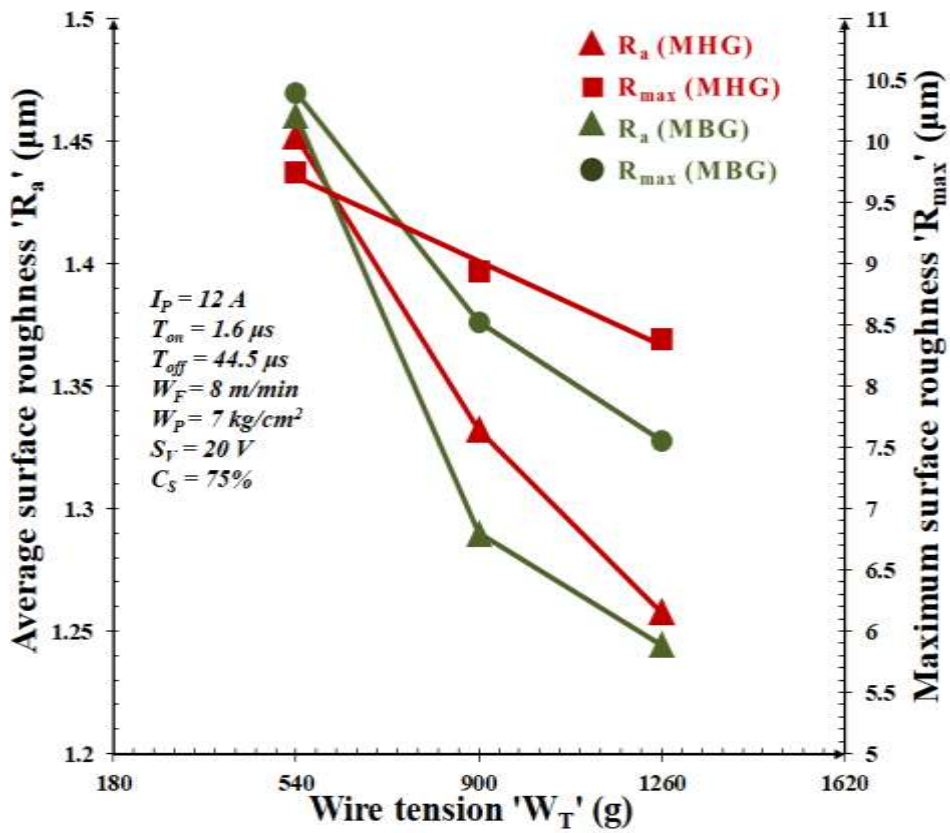


Fig. 4.3(f)

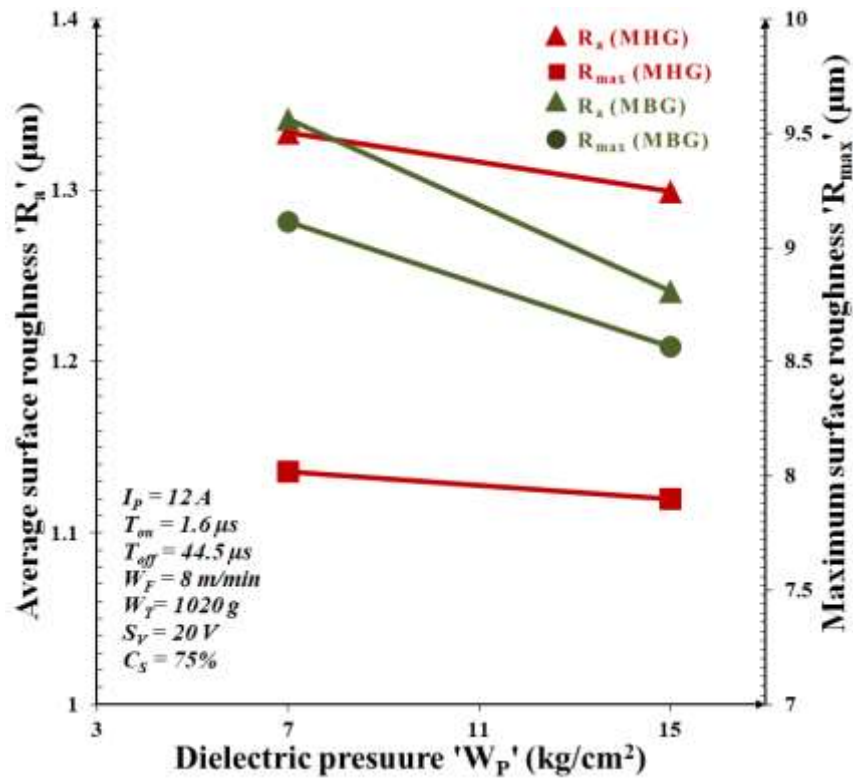


Fig. 4.3(g)

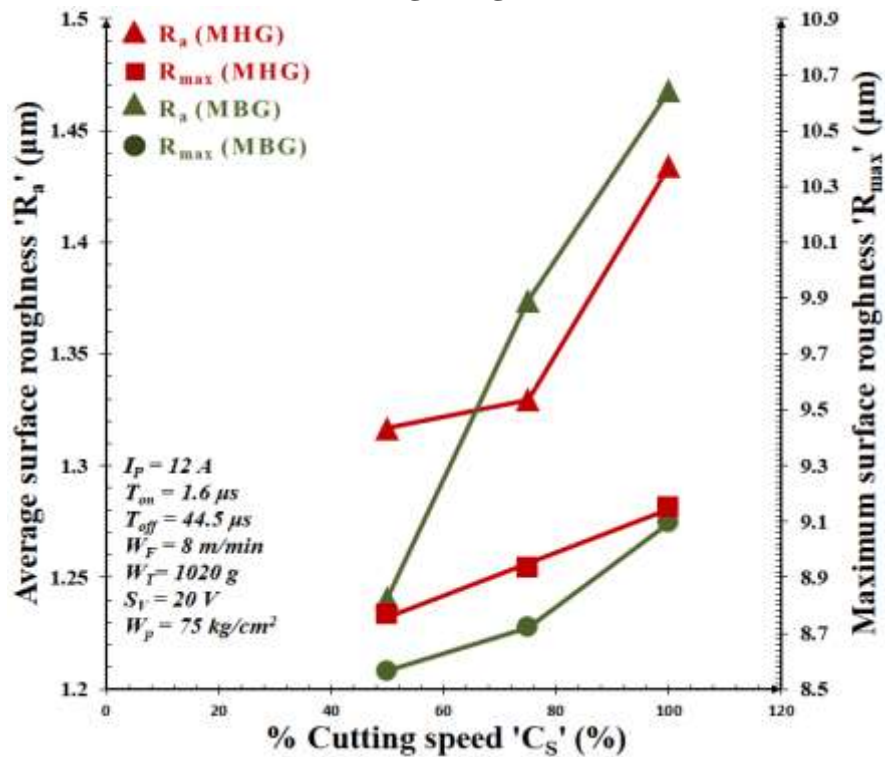


Fig. 4.3(h)

Fig. 4.3: Variation in average surface roughness and maximum surface roughness with WSEM process parameters for MBG and MHG: (a) peak current; (b) servo voltage; (c) pulse-on time; (d) pulse-off time; (e) wire feed rate; (f) wire tension; (g) dielectric pressure; and (h) % cutting speed.

### 4.2.3 Analysis of MBG and MHG having Minimum Microgeometry Errors

Details investigations on microgeometry errors, surface roughness parameters, flank surface topography, microhardness, and microstructure were carried for the MBG and MHG found to have minimum errors in their microgeometry from the pilot experiments and these are being referred as ‘better quality MBG and MHG’. It can be observed from Table 4.1 that better quality of MBG and MHG were manufactured in experiments number 26 and 23 respectively which have parametric combination of 12 A peak current; 20 volts servo voltage; 1.6  $\mu\text{s}$  pulse-on time; 44.5  $\mu\text{s}$  pulse-off time; 1020 g wire tension; 15  $\text{kg}/\text{cm}^2$  dielectric pressure; and 75% of the cutting speed. Only difference is in the wire feed rate. Better quality MBG (exp. no. 26) and MHG (exp. no. 23) were achieved using 8 m/min and 15 m/min wire feed rate respectively. Following paragraphs describe their results and analysis of the better quality MBG and MHG.

#### 4.2.3.1 Microgeometry

Microgeometry parameters of MBG and MHG were measured against DIN 8 and DIN 9 standard respectively on both left and right tooth flank of randomly selected three teeth for measurement of total profile error ‘ $F_a$ ’ and on both right and left hand flanks of all the teeth for measurement of locations error (i.e. single pitch error ‘ $f_p$ ’, adjacent pitch error ‘ $f_u$ ’, total cumulative pitch error ‘ $F_p$ ’ and radial runout ‘ $F_r$ ’) and average of the measured values were used for further analysis. Table 4.3 presents summary of these microgeometry parameters for the better quality MBG and MHG. It can be observed from this table that (i) quality of MHG is better than MBG for single pitch error, total cumulative pitch error and radial runout; and (ii) quality of MBG is better than MHG for adjacent pitch error.

**Table 4.3:** Summary of microgeometry errors for better quality MBG and MHG.

Microgeometry parameter	Value for better quality MBG			DIN quality	Value for better quality MHG			DIN quality
	RHF	LHF	Avg.		RHF	LHF	Avg.	
Total profile error ‘ $F_a$ ’ ( $\mu\text{m}$ )	NA	NA	NA	NA	7.5	10.8	9.15	DIN 7
Single pitch error ‘ $f_p$ ’ ( $\mu\text{m}$ )	9.4	12.1	10.75	DIN 7	8.6	8.4	8.5	DIN 6
Adjacent pitch error ‘ $f_u$ ’ ( $\mu\text{m}$ )	11.3	14.0	12.65	DIN 7	13.2	15.5	14.35	DIN 8
Total cumulative pitch error ‘ $F_p$ ’ ( $\mu\text{m}$ )	21.8	27.7	24.75	DIN 7	12.8	11.3	12.05	DIN 6
Radial runout ‘ $F_r$ ’ ( $\mu\text{m}$ )		46.3		DIN 10		20.2		DIN 8

Figure 4.4 presents report of microgeometry investigations for single pitch error, adjacent pitch error [Fig 4.4(a)] and total cumulative pitch error and radial runout [Fig. 4.4(b)] for better quality MBG indicating DIN quality number 7 corresponding to single pitch error value of 10.75  $\mu\text{m}$ , DIN quality number 7 for adjacent pitch error value of

12.65  $\mu\text{m}$  and *DIN* quality number 7 for total cumulative pitch error value of 24.75  $\mu\text{m}$ ; and *DIN* quality number 10 corresponding to radial runout value of 46.3  $\mu\text{m}$ .

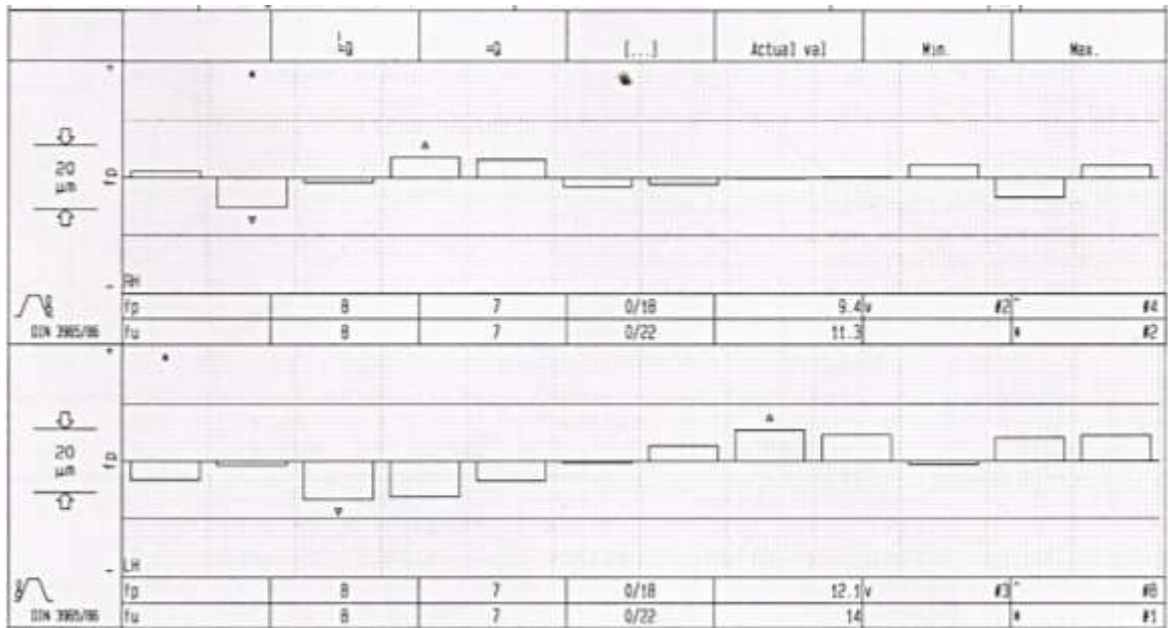


Fig. 4.4(a)

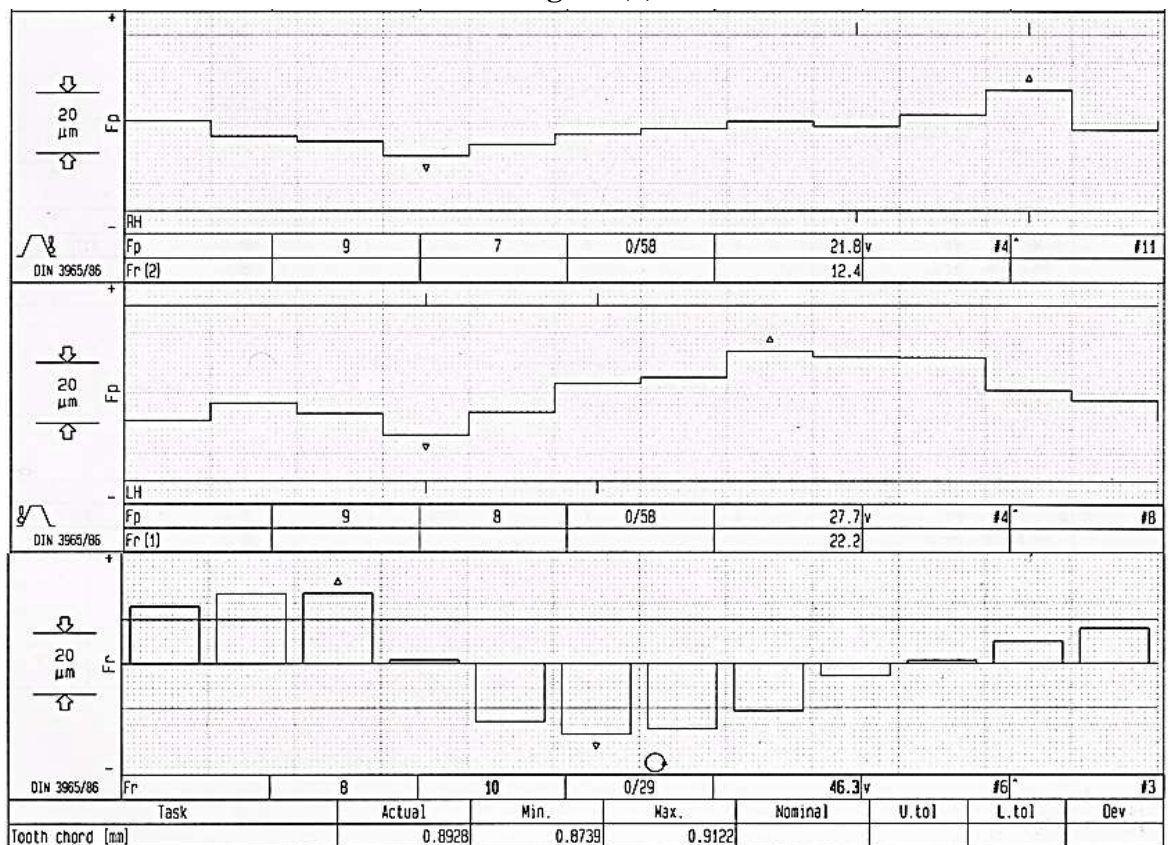


Fig. 4.4(b)

**Fig. 4.4:** Microgeometry investigation graphs showing *DIN* quality number for both left and right hand flanks of better quality MBG: (a) single pitch error ' $f_p$ ', adjacent pitch error ' $f_u$ '; and (b) total cumulative pitch error ' $F_p$ ' and radial runout ' $F_r$ '.

Figure 4.5(a) shows microgeometry graphs of the total profile errors ( $F_a$ ) for left flank (LHF) and for right flank (RHF) of three randomly chosen teeth (i.e. tooth no. 1; 4; and 8) of the better quality MHG, their mean values ( $x$ ) and *DIN* quality number. Blue colored vertical straight lines represent the best fit curves to the black colored actual profiles of MHG teeth indicating total profile error value of  $9.15 \mu\text{m}$  and accordingly *DIN* quality number 7. Figure 4.5(b) depicts graphical representation of single pitch error and adjacent pitch error showing *DIN* quality numbers 6 and 8 and corresponding values of  $8.5 \mu\text{m}$  and  $14.35 \mu\text{m}$  respectively. Figure 4.5(c) shows microgeometry graphs for total cumulative pitch error and radial runout showing their values as  $12.05 \mu\text{m}$  and  $20.2 \mu\text{m}$  and corresponding *DIN* quality numbers as 6 and 8 respectively for the better quality MHG.

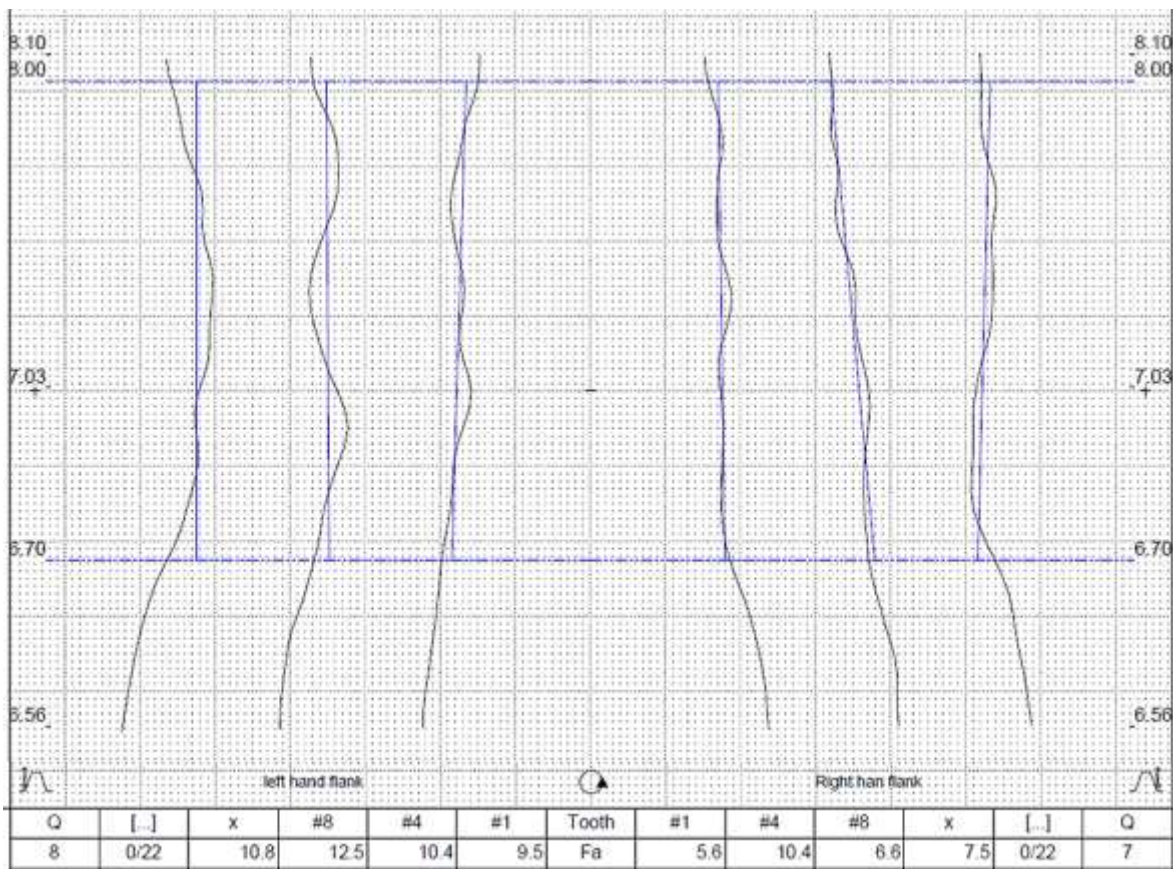


Fig. 4.5(a)



Fig. 4.5(b)



Fig. 4.5(c)

**Fig. 4.5:** Microgeometry investigation graphs showing DIN quality number for both left and right hand flanks of better quality MHG: (a) total profile error ' $F_a$ '; (b) single pitch error ' $f_p$ ' and adjacent pitch error ' $f_u$ ' and (c) total cumulative pitch error ' $F_p$ ' and radial runout ' $F_r$ '.

### 4.2.3.2 Flank Surface Topography

Topography of the left and right hand flanks of randomly chosen tooth of the better quality MBG and MHG was obtained to get complete information of their tooth flank surfaces in single measurement and they are depicted in Figures 4.6(a) and 4.6(b) respectively. The tooth flank surfaces of these meso-gears were divided into nine equal segments along the face width or lead and four equal segments from tip to root along the tooth profile. Grids formed by these segments help in the analyzing flank surface at any specific location. In figures 4.6(a) and 4.6(b), theoretical flank surfaces are represented in blue color grid lines and the actual flank surfaces in green color grid lines for MBG and in black color grid lines for MHG. Red coloured vertical line represents amount of deviation. It can be seen from Fig. 4.6(a) that average values (taken from right and left hand flanks) of deviations for MBG at root and tip of heel side are  $-7.7 \mu\text{m}$  and  $4.8 \mu\text{m}$  respectively and at root and tip of toe side are  $-4.5 \mu\text{m}$  and  $4.6 \mu\text{m}$  respectively. It is evident from Fig. 4.6(b) that amount of deviations for MHG are also less than  $20 \mu\text{m}$

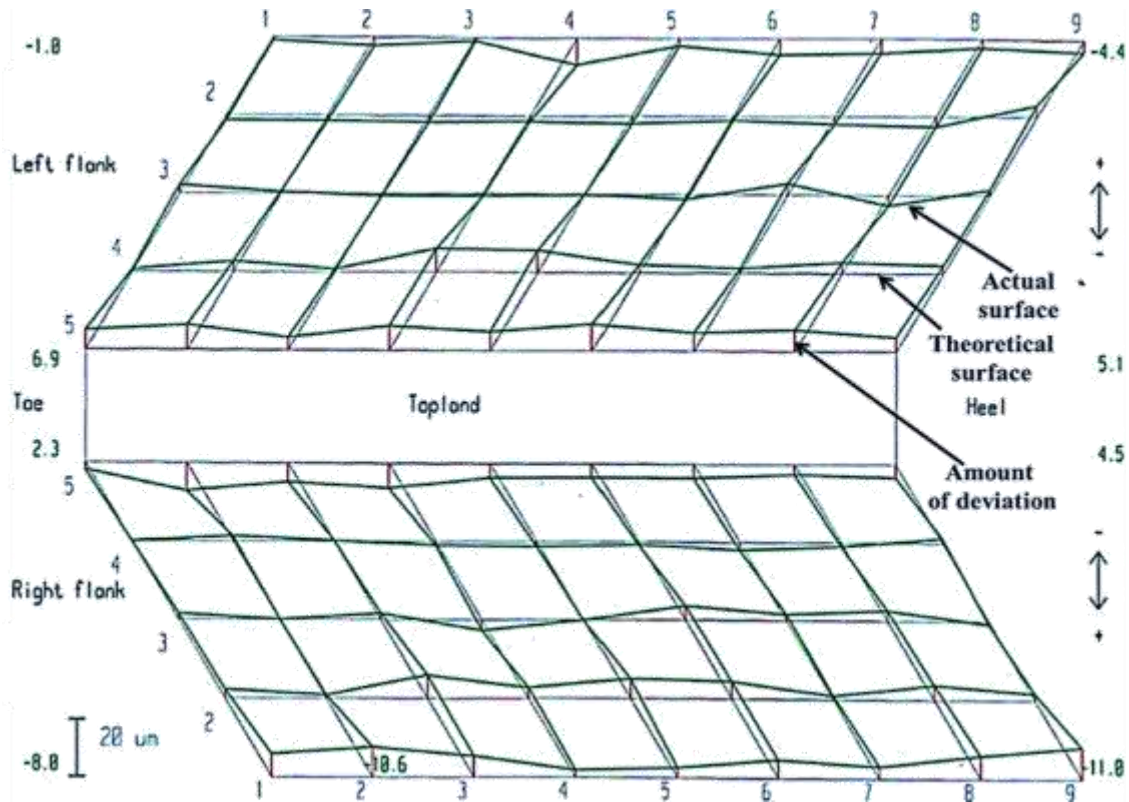
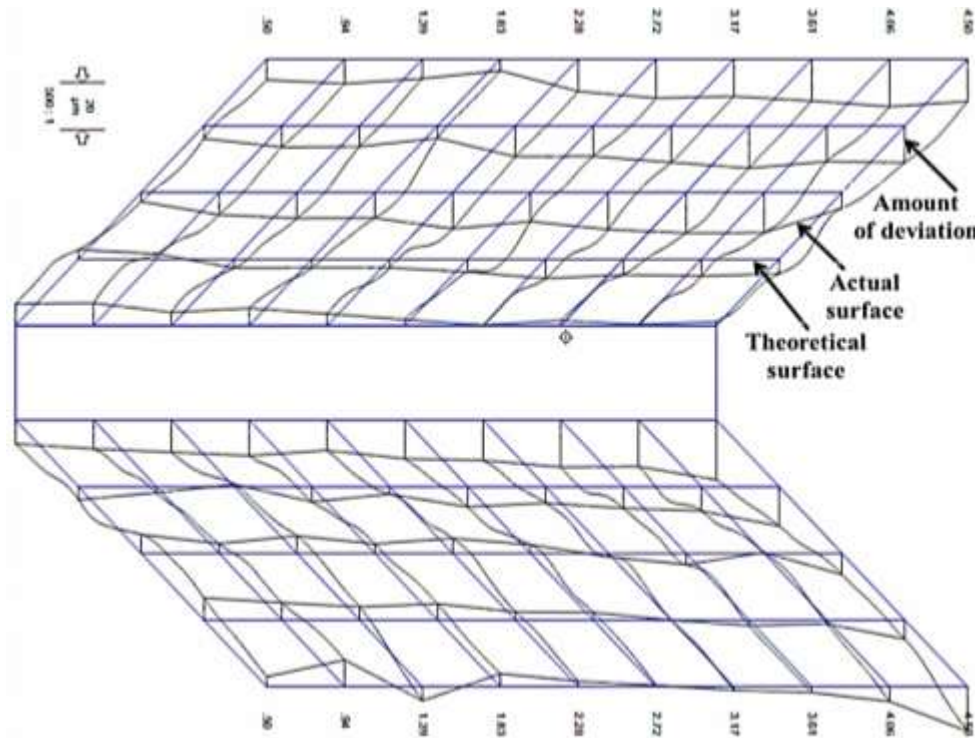


Fig. 4.6(a)



**Fig. 4.6(b)**

**Fig. 4.6:** Flank surface topography of the better quality (a) MBG; and (b) MHG.

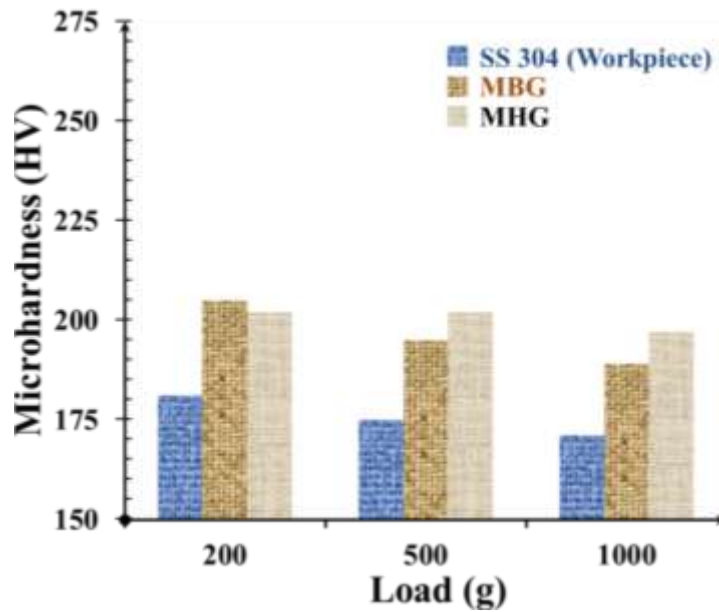
#### 4.2.3.3 Surface Roughness

Average surface roughness ' $R_a$ ' values and maximum surface roughness ' $R_{max}$ ' values for the better quality MBG and MHG were found to be 1.24 and 1.33  $\mu\text{m}$ ; and 7.56 and 7.67  $\mu\text{m}$  respectively.

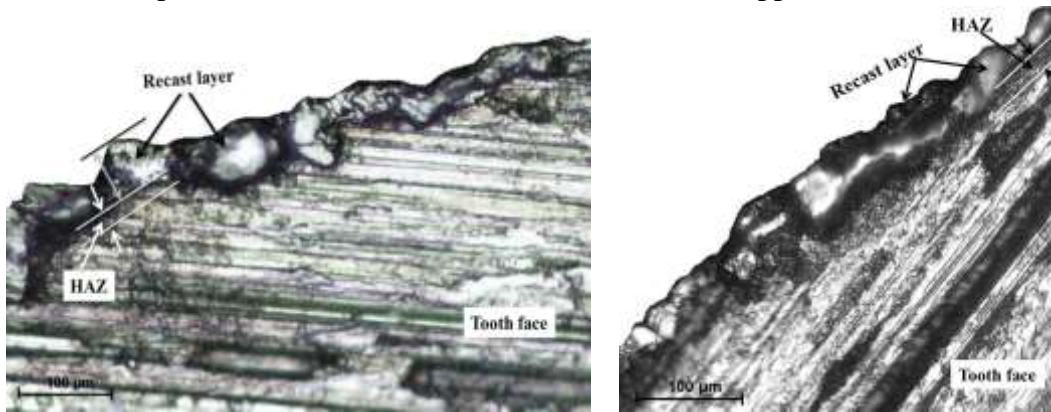
#### 4.2.3.4 Microhardness

Figure 4.7 depicts the microhardness of the better quality MBG and MHG manufactured by WSEM process and their material (i.e. SS 304) for three different values of the applied load. It reveals that microhardness of better quality MBG and MHG is higher than their material at all three values of the applied load due to formation of very thin recast layer (i.e. re-deposition of the eroded particles on top surface of the machined surface) on tooth flank surfaces of MBG and MHG shown in Figures 4.8(a) and 4.8(b) respectively. Microstructure and surface characteristics of this recast layer are different than the parent material and this is true for stainless steel also. If microcracks and non-uniform deeper and wider craters exist in the recast layer then it will adversely affect fatigue strength, surface quality and service life of the meso-gears (Zhang, 2011). This recast layer is sometime difficult to remove due to its higher hardness and cohesion. Rapid quenching in the WSEM may cause existence of heat affected zone (HAZ) to a certain depth just below the recast layer. Increase in microhardness of WSEM manufactured

MBG and MHG is welcome provided it does not induce any microcracks and HAZ to such an extent that it adversely affects their fatigue strength. It can also be seen in Figure 4.6 that microhardness values of MBG and MHG are different at different applied load. Better quality MBG has higher microhardness than better quality MHG for applied load of 200 g but this trend reverses for 500 g and 1000 g load. This can be explained by the fact that MBG is cut on the conical blank therefore its tooth thickness and gap between two consecutive teeth are continuously decreasing from its heel to toe side which makes flushing of the debris from IEG in more difficult. This causes formation of uneven recast layer on their flank surfaces. Formation of this layer on heel side is more than toe side. Whereas, chances of formation of uneven recast layer in MHG are very less due to uniform thickness of its teeth and uniform gap between two consecutive teeth.



**Fig. 4.7:** Microhardness of the better quality MBG and MHG manufactured by WSEM process and their material SS 304 at different applied load.



**Fig. 4.8(a)**

**Fig. 4.8(b)**

**Fig. 4.8:** Microscopic image of the recast layer and heat affected zone (HAZ) on tooth flank surface of the better quality (a) MBG; and (b) MHG.

#### 4.2.3.5 Microstructure

Analysis of microstructure of tooth profile and flank surfcess of the better quality MBG and MHG were studied to determine the accuracy of tooth profile and to find out presence of surface defects such as burrs, cracks, nicks, and asperities on their tooth flank surface. Figure 4.9 depicts SEM images showing tooth profiles [Fig. 4.9(a) and 4.9(c)] and microstructure of tooth flank surface [Figs. 4.9(b) and 4.9(d)] of better quality MBG and MHG. Figures 4.9(a) and 4.9(b) show that the WSEM manufactured better quality MBG and MHG have burr-free, uniform and accurate tooth profile without any undercut at root, no sharp edges on both end faces of the gears. Figures 4.9(c) and 4.9(d) depict that the microstructure of tooth flank surfaces of these gears are free from micro-cracks, nicks and asperities.

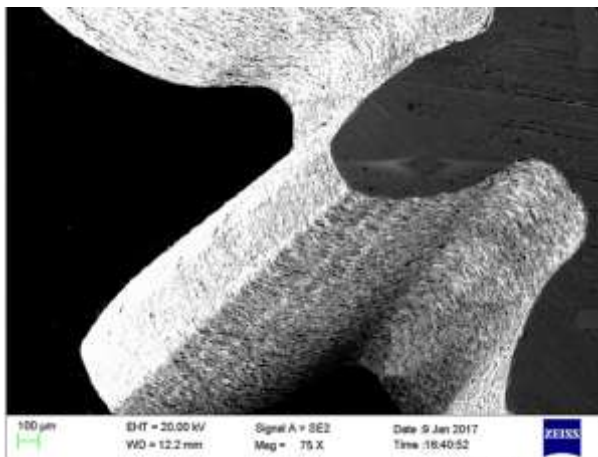


Fig. 4.9(a)

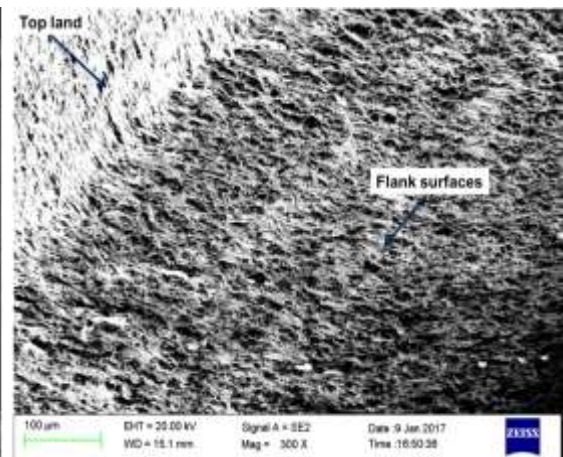


Fig. 4.9(b)

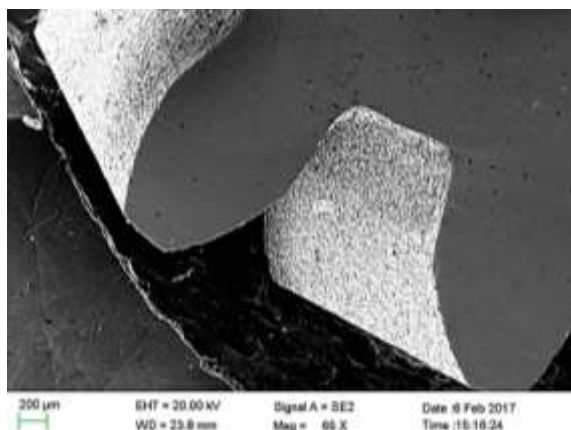


Fig. 4.9(c)

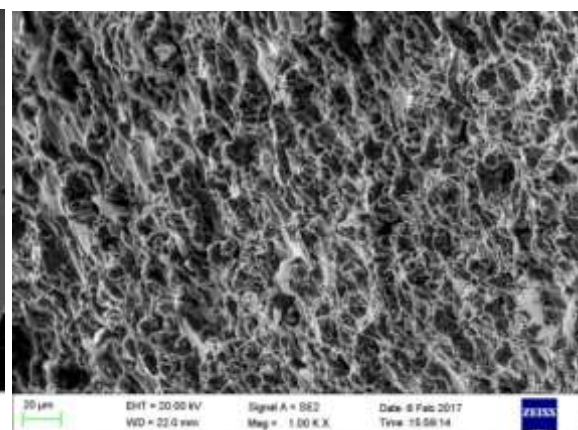


Fig. 4.9(d)

**Fig. 4.9:** SEM images showing tooth profile and microstructure of tooth flank surface of the better quality (a), (b) MBG; and (c), (d) MHG, respectively.

#### 4.2.4 Conclusions of the Pilot Experiments

Following conclusions can be drawn from results of the pilot experiments and their interpretation and analysis:

- Irregular shaped craters, sparks having higher discharge energy, non-uniform sparks, wire-lag, recast layer, non-flatness of the gear plate, and error in its positioning with respect to wire feed are main factors which affect microgeometry errors and surface roughness of MBG and MHG.
- There exist optimum ranges of servo-voltage and pulse-on time, and optimum value of % cutting speed to minimize microgeometry errors and surface roughness of MBG and MHG. Higher values of servo voltage and pulse-on time should be avoided for stable sparking to improve the quality and surface finish of MBG and MHG.
- Better gear quality and surface finish of MBG and MHG can be achieved using higher values of wire feed rate, wire tension and dielectric pressure because this will minimize the wire breakage frequency which will minimize microgeometry errors and surface roughness of MBG and MHG simultaneously.
- Conflict exists for peak current and pulse-off time. Higher value of peak current minimizes microgeometry errors of MBG and MHG whereas lower value of peak current minimizes surface roughness of MBG and MHG. In order to give more importance to microgeometry parameters, it was decided to keep higher value of peak current for further investigations. Similarly, optimum range of pulse-off time exists to minimize microgeometry errors of MBG and MHG whereas, minimization of surface roughness of MBG and MHG requires higher value of pulse-off time.
- Minimizing microgeometry errors and surface roughness of MBG and MHG but giving more preference to minimizing microgeometry errors than surface roughness resulted in narrowing down 10-20 volts for servo voltage, 1.0-1.6  $\mu\text{s}$  for pulse-on time, 44.5-48.5  $\mu\text{s}$  for pulse-off time; and 9-15 m/min for wire feed rate were as their optimum ranges for further investigations. It also identified 12 A for peak current; 1260 g for wire tension, 15 kg/cm<sup>2</sup> for dielectric pressure and 75% of the cutting speed as their optimum values for the conducting the further experimental investigations.
- MBG and MHG possessing minimum errors in their microgeometry (referred as better quality MBG and MHG) were identified for more detailed investigation on their microgeometry, flank surface topography, microhardness, and microstructure. These gears had 1.24 and 1.33  $\mu\text{m}$  as average surface roughness and 7.56 and 7.67  $\mu\text{m}$  for

maximum surface roughness, respectively. Their flank surface topography revealed very small amount of deviation of the actual flank surfaces from its theoretical form.

- Microhardness of flank surfaces of better quality MBG and MHG is higher than parent materials due to formation of very thin recast layers. Moreover, it does not induce any micro-cracks and heat affected zone to such an extent that it adversely affects fatigue strength of meso-gears.
- Analysis of microstructure of the better quality MBG and MHG revealed their tooth profile to be burr-free, uniform, accurate, no undercutting at the root and no sharp edges on both end faces of the meso-gears.
- Microstructural examination of flank surfaces of better quality MBG and MHG had shown smoother surface free from cracks, nicks and asperities.
- These results prove potential and capabilities of WSEM process to manufacture high quality MBG and MHG and that further investigations are needed for more detailed study of influence of WSEM parameters and their interactions on MBG and MHG microgeometry, surface finish and WSEM productivity and their optimization.

### **4.3 Results and Analysis of the Main Experiments**

Twenty nine main experiments with two replicate each for MBG and MHG were conducted using Box–Behnken design (BBD) of response surface methodology (RSM) by varying servo voltage, pulse-on time, pulse-off time and wire feed rate at three levels each in their identified optimum ranges and keeping other parameters fixed (as mention in Table 3.2). Table 4.4 presents values of microgeometry errors, average and maximum surface roughness values and volumetric gear cutting rate of MBG for two replicates (*R1* and *R2*) of the main experiments with along with corresponding variable parameters of WSEM process. Table 4.5 presents the same for MHG.

**Table 4.4:** Values of microgeometry errors, average and maximum surface roughness values and volumetric gear cutting rate of MBG for two replicates (*R1* and *R2*) of the main experiments with along with corresponding variable parameters of WSEM process.

Ex. no.	Variable parameters of WSEM				Responses														
	$T_{on}$ ( $\mu s$ )	$T_{off}$ ( $\mu s$ )	$S_V$ (Volts)	$W_F$ (m/min)	Single pitch error ' $f_P$ ' ( $\mu m$ )			Total cumulative pitch error ' $F_P$ ' ( $\mu m$ )			Avg. surface roughness ' $R_a$ ' ( $\mu m$ )			Max. surface roughness ' $R_{max}$ ' ( $\mu m$ )			Volumetric gear cutting rate ' $VGCR$ ' ( $mm^3/min$ )		
					<i>R1</i>	<i>R2</i>	Avg.	<i>R1</i>	<i>R2</i>	Avg.	<i>R1</i>	<i>R2</i>	Avg.	<i>R1</i>	<i>R2</i>	Avg.	<i>R1</i>	<i>R2</i>	Avg.
1	1.3	46.5	10	15	13.65	11.70	12.68	23.65	18.35	21.00	1.24	1.18	1.21	6.077	7.845	6.96	4.01	4.19	4.09
2	1.0	44.5	15	12	15.10	13.46	14.28	26.45	12.20	19.33	1.29	1.42	1.36	6.630	9.165	7.90	3.28	3.24	3.20
3	1.3	46.5	15	12	19.10	20.30	19.70	16.50	19.05	17.78	0.95	1.17	1.06	6.28	8.32	7.30	3.13	3.88	3.50
4	1.6	48.5	15	12	11.10	11.95	11.53	26.35	27.40	26.88	1.44	1.51	1.48	7.05	8.54	7.80	4.52	4.68	4.60
5	1.6	46.5	15	15	13.26	14.60	13.93	30.65	19.90	25.28	1.41	1.25	1.33	8.33	7.91	8.12	4.78	5.22	5.00
6	1.3	46.5	15	12	19.50	20.10	19.80	16.05	18.65	17.35	0.86	1.16	1.01	5.48	7.64	6.56	3.53	4.07	3.80
7	1.3	44.5	20	12	18.10	18.85	18.48	23.55	27.15	25.35	1.56	1.51	1.54	9.29	8.99	9.14	5.45	5.75	5.60
8	1.3	48.5	15	15	10.95	08.00	09.48	17.15	19.15	18.50	1.13	1.07	1.10	5.48	7.56	6.52	3.90	3.70	3.80
9	1.6	46.5	10	12	13.10	14.10	13.58	19.40	25.40	22.40	1.33	1.42	1.38	8.87	10.05	9.46	4.20	4.60	4.40
10	1.3	44.5	15	15	14.50	15.75	15.13	26.25	24.45	25.35	1.18	1.37	1.28	7.52	10.24	8.88	4.70	4.90	4.80
11	1.3	48.5	20	12	19.75	20.65	20.20	29.95	25.65	27.80	1.53	1.51	1.52	9.01	10.11	9.56	5.35	5.45	5.40
12	1.3	46.5	20	15	14.05	15.10	14.58	25.75	19.75	22.75	1.23	1.53	1.38	7.62	8.66	8.14	5.20	5.50	5.35
13	1.3	48.5	10	12	07.75	09.75	<b>08.75</b>	18.30	13.60	15.95	1.06	0.94	<b>1.00</b>	5.52	7.56	6.54	2.90	3.10	3.00
14	1.0	46.5	15	15	12.60	13.15	12.88	16.80	18.75	17.78	1.10	1.38	1.24	6.82	6.62	6.72	3.30	3.70	3.50
15	1.3	46.5	20	9	21.30	20.85	21.08	37.65	34.20	35.93	1.62	1.86	1.74	10.04	10.48	10.22	4.82	4.78	4.80
16	1.6	46.5	15	9	24.45	19.25	21.85	39.35	35.85	37.60	1.83	1.46	1.65	11.22	10.78	11.00	4.82	5.78	5.30
17	1.3	44.5	15	9	15.65	18.10	16.88	25.95	27.95	26.95	1.47	1.43	1.45	9.29	8.95	9.12	4.10	3.90	4.00
18	1.3	48.5	15	9	18.00	14.45	16.23	22.75	23.65	23.20	1.43	1.41	1.42	8.13	8.73	8.43	3.32	3.28	3.30
19	1.0	46.5	20	12	12.50	13.70	13.10	17.80	19.70	18.75	1.26	1.28	1.27	8.18	8.25	8.21	3.42	3.58	3.50
20	1.0	46.5	15	9	13.85	13.75	13.80	17.90	20.30	19.10	1.18	1.44	1.31	6.57	7.03	6.80	2.80	3.00	2.90
21	1.3	46.5	15	12	19.50	20.10	19.80	17.95	18.75	18.35	1.20	1.03	1.12	6.65	7.76	7.20	3.25	3.55	3.40
22	1.3	46.5	15	12	22.65	20.95	21.80	19.10	22.90	21.00	1.10	1.22	1.16	6.24	8.56	7.40	3.68	3.52	3.60
23	1.0	46.5	10	12	09.50	09.90	09.70	13.80	20.30	17.05	0.95	1.25	1.10	5.39	7.37	<b>6.38</b>	2.68	2.88	2.78
24	1.0	48.5	15	12	09.60	12.90	11.25	14.50	16.40	<b>15.45</b>	0.97	1.15	1.06	6.15	7.76	6.96	3.10	3.30	3.20
25	1.6	44.5	15	12	20.25	22.85	21.55	34.10	47.90	41.00	1.48	1.58	1.53	10.05	11.67	10.86	6.10	6.30	6.20
26	1.3	46.5	10	9	08.15	14.40	11.28	25.75	19.70	22.73	1.14	1.22	1.18	6.27	7.69	6.98	3.30	3.50	3.40
27	1.3	46.5	15	12	20.75	18.65	19.70	22.35	18.65	20.50	1.05	1.11	1.08	5.75	8.46	7.10	3.60	3.40	3.50
28	1.6	46.5	20	12	24.85	22.25	23.55	36.85	35.00	35.93	1.83	1.75	1.79	9.47	8.81	9.14	6.30	6.50	<b>6.40</b>
29	1.3	44.5	10	12	18.10	10.10	14.10	20.90	27.40	24.15	1.29	1.27	1.28	8.63	8.31	8.47	4.38	4.62	4.50

**Table 4.5:** Values of microgeometry errors, average and maximum surface roughness values and volumetric gear cutting rate of MHG for two replicates (*R1* and *R2*) of the main experiments with along with corresponding variable parameters of WSEM process.

Ex. No.	Variable parameters of WSEM				Responses														
	$T_{on}$ ( $\mu s$ )	$T_{off}$ ( $\mu s$ )	$S_V$ (Volts)	$W_F$ (m/min)	Total profile error ' $F_a$ ' ( $\mu m$ )			Total cumulative pitch error ' $F_p$ ' ( $\mu m$ )			Avg. surface roughness ' $R_a$ ' ( $\mu m$ )			Max. surface roughness ' $R_{max}$ ' ( $\mu m$ )			Volumetric gear cutting rate ' $VGCR$ ' ( $mm^3/min$ )		
					<i>R1</i>	<i>R2</i>	Avg.	<i>R1</i>	<i>R2</i>	Avg.	<i>R1</i>	<i>R2</i>	Avg.	<i>R1</i>	<i>R2</i>	Avg.			
1	1.3	46.5	10	15	09.75	09.65	09.70	18.50	18.65	18.58	1.10	1.16	1.13	7.25	7.89	7.57	4.46	5.10	4.78
2	1.0	44.5	15	12	09.25	11.60	10.43	20.75	20.75	20.75	1.34	1.56	1.45	8.43	7.20	7.82	3.40	3.80	3.60
3	1.3	46.5	15	12	09.65	09.15	09.40	17.30	15.05	16.15	1.05	1.19	1.12	8.02	7.12	7.57	3.50	4.10	3.80
4	1.6	48.5	15	12	10.65	10.85	10.75	17.15	17.15	17.15	1.51	1.45	1.48	8.00	9.13	8.57	5.10	5.30	5.20
5	1.6	46.5	15	15	12.31	11.45	11.88	22.15	19.90	21.00	1.31	1.42	1.36	8.05	8.55	8.33	5.30	5.50	5.40
6	1.3	46.5	15	12	08.65	08.55	08.50	15.50	14.10	14.80	1.19	1.01	1.10	7.51	6.84	7.17	3.50	3.70	3.60
7	1.3	44.5	20	12	11.15	13.25	12.20	27.55	29.75	28.65	1.41	1.44	1.42	8.79	9.05	8.92	6.52	5.21	5.86
8	1.3	48.5	15	15	11.30	08.75	10.03	17.90	12.75	15.33	0.94	1.18	1.06	7.60	8.92	8.26	4.28	4.12	4.20
9	1.6	46.5	10	12	11.05	11.65	11.35	19.30	22.70	21.00	1.05	1.46	1.25	8.48	8.62	8.55	5.35	5.25	5.30
10	1.3	44.5	15	15	08.90	13.70	11.30	28.55	15.00	21.78	1.38	1.19	1.29	8.44	8.28	8.36	5.40	5.20	5.30
11	1.3	48.5	20	12	13.15	13.61	13.38	29.90	29.90	29.90	1.43	1.33	1.38	10.36	9.10	9.73	5.75	4.95	5.35
12	1.3	46.5	20	15	13.05	13.15	13.10	22.85	22.10	22.48	1.18	1.24	1.21	9.61	9.60	9.60	5.35	5.65	5.50
13	1.3	48.5	10	12	08.10	08.56	<b>08.33</b>	14.60	13.45	<b>14.03</b>	1.04	1.28	1.16	6.61	7.62	<b>7.11</b>	3.70	2.90	3.30
14	1.0	46.5	15	15	10.30	10.15	10.23	18.70	17.56	18.13	1.13	1.23	1.18	7.78	8.48	8.13	4.35	4.06	4.20
15	1.3	46.5	20	9	12.25	11.95	12.10	38.85	30.70	33.28	1.55	1.45	1.50	8.37	9.10	8.73	5.74	4.76	5.25
16	1.6	46.5	15	9	15.01	15.85	15.43	35.75	25.20	30.48	1.25	1.64	1.44	7.90	11.75	9.82	5.40	5.35	5.38
17	1.3	44.5	15	9	14.0	14.20	14.10	34.80	21.15	27.98	1.44	1.48	1.46	8.68	10.69	9.69	4.90	4.70	4.80
18	1.3	48.5	15	9	11.25	10.50	10.88	24.95	24.00	24.48	1.24	1.18	1.21	8.56	8.64	8.60	4.55	4.25	4.40
19	1.0	46.5	20	12	08.10	13.70	10.90	21.85	21.05	21.45	1.25	1.29	1.27	7.71	8.19	7.95	4.28	4.12	4.20
20	1.0	46.5	15	9	10.70	11.45	11.08	18.25	18.45	18.35	1.11	1.26	1.19	7.48	8.18	7.83	3.25	3.15	3.20
21	1.3	46.5	15	12	08.90	09.40	09.15	18.70	21.66	20.18	0.98	1.06	1.02	7.43	8.16	7.80	3.50	4.10	3.80
22	1.3	46.5	15	12	10.65	10.75	10.70	17.25	18.95	18.10	1.08	1.16	1.12	7.98	7.82	7.90	3.65	4.35	4.00
23	1.0	46.5	10	12	11.61	10.85	11.03	15.50	15.75	15.63	1.22	1.18	1.20	7.59	8.05	7.82	2.90	2.70	2.80
24	1.0	48.5	15	12	09.60	10.85	10.23	23.85	08.70	16.28	1.02	0.94	<b>0.98</b>	8.14	8.23	8.19	3.10	4.02	3.56
25	1.6	44.5	15	12	15.05	15.85	15.45	32.70	37.85	35.28	1.39	1.41	1.40	10.38	10.48	10.43	6.20	6.50	<b>6.35</b>
26	1.3	46.5	10	9	12.00	15.45	13.73	16.15	16.70	16.43	1.18	1.16	1.17	8.98	9.88	9.43	3.80	3.20	3.50
27	1.3	46.5	15	12	09.15	09.40	09.28	18.70	18.26	18.48	1.16	0.98	1.07	7.49	8.97	8.23	4.61	3.59	4.10
28	1.6	46.5	20	12	15.01	15.85	15.43	37.30	36.95	37.13	1.78	1.56	1.67	10.98	11.06	11.02	5.65	5.55	5.60
29	1.3	44.5	10	12	12.15	10.30	11.23	32.80	18.15	25.48	1.26	1.59	1.43	8.05	8.55	8.30	5.22	4.93	5.08

### 4.3.1 Development of Response Surface Models

Response surface models were developed for the considered microgeometry errors, average and maximum surface roughness, and volumetric gear cutting rate of MBG and MHG using the results of the main experiments (presented in Tables 4.4 and 4.5) and using statistical concepts of sequential model sum of squares (SMSS), lack-of-fit and model summary statistics (MSS) in the 10<sup>th</sup> version of *Design Expert* software. All these tests suggested 2<sup>nd</sup> order polynomial for all the considered responses of MBG and MHG. Subsequently, analysis of variance (ANOVA) was used to determine significance of the developed response surface models, and significant WSEM parameters and their interactions in these models using 95% confidence interval. Results of ANOVA are presented in Tables E1 (for MBG) and E2 (for MHG) of Appendix-E. Following conclusions can be drawn from the ANOVA results:

- Servo voltage, pulse-on time, pulse-off time and wire feed rate, and their squared terms were found to be significant for the considered parameters of microgeometry and surface roughness, and volumetric gear cutting rate of MBG and MHG;
- Interactions between  $T_{on}$  and  $T_{off}$ ,  $T_{on}$  and  $S_V$ ,  $T_{on}$  and  $W_F$ ,  $T_{off}$  and  $S_V$ , and  $S_V$  and  $W_F$  (except  $T_{on}$  and  $W_F$  for  $R_a$  of MHG) were found to be significant for the considered parameters of microgeometry and surface roughness of MBG and MHG;
- Interactions between  $T_{on}$  and  $T_{off}$ ,  $T_{on}$  and  $S_V$ , and  $T_{off}$  and  $S_V$  were found to be significant for volumetric gear cutting rate of MBG and MHG.

The develop response surface models were modified to reflect the above-mentioned conclusions from the ANOVA. The details of adequacy testing and residual analysis of these models are discussed in the following section.

#### 4.3.1.1 For Microgeometry Errors of MBG and MHG

The statistical tests suggested 2<sup>nd</sup> order polynomial response surface models for microgeometry errors of MBG (i.e.  $f_p$  and  $F_p$ ) and MHG (i.e.  $F_a$  and  $F_p$ ). The residual analysis was used as the primary diagnostic tool and the graphs of normal probability plot of residuals have been drawn for the considered microgeometry errors of MBG and MHG and are presented in Fig. 4.10. It can be seen from these graphs that residuals are normally distributed as most of them are accumulated around a straight line.

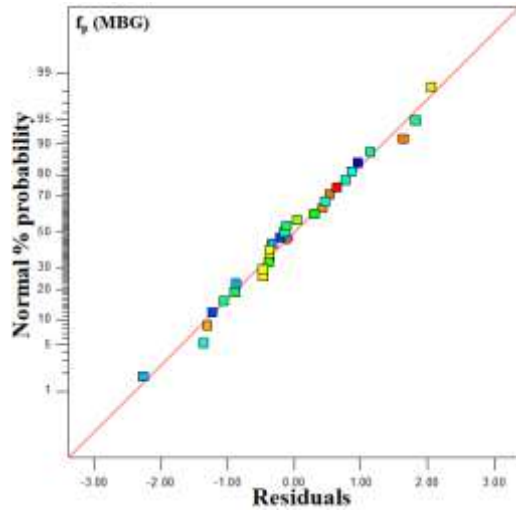


**Fig. 4.10(a)**

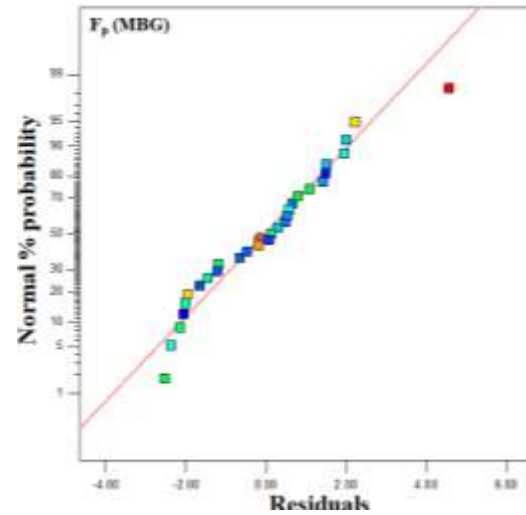


**Fig. 4.10(b)**

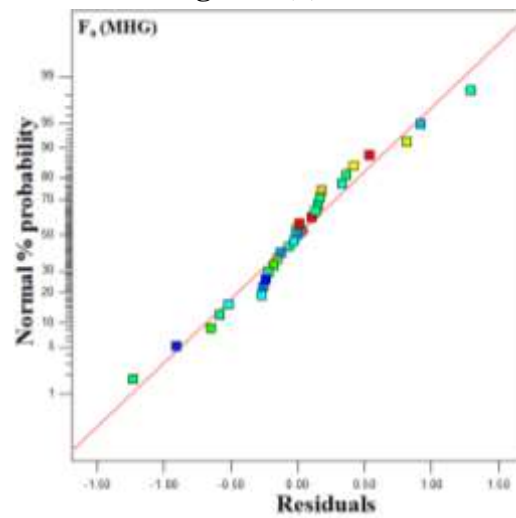


**Fig. 4.10(c)**

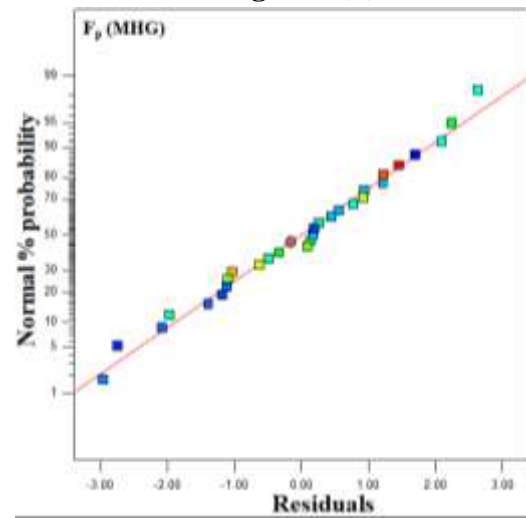


**Fig. 4.10(d)**

**Fig. 4.10:** Normal plot of residuals for (a) single pitch error ' $f_p$ '; and (b) total cumulative pitch error ' $F_p$ ' of MBG; and (c) total profile error ' $F_a$ '; and (d) total cumulative pitch error ' $F_p$ ' of MHG.

The F-value for the developed model implies that the 2<sup>nd</sup> order polynomial based response surface models are significant. P-values of (Prob > F) less than 0.05 indicate model terms are significant. The *lack of fit* test of these models is not significant (i.e. p-values are greater than .05) relative to the pure error. Non-significant *lack of fit* is desirable. The values of PRESS are: 151.94 for  $f_p$  and 416.69 for  $F_p$  of MBG and 33.45 for  $F_a$  and 268.07 for  $F_p$  of MHG; and values of R-Squared are 0.944 for  $f_p$  and 0.9377 for  $F_p$  of MBG, and 0.9310 for  $F_a$  and 0.9949 for  $F_p$  of MHG (i.e. close to 1) which confirms adequacy of the developed models. Values of the 'predicted R-Squared' of these models are in reasonable agreement with the 'adjusted R-Squared' because the difference is less than 0.2. It indicates high correlation between the experimental and the model predicted

values. The ‘adequate precision’ measures the signal to noise ratio. A ratio greater than 4 is desirable. The values of adequate precision are 14.645 for  $f_p$  and 13.599 for  $F_p$  of MBG, and 12.851 for  $f_p$  and 15.756 for  $F_p$  of MHG suggest that the quadratic models are a good predictor for the considered responses. Following equations represent the response surface model for considered microgeometry parameters of MBG and MHG in terms of significant variable parameters and their interactions.

(i) **For MBG**

$$f_{P_b} = -1796.83 + 221.71 T_{on} + 68.76 T_{off} - 4.45 S_V + 20.5 W_F - 27.22 T_{on}^2 - 0.71 T_{off}^2 - 0.1 S_V^2 - 0.29 W_F^2 - 2.91 T_{on}T_{off} + 1.1 T_{on}S_V - 1.94 T_{on}W_F + 0.18 T_{off} S_V - 0.13 S_VW_F \quad (4.1a)$$

$$F_{P_b} = 1263.11 + 147.65 T_{on} - 53.02 T_{off} - 14.66 S_V + 3.68 W_F + 35.5 T_{on}^2 + 0.59 T_{off}^2 + 0.09 S_V^2 + 0.34 W_F^2 - 4.52 T_{on}T_{off} + 1.972 T_{on}S_V - 3.06 T_{on}W_F + 0.27 T_{off}S_V - 0.19 S_VW_F \quad (4.1b)$$

(ii) **For MHG**

$$F_{a_h} = 524.43 + 53.03 T_{on} - 18.73 T_{off} - 8.03 S_V - 7.54 W_F + 15.48 T_{on}^2 + 0.19 T_{off}^2 + 0.05 S_V^2 + 0.15 W_F^2 - 1.88 T_{on} T_{off} + 0.7 T_{on}S_V - 1.03 T_{on}W_F + 0.1 T_{off}S_V + 0.08 S_VW_F \quad (4.2a)$$

$$F_{P_h} = 1518.6 + 216.21 T_{on} - 65.23 T_{off} - 17.91 S_V + 6.54 W_F + 26.1 T_{on}^2 + 0.73 T_{off}^2 + 0.15 S_V^2 + 0.2 W_F^2 - 5.69 T_{on}T_{off} + 1.72 T_{on}S_V - 2.57 T_{on}W_F + 0.32 T_{off}S_V - 0.22 S_VW_F \quad (4.2b)$$

**4.3.1.2 For Surface Roughness of MBG and MHG**

The statistical tests suggested 2<sup>nd</sup> order polynomial response surface models for average and maximum surface roughness of MBG and MHG. It can be seen from the normal probability plots of residuals for both  $R_a$  and  $R_{max}$  of MBG and MHG (Fig. 4.11) that they are normally distributed. Following equations present the response surface model for  $R_a$  and  $R_{max}$  of MBG and MHG in terms of significant variable parameters and their interactions using the concepts mentioned in subsection 4.3.1.1 to interpret the concerned ANOVA results.

(i) **For MBG**

$$R_{a_b} = 69.04 - 8.76 T_{on} - 2.55 T_{off} - 0.42 S_V + 0.09 W_F + 1.79 T_{on}^2 + 0.03 T_{off}^2 + 0.01 S_V^2 + 0.01 W_F^2 - +0.1 T_{on} T_{off} + 0.04 T_{on}S_V - 0.07 T_{on}W_F + 0.01 T_{off}S_V - 0.01 S_VW_F \quad (4.1c)$$

$$R_{max_b} = 345.81 + 42.18 T_{on} - 15.61 T_{off} - 2.39 S_V + 3.45 W_F + 6.66 T_{on}^2 + 0.16 T_{off}^2 + 0.02 S_V^2 + 0.05 W_F^2 - 0.88 T_{on}T_{off} - 0.36 T_{on}S_V - 0.78 T_{on}W_F + 0.06 T_{off}S_V - 0.03 S_VW_F \quad (4.1d)$$

(ii) For MHG

$$R_{ah} = 90.86 - 14.61 T_{on} - 3.25 T_{off} - 0.41 S_V - 0.12 W_F + 1.47 T_{on}^2 + 0.03 T_{off}^2 + 0.005 S_V^2 + 0.01 W_F^2 + 0.23 T_{on} T_{off} + 0.05 T_{on}S_V + 0.01 T_{off}S_V - 0.004 S_VW_F \quad (4.2c)$$

$$R_{max_h} = 274.92 + 31.6 T_{on} - 10.21 T_{off} - 3.89 S_V - 3.34 W_F + 5.47 T_{on}^2 + 0.11 T_{off}^2 + 0.02 S_V^2 + 0.05 W_F^2 - 0.93 T_{on}T_{off} + 0.39 T_{on}S_V - 0.5 T_{on}W_F + 0.05 T_{off}S_V + 0.05 S_VW_F \quad (4.2d)$$

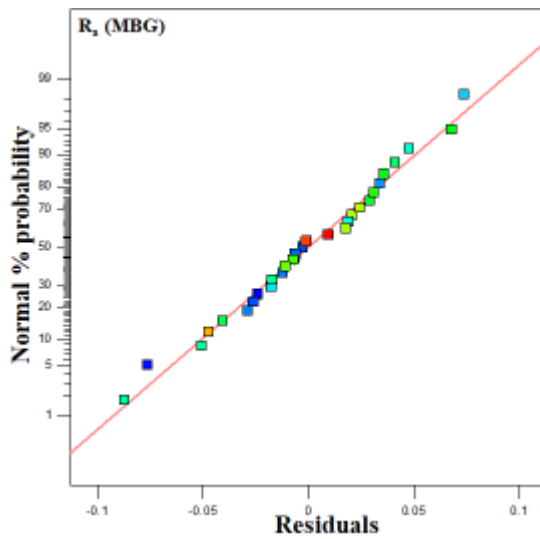


Fig. 4.11(a)

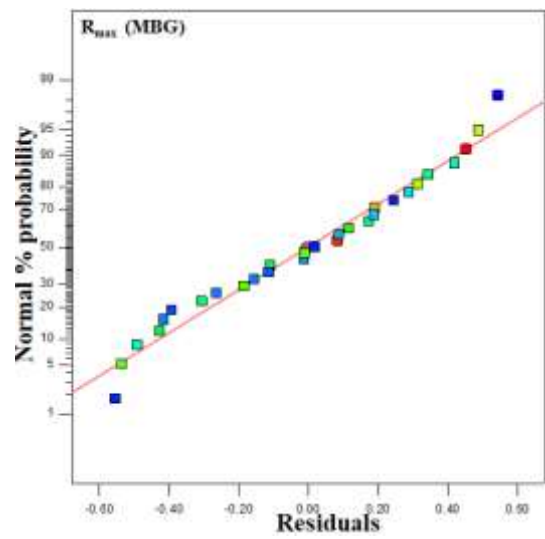


Fig. 4.11(b)

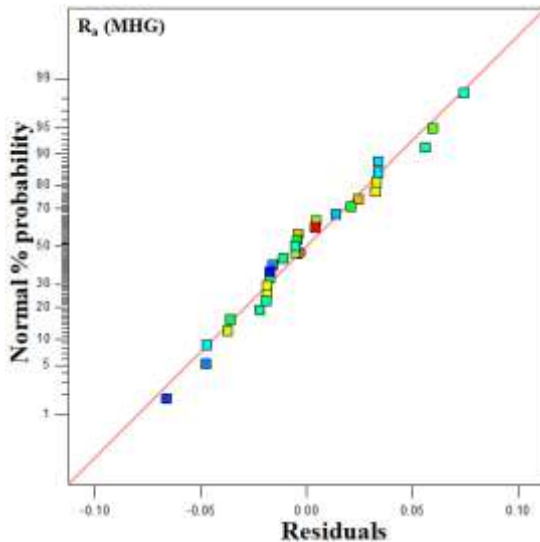


Fig. 4.11(c)

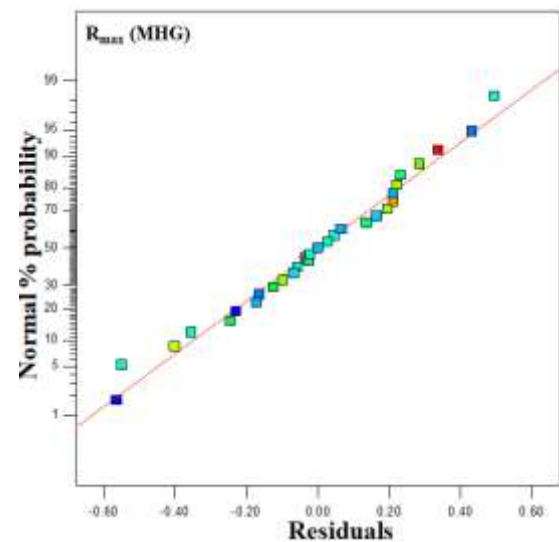


Fig. 4.11(d)

Fig. 4.11: Normal plot of residuals for average and maximum surface roughness of (a); (b) MBG; and (c) and (d) MHG, respectively.

#### 4.3.1.3 For Volumetric Gear Cutting Rate of MBG and MHG

The statistical tests suggested 2<sup>nd</sup> order polynomial response surface models for volumetric gear cutting rate (VGCR) of MBG and MHG. The normal probability plots (Fig. 4.12) depict the normal distribution of the data for these models. Following equations present the response surface model for VGCR of MBG and MHG in terms of significant variable parameters and their interactions using the concepts mentioned in subsection 4.3.1.1 to interpret the concerned ANOVA results.

##### (i) For MBG

$$VGCR_b = 198.678 + 25.7065T_{on} - 8.446T_{off} - 2.308S_V + 0.467W_F + 3.328T_{on}^2 + 0.094T_{off}^2 + 0.023S_V^2 + 0.023W_F^2 - 0.667T_{on}T_{off} + 0.213T_{on}S_V + 0.0325T_{off}S_V \quad (4.1e)$$

##### (ii) For MHG

$$VGCR_h = 271.736 + 23.6145T_{on} - 11.91T_{off} - 1.472S_V + 1.0135W_F + 2.75T_{on}^2 + 0.131T_{off}^2 + 0.0185S_V^2 + 0.043W_F^2 - 0.463T_{on}T_{off} - 0.183T_{on}S_V + 0.032T_{off}S_V \quad (4.2e)$$

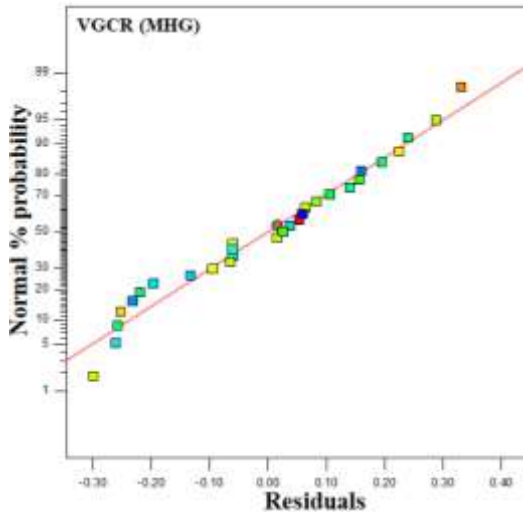


Fig. 4.12(a)

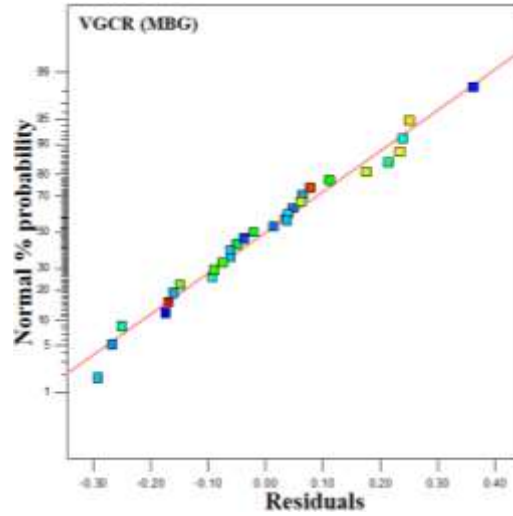


Fig. 4.12(b)

Fig. 4.12: Normal plot of residuals for volumetric gear cutting rate VGCR of (a) MBG; and (b) MHG.

#### 4.3.2 Influence of WSEM Parameters

Figure 4.13 depicts variation of single pitch error (blue color graph) and total cumulative pitch error (red color graph), average surface roughness (green color graph), and maximum surface roughness (purple color graph) with servo voltage [Fig. 4.13(a)], pulse-on time [Fig. 4.13(b)], pulse-off time [Fig. 4.13(c)], and wire feed rate [Fig. 4.13(d)] for MBG showing experimental points along with the equation of the best fit

curve to the results of the main experiments. Figure 4.14 illustrates same for MHG with the only difference that total profile error has been used in place of single pitch error. Following subsections describe observations from these graphs along with their explanation.

#### **4.3.2.1 On Microgeometry and Surface Roughness**

It can be seen from Figs. 4.13(a), 4.13(b), 4.14(a), and 4.14(b) that (i) single pitch error for MBG and total cumulative pitch error and maximum surface roughness for both MBG and MHG increase considerably with increase in servo voltage and pulse-on time; (ii) total profile error for MHG increases slightly with servo voltage and pulse-on time; (iii) values and variation of total cumulative pitch error is more than single pitch error for MBG and total profile error for MHG; (iv) values and variation in maximum surface roughness is higher than average surface roughness; and (v) servo voltage and pulse-on time have insignificant effect on average surface roughness of MBG and MHG. These observations can be explained by the fact that higher values of pulse-on time and servo voltage increase energy of sparks making them violent which leads to formation of irregular shaped craters on flank surface thus increasing microgeometry errors and surface roughness of MBG and MHG.

It can be observed from Figs. 4.13(c), and 4.14(c) that (i) total cumulative pitch error and maximum surface roughness decrease with increase in pulse-off time for both MBG and MHG; (ii) single pitch error decrease significantly with increase in pulse-off time for MBG; (iii) total profile error for MHG decreases slightly with pulse-off time; and (iv) pulse-off time has insignificant effect on average surface roughness for both MBG and MHG and; and. This is due to the fact that higher pulse-off time decreases frequency of sparks making them more stable which leads to formation of uniformly shaped craters resulting in uniform WSEM of tooth profile and meso-gear flank surfaces thus reducing microgeometry errors and surface roughness of MBG and MHG.

It is evident from Figs. 4.13(d) and 4.14(d) that (i) total cumulative pitch error and maximum surface roughness of both MBG and MHG decrease with increase in wire feed rate; (ii) single pitch error ' $f_p$ ' for MBG and total profile error for MHG decrease considerably during 12-15 and 9-12 m/min range of wire feed rate respectively; and (iii) average surface roughness is insignificantly affected by increase in wire feed rate for both MBG and MHG. These observation can explained by fact that higher wire feed rate significantly decreases duration of spark concentration at a certain location on the wire and

prevents its frequent breakage which adversely affects microgeometry, surface quality, and manufacturing time of MBG and MHG.

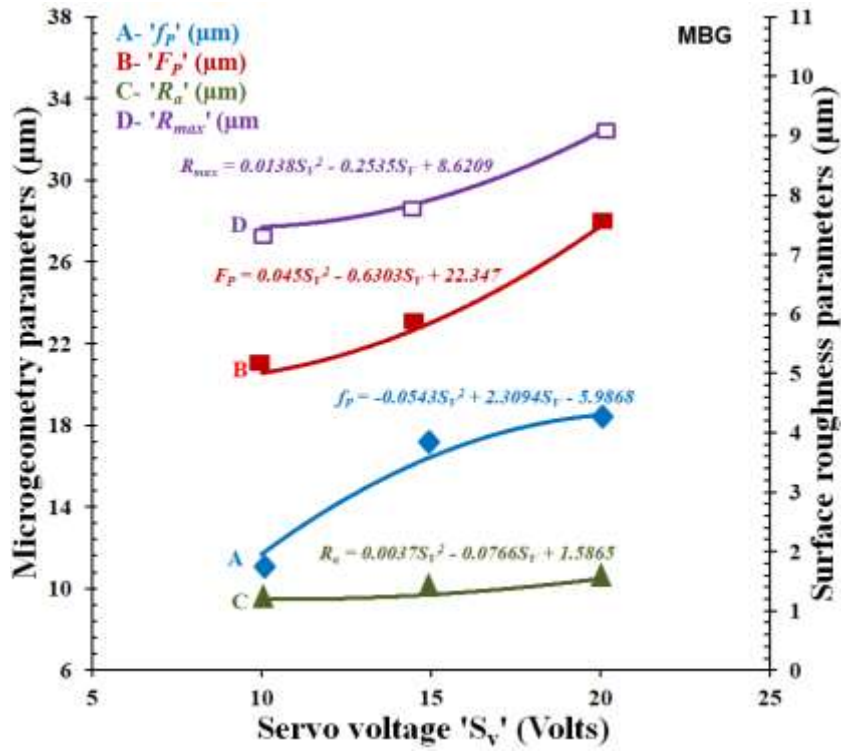


Fig. 4.13(a)

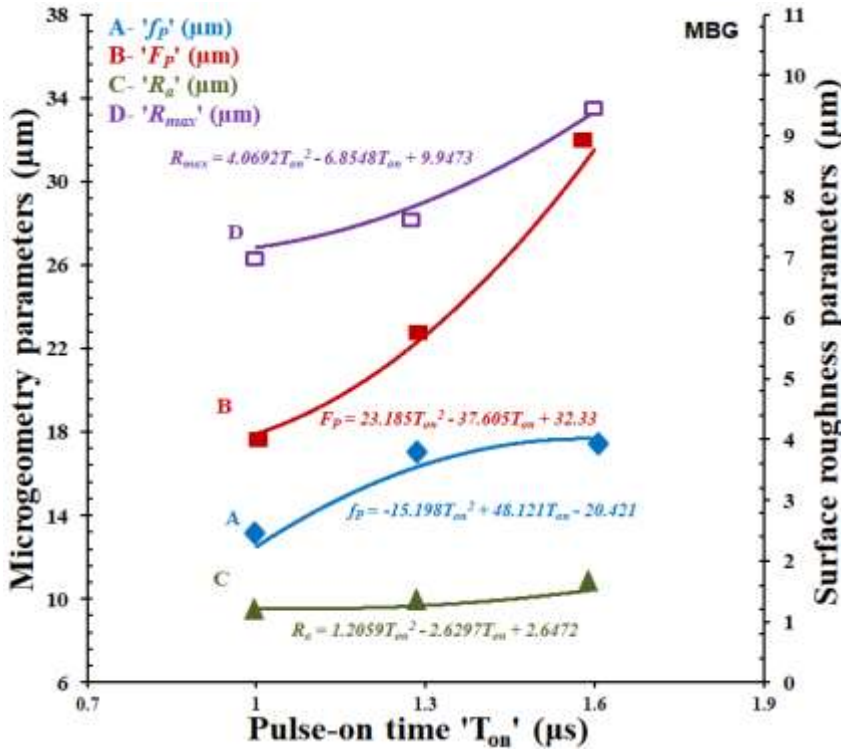


Fig. 4.13(b)

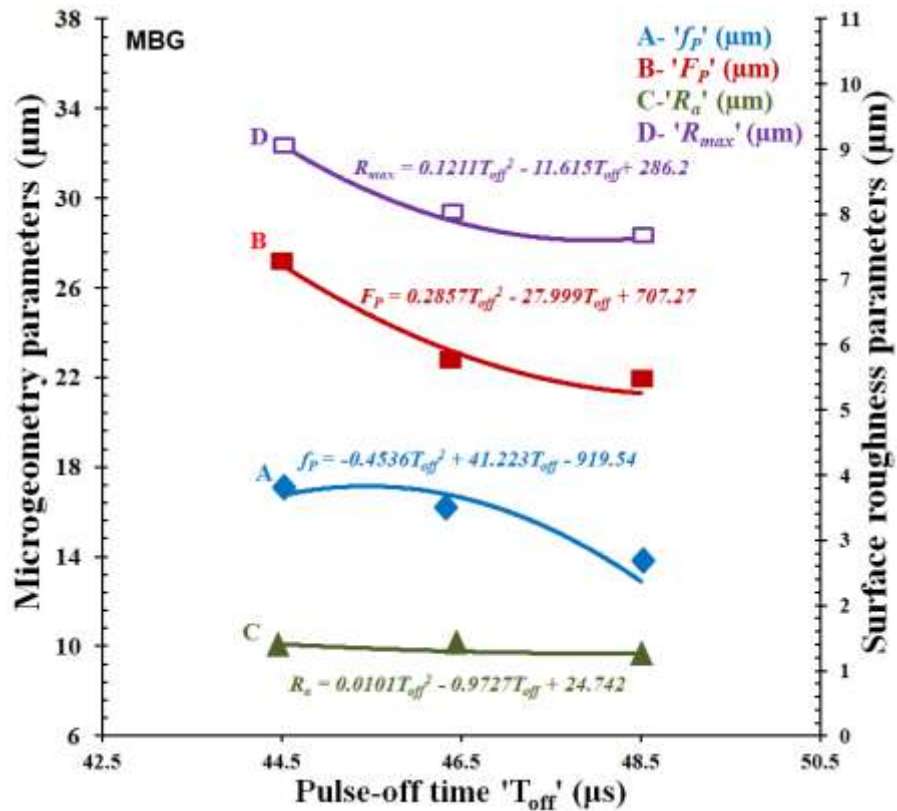


Fig. 4.13(c)

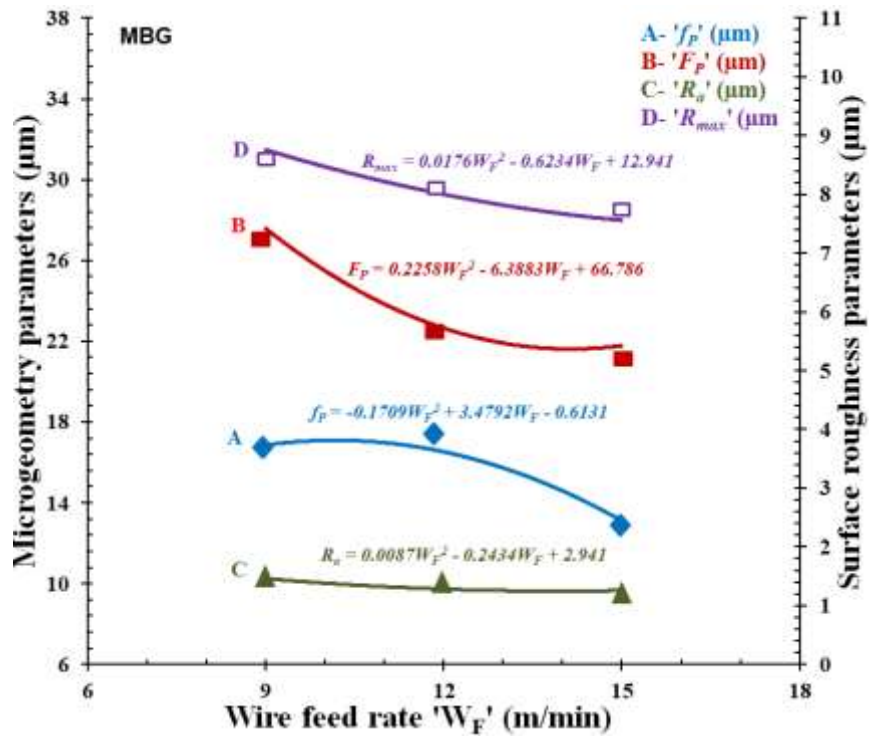


Fig. 4.13(d)

Fig. 4.13: Variation of surface roughness parameters and microgeometry errors of MBG with (a) servo voltage; (b) pulse-on time; (c) pulse-off time, and (d) wire feed rate.

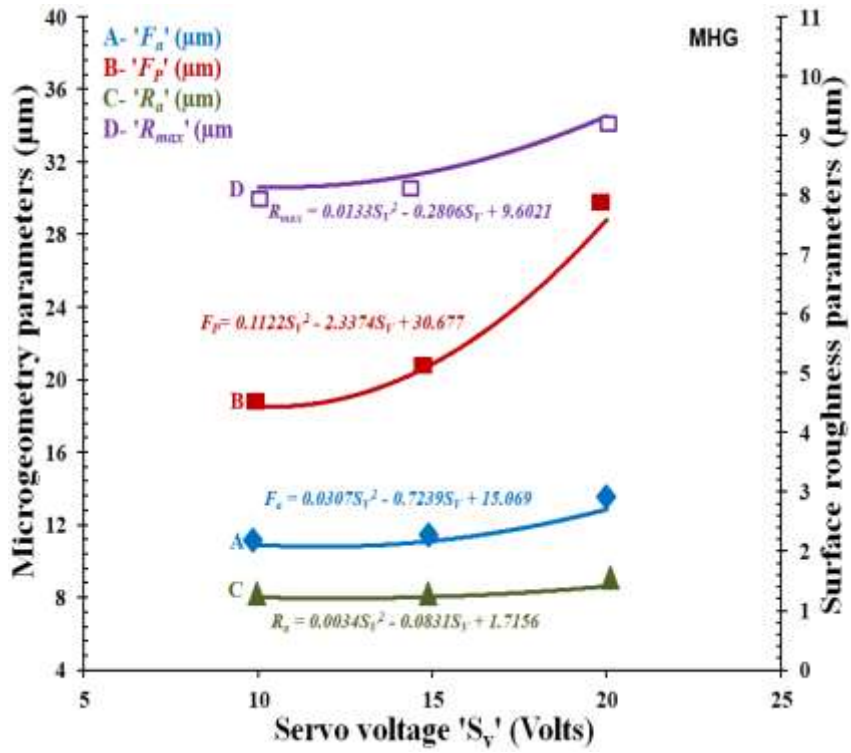


Fig. 4.14(a)

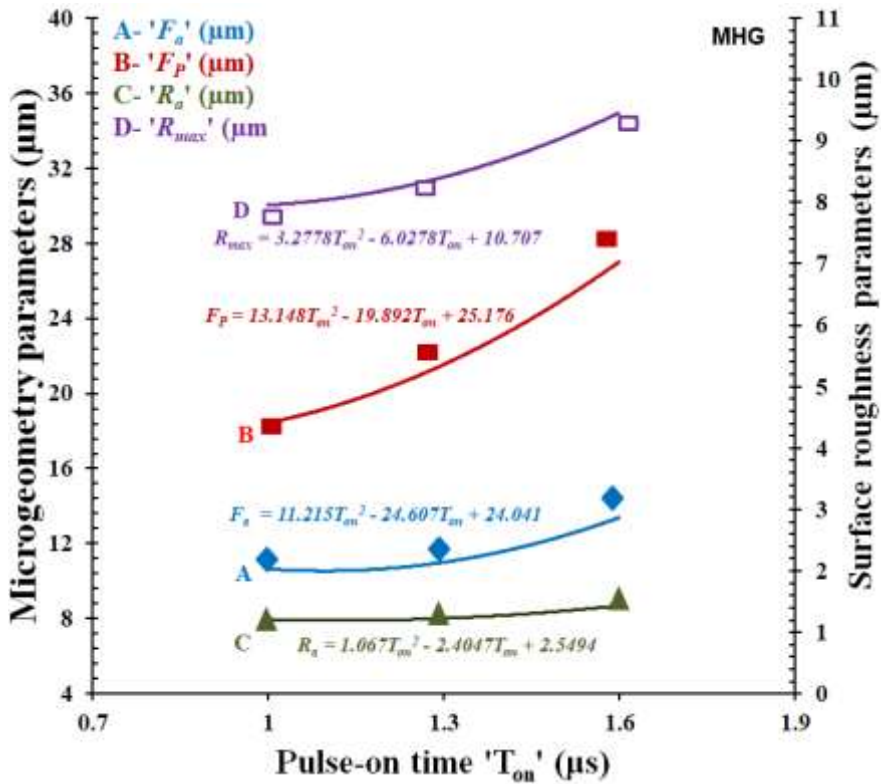


Fig. 4.14(b)

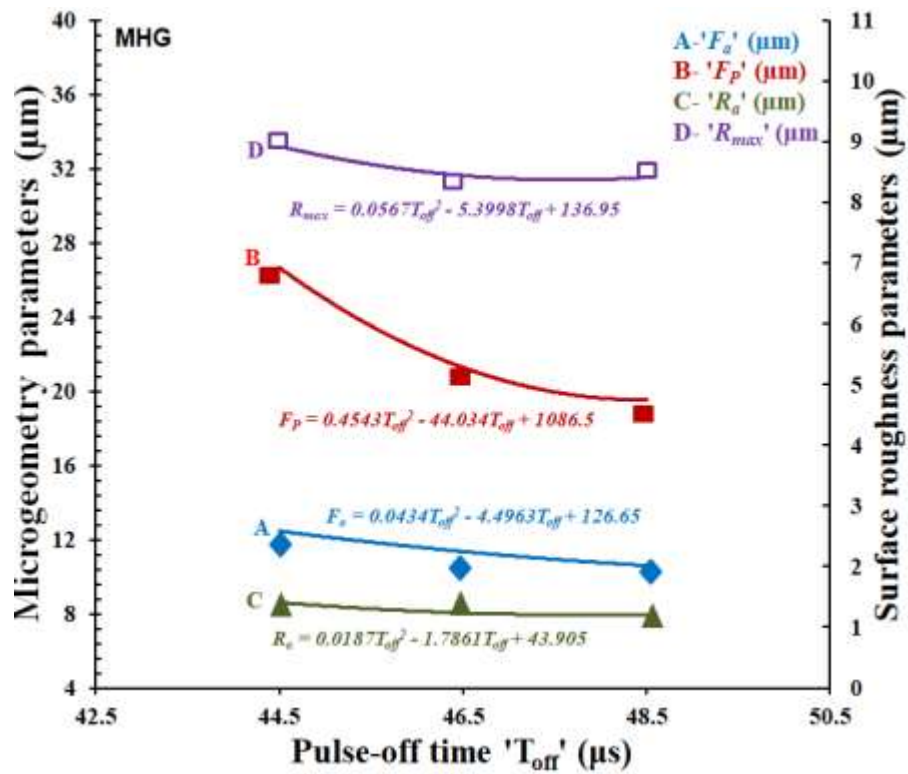


Fig. 4.14(c)

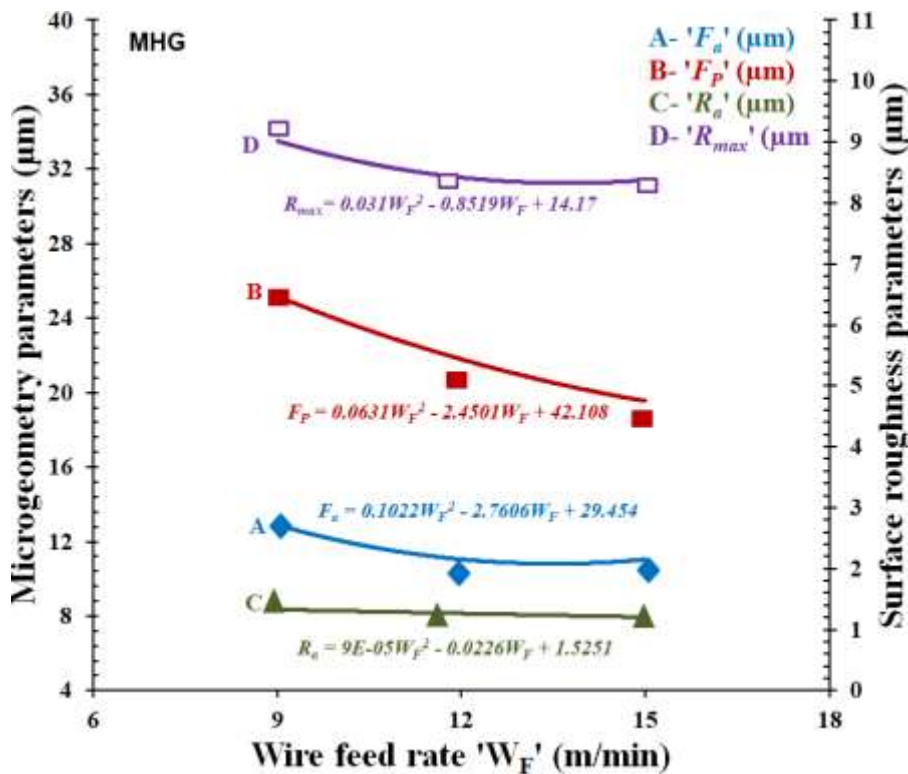


Fig. 4.14(d)

Fig. 4.14: Variation of surface roughness parameters and microgeometry errors of MHG with (a) servo voltage; (b) pulse-on time; (c) pulse-off time; and (d) wire feed rate.

#### 4.3.2.2 On Volumetric Gear Cutting Rate

Figure 4.15 depicts influences of pulse-on time, pulse-off time, servo voltage, and wire feed rate on the VGCR of MBG [Fig. 4.15(a)] and MHG [Fig. (4.15b)]. It can be seen from these figures that (i) VGCR increases with increase in servo voltage and pulse-on time due to occurrence of high discharge energy sparks between wire and meso-gear blank which accelerate the formation of irregular shaped craters on flank surfaces results in higher erosion of material; (ii) VGCR decreases with increase in pulse-off time due to fact that at higher value of pulse-off time decrease frequency of sparks between wire and workpiece resulting in removal of less material from workpiece per unit time; (iii) VGCR slightly increases with increase in wire feed rate because higher feed rate ensures that fresh wire is always available for sparking in WSEM process. It results in minimum deflection of wire and generation of more stable sparks between wire and workpiece which improves the material removal rate.

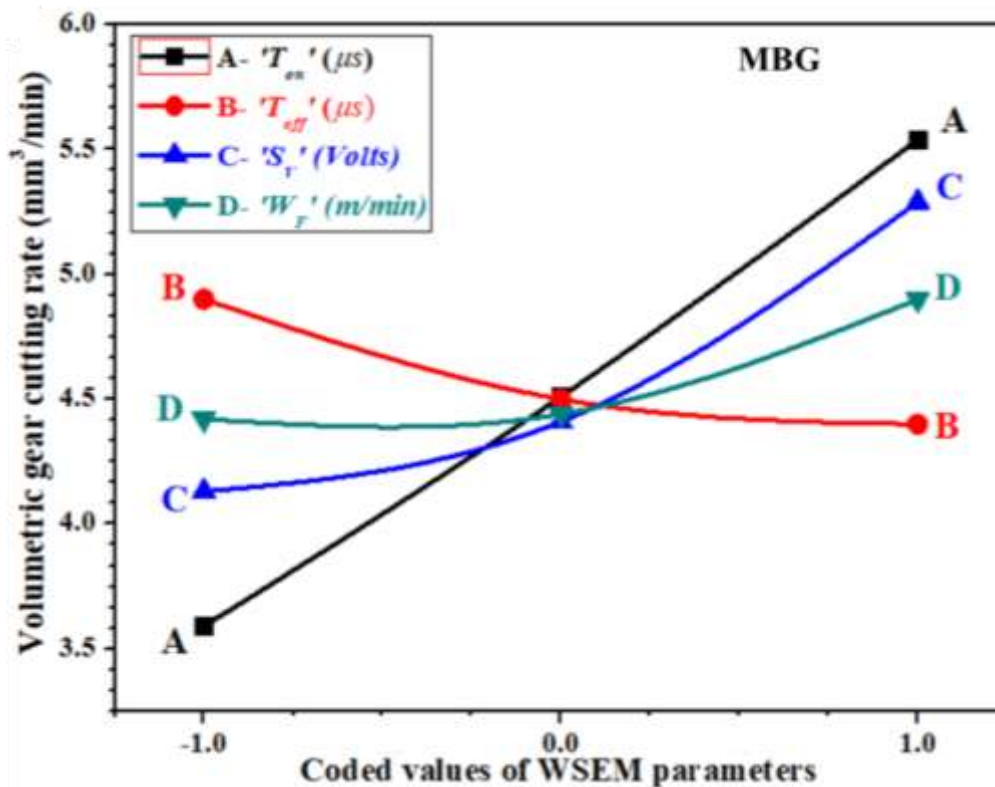


Fig. 4.15(a)

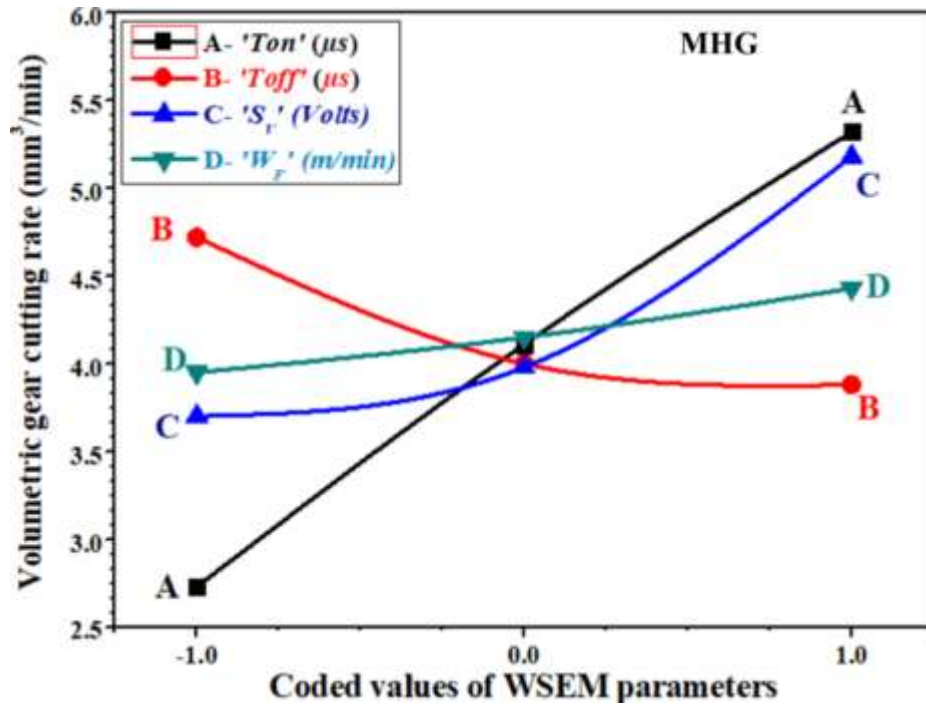


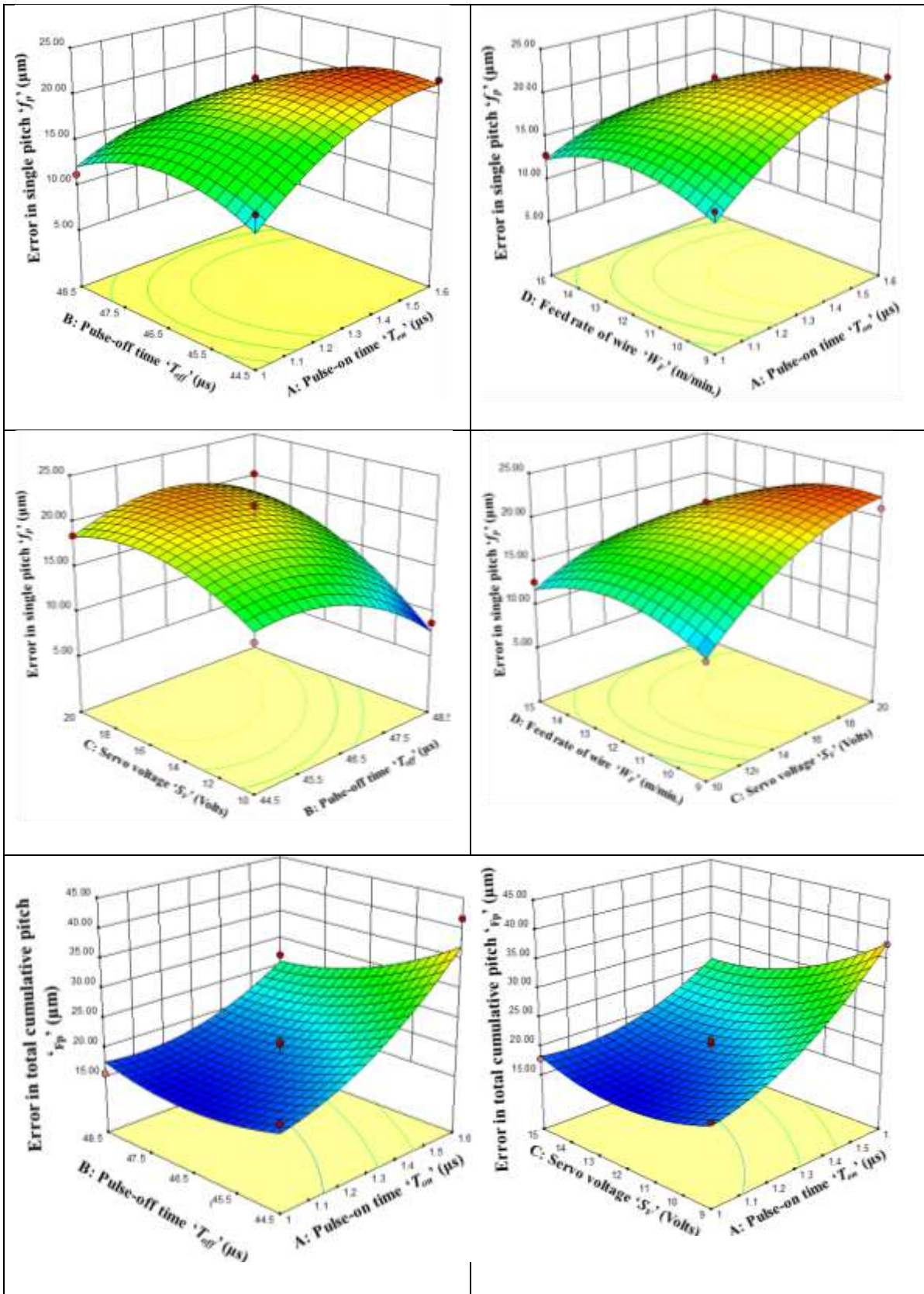
Fig. 4.15(b)

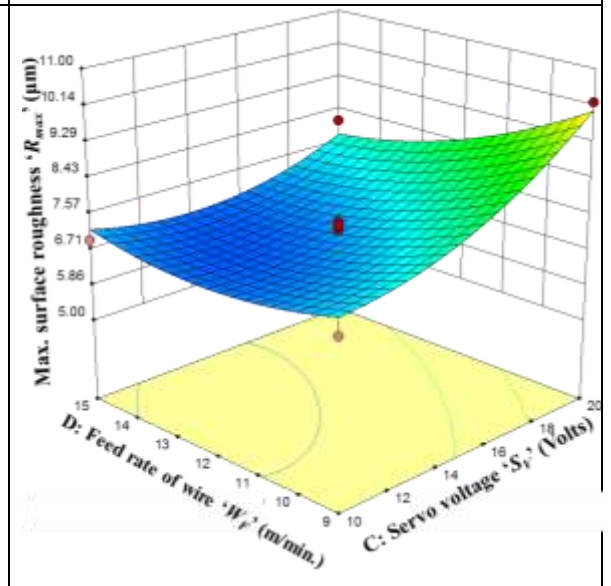
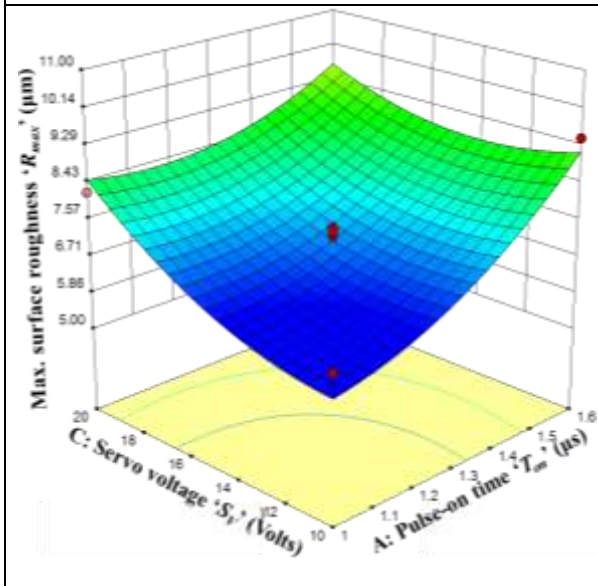
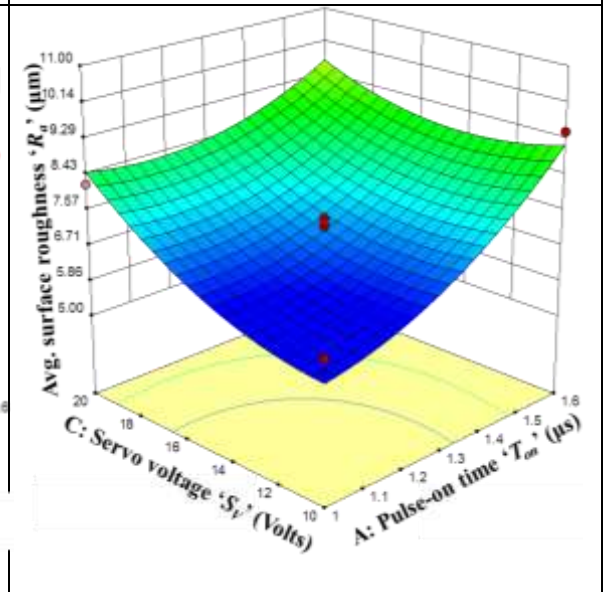
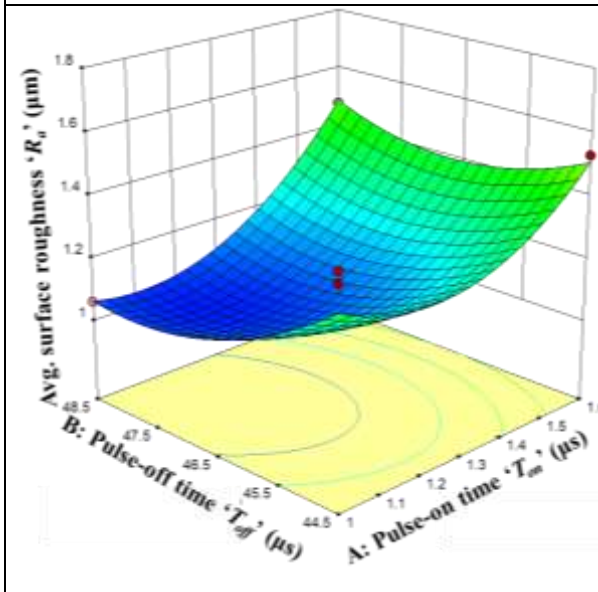
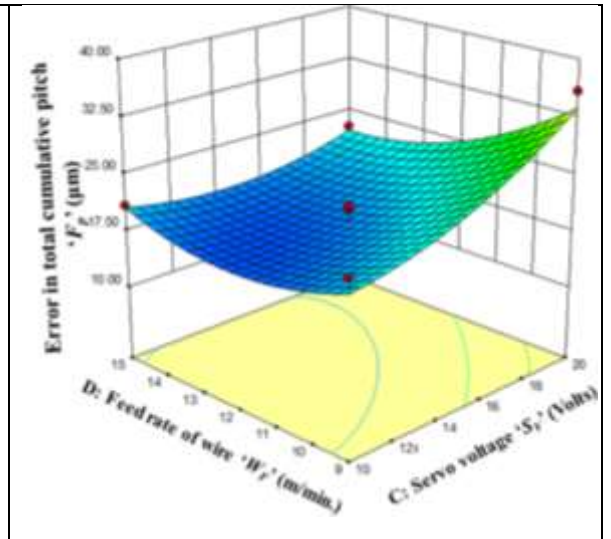
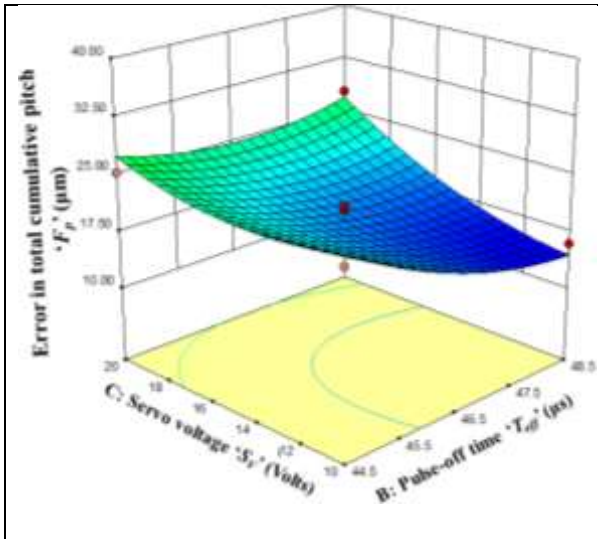
Fig. 4.15: Variation of volumetric gear cutting rate with WSEM parameters for: (a) MBG; and (b) MHG.

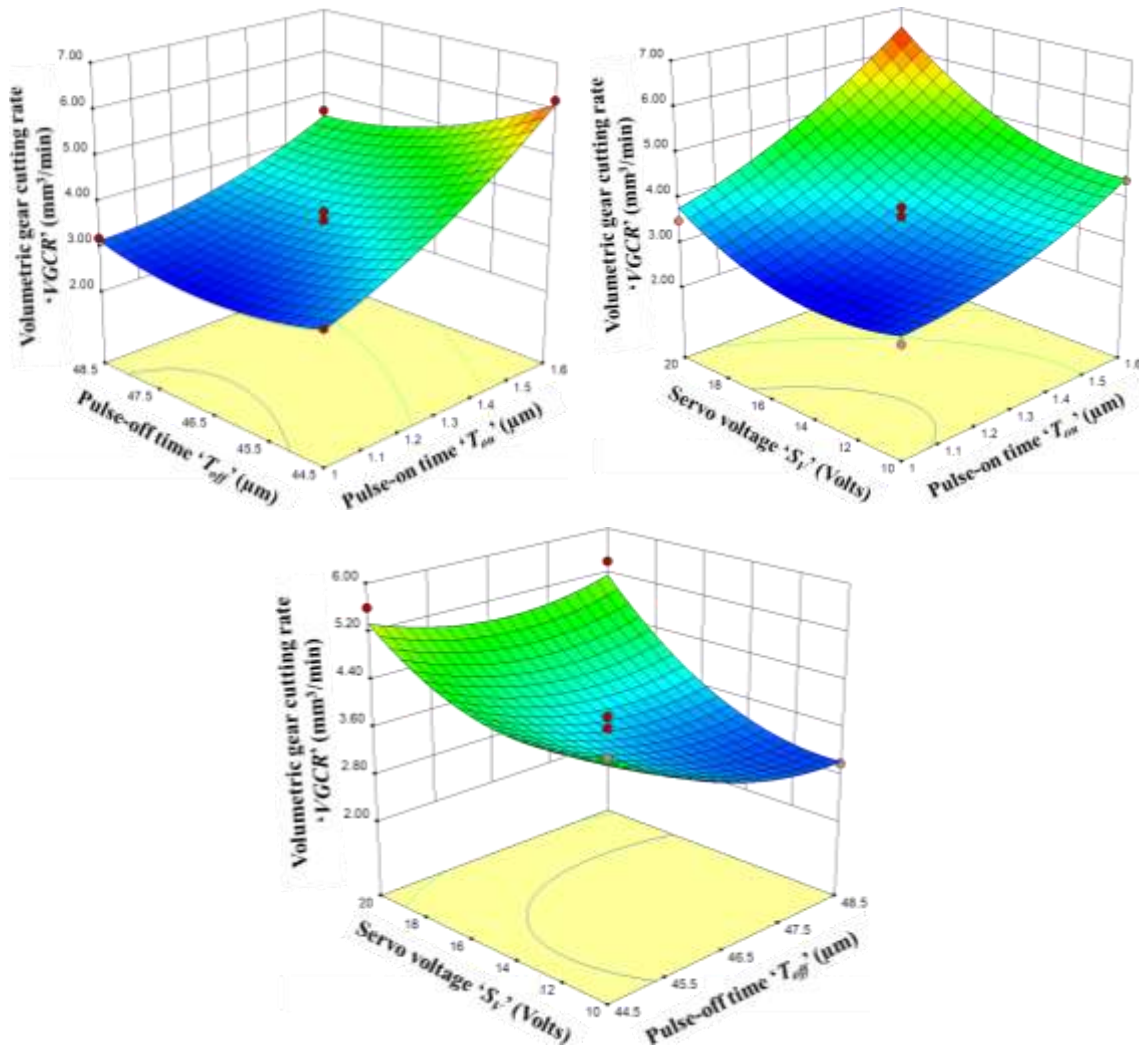
### 4.3.3 Influence of Significant Interactions of WSEM Parameters

Some significant interactions between the considered four WSEM parameters affecting the responses were found by ANOVA study. These interaction effects were plotted using the values of the responses predicted by the response surface models. For microgeometry errors and average and maximum surface roughness of MBG and MHG, interactions between  $T_{on}$  and  $T_{off}$ ,  $T_{on}$  and  $S_V$ ,  $T_{on}$  and  $W_F$ ,  $T_{off}$  and  $S_V$ , and  $S_V$  and  $W_F$  (except  $T_{on}$  and  $W_F$  for  $R_a$  of MHG) were found to be significant. While, for volumetric gear cutting rate, interactions between  $T_{on}$  and  $T_{off}$ ,  $T_{on}$  and  $S_V$ , and  $T_{off}$  and  $S_V$  were found to be significant. Figures 4.16 and 4.17 present the surface plots for MBG and MHG respectively showing the variation of the considered responses with the identified significant interactions of the WSEM parameters. It can be observed from these surface plots that minimum error in microgeometry and surface roughness parameters can be achieved by following combinations: (i) lower values of  $T_{on}$  and higher values of  $T_{off}$ , (ii) lower values of  $T_{on}$  and lower values of  $S_V$ , (iii) lower values of  $T_{on}$  and higher values of  $W_F$  (iv) higher values of  $T_{off}$  and lower values of  $S_V$ , and (iv) lower values of  $S_V$  and higher values of  $W_F$ . Maximum volumetric gear cutting rate has been achieved for following combinations: (i) higher values of pulse-on time and lower values of pulse-off time, (ii) higher values of

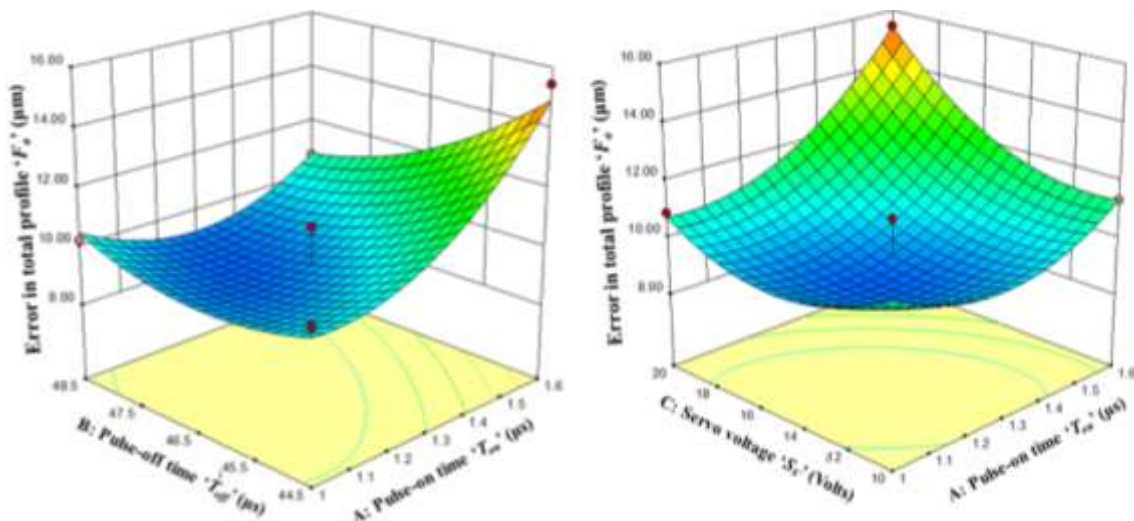
pulse-on time and servo voltage, and (iii) lower values of pulse-off time and higher values of servo voltage.

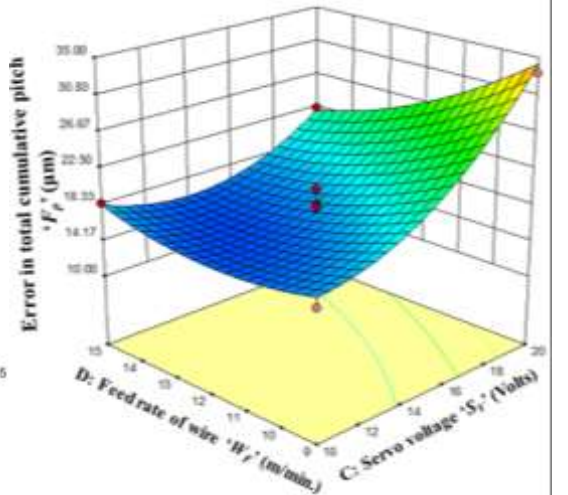
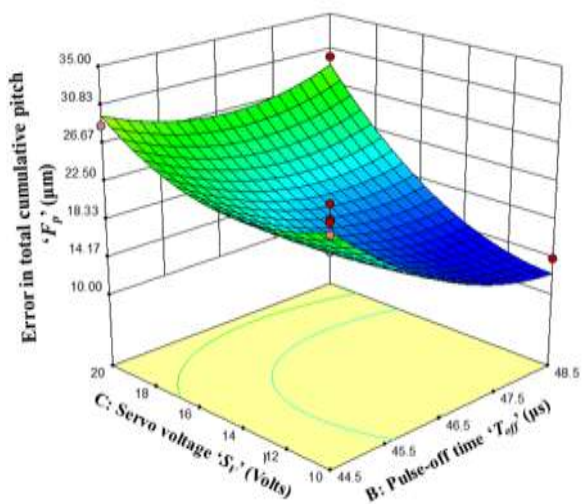
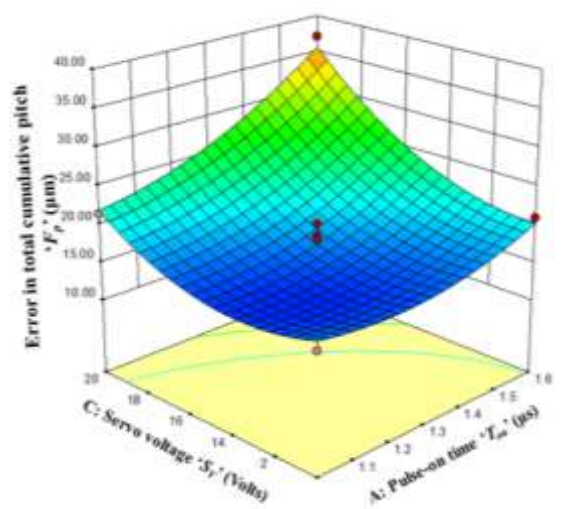
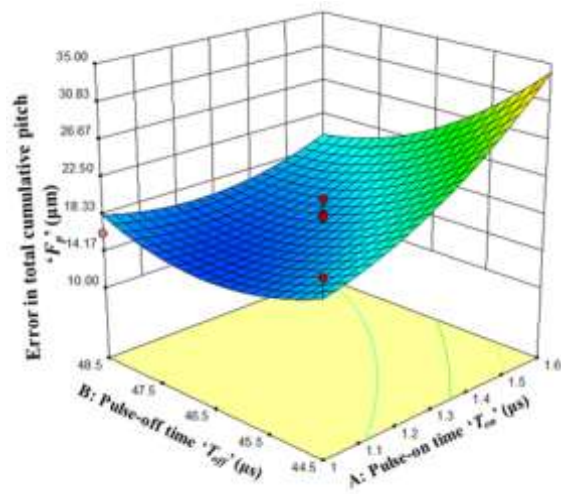
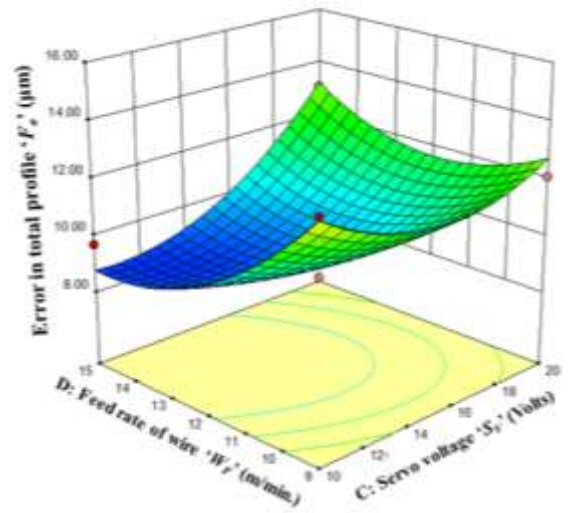
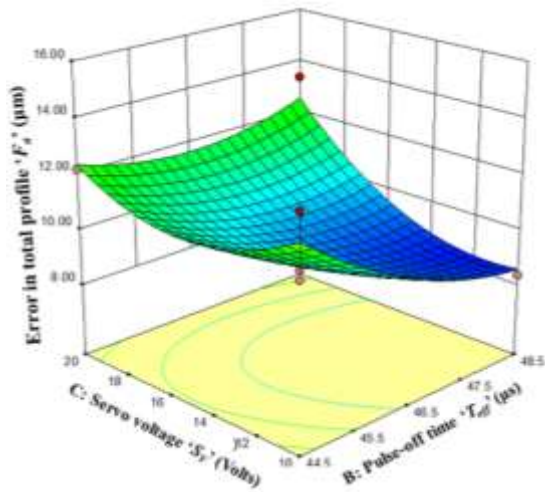


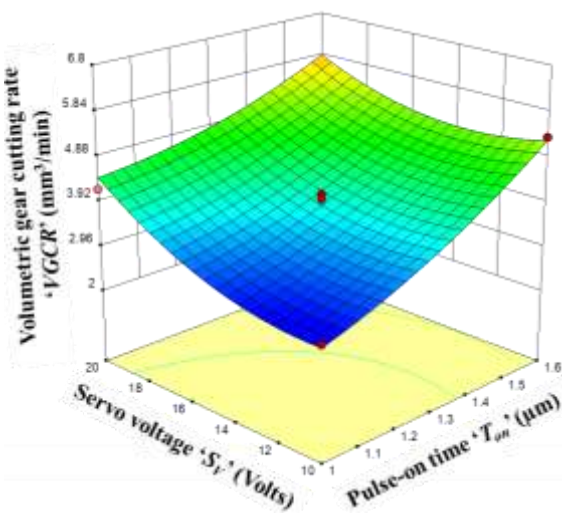
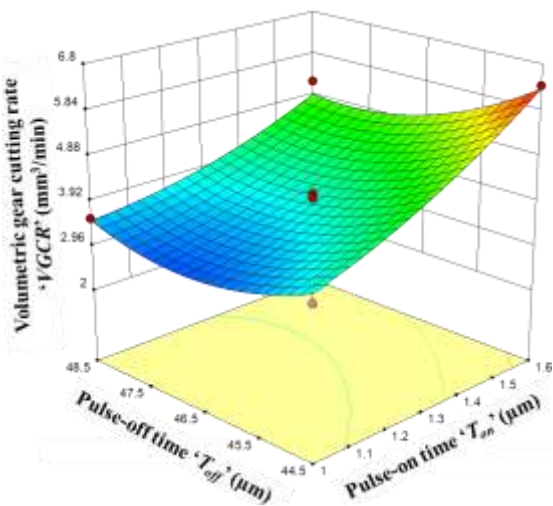
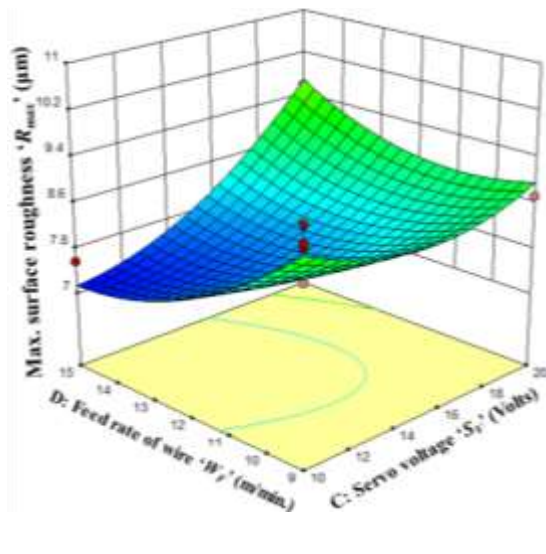
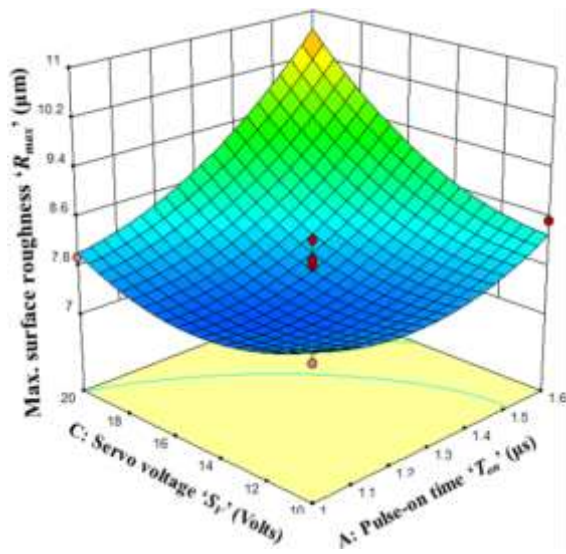
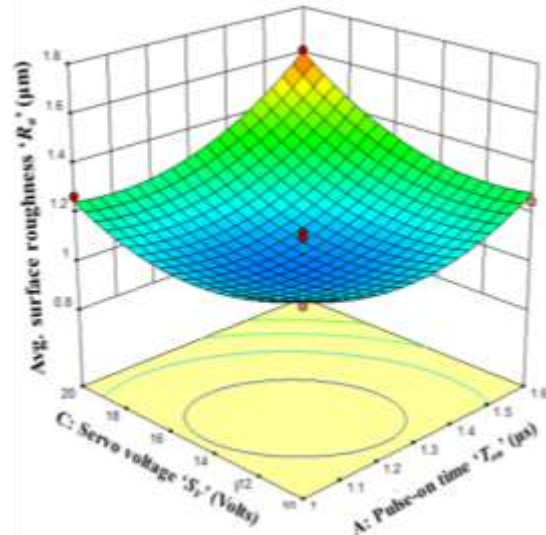
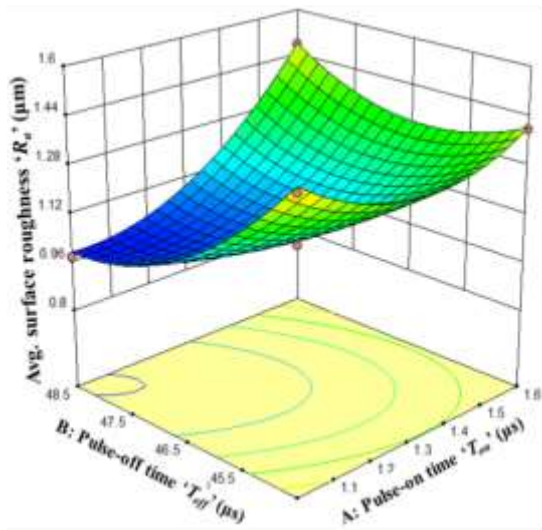




**Fig. 4.16:** Surface plots showing effects of the identified significant interactions on the considered responses of MBG.







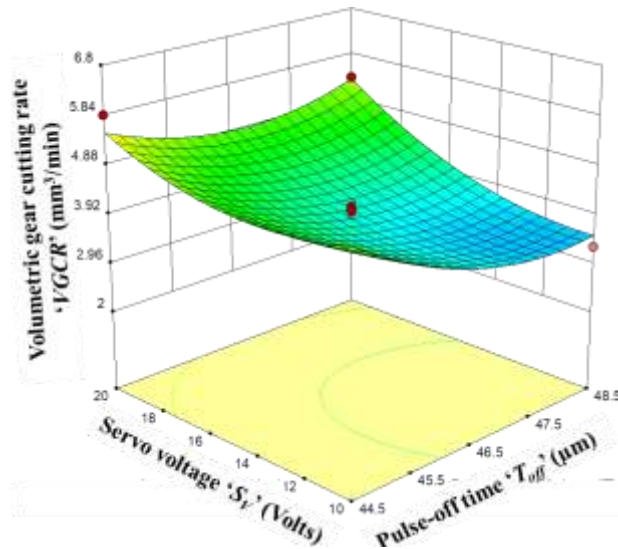


**Fig. 4.17:** Surface plots showing effects of the identified significant interactions on the considered responses of MHG.

#### 4.3.4 Conclusions of the Main Experiments

Following major conclusions can be drawn from the analyses of the experimental observations of the main experiments:

- Violent and non-uniform distribution of sparks, generation of irregular shaped craters on flank surfaces and wire vibration or wire lag are primarily responsible for determining overall quality of the WSEM manufactured MBG and MHG.
- Servo voltage, pulse-on-time, pulse-off-time and wire feed rate are found to be significant parameters affecting microgeometry errors and surface roughness of MBG and MHG during their manufacturing by WSEM process.
- Total profile error, single pitch error, total cumulative pitch error and maximum surface roughness decrease with decrease in pulse-on time and servo voltage, and with increase in wire feed rate and pulse-off time. Whereas, volumetric gear cutting rate increase with increase in of pulse-on time and servo voltage, decrease with increase in pulse-off time, and slightly increase with increase in wire feed rate. Therefore, lower values of pulse-on-time and servo voltage and higher values of pulse-off time and wire feed rate are recommended to manufacture higher accuracy and better quality MBG and MHG by WSEM process but at the cost of WSEM productivity.
- Single pitch error for MBG and total profile error for MHG decrease considerably during 12-15 and 9-12 m/min range of wire feed rate respectively
- Average surface roughness of MBG and MHG is insignificantly affected by four considered parameters of WSEM.

The *next chapter* describes modeling of the considered responses of MBG and MHG using ANN models, single-objective optimization of WSEM parameters using desirability function analysis, and multi-objective optimization of WSEM parameters using desirability function analysis and real-coded genetic algorithms with objectives to minimize microgeometry errors and surface roughness and maximize volumetric gear cutting rate of MBG and MHG.

## Chapter 5

### Modeling and Optimization

This presents modeling of the microgeometry errors, average and maximum surface roughness and volumetric gear cutting rate of MBG and MHG using ANN models, comparison of results predicted by response surface and ANN models, single-objective optimization of WSEM parameters using desirability function analysis (DFA), and multi-objective optimization of WSEM parameters using desirability function analysis and real-coded genetic algorithms with objectives to minimize microgeometry errors and surface roughness and maximize volumetric gear cutting rate of MBG and MHG.

#### 5.1 Modeling using Artificial Neural Network (ANN)

Performance and responses of many manufacturing processes are random, unpredictable, non-linear, and stochastic due to many parameters affecting them. WSEM process also belongs to this category. This makes a very experienced and skilled operator to select optimum process parameters and anticipate process performance. An effective solution to this problem is to establish relationships between the process performance measures and process parameters through appropriate modeling technique and then to optimize the process parameters. Effective and efficient optimization depends on the relationship established between process parameters and process performance measures (Zhang et al., 2013; Khan and Rajput, 2012). The relationship between WSEM process parameters and its performance measures can be established by analytical modelling, different empirical modelling techniques which may be explicit such as response surface models or implicit such as Taguchi orthogonal arrays, artificial neural network (ANN), group method of data handling (GMDH). Development of analytical models for microgeometry errors, average and maximum surface roughness and volumetric gear cutting rate of MBG and MHG are very difficult to develop due to their nature and many WSEM parameters affecting them. ANN modelling is very effective when sufficient reliable experimental data are available their training, validation, and testing purposes. It has capability to overcome the disadvantages of statistical modelling techniques which do not predict accurate results due to occurrence of noise in variables of a process. Therefore, feed forward back-propagation neural network (FF-BPNN) has been used in the present research work to develop models of the considered responses of MBG and MHG and process parameters of WSEM using logarithmic sigmoid transfer function as the activation function for the hidden and output layers and *Levenberg–Marquardt* reduction scheme to

train FF-BPNN. Results of 29 main experiments (as given in Table 4.4 and 4.5) were divided into training, validation and testing in the proportion of 60% (i.e. 17 data sets), 20% (i.e. 6 data sets), and 20% (6 data sets) for the purpose of developing the models, stopping the training, and estimating the considered responses respectively. Minimum value of mean square error was achieved by training the several FF-BPNN by varying number of the neurons in their hidden layer. Once it is achieved then that FF-BPNN was tested using 20% of experimental data meant for it. Ccorrelation coefficient indicates that how closely responses predicted by FF-BPNN agree with their actual values. Closeness of its value to 1 indicates prediction ability of FF-BPNN.

Performance of ANN depends upon number of neurons in input layers, hidden layers and output layers used in FF-BPNN. The developed models for prediction of microgeometry errors of MBG (i.e.  $f_{P_b}$  and  $F_{P_b}$ ) and of MHG (i.e.  $F_{a_h}$  and  $F_{P_h}$ ), average and maximum surface roughness of MBG and MHG (i.e.  $R_{a_b}$ ,  $R_{a_h}$ ,  $R_{max_b}$ , and  $R_{max_h}$ ) and volumetric gear cutting rate of MBG and MHG (i.e.  $VGCR_b$  and  $VGCR_h$ ) consisted of four neurons in their input layer corresponding to pulse-on time, pulse-off time, servo voltage, and wire feed rate, one hidden layer and one neurons (i.e. individual microgeometry parameters) in output layer. After various trial runs, the closest predicted results were obtained using 10 neurons in the hidden layer. Figure 5.1 depicts architecture of developed ANN model for each individual parameter of microgeometry, surface roughness and volumetric gear cutting rate of MBG and MHG and Table 5.1 presents their details.

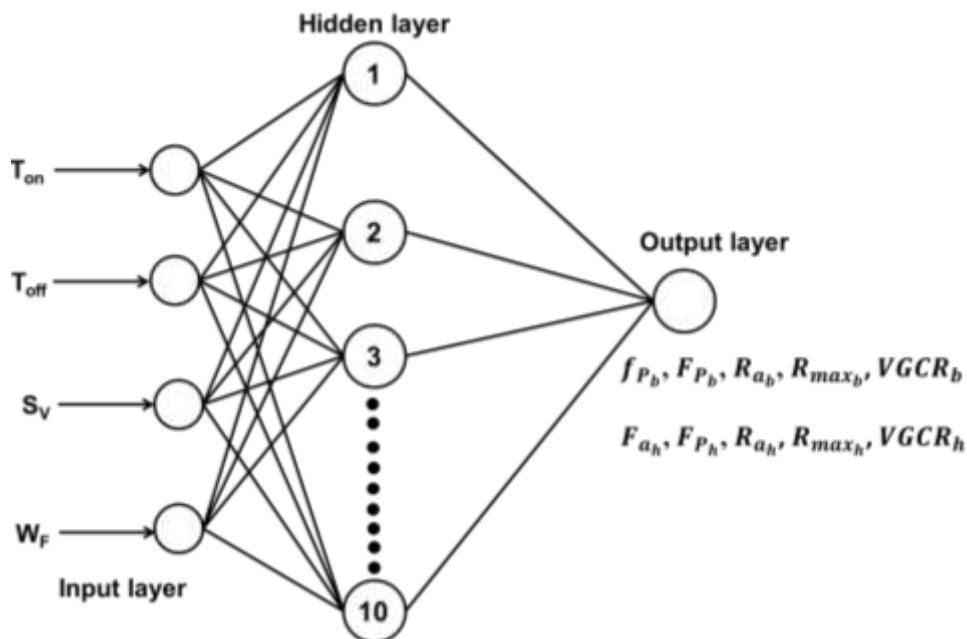


**Fig. 5.1:** Architecture of the ANN models for the considered responses of MBG and MHG.

**Table 5.1:** Details of the ANN models for the considered responses of MBG and MHG.

Responses	No. of neurons in input layer	No. of neurons in output layer	No. of neurons in hidden layer	No. of iterations used in training	Correlation coefficient
<i>Microgeometry parameters</i>					
$f_{P_b}$	4	1	10	100	0.976
$F_{P_b}$	4	1	10	400	0.992
$F_{a_h}$	4	1	10	300	0.977
$F_{P_h}$	4	1	10	100	0.999
<i>Surface roughness parameters</i>					
$R_{a_p}$	4	1	10	300	0.993
$R_{max_p}$	4	1	10	100	0.987
$R_{a_h}$	4	1	10	250	0.999
$R_{max_h}$	4	1	10	100	0.961
<i>Volumetric Gear Cutting Rate</i>					
$VGCR_b$	4	1	10	600	0.994
$VGCR_h$	4	1	10	200	0.987

## 5.2 Comparison of the Response Surface and ANN Models

Tables 5.2 and 5.3 present values of the considered responses of MBG and MHG predicted by their response surface models and ANN models. It can be observed from Tables 5.2 and 4.4 (for MBG), and Tables 5.3 and 4.5 (for MHG) that the values of microgeometry errors, average and maximum surface roughness, and volumetric gear cutting rate predicted by ANN models are better (smaller values for microgeometry errors and average and maximum surface roughness value ) than those predicted by their response surface models, more closer to the corresponding experimental values (presented in Tables 4.4 and 4.5) because of lower average value of the prediction error (PE) calculated using Eq. 5.1. The average prediction errors of ANN models are 2.04 and 2.08 % for MBG and MHG respectively. While, for response surface these errors are 4.2 and 3.58 % for MBG and MHG respectively.

$$PE (\%) = \frac{\text{Experimental value} - \text{Predicted value}}{\text{Experimental value}} \times 100 \quad (5.1)$$

**Table 5.2:** Response surface and ANN model predicted values of the considered responses of MBG.

Expt. No.	Variable input parameters				Responses									
	$T_{on}$	$T_{off}$	$S_V$	$W_F$	$f_{P_b}$ ( $\mu\text{m}$ )		$F_{P_b}$ ( $\mu\text{m}$ )		$R_{a_b}$ ( $\mu\text{m}$ )		$R_{max_b}$ ( $\mu\text{m}$ )		$VGCR_b$ ( $\text{mm}^3/\text{min}$ )	
	( $\mu\text{s}$ )	( $\mu\text{s}$ )	(Volts)	(m/min)	RM	ANN	RM	ANN	RM	ANN	RM	ANN	RM	ANN
1	1.3	46.5	10	15	11.82	12.80	20.69	21.22	1.19	1.16	7.23	6.93	3.9	3.5
2	1.0	44.5	15	12	12.46	14.11	17.90	19.21	1.33	1.36	7.49	7.84	3.2	3.16
3	1.3	46.5	15	12	20.16	19.63	18.99	18.53	1.09	1.10	7.12	7.12	3.6	3.57
4	1.6	48.5	15	12	13.79	11.50	25.78	26.70	1.49	1.48	8.30	7.10	4.5	4.52
5	1.6	46.5	15	15	14.08	13.92	26.45	25.55	1.37	1.33	7.96	8.29	5.1	5.17
6	1.3	46.5	15	12	20.16	19.63	18.99	18.53	1.09	1.10	7.12	7.12	3.6	3.57
7	1.3	44.5	20	12	18.44	18.50	27.48	25.76	1.52	1.54	9.33	8.66	5.3	5.66
8	1.3	48.5	15	15	09.69	09.43	17.83	18.09	1.11	1.12	6.51	6.55	3.9	3.83
9	1.6	46.5	10	12	12.81	13.75	24.75	23.44	1.31	1.37	9.16	8.14	4.4	4.58
10	1.3	44.5	15	15	16.02	15.24	25.21	25.64	1.33	1.29	8.77	8.79	4.9	4.77
11	1.3	48.5	20	12	18.14	19.00	26.98	25.86	1.50	1.52	9.08	8.69	5.2	5.38
12	1.3	46.5	20	15	14.69	14.70	22.17	23.15	1.34	1.33	7.81	7.28	5.3	5.08
13	1.3	48.5	10	12	07.79	08.93	14.45	16.28	1.02	1.05	6.30	6.52	3.0	3.02
14	1.0	46.5	15	15	12.41	13.84	18.25	18.43	1.19	1.24	7.12	6.75	3.5	3.49
15	1.3	46.5	20	9	22.38	21.10	33.71	35.80	1.74	1.74	10.04	9.38	4.9	4.7
16	1.6	46.5	15	9	21.32	21.90	37.76	37.95	1.70	1.65	10.56	8.90	5.1	5.37
17	1.3	44.5	15	9	17.26	16.88	29.47	28.96	1.46	1.38	9.14	9.11	4.2	4.06
18	1.3	48.5	15	9	15.93	15.97	25.19	22.89	1.39	1.40	8.55	9.03	3.6	3.35
19	1.0	46.5	20	12	14.46	12.48	18.25	17.20	1.36	1.25	8.52	8.26	3.8	4.02
20	1.0	46.5	15	9	12.65	13.93	18.56	19.10	1.27	1.35	6.92	8.68	2.5	2.9
21	1.3	46.5	15	12	20.16	19.63	18.99	18.53	1.09	1.10	7.12	7.12	3.6	3.57
22	1.3	46.5	15	12	20.16	19.63	18.99	18.53	1.09	1.10	7.12	7.12	3.6	3.57
23	1.0	46.5	10	12	10.93	09.87	16.96	17.75	1.13	1.09	5.85	6.58	3.0	2.89
24	1.0	48.5	15	12	12.12	11.58	17.49	15.99	1.06	1.07	7.12	6.88	3.2	3.23
25	1.6	44.5	15	12	21.12	20.49	37.02	40.27	1.51	1.67	10.78	10.30	6.1	6.09
26	1.3	46.5	10	9	11.61	13.51	20.78	24.60	1.20	1.15	7.40	7.25	3.3	3.39
27	1.3	46.5	15	12	20.16	19.63	18.99	18.53	1.09	1.10	7.12	7.12	3.6	3.57
28	1.6	46.5	20	12	22.91	23.53	37.87	35.79	1.78	1.78	9.68	8.49	6.6	6.36
29	1.3	44.5	10	12	15.16	14.73	25.60	23.62	1.30	1.28	8.90	8.88	4.5	4.28

**Table 5.3:** Response surface and ANN model predicted values of the considered responses of MHG.

Expt. No.	Variable input parameters				Responses									
	$T_{on}$ ( $\mu s$ )	$T_{off}$ ( $\mu s$ )	$S_V$ (Volts)	$W_F$ (m/min)	$F_{a_h}$ ( $\mu m$ )		$F_{P_h}$ ( $\mu m$ )		$R_{a_h}$ ( $\mu m$ )		$R_{max_h}$ ( $\mu m$ )		$VGCR_h$ ( $mm^3/min$ )	
					RM	ANN	RM	ANN	RM	ANN	RM	ANN	RM	ANN
1	1.3	46.5	10	15	08.79	11.15	18.41	18.58	1.18	1.13	7.13	7.58	4.56	4.50
2	1.0	44.5	15	12	10.10	10.42	18.66	20.75	1.47	1.45	7.60	7.11	3.73	3.59
3	1.3	46.5	15	12	09.41	09.44	17.55	16.15	1.09	1.12	7.73	7.78	3.77	3.90
4	1.6	48.5	15	12	10.82	10.77	20.11	17.15	1.49	1.48	8.59	7.12	4.80	4.99
5	1.6	46.5	15	15	11.47	11.88	20.87	21.00	1.30	1.36	8.68	7.11	5.35	5.51
6	1.3	46.5	15	12	09.41	09.44	17.55	16.95	1.09	1.10	7.73	7.78	3.77	3.90
7	1.3	44.5	20	12	12.38	12.20	29.76	28.65	1.46	1.42	9.04	8.92	5.40	5.94
8	1.3	48.5	15	15	10.06	10.64	15.15	15.33	1.11	1.06	8.31	8.27	4.33	4.02
9	1.6	46.5	10	12	11.36	11.35	20.24	21.00	1.29	1.25	8.31	8.55	5.16	5.30
10	1.3	44.5	15	15	10.94	11.30	23.75	21.78	1.30	1.29	8.33	8.37	5.51	5.29
11	1.3	48.5	20	12	12.57	13.35	28.99	29.90	1.38	1.38	9.53	11.02	5.21	5.45
12	1.3	46.5	20	15	13.26	13.10	22.23	22.48	1.23	1.21	9.69	9.62	5.15	5.43
13	1.3	48.5	10	12	08.57	08.41	12.35	14.03	1.09	1.16	7.34	7.12	3.47	3.34
14	1.0	46.5	15	15	10.75	10.43	16.92	18.13	1.13	1.18	8.08	8.14	3.94	4.27
15	1.3	46.5	20	9	12.76	12.09	34.32	33.28	1.48	1.50	8.97	8.67	5.19	5.23
16	1.6	46.5	15	9	15.33	15.43	31.11	30.48	1.46	1.44	10.22	9.80	5.36	5.41
17	1.3	44.5	15	9	13.93	14.06	27.89	27.98	1.43	1.46	9.46	8.38	4.68	4.93
18	1.3	48.5	15	9	11.10	11.03	22.25	24.48	1.22	1.21	8.46	8.97	4.20	4.49
19	1.0	46.5	20	12	10.75	10.89	21.95	21.45	1.25	1.27	8.01	7.94	4.36	4.35
20	1.0	46.5	15	9	10.92	11.18	17.91	18.35	1.21	1.19	7.83	9.27	2.97	3.10
21	1.3	46.5	15	12	09.41	09.44	17.55	18.29	1.09	1.02	7.73	7.78	3.77	3.90
22	1.3	46.5	15	12	09.41	09.44	17.55	18.10	1.09	1.12	7.73	7.78	3.77	3.90
23	1.0	46.5	10	12	10.90	10.87	16.82	15.63	1.22	1.20	7.99	7.90	2.70	3.12
24	1.0	48.5	15	12	10.50	10.23	18.37	16.28	1.00	0.98	8.21	8.21	3.45	3.56
25	1.6	44.5	15	12	14.92	15.42	34.07	35.28	1.41	1.40	10.22	10.37	6.18	6.17
26	1.3	46.5	10	9	13.31	13.79	17.56	16.43	1.18	1.17	9.14	9.38	3.57	3.30
27	1.3	46.5	15	12	09.41	09.44	17.55	18.48	1.09	1.07	7.73	7.78	3.77	3.90
28	1.6	46.5	20	12	15.42	15.41	35.68	37.13	1.61	1.67	10.68	11.02	5.70	5.56
29	1.3	44.5	10	12	12.46	11.24	25.82	25.48	1.40	1.43	8.85	8.31	4.94	5.04

### 5.3 Optimization Using Desirability Function Analysis

Optimization of WSEM process was done using desirability function analysis for (i) simultaneous minimization of microgeometry errors of MBG (i.e.  $f_{P_b}$  and  $F_{P_b}$ ) and MHG ( $F_{a_h}$  and  $F_{P_h}$ ) and their average and maximum surface roughness values (i.e.  $R_{a_b}$ ,  $R_{a_h}$ ,  $R_{max_b}$ , and  $R_{max_h}$ ); and (ii) and maximizing their volumetric gear cutting rates (i.e.  $VGCR_b$  and  $VGCR_h$ ). Desirability function analysis (DFA) is a useful technique for simultaneous optimization of the multiple responses. It involves computation of desirability ' $d_i$ ' ( $0 \leq d_i \leq 1$ ) of each response ' $y_i$ ' and then computing overall desirability ' $D$ ' ( $0 \leq D \leq 1$ ) which is geometrical mean of the computed desirabilities of all the considered responses. Equation 5.2 can be used to compute the overall desirability ' $D_j$ ' for  $j^{th}$  experimental observation (Montgomery, 2009).

$$D_j = \left( \prod_{i=1}^m d_{ij} \right)^{\frac{1}{\sum_{i=1}^m w_i}} \quad (5.2)$$

Where,  $m$  is total number of the responses;  $w_i$  is relative weightage assigned to  $i^{th}$  response; and  $d_{ij}$  is the desirability of the  $i^{th}$  response for the  $j^{th}$  experimental observation which can be computed using following Equations depending upon the type of the objective function.

For *minimization* of the responses (i.e. *smaller-the-better type*)

$$d_i = \left( \frac{U_i - y_{ij}}{U_i - T_i} \right)^{w_i} \quad (5.3)$$

For *maximization* of the responses (i.e. *larger-the-better type*)

$$d_i = \left( \frac{y_{ij} - L_i}{T_i - L_i} \right)^{w_i} \quad (5.4)$$

Here,  $T_i$  is the target value of the  $i^{th}$  response;  $U_i$  is permissible upper value of the  $i^{th}$  response;  $L_i$  is permissible lower value of the  $i^{th}$  response;  $y_{ij}$  is the value of  $i^{th}$  response in  $j^{th}$  experimental observation; and  $w_i$  is relative weightage assigned to  $i^{th}$  response. If  $w_i$  is selected to be equal to 1 then it makes the desirability function linear. Using  $w_i$  more than 1 puts more importance on being close to the target value; and selecting  $0 < w_i < 1$  makes this less important (Montgomery, 2014). DFA approach was employed for simultaneous minimization of the considered microgeometry errors and surface roughness parameters of MBG and MHG using the Eq. 5.3 and to maximize the VGCR of MBG and MHG using Eq. 5.4. Following subsections describe their details.

### 5.3.1 Minimization of Microgeometry Errors and Surface Roughness

Concept of DFA was used to find optimum values of four parameters of WSEM (i.e. pulse-on time, pulse-off time, servo voltage, and wire feed rate) through simultaneous minimisation of the considered microgeometry errors of MBG and MHG and their average and maximum surface roughness values (i.e. all the responses are smaller-the-better type) and assigning equal weightage to each response. Equations 5.5 to 5.9 were used to compute the desirability of each response for the  $j^{th}$  experimental observation and using target value equal to minimum value of a response identified from its experimental values:

$$\text{For MBG only} \quad (d_{f_p})_j = \left[ \frac{f_{p_{max}} - f_{p_j}}{f_{p_{max}} - f_{p_{min}}} \right]^{0.25} \quad (5.5)$$

$$\text{For MHG only} \quad (d_{F_a})_j = \left[ \frac{F_{a_{max}} - F_{a_j}}{F_{a_{max}} - F_{a_{min}}} \right]^{0.25} \quad (5.6)$$

$$\text{For both MBG and MHG} \quad (d_{F_p})_j = \left[ \frac{F_{p_{max}} - F_{p_j}}{F_{p_{max}} - F_{p_{min}}} \right]^{0.25} \quad (5.7)$$

$$\text{For both MBG and MHG} \quad (d_{R_a})_j = \left[ \frac{R_{a_{max}} - R_{a_j}}{R_{a_{max}} - R_{a_{min}}} \right]^{0.25} \quad (5.8)$$

$$\text{For both MBG and MHG} \quad (d_{R_{max}})_j = \left[ \frac{R_{max_{max}} - R_{max_j}}{R_{max_{max}} - R_{max_{min}}} \right]^{0.25} \quad (5.9)$$

Where,  $f_{p_{min}}, F_{p_{min}}, F_{a_{min}}, R_{a_{min}}, R_{max_{min}}, f_{p_{max}}, F_{p_{max}}, F_{a_{max}}, R_{a_{max}}$  and  $R_{max_{max}}$  are the minimum and maximum values of single pitch error, total cumulative pitch error, total profile error, average and maximum surface roughness values identified from the experimental results. These values were selected from the results of 29 main experiments presented in Tables 4.4 (for MBG) and 4.5 (for MHG). Minimum values used for MBG included 8.75  $\mu\text{m}$  for  $f_p$ ; 15.45  $\mu\text{m}$  for  $F_p$ ; 1.0  $\mu\text{m}$  for  $R_a$ ; and 6.38  $\mu\text{m}$  for  $R_{max}$  with corresponding maximum values being 23.55  $\mu\text{m}$ ; 41.6  $\mu\text{m}$ ; 1.79  $\mu\text{m}$ ; and 11.0  $\mu\text{m}$ . For MHG, minimum values used were 8.33  $\mu\text{m}$  for  $F_a$ ; 14.03  $\mu\text{m}$  for  $F_p$ ; 0.98  $\mu\text{m}$  for  $R_a$ ; and 7.11  $\mu\text{m}$  for  $R_{max}$  with their maximum values being 15.43  $\mu\text{m}$ ; 37.13  $\mu\text{m}$ ; 1.61  $\mu\text{m}$ ; and 11.02  $\mu\text{m}$ . Overall desirability for the  $j^{th}$  experimental observation of MBG and MHG were computed by *Design Expert (version 10)* software using Equations 5.10 and 5.11 respectively.

**For MBG:**

$$D_{jb} = \left[ \left\{ (d_{f_p})_j \right\}^{0.25} \left\{ (d_{F_p})_j \right\}^{0.25} \left\{ (d_{R_a})_j \right\}^{0.25} \left\{ (d_{R_{max}})_j \right\}^{0.25} \right]^{\frac{1}{0.25 + 0.25 + 0.25 + 0.25}}$$

$$\Rightarrow D_{jb} = \left[ (d_{f_p})_j (d_{F_p})_j (d_{R_a})_j (d_{R_{max}})_j \right]^{0.25} \quad (5.10)$$

**For MHG:**

$$D_{jh} = \left[ \{(d_{Fa})_j\}^{0.25} \{(d_{Fp})_j\}^{0.25} \{(d_{Ra})_j\}^{0.25} \{(d_{Rmax})_j\}^{0.25} \right]^{\frac{1}{0.25 + 0.25 + 0.25 + 0.25}}$$

$$\Rightarrow D_{jh} = \left[ (d_{Fa})_j (d_{Fp})_j (d_{Ra})_j (d_{Rmax})_j \right]^{0.25} \quad (5.11)$$

Once values of overall desirability for all the experimental observations are calculated then the software identifies that parametric combination as optimum which gives maximum possible value of overall desirability (i.e. either equal to 1 or nearest to 1). Table 5.5 presents the obtained optimum values of WSEM parameters along with optimum values of the corresponding responses for MBG and MHG.

### 5.3.2 Maximization of Volumetric Gear Cutting Rate

DFA was also used to identify the optimum value of  $T_{on}$ ,  $T_{off}$ ,  $S_V$ , and  $W_F$  with single objective function to maximize the volumetric gear cutting rate ‘VGCR’ of MBG and MHG i.e. (larger-the-better type response) and assigning weightage of 1. Eq. 5.12 was used to compute the desirability for the  $j^{th}$  experimental observation.

$$\text{For both MBG and MHG} \quad (d_{VGCR})_j = \left[ \frac{VGCR_j - VGCR_{min}}{VGCR_{max} - VGCR_{min}} \right] \quad (5.12)$$

Where  $VGCR_{min}$  and  $VGCR_{max}$  are the minimum and maximum values of VGCR of MBG (or MHG) identified from the results of 29 main experiments presented in Tables 4.4 (for MBG) and 4.5 (for MHG). This gave minimum and maximum values of VGCR as 2.78 and 6.4 mm<sup>3</sup>/min for MBG and 2.8 and 6.35 for MHG, respectively. Overall desirability for the  $j^{th}$  experimental observation of VGCR for MBG and MHG was computed using Eq. 5.13 by *Design Expert (version 10)* software. Table 5.5 presents the obtained optimum values of WSEM parameters along with optimum values of VGCR of MBG and MHG.

$$D_j = (d_{VGCR})_j \quad (5.13)$$

### 5.4 Multi-Objective Optimization

Simultaneous minimization of microgeometry errors, average surface roughness, and maximum surface roughness, and maximization of volumetric gear cutting rate have been found to conflict each other for both MBG and MHG based up on observations of main experiments. Therefore, concept of multi-objective optimization was employed using desirability function analysis and real-coded genetic algorithm to identify optimum values of  $T_{on}$ ,  $T_{off}$ ,  $S_V$ , and  $W_F$ . They are mentioned in following subsections:

#### 5.4.1 Using Desirability Function Analysis

The multi-objective optimization by DFA was accomplished by assigning equal weights to all the microgeometry errors of MBG (i.e.  $f_{P_b}$  and  $F_{P_b}$ ) and MHG ( $F_{a_h}$  and  $F_{P_h}$ ) and their average and maximum surface roughness values (i.e.  $R_{a_b}$ ,  $R_{a_h}$ ,  $R_{max_b}$ , and  $R_{max_h}$ ); and their volumetric gear cutting rates (i.e.  $VGCR_b$  and  $VGCR_h$ ) i.e. 0.2 to objective to achieve value of overall desirability nearest to 1. Equations 5.5 to 5.9 were used to compute individual desirability of microgeometry errors, and average and maximum surface roughness of MBG and MHG and Eq. 5.12 was used to compute individual desirability of VGCR of MBG and MHG for the  $j^{th}$  experimental observation by assigning weightage as 0.2. Overall desirabilities corresponding to the  $j^{th}$  experimental observation of MBG and MHG for multi-objective optimization were computed by *Design Expert (version 10)* software using Equations 5.14 and 5.15 respectively.

**For MBG**

$$D_{jbm} = \left[ \left\{ (d_{f_p})_j \right\}^{0.2} \left\{ (d_{F_p})_j \right\}^{0.2} \left\{ (d_{R_a})_j \right\}^{0.2} \left\{ (d_{R_{max}})_j \right\}^{0.2} \left\{ (d_{VGCR})_j \right\}^{0.2} \right]^{\frac{1}{0.2+0.2+0.2+0.2+0.2}}$$

$$\Rightarrow D_{jbm} = \left[ (d_{f_p})_j (d_{F_p})_j (d_{R_a})_j (d_{R_{max}})_j (d_{VGCR})_j \right]^{0.2} \quad (5.14)$$

**For MHG**

$$D_{jhm} = \left[ \left\{ (d_{F_a})_j \right\}^{0.2} \left\{ (d_{F_p})_j \right\}^{0.2} \left\{ (d_{R_a})_j \right\}^{0.2} \left\{ (d_{R_{max}})_j \right\}^{0.2} \left\{ (d_{VGCR})_j \right\}^{0.2} \right]^{\frac{1}{0.2+0.2+0.2+0.2+0.2}}$$

$$\Rightarrow D_{jhm} = \left[ (d_{F_a})_j (d_{F_p})_j (d_{R_a})_j (d_{R_{max}})_j (d_{VGCR})_j \right]^{0.2} \quad (5.15)$$

Once values of overall desirability for all the experimental observations are calculated then the software identifies that parametric combination as optimum which gives maximum possible value of overall desirability (i.e. either equal to 1 or nearest to 1). Table 5.5 presents the obtained optimum values of WSEM parameters along with optimum values of the corresponding responses for MBG and MHG. Comparing results of optimization done by DFA considering different objectives reveals that multi-objective optimization by DFA as compared to simultaneous optimization of microgeometry errors and surface roughness (i) increases microgeometry errors, avg. and max. surface roughness of MBG; (ii) does not significantly change microgeometry errors, avg. and max. surface roughness of MHG; (iii) decreases values of VGCR of MBG and MHG; and (iv) decreases maximum value of overall desirability.

### 5.4.2 Using Real-coded Genetic Algorithm

Real-coded genetic algorithm (RCGA) was used for multi-objective optimization of conflicting objectives of minimizing microgeometry errors of MBG (i.e.  $f_{P_b}$  and  $F_{P_b}$ ) and MHG ( $F_{a_h}$  and  $F_{P_h}$ ) and their average and maximum surface roughness values (i.e.  $R_{a_b}$ ,  $R_{a_h}$ ,  $R_{max_b}$ , and  $R_{max_h}$ ); and maximizing their volumetric gear cutting rates (i.e.  $VGCR_b$  and  $VGCR_h$ ) using their corresponding response surface models (i.e. Equations 4.1a to 4.1e for MBG and Equations 4.2a to 4.2e for MHG) as objective functions. Figure 5.2 depicts flow chart of using RCGA for multi-objective optimization. It used ranges of four WSEM parameters (namely pulse-on time, pulse-off time, servo voltage and wire feed rate) used in the main experiments as their variable bounds also presented in Table 5.4 along with RCGA parameters used in the present work. Table 5.5 presents the RCGA optimized values of WSEM parameters along with optimum values of the corresponding responses for MBG and MHG.

**Table 5.4:** Variable bounds of the WSEM parameters and RCGA parameters used in multi-objective optimization.

Pulse-on time ' $T_{on}$ ' ( $\mu$ s)	$1 \leq T_{on} \leq 1.6$
Pulse-off time ' $T_{off}$ ' ( $\mu$ s)	$44.5 \leq T_{off} \leq 48.5$
Servo voltage ' $S_V$ ' (Volts)	$10 \leq S_V \leq 20$
Wire feed rate ' $W_F$ ' (m/min)	$9 \leq W_F \leq 15$
<b>Details of RCGA parameters</b>	
Population size	50
Number of generations	164 (MBG), 120 (MHG)
Reproduction operator	Tournament
Crossover function	Intermediate
Crossover probability	0.8
Mutation function	Uniform
Mutation probability	0.01

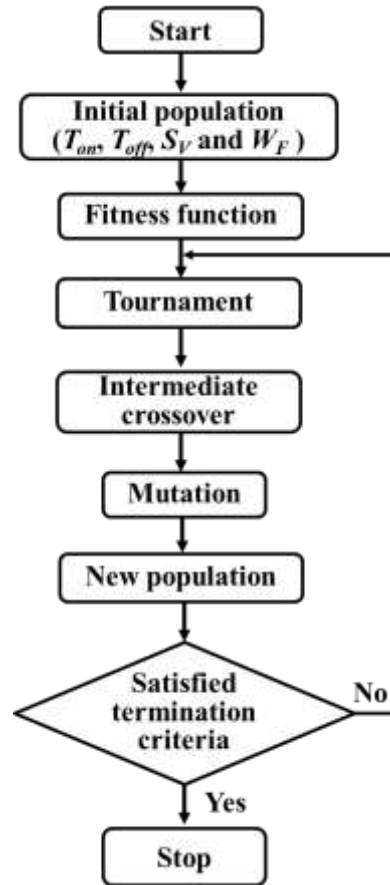


**Fig. 5.2:** Flow chart of the real-coded genetic algorithm used in multi-objective optimization.

### 5.5 Validation of the Optimization Results

Results of optimization by DFA and RCGA discussed in the previous sections were confirmed by conducting validation experiments using those standard values available on the WSEM machine which were nearest to the optimized values of WSEM parameters. Using the standard optimum values, 8 validation experiments were conducted separately for MBG and MHG to confirm the optimum values of their considered responses in four different types of optimizations. Two validation experiments were conducted for MBG and MHG separately to confirm results of simultaneous optimization of  $f_{P_b}$ ,  $F_{P_b}$ ,  $R_{max_b}$ ,  $R_{a_b}$  and  $VGCR_b$  of MBG and  $F_{a_h}$ ,  $F_{P_h}$ ,  $R_{a_h}$ ,  $R_{max_h}$  and  $VGCR_h$  of MHG by DFA. Table 5.6 presents optimized WSEM parameters and the considered responses for MBG and MHG along with their corresponding values from the experimental validation. It reveals that there is very good agreement between the experimental results and optimization results given by DFA. Validation experiments assigned the gear quality DIN 6 for  $f_p$  and  $F_p$  of MBG, and DIN 7 and DIN 6 for  $F_a$  and  $F_p$  of MHG, respectively.

**Table 5.5:** Optimized values of four parameters of WSEM given by DFA and RCGA along with corresponding values of considered responses of MBG and MHG.

Optimum values of WSEM parameters				Optimum values of responses ( $\mu\text{m}$ )					Maximum value of overall desirability
$T_{on}$ ( $\mu\text{s}$ )	$T_{off}$ ( $\mu\text{s}$ )	$S_V$ (Volts)	$W_F$ (m/min)	$f_{P_b}$	$F_{P_b}$	$R_{a_b}$	$R_{max_b}$	$VGCR_b$	$D_{j_b}$
<b>For MBG</b>				$f_{P_b}$	$F_{P_b}$	$R_{a_b}$	$R_{max_b}$	$VGCR_b$	$D_{j_b}$
1.14	48.38	10.49	12.12	8.41	15.06	0.99	5.93	--	1.0
<b>For MHG</b>				$F_{a_h}$	$F_{P_h}$	$R_{a_h}$	$R_{max_h}$	$VGCR_h$	$D_{j_h}$
1.25	47.73	11.7	13.3	8.33	13.4	1.03	7.02	--	0.99
<b>Objective:</b> Simultaneous minimization of microgeometry errors, avg. and max. surface roughness by DFA									
<b>For MBG</b>				$f_{P_b}$	$F_{P_b}$	$R_{a_b}$	$R_{max_b}$	$VGCR_b$	$D_{j_b}$
1.58	46.03	19.12	12.17	--	--	--	--	6.5	0.99
<b>For MHG</b>				$F_{a_h}$	$F_{P_h}$	$R_{a_h}$	$R_{max_h}$	$VGCR_h$	$D_{j_h}$
1.5	44.6	10.3	14.8	--	--	--	--	6.8	0.98
<b>Objective:</b> Maximization of volumetric gear cutting rate by DFA									
<b>For MBG</b>				$f_{P_b}$	$F_{P_b}$	$R_{a_b}$	$R_{max_b}$	$VGCR_b$	$D_{j_{bm}}$
1.41	48.5	14.92	15	8.94	18.73	1.16	6.53	4.1	0.94
<b>For MHG</b>				$F_{a_h}$	$F_{P_h}$	$R_{a_h}$	$R_{max_h}$	$VGCR_h$	$D_{j_{hm}}$
1.44	47.3	11.3	15	8.32	14.91	1.19	7.1	4.7	0.96
<b>Objective:</b> Multi-objective optimization i.e. simultaneous minimization of microgeometry errors, avg. and max. surface roughness and maximization of volumetric gear cutting rate by DFA									
<b>For MBG</b>				$f_{P_b}$	$F_{P_b}$	$R_{a_b}$	$R_{max_b}$	$VGCR_b$	
1.21	47.15	10.86	11.24	9.39	16.66	1.04	6.43	3.02	
<b>For MHG</b>				$F_{a_h}$	$F_{P_h}$	$R_{a_h}$	$R_{max_h}$	$VGCR_h$	
1.23	46.31	11.41	11.68	9.46	15.37	1.09	7.65	3.33	

Two validation experiments were conducted for MBG and MHG separately to confirm results of optimization of VGCR of MBG and MHG by DFA and its results are presented in Table 5.6 along with their corresponding values from the experimental validation. Very good agreement between the experimental results and optimization results given by desirability function analysis.

Two validation experiments were conducted for MBG and MHG separately to confirm multi-objective optimization of microgeometry errors, average and maximum surface roughness and VGCR of MBG and MHG by DFA and two validation experiment to confirm multi-objective optimization results by RCGA. Table 5.6 presents optimized

WSEM parameters along multi-objective optimized values of the considered responses of MBG and MHG along with their corresponding values from the experimental validation. Very good agreement between the experimental results and optimization results obtained by them. Gear quality DIN 7 for microgeometry parameters of MBG (i.e.  $f_p$  and  $F_a$ ) and MHG (i.e.  $F_a$  and  $F_p$ ) were achieved by both DFA and RCGA.

**Table 5.6:** Optimized values of WSEM parameters and responses along with their corresponding values from the experimental validation.

<b>Objective:</b> Simultaneous minimization of microgeometry errors, avg. and max. surface roughness by DFA										
Optimum values of WSEM parameters					Optimum values of responses					
	$T_{on}$	$T_{off}$	$S_V$	$W_F$	(μm)					
	(μs)	(μs)	(Volts)	(m/min)						
<b>For MBG</b>					$f_{P_b}$	$F_{P_b}$	$R_{a_b}$	$R_{max_b}$	$VGCR_b$	
By DFA	1.14	48.38	10.49	12.12	8.41	15.06	0.99	5.93	--	
Validation Exp.	1.1	48.5	10	12	7.75	14.5	0.95	6.1	--	
<b>For MHG</b>					$F_{a_h}$	$F_{P_h}$	$R_{a_h}$	$R_{max_h}$	$VGCR_h$	
By DFA	1.25	47.73	11.7	13.3	8.33	13.4	1.03	7.02	--	
Validation Exp.	1.2	47.5	12	13	8.8	13.2	1.0	7.04	--	
<b>Objective:</b> Maximization of volumetric gear cutting rate by DFA										
<b>For MBG</b>					$f_{P_b}$	$F_{P_b}$	$R_{a_b}$	$R_{max_b}$	$VGCR_b$	
By DFA	1.58	46.03	19.12	12.17	--	--	--	--	6.5	
Validation Exp.	1.6	45.5	20	12	--	--	--	--	6.3	
<b>For MHG</b>					$F_{a_h}$	$F_{P_h}$	$R_{a_h}$	$R_{max_h}$	$VGCR_h$	
By DFA	1.5	44.6	10.3	14.8	--	--	--	--	6.8	
Validation Exp.	1.5	44.5	10	15	--	--	--	--	6.7	
<b>Objective:</b> Multi-objective optimization i.e. simultaneous minimization of microgeometry errors, avg. and max. surface roughness and maximization of volumetric gear cutting rate by DFA										
<b>For MBG</b>					$f_{P_b}$	$F_{P_b}$	$R_{a_b}$	$R_{max_b}$	$VGCR_b$	
By DFA	1.41	48.5	14.92	15	8.94	18.73	1.16	6.53	4.1	
Validation Exp.	1.4	48.5	15	15	9.55	19.7	1.13	6.9	4.4	
<b>For MHG</b>					$F_{a_h}$	$F_{P_h}$	$R_{a_h}$	$R_{max_h}$	$VGCR_h$	
By DFA	1.44	47.3	11.3	15	8.32	14.91	1.19	7.1	4.7	
Validation Exp.	1.4	47.5	11	15	8.85	15.7	1.15	7.3	5.0	
<b>Objective:</b> Multi-objective optimization i.e. simultaneous minimization of microgeometry errors, avg. and max. surface roughness and maximization of volumetric gear cutting rate by RCGA										
<b>For MBG</b>					$f_{P_b}$	$F_{P_b}$	$R_{a_b}$	$R_{max_b}$	$VGCR_b$	
By RCGA	1.21	47.15	10.86	11.24	9.39	16.66	1.04	6.43	3.02	
Validation Exp.	1.2	47.5	11	11	9.5	17.5	1.1	6.7	3.3	
<b>For MHG</b>					$F_{a_h}$	$F_{P_h}$	$R_{a_h}$	$R_{max_h}$	$VGCR_h$	
By RCGA	1.23	46.31	11.41	11.68	9.46	15.37	1.09	7.65	3.33	
Validation Exp.	1.2	46.5	11	12	9.05	16.8	1.02	7.1	3.8	

## 5.6 Investigations on the Best quality MBG and MHG

Among all the MBG and MHG obtained from different optimization approaches, the MBG and MHG obtained from simultaneous optimization of their microgeometry errors, and average and maximum surface roughness by DFA were found to have minimum microgeometry errors and are referred as the *best quality MBG and MHG*. Further detailed investigation on their microgeometry, flank surface topography, surface roughness, microstructure of flank surfaces were carried out on these meso-gears which is described in the following subsections.

### 5.6.1 Microgeometry

Figure 5.3 (for MBG) and 5.4 (for MHG) present the reports of metrological investigations for the best quality MBG and MHG manufactured by using standard values of WSEM parameters which were nearest to their optimized values by DFA and were available on the WSEM machine. It can be observed from Fig. 5.3 that the best quality MBG has 7.75  $\mu\text{m}$  as single pitch error thus getting assigned DIN 6 quality; 11.8  $\mu\text{m}$  as adjacent pitch error ' $f_u$ ' securing DIN 7 quality; 14.5  $\mu\text{m}$  as total cumulative pitch error which got it DIN 6 quality; and 14.9  $\mu\text{m}$  as radial runout corresponding to DIN 6 quality. Whereas, the best quality MHG (Fig. 5.4) has 7.6  $\mu\text{m}$  as single pitch error thus securing DIN 6 quality; 11.4  $\mu\text{m}$  as adjacent pitch error which got it assigned DIN 7 quality; 13.2  $\mu\text{m}$  as total cumulative pitch error corresponding to DIN 6 quality; 13.8  $\mu\text{m}$  as radial runout which secured it DIN 6 quality; and 8.8  $\mu\text{m}$  as total profile error giving it DIN 7 quality.

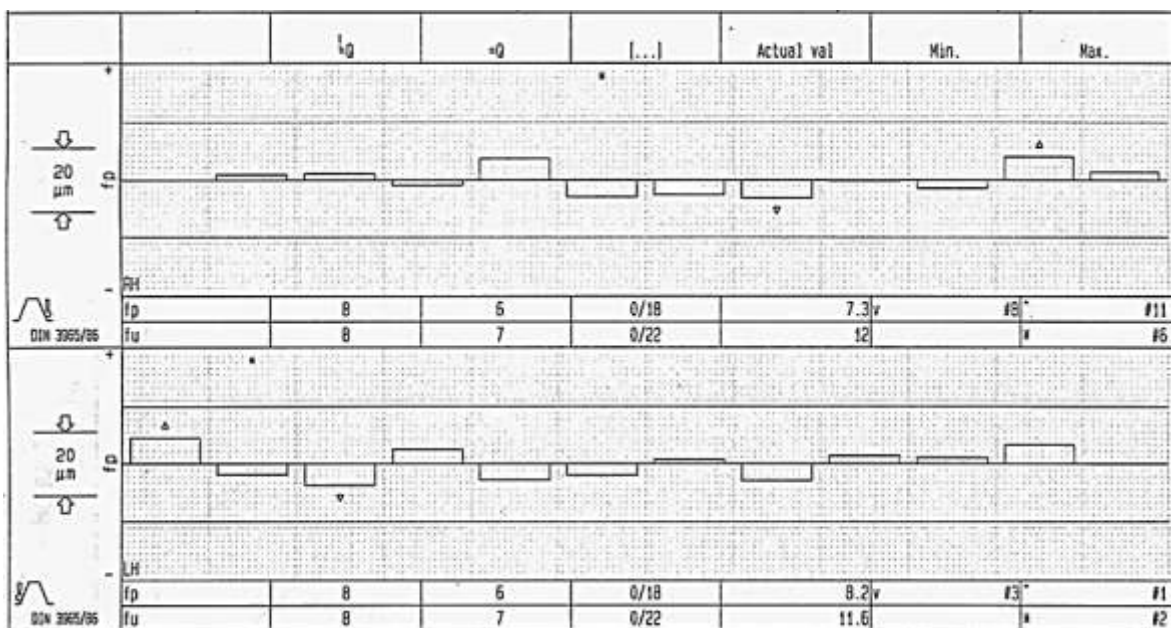


Fig. 5.3(a)

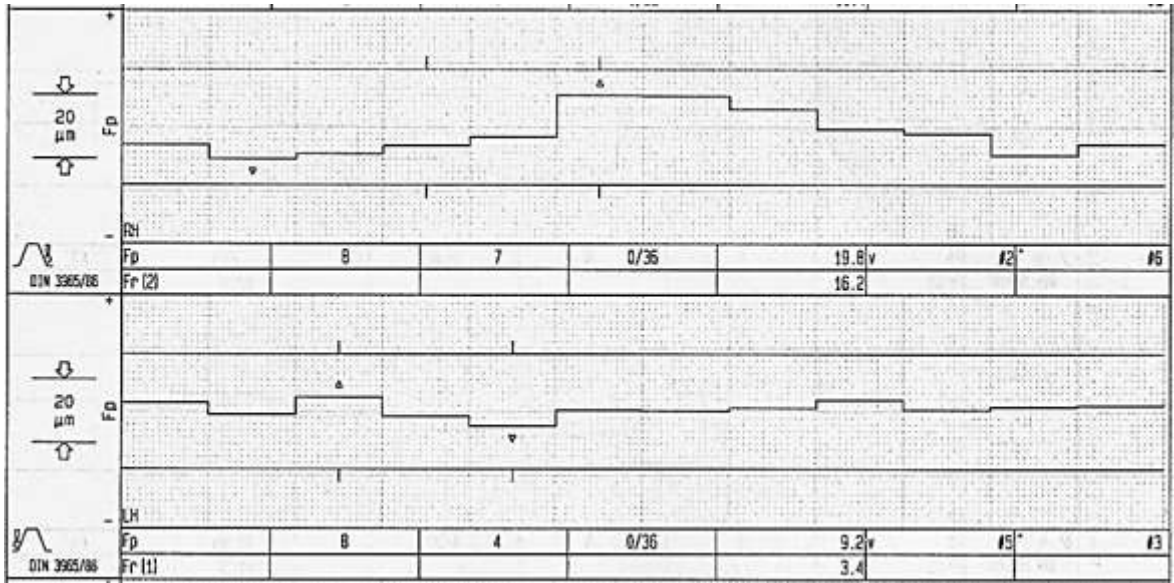


Fig. 5.3(b)

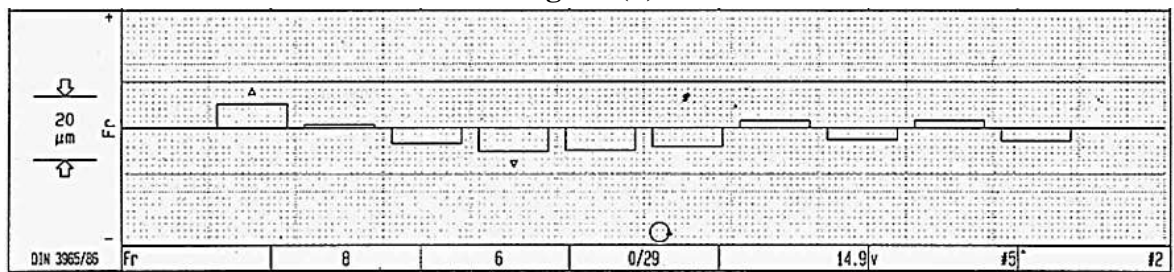


Fig. 5.3(c)

Fig. 5.3: Reports of metrological investigation for the best quality MBG manufactured using the optimized WSEM parameters: (a) single pitch error ' $f_p$ ' and adjacent pitch error ' $f_u$ '; (b) total cumulative pitch error ' $F_p$ '; and (c) radial runout ' $F_r$ '.

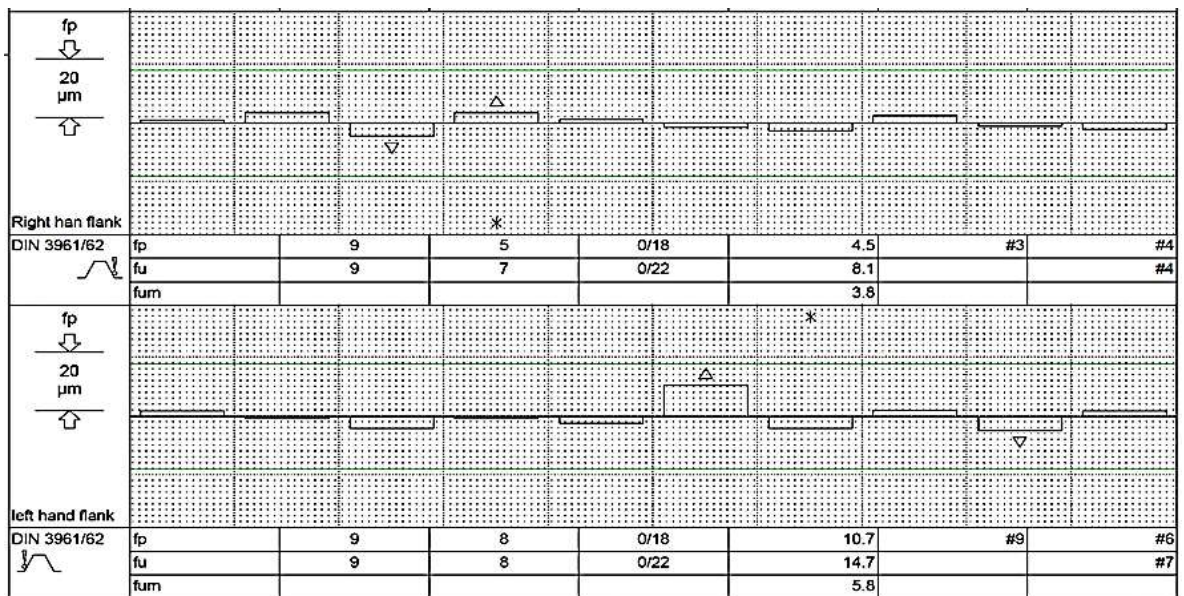


Fig. 5.4(a)



Fig. 5.4(b)

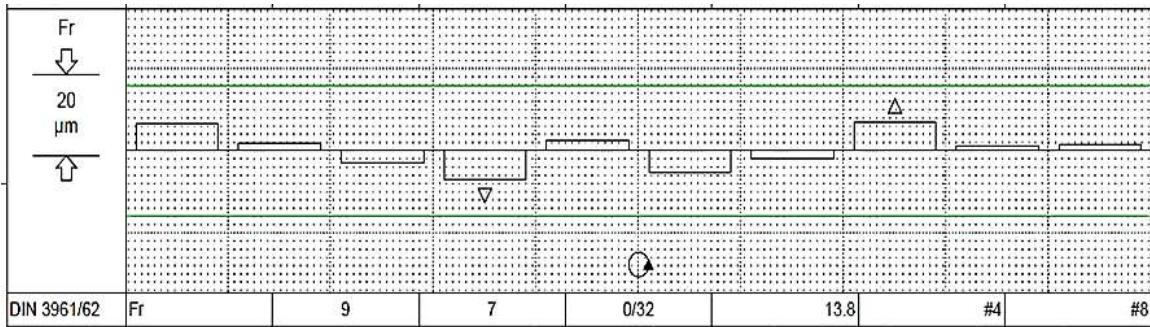


Fig. 5.4(c)

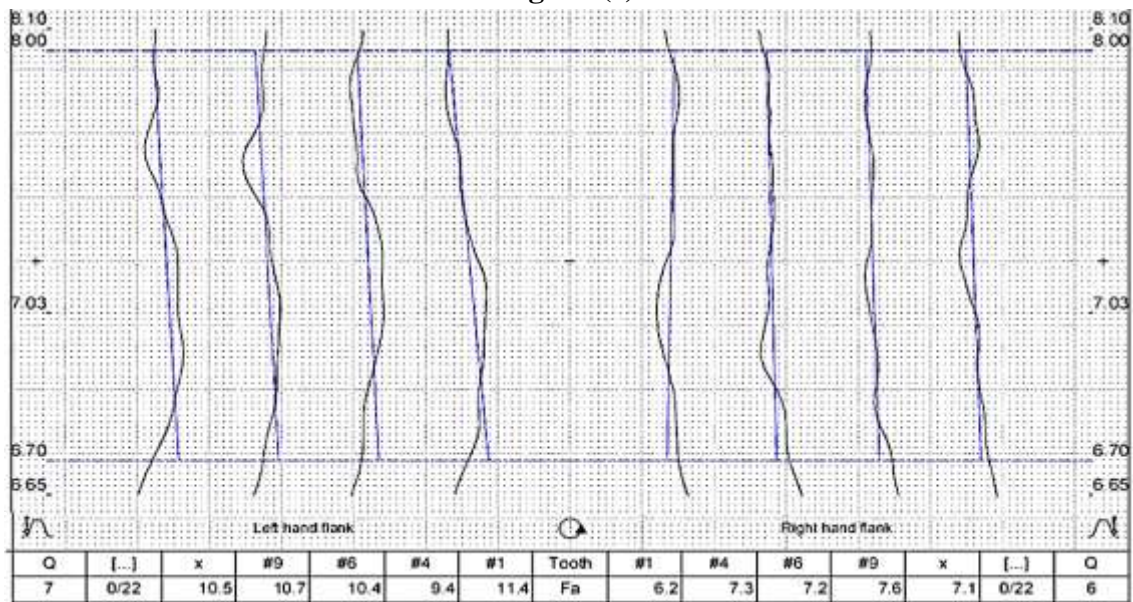


Fig. 5.4(d)

Fig. 5.4: Reports of metrological investigation for the best quality MHG manufactured using optimized WSEM parameters: (a) single pitch error ' $f_p$ ' and adjacent pitch error ' $f_u$ '; (b) total cumulative pitch error ' $F_p$ '; (c) radial runout ' $F_r$ '; and (d) total profile error ' $F_a$ '.

### 5.6.2 Flank Surface Topography

Measurement of topography of flank surfaces of the best quality MBG and MHG revealed very small amount of deviations on right and hand flank surfaces. Average values of deviations (computed by taking arithmetic mean of deviations present on right and left hand flanks) of the actual flank surface with respect to theoretical flank surface of the best quality MBG were found to be  $8.2 \mu\text{m}$  and  $6.05 \mu\text{m}$  on toe and heel side respectively.

### 5.6.3 Surface Roughness

The best quality MBG and MHG had  $0.95 \mu\text{m}$  and  $1.00 \mu\text{m}$  as avg. surface roughness values and  $6.1 \mu\text{m}$  and  $7.04 \mu\text{m}$  as max. surface roughness values respectively.

### 5.6.4 Microstructure

Figure 5.5 depicts the microstructures of tooth profile, bore and flank surfaces of the best quality MBG [Figs. 5.5(a) and 5.5(c)] and MHG [Figs. 5.5(b) and 5.5(d)] respectively. It can be seen from the SEM images that the best quality MBG and MHG have uniform and accurate tooth profile, flank surfaces and bore without any undercut at root and also are free from burrs and sharp edges on their both end faces. Examination of microstructure of the flank surfaces of the best quality MBG and MHG [Fig. 5.5(c) and 5.5(d)] reveals that they are free from cracks, globules and pores.

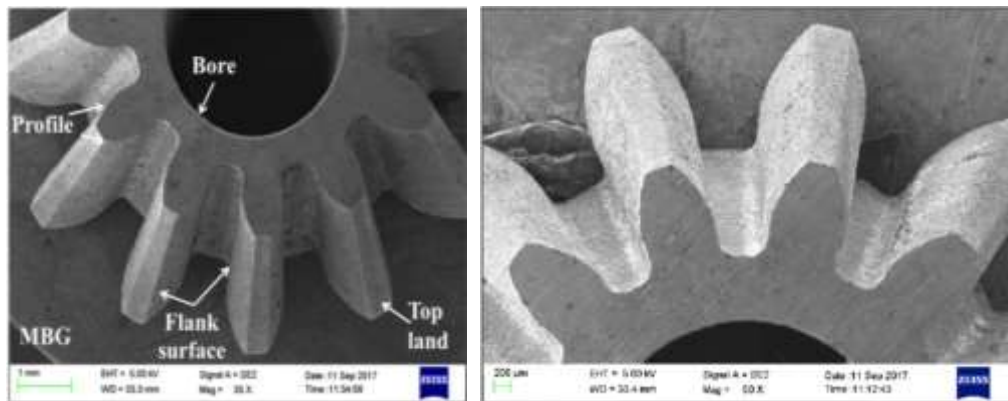


Fig. 5.5(a)

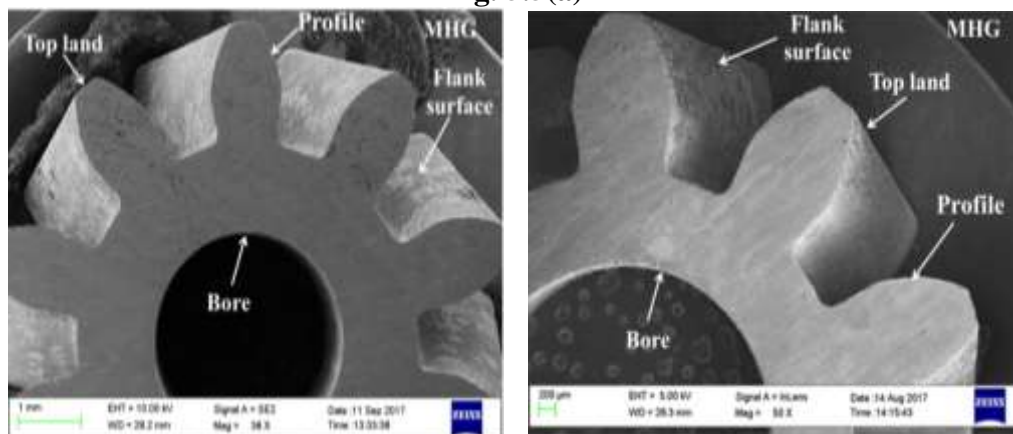
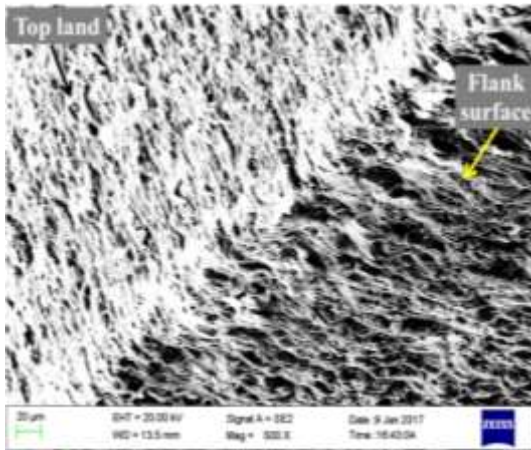
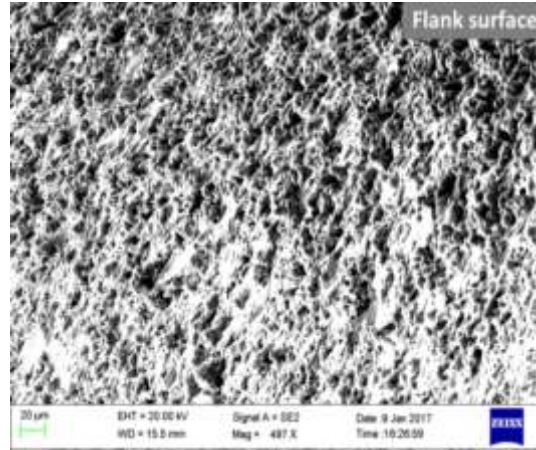


Fig. 5.5(b)



**Fig. 5.5(c)**



**Fig. 5.5(d)**

**Fig. 5.5:** SEM images showing bore, tooth profile, and flank surfaces of the best quality meso-gears manufactured by WSEM (a) MBG; (b) MHG; microstructures of the flank surfaces of the best quality; (c) MBG; and (d) MHG.

The *next chapter* describes the comparative evaluation of WSEM with milling and hobbing processes for manufacturing MBG and MHG.

## Chapter-6

### Comparison of WSEM with Traditional Processes

This chapter presents the comparative study of WSEM with traditional processes namely milling and hobbing processes for manufacturing MBG and MHG in terms of their microgeometry, macrogeometry (for MHG only) and surface roughness, flank surface topography, manufacturing cost, manufacturing time and microstructure of flank surfaces as a criteria for evaluation.

#### 6.1 Details of Experimentation

Three MBG were manufactured by milling and WSEM each and three MHG were manufactured by hobbing and WSEM each to evaluate their manufacturing capabilities. Austenitic stainless steel (SS 304) was again selected as material for manufacturing MBG and MHG for the comparative study due to its useful properties as mentioned in Chapter 3. Specifications of MHG were changed slightly from those mentioned in Table 3.1 keeping in view constraints of the hobbing machine used for their manufacturing. Table 6.1 presents the specifications of MBG and MHG along with details of machine tool, cutting tool and machining medium used in the comparative study.

Same activities and their same sequence was used in manufacturing MBG and MHG by WSEM as mentioned in subsection 3.4.2 and Fig. 3.4. Whereas, concept of manufacturing MHG by hobbing and MBG by milling are depicted in Figs. 6.1(a) and 6.1(b) respectively. Horizontal hobbing machine (model PW10 from Penasott-EZIO, Italy) was used to manufacture three MHG from the cylindrical gear blank having 8.7 mm diameter; and 5 mm face width. Whereas, universal milling machine was used to manufacture three MBG from the truncated conical gear blank having 9.8 mm diameter at base; 7.0 mm diameter at top;  $32^{\circ}$  cone angle; and 5 mm face width. Rotational speed and feed rate of the hobbing and milling cutters were kept at 40 rpm and 10  $\mu\text{m}$  per revolution of the meso-gear blank respectively. These values were identified by conducting six trial experiments for milling and hobbing each by varying rotational speed and feed rate of their cutters at 30, 40, and 60 rpm and 10, 20, and 30  $\mu\text{m}$  per revolution of the gear blank respectively. Those values which minimized wear and damage of hobbing and milling cutters were considered as the optimum values because wear of hobbing and milling cutters deteriorates the quality, surface finish, manufacturing time and cost of the meso-gears. Servo cut 335 cutting oil was used to remove the heat and chips produced during the hobbing and milling processes so as to minimize the wear and tear of their cutters and

achieve better surface finish and quality of the MBG and MHG. Figure 6.2 shows 3D views of WSEM manufactured MBG and MHG, milled MBG and hobbed MHG.

**Table 6.1:** Details of the processes used to manufacture MBG and MHG along with their specifications.

Details of the manufacturing process				
Type of meso-gear		Meso-bevel gear (MBG)		Meso-helical gear (MHG)
Manufacturing Process		<i>Milling</i>	<i>WSEM</i>	<i>WSEM</i>
				<i>Hobbing</i>
Specifications of meso-gears				
Module		0.7 mm	0.7 mm	0.66 mm
No. of teeth		12	12	10
Major diameter		9.8 mm	9.8 mm	8.35 mm
Minor diameter		7.0 mm	7.0 mm	---
Angle		32° (cone angle)	32° (cone angle)	20° helix angle (right hand type)
				15° helix angle (left hand type)
Machine	Type	Universal	4-axes (X, Y, U and V) flushing CNC	
	Model	--	Sprintcut-win	
	Make	KMT Mumbai (India)	Electronica India Ltd. Pune	
Cutting tool		M2/M35 HSS milling cutter of 0.7 mm module	0.25 mm dia. of soft plain brass wire (tensile strength: 470-510 N/mm <sup>2</sup> )	
Machining medium		Servo cut 335 cutting oil	Deionized water	
			Servo cut 335 cutting oil	

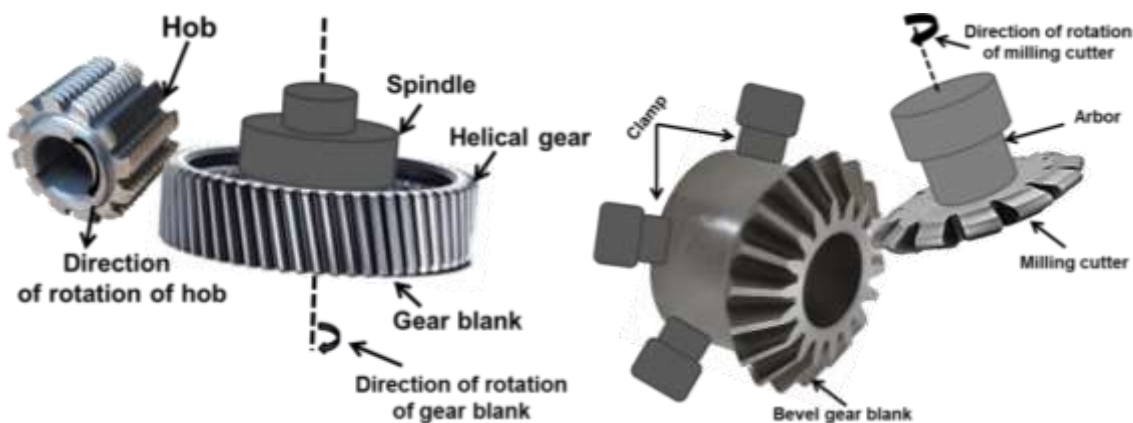


**Fig. 6.1(a)**

**Fig. 6.1(b)**

**Fig. 6.1:** Concepts of manufacturing: (a) MHG by hobbing; and (b) MBG by milling process.

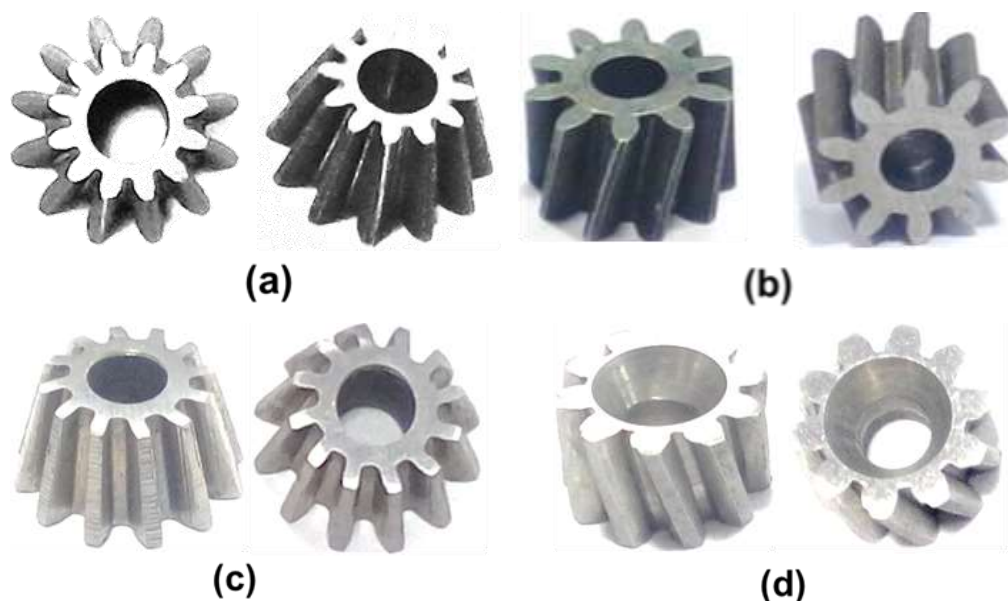


**Fig. 6.2:** Photographs showing 3D views of (a) WSEM manufactured MBG; (b) WSEM manufactured MHG; (c) milled MBG; and (d) hobbed MHG.

## 6.2 Comparison of WSEMed, Milled and Hobbed Gears

Table 6.2 presents comparison of WSEM manufactured MBG and MHG with milled MBG and hobbed MHG on basis of their microgeometry, macrogeometry, surface roughness parameters, flank surface topography, actual manufacturing time, setup time, total manufacturing time, required skills of the operator, consumption of machining medium, loss of the meso-gear material, and total manufacturing cost. Following paragraphs discuss them in detail along with comparative study of their microhardness, and flank surface microstructure.

### 6.2.1 Microgeometry

It can be seen from Table 6.2 that the best quality MBG manufactured by WSEM has  $6.9 \mu\text{m}$  as single pitch error;  $11.5 \mu\text{m}$  as adjacent pitch error;  $17.5 \mu\text{m}$  as total cumulative pitch error; and  $12.3 \mu\text{m}$  as radial runout securing assignment of DIN 6; DIN 7; DIN 6; DIN 6 standard respectively. While, corresponding values of these parameters for the milled MBG are:  $63.2 \mu\text{m}$ ;  $47.2 \mu\text{m}$ ;  $163.2 \mu\text{m}$ ; and  $151.8 \mu\text{m}$  respectively which cause assignment of DIN 11, DIN 10; DIN 12; and greater than DIN 12 standard to it. The best quality MHG manufactured by WSEM process has total profile error of  $8.8 \mu\text{m}$ ; single pitch error of  $7.2 \mu\text{m}$ ; adjacent pitch error of  $12.3 \mu\text{m}$ ; total cumulative pitch error of  $8.7 \mu\text{m}$ ; and radial runout of  $10.3 \mu\text{m}$ . These values enable assignment of DIN 6; DIN 7; DIN 7; DIN 5; and DIN 6 respectively to it. Corresponding values of these parameters for the

hobbed MHG are: 30.9  $\mu\text{m}$ ; 8.8  $\mu\text{m}$ ; 9.2  $\mu\text{m}$ ; 18.5  $\mu\text{m}$  and 14.9  $\mu\text{m}$  respectively, which get it assigned DIN 10, DIN 8, DIN 7, DIN 7 and DIN 7 for these parameters.

**Table 6.2:** Microgeometry, flank surface topography, macrogeometry, and surface roughness parameters for the meso-gears manufactured by WSEM, milling and hobbing.

Criterion for comparison	Best quality MHG manufactured by		Best quality MBG manufactured by	
	WSEM	Hobbing	WSEM	Milling
<b>Value of microgeometry error and corresponding quality in DIN standard</b>				
Total profile error ( $\mu\text{m}$ )	8.8 (DIN 6)	30.9 (DIN 10)	Not applicable	
Single pitch error ( $\mu\text{m}$ )	7.2 (DIN 7)	8.8 (DIN 8)	6.9 (DIN 6)	63.2 (DIN 11)
Adjacent pitch error ( $\mu\text{m}$ )	12.3 (DIN 7)	9.2 (DIN 7)	11.5 D(IN 7)	47.2 (DIN 10)
Total pitch error ( $\mu\text{m}$ )	8.7 (DIN 5)	18.5 (DIN 7)	17.5 (DIN 6)	163.2 (DIN 12)
Radial runout ( $\mu\text{m}$ )	10.3 (DIN 6)	14.9 (DIN 7)	12.3 (DIN 6)	151.8 (>DIN 12)
<b>Value of the considered parameters of macrogeometry</b>				
Deviation in span ( $\mu\text{m}$ )	29	373	Not applicable	
Deviation in tooth thickness ( $\mu\text{m}$ )	33	351	Not applicable	
Deviation in outside dia. ( $\mu\text{m}$ )	46	250	Not applicable	
<b>Value of the considered parameters of surface roughness</b>				
Average roughness ( $\mu\text{m}$ )	1.07	0.48	1.04	0.45
Maximum roughness ( $\mu\text{m}$ )	6.60	4.11	6.16	3.77
Skewness	-0.19	-0.188	-0.05	-0.56
Kurtosis	2.77	2.56	2.70	2.98
<b>Economic aspects</b>				
Actual manufacturing time per meso-gear (minutes)	20	120	25	150
Setup time (minutes)	15	70	15	90
Total manufacturing time per meso-gear (minutes)	35	190	40	240
Amount [in (ml)] and cost of machining medium consumption (US \$)	80-100 (\$ 0.08)	100 (\$ 0.31)	80-100 (\$ 0.08)	150 (\$0.46)
Loss of gear material per meso-gear (g)	0.75	1.29	0.7	1.18
Required skills of the operator	Average	High	Average	High
Total manufacturing cost (US \$)	4	8	4	10

### 6.2.2 Macrogeometry

It can also be observed from Table 6.2 that macrogeometry parameters namely deviation in span, deviation in tooth thickness and deviation in outside diameter of the hobbed MHG have very high values as compared to the WSEM manufactured MHG. Thus, it can be concluded that quality of MHG manufactured by WSEM process is much better than the hobbed MHG.

### **6.2.3 Flank Surface Topography**

It can be seen from Table 6.2 that deviation between the actual right and left flank surfaces and corresponding theoretical surfaces in milled MBG are much more on both heel and toe side than WSEM manufactured MBG. Comparison of flank surface topography of the WSEM manufactured MHG with the hobbed MHG revealed that former has small amount of deviations in flank surfaces than the hobbed MHG. Reasons for poor microgeometry, macrogeometry and topography of the milled MBG and hobbed MHG are: indexing error, inaccuracy in making the bore which was done on other drilling machine, difficulty in holding the conical blank (for MBG) and cylindrical blank (for MHG) on the milling and hobbing machine respectively, errors, wear and sharpness of the milling and hob cutter, vibrations, and difficulty in chip removal.

### **6.2.4 Surface Roughness**

It can be observed from Table 6.2 that the (i) hobbed MHG has smaller values of average surface roughness ( $0.48 \mu\text{m}$ ), maximum surface roughness ( $4.11 \mu\text{m}$ ), and kurtosis (2.56) than the WSEM manufactured MHG (i.e.  $1.07 \mu\text{m}$ ;  $6.60 \mu\text{m}$ ; and 2.77) with skewness values being comparable; and (ii) milled MBG has smaller values of average surface roughness ( $0.45 \mu\text{m}$ ), maximum surface roughness ( $3.77 \mu\text{m}$ ), and skewness (-0.56) but higher value kurtosis (2.98) than the values for the WSEM manufactured MBG (i.e.  $1.04 \mu\text{m}$ ;  $6.16 \mu\text{m}$ ; -0.05 and 2.77 respectively). Poor surface finish of WSEM manufactured MBG and MHG than the hobbed MHG and milled MBG is due to the fact that in WSEM process material removal takes by erosion caused by occurrence of series of spark between the gear blank and the wire. This causes formation of tiny craters on flank surfaces of the meso-gear increasing their maximum and average surface roughness values.

### **6.2.5 Microhardness**

Figure 6.3 depicts values of microhardness for the WSEM manufactured MBG and MHG, milled MBG and hobbed MHG at an indentation load of 500 and 1000 g showing that microhardness of the WSEM manufactured MBG and MHG is much higher than milled MBG and hobbed MHG at both indentation force. This is due to formation of a very thin recast layer on flank surfaces of the meso-gears in the WSEM process which is caused by resolidification of the some residual or unflushed removed material left over in the IEG due to inefficient flushing. This increases hardness of the meso-gears to a certain depth whereas hardness of core material remains unchanged. Higher microhardness is

beneficial provided it does not induce any micro-cracks and HAZ to such an extent that it adversely affects fatigue strength of the MBG and MHG.

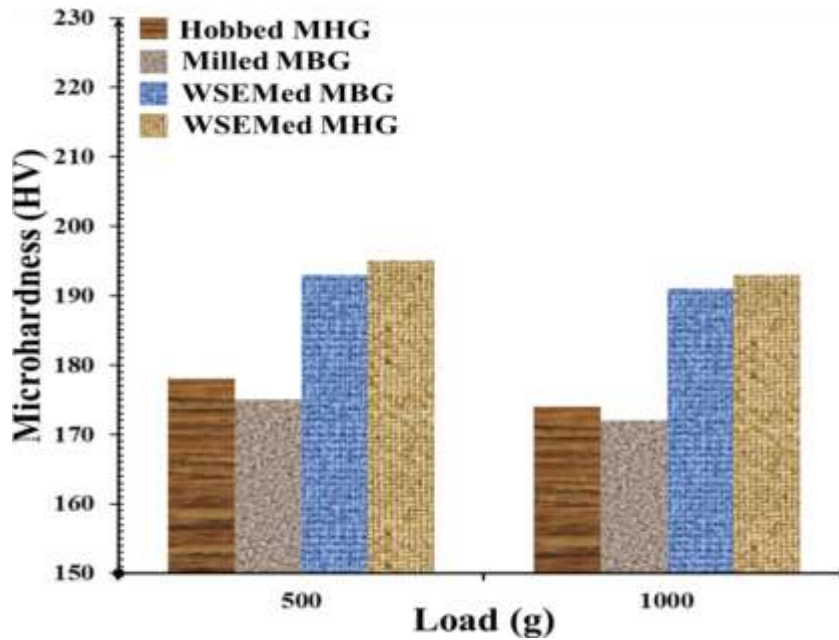


**Fig. 6.3:** Microhardness values of the hobbed MHG, milling MBG and WSEM manufactured MHG and MBG at different values of indentation load.

### 6.2.6 Economic Aspects

It can be seen from Table 6.2 that total manufacturing time and cost of the milled MBG and hobbed MHG are very high than WSEMed MBG and MHG i.e. total manufacturing time is 240 minutes per MBG for milling process and 190 minutes per MHG for hobbing process. Total manufacturing times by WSEM for MBG and MHG are 40 and 35 minutes respectively. Machine idle time is also high in hobbing and milling processes. Manufacturing of MBG and MHG by WSEM uses the same raw material and same brass wire as the cutting tool. This reduces idle and setting time thus reducing the total manufacturing time. Total manufacturing costs for the milled MBG and hobbed MHG are \$10 and \$8 respectively. This is \$4 per meso-gear for WSEM process. Total manufacturing cost of milling and hobbing processes is higher due to higher setting, idle time, actual manufacturing time, tooling costs and less flexibility of cutting tools i.e. different geometry meso-gears may require different hobbing and milling tools. WSEM generally uses brass wire, only few clamps for mounting the meso-gear plate on its worktable, and deionized water is used as machining medium. Loss of meso-gear material is also very high in milling and hobbing processes because they remove meso-gear material in chip form whereas WSEM removes it in fine particles form whose volume is negligible than that of the chips.

### 6.2.7 Microstructure

Figures 6.4(a) and 6.4(b) present the SEM images showing tooth profile, flank surface and bore of MBG manufactured by WSEM and milling respectively. It can be observed from these images that the milled MBG has non-uniform and inaccurate tooth profile, flank surface and bore whereas WSEM manufactured MBG has smoother and uniform tooth profile, flank surface and bore. SEM images of tooth profile, flank surface and bore of MHG manufactured by WSEM [Fig. 6.5(a)] and hobbing [Fig. 6.5(b)] show that hobbed MHG has worn and inaccurate tooth profile and bore with some particles of the removed material stuck to its flank surface whereas WSEM manufactured MHG has uniform tooth profile, bore and smoother and clean flank surface. The SEM images illustrating flank surface microstructure of the WSEM manufactured MBG [Fig. 6.4(c)], milled MBG [Fig. 6.4(d)], WSEM manufactured MHG [Fig. 6.5(c)], and hobbed MHG [Fig. 6.5(d)] clearly show that the flanks of the WSEM manufactured MBG and MHG do not have cracks, globules and pores whereas flanks of the milled MBG and the hobbed MHG show presence of small burrs and cutter marks.

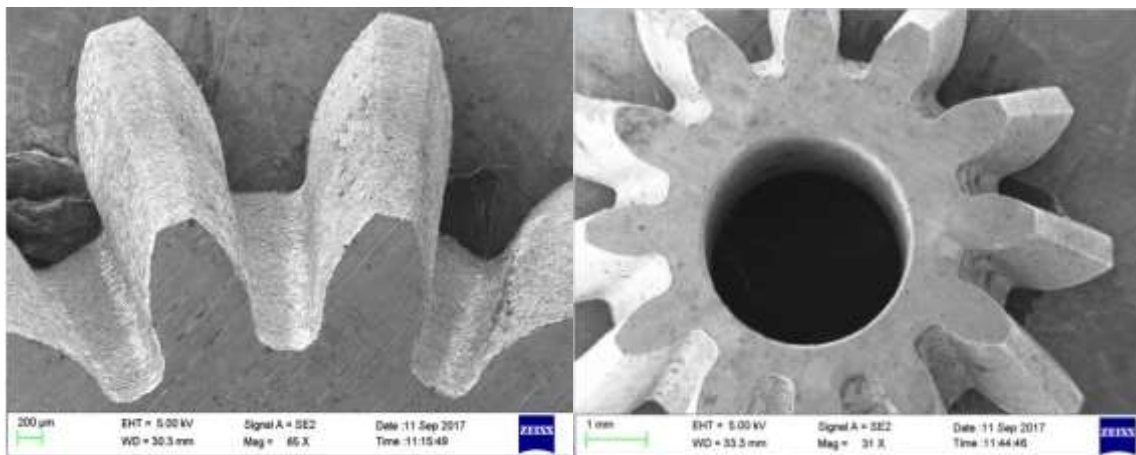


Fig. 6.4(a)

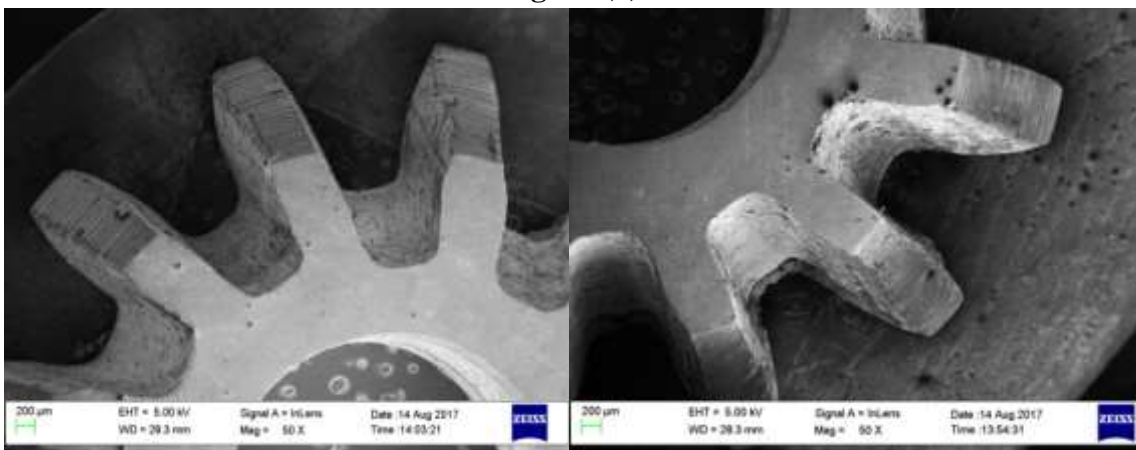
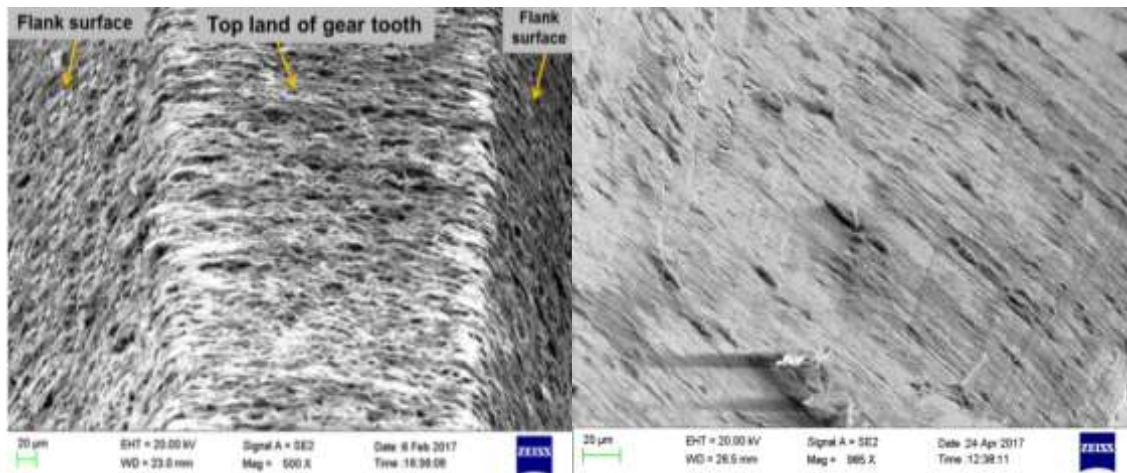


Fig. 6.4(b)



**Fig. 6.4(c)**

**Fig. 6.4(d)**

**Fig. 6.4:** SEM micrographs showing tooth profile, flank surface and bore of (a) WSEM manufactured MBG; (b) milled MBG, microstructure of tooth flank surface of (c) WSEM manufactured MBG; and (d) milled MBG.

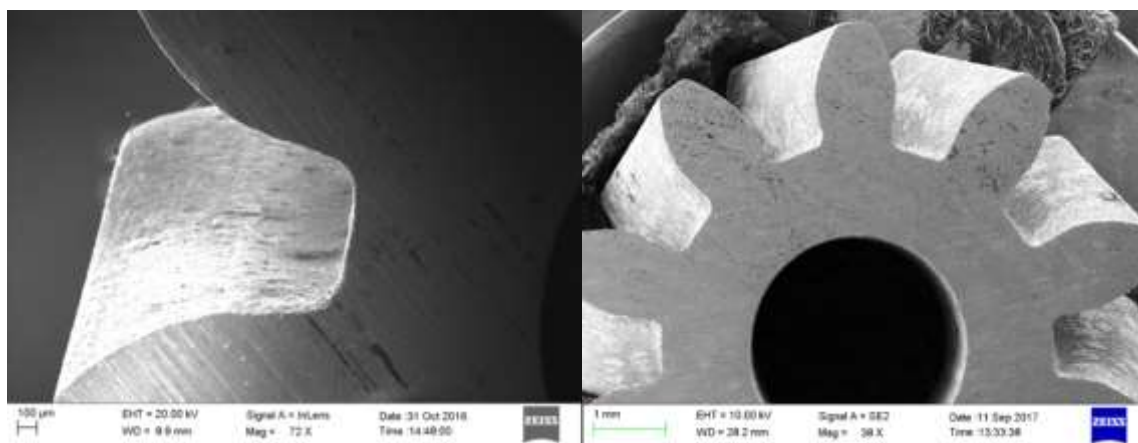


**Fig. 6.5(a)**

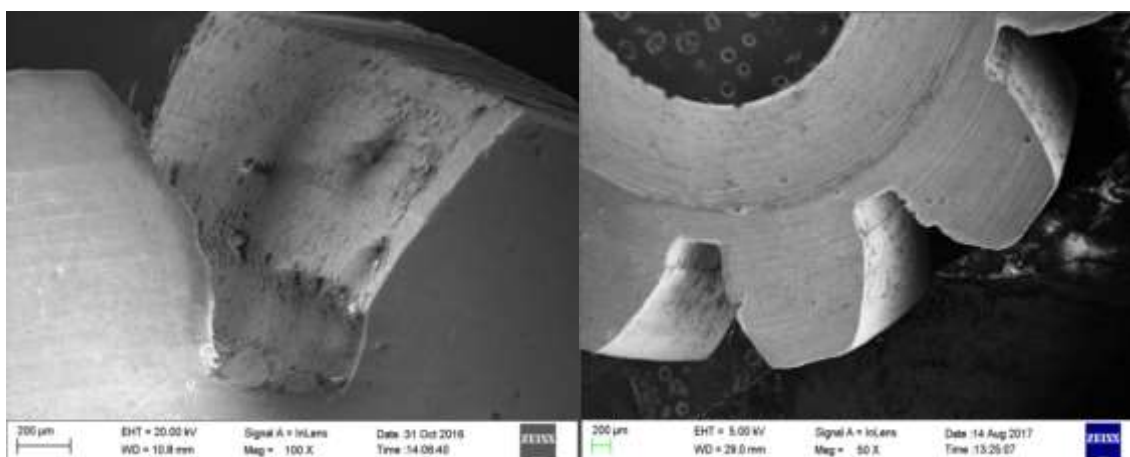


**Fig. 6.5(b)**

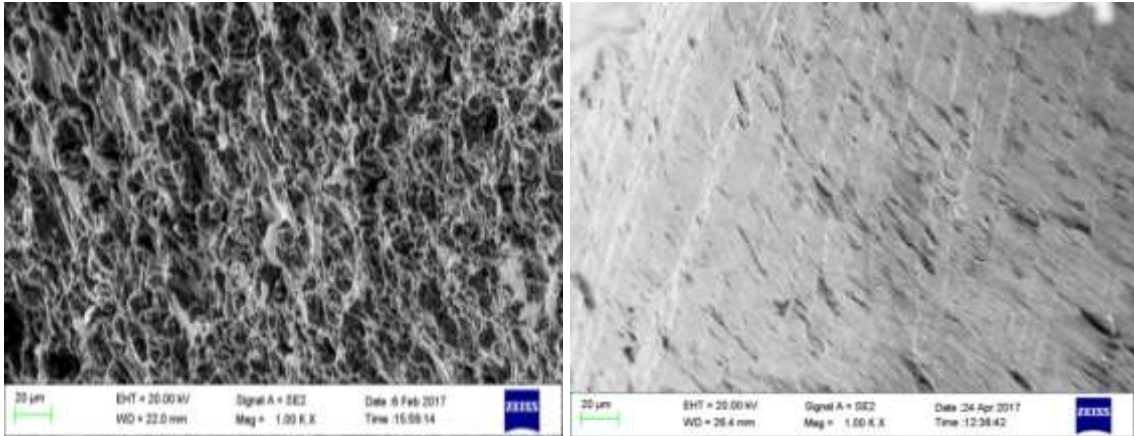


**Fig. 6.5(c)**

**Fig. 6.5(d)**

**Fig. 6.5:** SEM images showing tooth profile, flank surface and bore of (a) WSEM manufactured MHG; (b) hobbled MHG, microstructure of tooth flank surface of (c) WSEM manufactured MHG; and (d) hobbled MHG.

### 6.3 Conclusions from the Comparative Study

Aim of the study reported in this chapter was to prove superiority of WSEM process over hobbing and milling processes for manufacturing MBG and MHG. Following major conclusions can be drawn from this comparative study:

- Microgeometry and macrogeometry of WSEM manufactured MBG and MHG is better than milled MBG and hobbled MHG. But, surface finish of milled MBG and hobbing MHG is better than the WSEM manufactured MBG and MHG.
- Flank surface topography of WSEM manufactured MBG and MHG revealed very less deviation of actual surface from theoretical surface as compared to milled MBG and hobbled MHG.
- Microhardness of WSEM manufactured MBG and MHG is very high as compared to milled MBG and hobbled MHG which imparts better wear resistance to WSEM manufactured meso-gears.
- WSEM manufactured MBG and MHG exhibit smoother, cracks and burr free tooth flank surfaces whereas the milled MBG and hobbled MHG have presence of chip particles, burrs and cutter marks on its flank surfaces.
- WSEM manufactured MBG and MHG have accurate and uniform tooth profile than milled MBG and hobbled MHG.
- Total manufacturing time, total manufacturing cost, tooling cost and cost of the machining medium of milled MBG and hobbled MHG are very high as compared to the WSEM manufactured MBG and MHG.

- Loss of meso-gear material is very less in WSEM process. Moreover, it does not require any special tooling and fixture, lubricants, and harmful hydrocarbon-based machining medium as required in the milling and hobbing processes.
- WSEM process can manufacture different sizes of MBG and MHG (i.e. having different tip diameter, cone angle and helix angle) with bore and in large number from the same plate without changing the cutting tool as required in milling and hobbing processes. This minimizes the setup time and manufacturing cost.
- This study proves that WSEM is an economical, superior, flexible, material efficient and environment friendly process for manufacturing of better quality and higher accuracy meso-gears from any material with excellent repeatability. This eliminates need of any finishing and hardening process after WSEM. Results of this study will be very helpful and beneficial for those who work on manufacturing meso-gears. They can achieve better quality fine pitch meso-gears with minimum cost by reducing manufacturing steps, process and wastage of material by using optimal WSEM parametric setting.

The *last chapter* presents the significant achievements and conclusions drawn from the present research along with the scope of future work.

## Chapter 7

### Conclusions and Scope for the Future Work

The significant achievements of the present research work, conclusions drawn from it, and scope for future work are summarized in this chapter.

#### 7.1 Significant Achievements

Based upon the past literature available, present research work is first attempt to manufacture bored MBG and MHG by WSEM process and investigate on their microgeometry errors, flank surface topography, macrogeometry, surface roughness, microhardness, microstructure of their flank surfaces, and WSEM process productivity. Following are significant achievements of the present research work:

- Manufacturing high quality MBG and MHG by WSEM process.
- Investigating effects of variable parameters of WSEM on microgeometry errors, surface roughness parameters, and volumetric gear cutting rate of MBG and MHG which significantly affect their noise characteristics, operating performance, fatigue life, service life, and manufacturing productivity.
- Development of response surface and ANN models for microgeometry errors, surface roughness and volumetric gear cutting rate of WSEM manufactured MBG and MHG.
- Optimization of WSEM parameters by desirability function analysis and real-coded genetic algorithm to minimize the microgeometry and surface roughness parameters and maximize volumetric gear cutting rate of MBG and MHG simultaneously.
- Achieved gear quality of WSEM manufactured MBG and MHG up to DIN quality number 6 which is superior to the quality of the gears manufactured by the traditional processes.
- Establishing WSEM as a superior, economical, material efficient, and environment friendly process for near net-shape manufacturing of high quality MBG and MHG.

#### 7.2 Conclusions

Following conclusions can be drawn from the present research work:

- Irregular shaped craters, sparks having higher discharge energy, non-uniform sparks, wire-lag, recast layer, non-flatness of the gear plate, and error in its positioning with respect to wire feed are main factors which affect microgeometry errors and surface roughness of MBG and MHG.

- There exist optimum ranges of servo-voltage and pulse-on time, and optimum value of % cutting speed to minimize microgeometry errors and surface roughness of MBG and MHG. Higher values of servo voltage and pulse-on time should be avoided for stable sparking to improve the quality and surface finish of MBG and MHG.
- Better gear quality and surface finish of MBG and MHG can be achieved using higher values of wire feed rate, wire tension and dielectric pressure because this will minimize the wire breakage frequency which will minimize microgeometry errors and surface roughness of MBG and MHG simultaneously.
- Conflict exists for peak current and pulse-off time. Higher value of peak current minimizes microgeometry errors of MBG and MHG whereas lower value of peak current minimizes surface roughness of MBG and MHG. In order to give more importance to microgeometry parameters, it was decided to keep higher value of peak current for further investigations. Similarly, optimum range of pulse-off time exists to minimize microgeometry errors of MBG and MHG whereas, minimization of surface roughness of MBG and MHG requires higher value of pulse-off time.
- MBG and MHG possessing minimum errors in their microgeometry during the pilot experiments (referred as better quality MBG and MHG) were identified for more detailed investigation on their microgeometry, flank surface topography, microhardness, and microstructure. These gears had 1.24 and 1.33  $\mu\text{m}$  as average surface roughness and 7.56 and 7.67  $\mu\text{m}$  for maximum surface roughness, respectively. Their flank surface topography revealed very small amount of deviation of the actual flank surfaces from its theoretical form.
- Microhardness of flank surfaces of better quality MBG and MBG is higher than parent materials due to formation of very thin recast layers. Moreover, it does not induce any micro-cracks and heat affected zone to such an extent that it adversely affects fatigue strength of meso-gears.
- Analysis of microstructure of the better quality MBG and MHG revealed their tooth profile to be burr-free, uniform, accurate, no undercutting at the root and no sharp edges on both end faces of the meso-gears.
- Microstructural examination of flank surfaces of better quality MBG and MHG had shown smoother surface free from cracks, nicks and asperities.

- Violent and non-uniform distribution of sparks, generation of irregular shaped craters on flank surfaces and wire vibration or wire lag are primarily responsible for determining overall quality of the WSEM manufactured MBG and MHG.
- Servo voltage, pulse-on-time, pulse-off-time and wire feed rate are found to be significant parameters affecting microgeometry errors and surface roughness of MBG and MHG during their manufacturing by WSEM process.
- Interactions between  $T_{on}$  and  $T_{off}$ ,  $T_{on}$  and  $S_V$ ,  $T_{on}$  and  $W_F$ ,  $T_{off}$  and  $S_V$ , and  $S_V$  and  $W_F$  (except  $T_{on}$  and  $W_F$  for  $R_a$  of MHG) were found to be significant for the considered parameters of microgeometry and surface roughness of MBG and MHG. Interactions between  $T_{on}$  and  $T_{off}$ ,  $T_{on}$  and  $S_V$ , and  $T_{off}$  and  $S_V$  were found to be significant for volumetric gear cutting rate of MBG and MHG.
- Total profile error, single pitch error, total cumulative pitch error and maximum surface roughness decrease with decrease in pulse-on time and servo voltage, and with increase in wire feed rate and pulse-off time. Whereas, volumetric gear cutting rate increase with increase in of pulse-on time and servo voltage, decrease with increase in pulse-off time, and slightly increase with increase in wire feed rate. Therefore, lower values of pulse-on-time and servo voltage and higher values of pulse-off time and wire feed rate are recommended to manufacture higher accuracy and better quality MBG and MHG by WSEM process but at the cost of WSEM productivity.
- Single pitch error for MBG and total profile error for MHG decrease considerably during 12-15 and 9-12 m/min range of wire feed rate respectively
- Average surface roughness of MBG and MHG is insignificantly affected by four considered parameters of WSEM.
- The ANN models are very effective and superior to response surface models for prediction of the responses for MBG and MHG.
- Comparison of the results of optimization done by DFA considering different objectives reveals that multi-objective optimization by DFA as compared to simultaneous optimization of microgeometry errors and surface roughness (i) increases microgeometry errors, avg. and max. surface roughness of MBG; (ii) does not significantly change microgeometry errors, avg. and max. surface roughness of MHG; (iii) decreases values of VGCR of MBG and MHG; and (iv) decreases maximum value of overall desirability.

- There is very good agreement between the experimental results and optimization results given by DFA and RCGA. The best quality MBG and MHG manufactured during validation of the optimization attained quality up to DIN 6 in microgeometry, had 0.95  $\mu\text{m}$  and 1.00  $\mu\text{m}$  as average surface roughness, and 6.1 $\mu\text{m}$  and 7.04  $\mu\text{m}$  as maximum surface roughness.
- Microgeometry and macrogeometry of WSEM manufactured MBG and MHG is better than milled MBG and hobbled MHG. But, surface finish of milled MBG and hobbing MHG is better than the WSEM manufactured MBG and MHG.
- Flank surface topography of WSEM manufactured MBG and MHG revealed very less deviation of actual surface from theoretical surface as compared to milled MBG and hobbled MHG.
- Microhardness of WSEM manufactured MBG and MHG is very high as compared to milled MBG and hobbled MHG which imparts better wear resistance to WSEM manufactured meso-gears.
- WSEM manufactured MBG and MHG exhibit smoother, cracks and burr free tooth flank surfaces whereas the milled MBG and hobbled MHG have presence of chip particles, burrs and cutter marks on its flank surfaces.
- WSEM manufactured MBG and MHG have accurate and uniform tooth profile than milled MBG and hobbled MHG.
- Total manufacturing time, total manufacturing cost, tooling cost and cost of the machining medium of milled MBG and hobbled MHG are very high as compared to the WSEM manufactured MBG and MHG.
- Loss of meso-gear material is very less in WSEM process. Moreover, it does not require any special tooling and fixture, lubricants, and harmful hydrocarbon-based machining medium as required in the milling and hobbing processes.
- WSEM process can manufacture different sizes of MBG and MHG (i.e. having different tip diameter, cone angle and helix angle) with bore and in large number from the same plate without changing the cutting tool as required in milling and hobbing processes. This minimizes the setup time and manufacturing cost.
- This study proves that WSEM is an economical, superior, flexible, material efficient and environment friendly process for manufacturing of better quality and higher accuracy meso-gears from any material with excellent repeatability. This eliminates need of any finishing and hardening process after WSEM.

- Results of this research work will be very helpful and beneficial for those who work on manufacturing meso-gears. They can achieve better quality fine pitch meso-gears with minimum cost by reducing manufacturing steps, process and wastage of material by using optimal WSEM parametric setting.

### **7.3 Scope for the Future Work**

Since, the present work was the first attempt to establish WSEM as an alternative process of near net-shape manufacturing of high quality MBG and MHG. Therefore there is lot of scope for the future research work in this area which may include:

- Investigations on manufacturing of meso-helical bevel gears (i.e. spiral gears), internal helical gears and meso-sized non-circular gears by WSEM process.
- Investigations on manufacturing of MBG and MHG made of other gear materials (i.e. superalloys, titanium alloys, brass, bronze, aluminium, and different grade of stainless steel) by WSEM process.
- Measurements of other microgeometry parameters such as lead error (for MHG only), single pitch error (for MHG) and runout for both MBG and MHG.
- Investigation on macrogeometry, wear characteristics and residual of MBG and MHG.
- Manufacturing the MBG and MHG of comparatively small size by using wire of different material and dimension (i.e. smaller diameter).
- Development of a test rig for functional testing of MBG and MHG on quality aspects such as noise, vibration and wear-rate etc.
- Exploration of micro-spark-erosion based processes (i.e. micro-WSEM and micro-SEM) for manufacturing of high quality MBG and MHG.
- Explore other micro-manufacturing process for manufacturing of MBG and MHG.



## References

- AGMA 2000–A88, **1988. Gear Classification and Inspection Handbook: Tolerances and Measuring Methods for Unassembled Spur and Helical Gears** (Including Metric Equivalents). *American Gear Manufacturers Association*, Virginia, USA. ISBN: 1-55589-459-X
- Ali, M.Y., Karim, A.N.M., Adesta, Y.E.T., Ismail, A.F., Abdullah, A.A., Idris, M.N., **2010**. Comparative study of conventional and micro WEDM based on machining of meso/micro sized spur gear. **International Journal of Precision Engineering and Manufacturing**. 11(5), 779–784. DOI: 10.1007/s12541-010-0092-2
- Ali, M.Y., Mohammad A.S., **2008**. Experimental study of conventional WEDM for microfabrication. **Materials and Manufacturing Process**. 23(7). 641–645. DOI: 10.1080/10426910802316492
- Ali, M.Y., Rashidah, N.I., Azima, N.A., **2007**. Wire electrical discharge machining for micro fabrication. In: Proceedings of **International Conference on Mechanical Engineering**. December 29- 31, Dhaka, Bangladesh, 1-6.
- ANSI/AGMA2009-B01, **2001. Bevel Gear Classification, Tolerances and Measuring Methods**. *American Gear Manufacturers Association*. Virginia, USA. ISBN: 1-55589-794-0
- Bell, P.C., **1971. Mechanical Power Transmission**. *The Macmillan Press Limited*. Hampshire, UK. DOI 10.1007/978-1-349-01197-1
- Benavides, G.L., Bieg, L.F., Saavedra, M.P., Bryce, E.A., **2003**. High aspect ratio meso-scale parts enabled by wire micro-EDM. **Microsystems Technology**. 8, 395–401. DOI: 10.1007/s00542-002-0190-x
- Bouqueta, J., Hensgenb, L., Klinkb, A., Jacobsc, T., Klockeb, F., Lauwersa, B., **2014**. Fast production of gear prototypes-a comparison of technologies. **Procedia CIRP**. 14, 77-82. DOI: 10.1016/j.procir.2014.03.066
- Bralla, J.G., **1998. Design for Manufacturing Handbook**. *McGraw-Hill Publishing Company*, New York, USA. ISBN: 9780070071391
- Chaubey, S.K., Jain, N.K., **2018**. State-of-art review of past research on manufacturing of meso and micro cylindrical gears. **Precision Engineering**. 51, 702-728. DOI: 10.1016/j.precisioneng.2017.07.014
- Damir, J., **2012. Gears and Gear Drives**. *John Wiley & Sons Inc*. London, UK. ISBN: 978-1-119-94130-9

- Davim, J.P., **2010. Surface Integrity in Machining.** *Springer-Verlag*. London, UK. DOI: 10.1007/978-1-84882-874-2
- Davis, J.R., **2005. Gear Materials, Properties and Manufacture.** (1<sup>st</sup> ed.) *ASM International*, Ohio, USA. ISBN: 978-0-87170-815-1
- Di, S., Haung, R., Ch,i G., **2006.** Study on micro-machining by micro-WEDM. In: Proceedings of **1<sup>st</sup> International IEEE Conference on Nano/Micro Engineered and Molecular systems.** January 18-21, Zhuhai, China, 615-619. DOI: 10.1109/NEMS.2006.334857
- Farago, F.T., Curtis, M.A., **1994. Handbook of Dimensional Measurement.** *Industrial Press Inc.* New York, USA. ISBN: 0-8311-3053-9
- Ferreira, S.L.C., Bruns, R.E., Ferreira, H.S., Matos, G.D., David, J.M., Brandao, G.C., da Silva, E.G.P., Portugal, L.A., dos Reis, P.S., Souza, A.S., dos Santos, W.N.L., **2007.** Box-Behnken design: An alternative for the optimization of analytical methods. *Analytica Chimica Acta.* 597, 179–186. DOI:10.1016/j.aca.2007.07.011
- Goch, G., **2003.** Gear metrology. *CIRP Annals.* 52(2), 659-695. DOI: 10.1016/S0007-8506(07)60209-1
- Griffith, B., **2001. Manufacturing Surface Technology.** *Penton Press*, London, UK. ISBN: 1-8571-8029-1
- Grzesik W., **2008. Advanced Machining Process of Metallic Materials.** *Elsevier*, Oxford, UK. ISBN: 978-0-08-044534-2
- Gupta, K., Jain, N.K., **2013a.** On micro-geometry of miniature gears manufactured by Wire Electrical Discharge Machining. *Materials and Manufacturing Process.* 28(10), 1153-1159. DOI: 10.1080/10426914.2013.792422
- Gupta, K., Jain, N.K., **2013b.** Deviations in geometry of miniature gears fabricated by wire electrical discharge machining. In: Proceedings of **International Mechanical Engineering Congress and Exposition (IMECE 2013) of ASME.** November 13–21, San Diego, USA, V010T11A047. DOI: 10.1115/IMECE2013-66560
- Gupta, K., Jain, N.K., **2014a.** Comparative study of wire-EDM and hobbing for manufacturing high quality miniature gears. *Materials and Manufacturing Process.* 29(11-12), 1470-1476. DOI: 10.1080/10426914.2014.941865
- Gupta, K., Jain, N.K., **2014b.** Analysis and optimization of micro-geometry of miniature spur gears manufactured by wire electric discharge machining. *Precision Engineering.* 38(4), 728-737. DOI: org/10.1016/j.precisioneng.2014.03.009

- Gupta, K., Jain, N.K., **2014c**. On surface integrity of miniature spur gears manufactured by wire electrical discharge machining. **International Journal of Advanced Manufacturing Technology**. 72 (9-12), 1735-1745. DOI: 10.1007/s00170-014-5772-0
- Gupta, K., Jain, N.K., **2014d**. Analysis and optimization of the surface finish of the wire electrical discharge machined miniature gears. **In: Proceedings IMechE, Part B: Journal of Engineering Manufacture**. 228 (5), 673-681. DOI: 10.1007/s00170-014-5772-0
- Gupta, K., Jain, N.K., **2015**. Spark erosion machining of miniature gears: a critical review. **International Journal of Advanced Manufacturing Technology**. 80(9-12), 1863-1877. DOI: 10.1007/s00170-015-7130-2
- Gupta, K., Jain, N.K., **2016**. **Near Net Shape Manufacturing of Miniature Spur Gears By Spark Erosion Machining**. *Springer Nature*. Singapore. DOI: 10.1007/978-981-10-1563-2
- Gupta, K., Jain, N.K., Laubscher, R.F., **2017**. **Advanced Gear Manufacturing and Finishing: Classical and Modern Processes**. *Academic Press*. London, UK. DOI: 10.1016/B978-0-12-804460-5.00008-0.
- Ho, K.H., Newman, S.T., Rahimifard, S., Allen, R.D., **2004**. State of the art in wire electrical discharge machining (WEDM). **International Journal of Machine Tools and Manufacture**. 44, 1247–1259. DOI:10.1016/j.ijmachtools.2004.04.017
- Hori, K., Murata, Y., **1994**. Wire electrical discharge machining of micro-involute gears. **Transactions: The Japan Society of Mechanical Engineering**. Series C (60), 3957–3962. DOI: 10.1299/kikaic.60.3957
- Houser, R., **2009**. The effect of manufacturing microgeometry variations on the load distribution factor and on gear contact and root stresses. **Gear Technology**. 51-60.
- Hsu, T.R., **2008**. MEMS and Microsystems Design. Manufacture and Nano scale Engineering. **John Wiley and Sons**. New Jersey, USA. ISBN: 978-0-470-08301-7
- Hsue, A.W.J., Yan, M.T., Ke, S.H., **2007**. Comparison on linear synchronous motors and conventional rotary motors driven wire-EDM processes. **Journal of Materials Processing Technology**. 192–193, 478–485. DOI: 10.1016/j.jmatprotec.2007.04.046
- Jain, N.K., and Chaubey, S.K., **2016**. Review of Miniature Gear Manufacturing, **In: Comprehensive Materials Finishing-Vol. 1** (Ed. Hashmi, M.S.J.) pp. 504–538,

Elsevier, Oxford, UK. DOI: 10.1016/B978-0-12-803581-8.09159-1, (ISBN: 978-0-12-803581-8)

- Jaster, M., Snyder L., **2010**. Getting wired Into EDM technology emphasizes high accuracies and improved surface finishes. **Gear Technology**. 30-34.
- Khan, I.A. Rajput, T.S., **2012**. Modeling of wire electrical discharge machining of alloy steel (HCHCr). **International Journal of Precision Engineering and Manufacturing**. 13(11), 1989-1995. DOI: 10.1007/s12541-012-0262-5
- Liu, H., Li, J., Shen, Z., Qian, Q., Zhang, H., Wang, X., **2015**. Experimental and numerical simulation research on micro-gears fabrication by laser shock punching process. **Micromachines**. 6(8), 969-983. DOI: 10.3390/mi6080969
- Liu, H.T., Schubert, E., **2011**. Micro abrasive-waterjet technology. **Intech**. 205-234. DOI: 10.5772/30409
- Mahapatra, S.S., Patnaik, A., **2007**. Parametric optimization of wire electrical discharge machining (WEDM) Process using Taguchi Method. **Journal of the Brazilian Society of Mechanical Science and Engineering**. 28(4), 422-429. DOI: 10.1590/S1678-58782006000400006
- Moderow, R., **1992**. Gear inspection and measurement. **Gear Technology**. 44-49.
- Moldovean G., Butuc, Velicu, R., Gavrilă, C.C., B., **2011**. Mechanical efficiency of straight bevel gears used in photovoltaic trackers depending on geometrical accuracy. **13<sup>th</sup> World Congress in Mechanism and Machine Science**. 19-23 June, Guanajuato, Mexico. ISBN: 978-1-62993-077-0
- Montgomery, D.G., **2009**. **Design and Analysis of Experiments**. *John Willey and Sons*, USA. ISBN: 978-1-118-14692-7
- Okada, A., Konishi, T., Okamoto, Y., **2015**. H. Kurihara, Wire breakage and deflection caused by nozzle jet flushing in wire EDM. **CIRP Annals-Manufacturing Technology**. 64 (1), 233–236. DOI:10.1016/j.cirp.2015.04.034
- Pathak, S., Jain, N.K., Palani, I.A., **2016**. Investigations on micro-geometry improvement of straight bevel gears finished by electrochemical honing process. **International Journal of Advanced Manufacturing Technology**. 85, 2223-2234. DOI 10.1007/s00170-015-7725-7
- Puri, A.B., Bhattacharyya, B., **2003**. An analysis and optimization of the geometrical inaccuracy due to wire lag phenomenon in WEDM. **International Journal of Machine Tools and Manufacturer**. 43, 151-159. DOI: 10.1016/S0890-6955(02)00158-X

- Qin, Y., **2010**. Micro-manufacturing Engineering and Technology. **Elsevier**. Oxford, UK. ISBN: 978-0-8155-1545-6
- Radzevich, S.P., **2012**. **Dudley's Handbook of Practical Gear Design and Manufacture**. (2<sup>nd</sup> ed.) *CRC Press*, New York, USA. ISBN: 13: 978-1-4398-6602-3 (eBook-PDF)
- Ramakrishnan, R., Karunamoorthy, L., **2006**. Multi response optimization of Wire EDM operations using robust design of experiments. **International Journal of Advanced Manufacturing Technology**. 29, 105-112. DOI: 10.1007/s00170-004-2496-6
- Sarkar, S., Sekh, M., Bhattacharyya, B., **2006**. Parametric optimization of wire electrical discharge machining of  $\gamma$ -titanium aluminide alloy through an artificial neural network. **International Journal of Advanced Manufacturing Technology**. 27, 501-508. DOI 10.1007/s00170-004-2203-7
- Schoth, A., Forster, R., Menz, W., **2005**. Micro wire-EDM for high aspect ratio 3D microstructuring of ceramics and metals. **Microsystems Technology**. 11(4-5), 250–253. DOI:org/10.1007/s00542-004-0399-y
- Schulze, V., Weber, P., Ruhs, C., **2012**. Increase of process reliability in the micro-machining processes EDM-milling and laser ablation using on-machine sensors. **Journal of Materials Processing Technology**. 212(3), 625– 632. DOI: 10.1016/j.jmatprotec.2011.09.014
- Schumacher, B.M., **2004**. After 60 years of EDM the discharge process remains still disputed. **Journal of Materials Processing Technology**. 149, 376–381. DOI:10.1016/j.matprotec.2003.11.060
- Spedding, T.A., Wang, Z.Q., **1995**. Study on modeling of wire EDM process. **Journal of Materials Processing Technology**. 69(1997), 8-28. DOI: 10.1016/S0924-0136(96)00033-7
- Spedding, T.A., Wang, Z.Q., 1997. Parametric optimization and surface characterization of wire electrical discharge machining process. *Precision Engineering* 20(1), 5-15. DOI: 10.1016/S0141-6359(97)00003-2
- Suzumori, K., Hori, K., **1997**. Micro electrostatic wobble motor with toothed electrodes. In: **Proceedings of 10<sup>th</sup> IEEE International Workshop on Micro Electro Mechanical Systems**. 26-30 January, Nagoya, Japan, 227–232. DOI: 10.1109/MEMSYS.1997.581808

- Takeuchi, H., Nakamura, K., Shimizu, N., Shibaike, N., **2000**. Optimization of mechanical interface for a practical micro-reducer. In: Proceedings of **13<sup>th</sup> IEEE International Conference on Micro Electro Mechanical Systems**. 27-27 January, Miyazaki, Japan. 172-175. DOI: 10.1109/MEMSYS.2000.838511
- Takhata, K., Gianchandani, Y.B., **2002**. Batch mode micro-electrical-discharge Machining. **Journal of Micro Mechanical Systems**. 11(2), 102–110. DOI: 10.1109/84.993444
- Takhata, K., Shibaik, N., Guckel, H., **2000**. High-aspect-ratio WC-Co microstructure produced by the combination of LIGA and micro-EDM. **Microsystem Technology**. 6(5), 175–178. DOI: 10.1007/s005420000052
- Teili, Y., Kewei, H., Luling, A., **2011**. Research on micro gear design for WEDM. **Advanced Materials Research**. 211-212, 315-319. DOI: 10.4028/www.scientific.net/AMR.211-212.315
- Tong, H., Li, Y., Wang, Y., **2008**. Experimental research on vibration assisted EDM of micro-structures with non-circular cross-section. **Journal of Materials Processing Technology**. 208 (1-3), 289–298. DOI: 10.1016/j.jmatprotec.2007.12.126
- Totten, G.E., Howes, M.A.H., Inoue, T., **2002**. **Handbook of Residual Stress and Deformation of Steel**. *ASM International*, Ohio, USA. ISBN: 0-87170-729-2
- Townsend, D.P., **2011**. **Dudley's Gear Handbook**. (2<sup>nd</sup> Ed.) *Tata McGraw-Hill Education Private Limited*, New Delhi, India. ISBN-10: 0070179034
- Uhlmann, E., Piltz, S., Doll, U., **2005**. Machining of micro/miniature dies and moulds by electrical discharge machining-recent development. **Journal of Materials Processing Technology**. 167 (2-3), 488–493. DOI: 10.1016/j.jmatprotec.2005.06.013
- Yan, M.T., Chiang, T.L., **2009**. Design and experimental study of a power supply for micro-wire EDM. **International Journal of Advanced Manufacturing Technology**. 40 (11-12), 1111–1117. DOI: 10.1007/s00170-008-1431-7
- Youn, S.W., Takahashi, M., Goto, H., Maeda, R., **2007**. Fabrication of micro-mold for glass embossing using focused ion beam, femto-second laser, excimer laser and dicing techniques. **Journal of Materials Processing Technology**. 187-188, 326–330. DOI: 10.1016/j.jmatprotec.2006.11.120
- Yude, L., Xingbing, X. W., Yu, Y., Wentian, S., **2009**. Processing micro-gear based on bio-etching method. **Applied Mechanics and Materials**. 16-19, 120-123. DOI:10.4028/www.scientific.net/AMM.16-19.120

- Zhang, G., Zhang, Z., Guo, J., Ming, W., Huang, Y., **2013**. Modeling and optimization of medium-speed WEDM process parameters for machining SKD11. **Materials and Manufacturing Process**. 8(10), 1124-1132. DOI: 10.1080/10426914.2013.773024
- Zhang, Y., Liu, Y., Ji, R., Cai, B., **2011**. Study of the recast layer of a surface machined by sinking electrical discharge machining using water-in-oil emulsion as dielectric. **Applied Surface Science**. 257(14), 5989–5997. DOI: 10.1016/j.apsusc.2011.01.083.
- Zhao, L., Du, M., Yang, Y., **2018**. Optimizing gear micro geometry for minimum transmission error when considering manufacturing deviation. **International Journal of Materials, Mechanics and Manufacturing**. 6(1), 74-77. DOI: 10.18178/ijmmm.2018.6.1.350
- Zhong, J., Wu, X., Xu, B., Li, J., Luo, F., Cheng, R., Ruan, S., **2015**. Laminated fabrication of micro-stepped gear mold based on WEDM and thermal diffusion welding. **International Journal of Advanced Manufacturing Technology**. 78(5-8), 1233–1240. DOI: 10.1007/s00170-014-6746-y



## Appendix-A

### Chemical Composition of Meso-Gears Material

<h1 style="margin: 0;">Certificate</h1>					
					
6/3, MANORAMAGANJ, INDORE 452001 MADHYA PRADESH Phone : +91 731 4243888 (30 LINES) Fax : +91 731 2490593 Email : indore@choksilab.com Website : www.choksilab.com					
BOOKING NO. :	10348				
CERTIFICATE NO. :	10348/2017-2018				
<b>1. NAME OF MANUFACTURER/PARTY :</b> SUJEET KUMAR CHAUBEY RESEARCH SCHALAR IIT,INDORE INDORE MADHYA PRADESH					
1.MFG. LIC. NO.	: NM	5. REFERENCE NO. 1	: NM		
2. REFERENCE NO. OF LETTER	: NM	6. REFERENCE NO. 2	: NM		
3. DATE	: NM	7. REFERENCE NO. 3	: NM		
4. DATE OF RECEIPT	: 14/10/2017	8. NAME OF SAMPLE	: METAL PIECE (SS 304)		
<b>9. DETAILS OF RAW MATERIAL / FINAL PRODUCTS (In Bulk/Finished Pack)</b>					
(A) BATCH NO.	: 1	(G) SAMPLE QUANTITY	: 1 NO		
(B) BATCH SIZE	: NM	(H) SEALED	: UNSEALED		
(C) A.R. NO.	: NM	(I) PACKING	: OPEN		
(D) DATE OF MFG.	: NM	(J) STARTING DATE	: 14/10/2017		
(E) DATE OF EXPIRY	: NM	(K) ENDING DATE	: 14/10/2017		
(F) MFG NAME	: NM	(L) PAGE NO.	: Page 1 of 1		
<b>AS PER CUSTOMER SPECIFICATION</b>					
SR	TEST NAME	UNIT	RESULT	SPECIFICATIONS	METHOD OF TEST
(A)	Chemical Composition :-	---			
1	Carbon as C	%	0.053	Max. 0.08	CLL-IDR-STP-BM-004 (Spectro Analysis)
2	Silicon as Si	%	0.480	Max. 0.75	
3	Manganese as Mn	%	1.08	Max. 2.0	
4	Phosphorus as P	%	0.038	Max. 0.045	
5	Sulphur as S	%	0.017	Max. 0.03	
6	Chromium as Cr	%	18.04	18.0 to 20.0	
7	Nickel as Ni	%	8.32	8.0 to 10.0	
8	Nitrogen as N	%	0.098	Max. 0.1	
<b>Remarks :</b> 1. Certificate Issue Date: 14/10/2017					For Choksi Laboratories Ltd. Authorized Signatory   Sachin T. Patil Sr. Scientist (IND-00750) Building Materials QAIS : 57/04
<b>Note :</b> Please see overleaf for terms & conditions.					

## Appendix-B

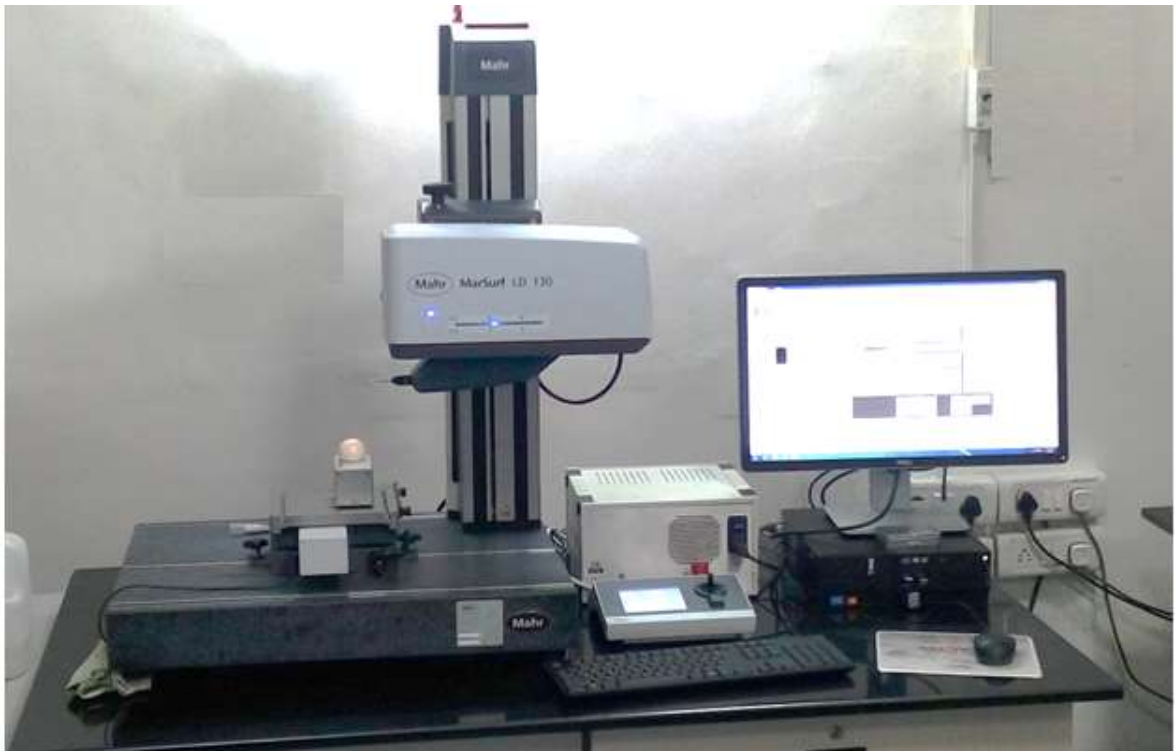
### Details of the Measuring Instruments Used

- CNC Gear Metrology Machine (Gear Research LAB, IIT Indore)



Model	SmartGear 500
Make	WenzelTec Germany
Diameter of work-piece minimum/maximum	5-270 mm
Internal Gear Diameter	>12 mm
Module range minimum/maximum	0.4-15 mm
Helix angle	<90 <sup>0</sup>
	MPE <sub>e</sub> = 4.5+L/250 μm
ISO 10360-2 accuracy for 3D measurement from	MPE <sub>thp</sub> = 5.0 μm
Measurable face width maximum	300 mm
Temperature range	20 <sup>0</sup> C +5k, -3k
	500 mm
Transverse Distance	450 mm
	400 mm
Distance between centres minimum/maximum	-
Table diameter	L200 mm
Rotary table load maximum	

- **3D Surface Roughness cum Contour Tracer (Gear Research LAB, IIT Indore)**



Make	Mahr GmbH
Model	MarSurf LD 130
Resolution	0.8 nm
Start of traversing length (in X)	0.1 mm
End of traversing length (in X)	130 mm
Positioning speed	0.02 mm/s to 200 mm/s
Measuring speed	0.02 mm/s to 10 mm/s; for roughness measurements 0.1 mm/s to 0.5 mm/s is recommended
Measuring range (mm)	13 mm (100 mm probe arm) 26 mm (200 mm probe arm)
Traversing lengths	0.1 mm - 130 mm
Measuring force (N)	0.5 mN to 30 mN, software-adjustable

- Scanning Electron Microscope (Sophisticated Instrument Centre, IIT Indore)



Make	Carl Zeiss NTS GmbH, Germany
Model	SUPRA 55
Resolution	1.0 nm @ 15 kV 1.7 nm @ 1 kV 4.0 nm @ 0.1 kV
Acceleration Voltage	0.1 - 30 kV
Magnification	12x - 900,000 x
Stages	5-Axes Motorised Eucentric Specimen Stage X = 130 mm, Y = 130mm, Z = 50mm, T = -3 - +70°, R = 360° (continuous)
Standard Detectors	High efficiency In-lens detector Everhart-Thornley Secondary Electron Detector

- **Microhardness Tester (AVTEC Limited, Pithampur (MP) India)**



---

Make: Zwick Roell, UK

---

Model: ZHV30

---

Load Range: 200 grams-5000 grams

---

Type of Indenter: Diamond square base hexagonal pyramid

---

- **Optical Microscope (Gear Research Lab, IIT Indore)**



<b>Specification of Optical Microscope</b>	
Model	Leica DM2500 M
Power supply	Stabilized universal power supply unit, 90–230 V for 12 V 30 W
Magnifying Range	10X, 100X
Software	Leica “QMW” for image analysis
Image Analysis	Digital
Attachment	Polarise

## Appendix-C Gear Part Program

- **Meso Bevel Gear (MBG)**

;27. 2.2016, 05:41:30 Bevel-7mm

G71

G9

G27

G40

G47

G50

G90

G75

; Wire Compensation Definitions

D0=0

D1=0.135

;**#1.0 Cavity=1 RoughCut**

G0 X0 Y0 U0 V0

M21

G42 D0 ;D0=0

G1 X0 Y1.5

G42 D1 ;D1=0.135

G2 X1.5 Y0 I0 J-1.5

G2 X-1.5 Y0 I-1.5 J0

G2 X0.1 Y1.496663 I1.5 J0

M0

G42 D0 ;D0=0

G1 X0 Y0

G40

M0

;27. 2.2016, 05:42:48

; Wire Compensation Definitions

D0=0

D1=0.165

;**#1.0 Cavity=1 RoughCut**

G74 Z10 B0 T5.5

G41 D0 ;D0=0

G0 X0 Y-12 G100 U0 V-12

M21

G1 X0 Y-4.9 G101 U0 V-3.5

G41 D1 ;D1=0.165

G2 X-0.217243 Y-4.895182 I0 J4.9 G102 U-0.155174 V-3.496558 P0 Q3.5

G2 X-0.366642 Y-4.656346 I1.478333 J1.090884 G102 U-0.261887 V-3.325961 P1.055952 Q0.779203

G2 X-0.47777 Y-4.397477 I1.627732 J0.852047 G102 U-0.341265 V-3.141055 P1.162666 Q0.608605

G2 X-0.54249 Y-4.154435 I1.738861 J0.593178 G102 U-0.387493 V-2.967454 P1.242043 Q0.423699

G2 X-0.57341 Y-3.904832 I1.80358 J0.350137 G102 U-0.409578 V-2.789166 P1.288271 Q0.250098

G1 X-0.483083 Y-3.28972 G101 U-0.345059 V-2.3498

G2 X-0.860573 Y-3.211703 I0.483083 J3.28972 G102 U-0.614695 V-2.294074 P0.345059 Q2.3498

G2 X-1.226498 Y-3.090522 I0.860573 J3.211703 G102 U-0.87607 V-2.207516 P0.614695 Q2.294074

G1 X-1.455829 Y-3.668389 G101 U-1.039878 V-2.620278

G2 X-1.607408 Y-3.869091 I-1.538457 J1.004315 G102 U-1.148148 V-2.763637 P-1.098898 Q0.717368

G2 X-1.784977 Y-4.047212 I-1.386878 J1.205017 G102 U-1.274984 V-2.890865 P-0.990627 Q0.860727

G2 X-2.010652 Y-4.215835 I-1.209308 J1.383138 G102 U-1.43618 V-3.01131 P-0.863792 Q0.987956  
G2 X-2.259453 Y-4.347973 I-0.983634 J1.551761 G102 U-1.613895 V-3.105695 P-0.702596 Q1.108401  
G2 X-2.45 Y-4.243524 I2.259453 J4.347973 G102 U-1.75 V-3.031089 P1.613895 Q3.105695  
G2 X-2.635729 Y-4.13073 I2.45 J4.243524 G102 U-1.882664 V-2.950522 P1.75 Q3.031089  
G2 X-2.645694 Y-3.849193 I1.825716 J0.205566 G102 U-1.889781 V-2.749423 P1.304083 Q0.146833  
G2 X-2.6125 Y-3.569441 I1.835681 J-0.075971 G102 U-1.866071 V-2.549601 P1.311201 Q-0.054265  
G2 X-2.547027 Y-3.326602 I1.802487 J-0.355723 G102 U-1.819305 V-2.376144 P1.28749 Q-0.254088  
G2 X-2.449003 Y-3.094979 I1.737015 J-0.598563 G102 U-1.749288 V-2.210699 P1.240725 Q-0.427545  
G1 X-2.063222 Y-2.60744 G101 U-1.47373 V-1.862457  
G2 X-2.35113 Y-2.35113 I2.063222 J2.60744 G102 U-1.679379 V-1.679379 P1.47373 Q1.862457  
G2 X-2.60744 Y-2.063222 I2.35113 J2.35113 G102 U-1.862457 V-1.47373 P1.679379 Q1.679379  
G1 X-3.094979 Y-2.449003 G101 U-2.210699 V-1.749288  
G2 X-3.326602 Y-2.547027 I-0.830185 J1.63899 G102 U-2.376144 V-1.819305 P-0.592989 Q1.170707  
G2 X-3.569441 Y-2.6125 I-0.598563 J1.737015 G102 U-2.549601 V-1.866071 P-0.427545 Q1.240725  
G2 X-3.849193 Y-2.645694 I-0.355723 J1.802487 G102 U-2.749423 V-1.889781 P-0.254088 Q1.28749  
G2 X-4.13073 Y-2.635729 I-0.075971 J1.835681 G102 U-2.950522 V-1.882664 P-0.054265 Q1.311201  
G2 X-4.243524 Y-2.45 I4.13073 J2.635729 G102 U-3.031089 V-1.75 P2.950522 Q1.882664  
G2 X-4.347973 Y-2.259453 I4.243524 J2.45 G102 U-3.105695 V-1.613895 P3.031089 Q1.75  
G2 X-4.215835 Y-2.010652 I1.6839 J-0.734833 G102 U-3.01131 V-1.43618 P1.202785 Q-0.52488  
G2 X-4.047212 Y-1.784977 I1.551761 J-0.983634 G102 U-2.890865 V-1.274984 P1.108401 Q-0.702596  
G2 X-3.869091 Y-1.607408 I1.383138 J-1.209308 G102 U-2.763637 V-1.148148 P0.987956 Q-0.863792  
G2 X-3.668389 Y-1.455829 I1.205017 J-1.386878 G102 U-2.620278 V-1.039878 P0.860727 Q-0.990627  
G1 X-3.090522 Y-1.226498 G101 U-2.207516 V-0.87607  
G2 X-3.211703 Y-0.860573 I3.090522 J1.226498 G102 U-2.294074 V-0.614695 P2.207516 Q0.87607  
G2 X-3.28972 Y-0.483083 I3.211703 J0.860573 G102 U-2.3498 V-0.345059 P2.294074 Q0.614695  
G1 X-3.904832 Y-0.57341 G101 U-2.789166 V-0.409578  
G2 X-4.154435 Y-0.54249 I0.100534 J1.8345 G102 U-2.967454 V-0.387493 P0.07181 Q1.310357  
G2 X-4.397477 Y-0.47777 I0.350137 J1.80358 G102 U-3.141055 V-0.341265 P0.250098 Q1.288271  
G2 X-4.656346 Y-0.366642 I0.593178 J1.738861 G102 U-3.325961 V-0.261887 P0.423699 Q1.242043  
G2 X-4.895182 Y-0.217243 I0.852047 J1.627732 G102 U-3.496558 V-0.155174 P0.608605 Q1.162666  
G2 X-4.9 Y0 I4.895182 J0.217243 G102 U-3.5 V0 P3.496558 Q0.155174  
G2 X-4.895182 Y0.217243 I4.9 J0 G102 U-3.496558 V0.155174 P3.5 Q0  
G2 X-4.656346 Y0.366642 I1.090884 J-1.478333 G102 U-3.325961 V0.261887 P0.779203 Q-1.055952  
G2 X-4.397477 Y0.47777 I0.852047 J-1.627732 G102 U-3.141055 V0.341265 P0.608605 Q-1.162666  
G2 X-4.154435 Y0.54249 I0.593178 J-1.738861 G102 U-2.967454 V0.387493 P0.423699 Q-1.242043  
G2 X-3.904832 Y0.57341 I0.350137 J-1.80358 G102 U-2.789166 V0.409578 P0.250098 Q-1.288271  
G1 X-3.28972 Y0.483083 G101 U-2.3498 V0.345059  
G2 X-3.211703 Y0.860573 I3.28972 J-0.483083 G102 U-2.294074 V0.614695 P2.3498 Q-0.345059  
G2 X-3.090522 Y1.226498 I3.211703 J-0.860573 G102 U-2.207516 V0.87607 P2.294074 Q-0.614695  
G1 X-3.668389 Y1.455829 G101 U-2.620278 V1.039878  
G2 X-3.869091 Y1.607408 I1.004315 J1.538457 G102 U-2.763637 V1.148148 P0.717368 Q1.098898  
G2 X-4.047212 Y1.784977 I1.205017 J1.386878 G102 U-2.890865 V1.274984 P0.860727 Q0.990627  
G2 X-4.215835 Y2.010652 I1.383138 J1.209308 G102 U-3.01131 V1.43618 P0.987956 Q0.863792  
G2 X-4.347973 Y2.259453 I1.551761 J0.983634 G102 U-3.105695 V1.613895 P1.108401 Q0.702596  
G2 X-4.243524 Y2.45 I4.347973 J-2.259453 G102 U-3.031089 V1.75 P3.105695 Q-1.613895  
G2 X-4.13073 Y2.635729 I4.243524 J-2.45 G102 U-2.950522 V1.882664 P3.031089 Q-1.75  
G2 X-3.849193 Y2.645694 I0.205566 J-1.825716 G102 U-2.749423 V1.889781 P0.146833 Q-1.304083  
G2 X-3.569441 Y2.6125 I-0.075971 J-1.835681 G102 U-2.549601 V1.866071 P-0.054265 Q-1.311201  
G2 X-3.326602 Y2.547027 I-0.355723 J-1.802487 G102 U-2.376144 V1.819305 P-0.254088 Q-1.28749  
G2 X-3.094979 Y2.449003 I-0.598563 J-1.737015 G102 U-2.210699 V1.749288 P-0.427545 Q-1.240725  
G1 X-2.60744 Y2.063222 G101 U-1.862457 V1.47373  
G2 X-2.35113 Y2.35113 I2.60744 J-2.063222 G102 U-1.679379 V1.679379 P1.862457 Q-1.47373

G2 X-2.063222 Y2.60744 I2.35113 J-2.35113 G102 U-1.47373 V1.862457 P1.679379 Q-1.679379  
G1 X-2.449003 Y3.094979 G101 U-1.749288 V2.210699  
G2 X-2.547027 Y3.326602 I1.63899 J0.830185 G102 U-1.819305 V2.376144 P1.170707 Q0.592989  
G2 X-2.6125 Y3.569441 I1.737015 J0.598563 G102 U-1.866071 V2.549601 P1.240725 Q0.427545  
G2 X-2.645694 Y3.849193 I1.802487 J0.355723 G102 U-1.889781 V2.749423 P1.28749 Q0.254088  
G2 X-2.635729 Y4.13073 I1.835681 J0.075971 G102 U-1.882664 V2.950522 P1.311201 Q0.054265  
G2 X-2.45 Y4.243524 I2.635729 J-4.13073 G102 U-1.75 V3.031089 P1.882664 Q-2.950522  
G2 X-2.259453 Y4.347973 I2.45 J-4.243524 G102 U-1.613895 V3.105695 P1.75 Q-3.031089  
G2 X-2.010652 Y4.215835 I-0.734833 J-1.6839 G102 U-1.43618 V3.01131 P-0.52488 Q-1.202785  
G2 X-1.784977 Y4.047212 I-0.983634 J-1.551761 G102 U-1.274984 V2.890865 P-0.702596 Q-1.108401  
G2 X-1.607408 Y3.869091 I-1.209308 J-1.383138 G102 U-1.148148 V2.763637 P-0.863792 Q-0.987956  
G2 X-1.455829 Y3.668389 I-1.386878 J-1.205017 G102 U-1.039878 V2.620278 P-0.990627 Q-0.860727  
G1 X-1.226498 Y3.090522 G101 U-0.87607 V2.207516  
G2 X-0.860573 Y3.211703 I1.226498 J-3.090522 G102 U-0.614695 V2.294074 P0.87607 Q-2.207516  
G2 X-0.483083 Y3.28972 I0.860573 J-3.211703 G102 U-0.345059 V2.3498 P0.614695 Q-2.294074  
G1 X-0.57341 Y3.904832 G101 U-0.409578 V2.789166  
G2 X-0.54249 Y4.154435 I1.8345 J-0.100534 G102 U-0.387493 V2.967454 P1.310357 Q-0.07181  
G2 X-0.47777 Y4.397477 I1.80358 J-0.350137 G102 U-0.341265 V3.141055 P1.288271 Q-0.250098  
G2 X-0.366642 Y4.656346 I1.738861 J-0.593178 G102 U-0.261887 V3.325961 P1.242043 Q-0.423699  
G2 X-0.217243 Y4.895182 I1.627732 J-0.852047 G102 U-0.155174 V3.496558 P1.162666 Q-0.608605  
G2 X0 Y4.9 I0.217243 J-4.895182 G102 U0 V3.5 P0.155174 Q-3.496558  
G2 X0.217243 Y4.895182 I0 J-4.9 G102 U0.155174 V3.496558 P0 Q-3.5  
G2 X0.366642 Y4.656346 I-1.478333 J-1.090884 G102 U0.261887 V3.325961 P-1.055952 Q-0.779203  
G2 X0.47777 Y4.397477 I-1.627732 J-0.852047 G102 U0.341265 V3.141055 P-1.162666 Q-0.608605  
G2 X0.54249 Y4.154435 I-1.738861 J-0.593178 G102 U0.387493 V2.967454 P-1.242043 Q-0.423699  
G2 X0.57341 Y3.904832 I-1.80358 J-0.350137 G102 U0.409578 V2.789166 P-1.288271 Q-0.250098  
G1 X0.483083 Y3.28972 G101 U0.345059 V2.3498  
G2 X0.860573 Y3.211703 I-0.483083 J-3.28972 G102 U0.614695 V2.294074 P-0.345059 Q-2.3498  
G2 X1.226498 Y3.090522 I-0.860573 J-3.211703 G102 U0.87607 V2.207516 P-0.614695 Q-2.294074  
G1 X1.455829 Y3.668389 G101 U1.039878 V2.620278  
G2 X1.607408 Y3.869091 I1.538457 J-1.004315 G102 U1.148148 V2.763637 P1.098898 Q-0.717368  
G2 X1.784977 Y4.047212 I1.386878 J-1.205017 G102 U1.274984 V2.890865 P0.990627 Q-0.860727  
G2 X2.010652 Y4.215835 I1.209308 J-1.383138 G102 U1.43618 V3.01131 P0.863792 Q-0.987956  
G2 X2.259453 Y4.347973 I0.983634 J-1.551761 G102 U1.613895 V3.105695 P0.702596 Q-1.108401  
G2 X2.45 Y4.243524 I-2.259453 J-4.347973 G102 U1.75 V3.031089 P-1.613895 Q-3.105695  
G2 X2.635729 Y4.13073 I-2.45 J-4.243524 G102 U1.882664 V2.950522 P-1.75 Q-3.031089  
G2 X2.645694 Y3.849193 I-1.825716 J-0.205566 G102 U1.889781 V2.749423 P-1.304083 Q-0.146833  
G2 X2.6125 Y3.569441 I-1.835681 J0.075971 G102 U1.866071 V2.549601 P-1.311201 Q0.054265  
G2 X2.547027 Y3.326602 I-1.802487 J0.355723 G102 U1.819305 V2.376144 P-1.28749 Q0.254088  
G2 X2.449003 Y3.094979 I-1.737015 J0.598563 G102 U1.749288 V2.210699 P-1.240725 Q0.427545  
G1 X2.063222 Y2.60744 G101 U1.47373 V1.862457  
G2 X2.35113 Y2.35113 I-2.063222 J-2.60744 G102 U1.679379 V1.679379 P-1.47373 Q-1.862457  
G2 X2.60744 Y2.063222 I-2.35113 J-2.35113 G102 U1.862457 V1.47373 P-1.679379 Q-1.679379  
G1 X3.094979 Y2.449003 G101 U2.210699 V1.749288  
G2 X3.326602 Y2.547027 I0.830185 J-1.63899 G102 U2.376144 V1.819305 P0.592989 Q-1.170707  
G2 X3.569441 Y2.6125 I0.598563 J-1.737015 G102 U2.549601 V1.866071 P0.427545 Q-1.240725  
G2 X3.849193 Y2.645694 I0.355723 J-1.802487 G102 U2.749423 V1.889781 P0.254088 Q-1.28749  
G2 X4.13073 Y2.635729 I0.075971 J-1.835681 G102 U2.950522 V1.882664 P0.054265 Q-1.311201  
G2 X4.243524 Y2.45 I-4.13073 J-2.635729 G102 U3.031089 V1.75 P-2.950522 Q-1.882664  
G2 X4.347973 Y2.259453 I-4.243524 J-2.45 G102 U3.105695 V1.613895 P-3.031089 Q-1.75  
G2 X4.215835 Y2.010652 I-1.6839 J0.734833 G102 U3.01131 V1.43618 P-1.202785 Q0.52488  
G2 X4.047212 Y1.784977 I-1.551761 J0.983634 G102 U2.890865 V1.274984 P-1.108401 Q0.702596

G2 X3.869091 Y1.607408 I-1.383138 J1.209308 G102 U2.763637 V1.148148 P-0.987956 Q0.863792  
G2 X3.668389 Y1.455829 I-1.205017 J1.386878 G102 U2.620278 V1.039878 P-0.860727 Q0.990627  
G1 X3.090522 Y1.226498 G101 U2.207516 V0.87607  
G2 X3.211703 Y0.860573 I-3.090522 J-1.226498 G102 U2.294074 V0.614695 P-2.207516 Q-0.87607  
G2 X3.28972 Y0.483083 I-3.211703 J-0.860573 G102 U2.3498 V0.345059 P-2.294074 Q-0.614695  
G1 X3.904832 Y0.57341 G101 U2.789166 V0.409578  
G2 X4.154435 Y0.54249 I-0.100534 J-1.8345 G102 U2.967454 V0.387493 P-0.07181 Q-1.310357  
G2 X4.397477 Y0.47777 I-0.350137 J-1.80358 G102 U3.141055 V0.341265 P-0.250098 Q-1.288271  
G2 X4.656346 Y0.366642 I-0.593178 J-1.738861 G102 U3.325961 V0.261887 P-0.423699 Q-1.242043  
G2 X4.895182 Y0.217243 I-0.852047 J-1.627732 G102 U3.496558 V0.155174 P-0.608605 Q-1.162666  
G2 X4.9 Y0 I-4.895182 J-0.217243 G102 U3.5 V0 P-3.496558 Q-0.155174  
G2 X4.895182 Y-0.217243 I-4.9 J0 G102 U3.496558 V-0.155174 P-3.5 Q0  
G2 X4.656346 Y-0.366642 I-1.090884 J1.478333 G102 U3.325961 V-0.261887 P-0.779203 Q1.055952  
G2 X4.397477 Y-0.47777 I-0.852047 J1.627732 G102 U3.141055 V-0.341265 P-0.608605 Q1.162666  
G2 X4.154435 Y-0.54249 I-0.593178 J1.738861 G102 U2.967454 V-0.387493 P-0.423699 Q1.242043  
G2 X3.904832 Y-0.57341 I-0.350137 J1.80358 G102 U2.789166 V-0.409578 P-0.250098 Q1.288271  
G1 X3.28972 Y-0.483083 G101 U2.3498 V-0.345059  
G2 X3.211703 Y-0.860573 I-3.28972 J0.483083 G102 U2.294074 V-0.614695 P-2.3498 Q0.345059  
G2 X3.090522 Y-1.226498 I-3.211703 J0.860573 G102 U2.207516 V-0.87607 P-2.294074 Q0.614695  
G1 X3.668389 Y-1.455829 G101 U2.620278 V-1.039878  
G2 X3.869091 Y-1.607408 I-1.004315 J-1.538457 G102 U2.763637 V-1.148148 P-0.717368 Q-1.098898  
G2 X4.047212 Y-1.784977 I-1.205017 J-1.386878 G102 U2.890865 V-1.274984 P-0.860727 Q-0.990627  
G2 X4.215835 Y-2.010652 I-1.383138 J-1.209308 G102 U3.01131 V-1.43618 P-0.987956 Q-0.863792  
G2 X4.347973 Y-2.259453 I-1.551761 J-0.983634 G102 U3.105695 V-1.613895 P-1.108401 Q-0.702596  
G2 X4.243524 Y-2.45 I-4.347973 J2.259453 G102 U3.031089 V-1.75 P-3.105695 Q1.613895  
G2 X4.13073 Y-2.635729 I-4.243524 J2.45 G102 U2.950522 V-1.882664 P-3.031089 Q1.75  
G2 X3.849193 Y-2.645694 I-0.205566 J1.825716 G102 U2.749423 V-1.889781 P-0.146833 Q1.304083  
G2 X3.569441 Y-2.6125 I0.075971 J1.835681 G102 U2.549601 V-1.866071 P0.054265 Q1.311201  
G2 X3.326602 Y-2.547027 I0.355723 J1.802487 G102 U2.376144 V-1.819305 P0.254088 Q1.28749  
G2 X3.094979 Y-2.449003 I0.598563 J1.737015 G102 U2.210699 V-1.749288 P0.427545 Q1.240725  
G1 X2.60744 Y-2.063222 G101 U1.862457 V-1.47373  
G2 X2.35113 Y-2.35113 I-2.60744 J2.063222 G102 U1.679379 V-1.679379 P-1.862457 Q1.47373  
G2 X2.063222 Y-2.60744 I-2.35113 J2.35113 G102 U1.47373 V-1.862457 P-1.679379 Q1.679379  
G1 X2.449003 Y-3.094979 G101 U1.749288 V-2.210699  
G2 X2.547027 Y-3.326602 I-1.63899 J-0.830185 G102 U1.819305 V-2.376144 P-1.170707 Q-0.592989  
G2 X2.6125 Y-3.569441 I-1.737015 J-0.598563 G102 U1.866071 V-2.549601 P-1.240725 Q-0.427545  
G2 X2.645694 Y-3.849193 I-1.802487 J-0.355723 G102 U1.889781 V-2.749423 P-1.28749 Q-0.254088  
G2 X2.635729 Y-4.13073 I-1.835681 J-0.075971 G102 U1.882664 V-2.950522 P-1.311201 Q-0.054265  
G2 X2.45 Y-4.243524 I-2.635729 J4.13073 G102 U1.75 V-3.031089 P-1.882664 Q2.950522  
G2 X2.259453 Y-4.347973 I-2.45 J4.243524 G102 U1.613895 V-3.105695 P-1.75 Q3.031089  
G2 X2.010652 Y-4.215835 I0.734833 J1.6839 G102 U1.43618 V-3.01131 P0.52488 Q1.202785  
G2 X1.784977 Y-4.047212 I0.983634 J1.551761 G102 U1.274984 V-2.890865 P0.702596 Q1.108401  
G2 X1.607408 Y-3.869091 I1.209308 J1.383138 G102 U1.148148 V-2.763637 P0.863792 Q0.987956  
G2 X1.455829 Y-3.668389 I1.386878 J1.205017 G102 U1.039878 V-2.620278 P0.990627 Q0.860727  
G1 X1.226498 Y-3.090522 G101 U0.87607 V-2.207516  
G2 X0.860573 Y-3.211703 I-1.226498 J3.090522 G102 U0.614695 V-2.294074 P-0.87607 Q2.207516  
G2 X0.483083 Y-3.28972 I-0.860573 J3.211703 G102 U0.345059 V-2.3498 P-0.614695 Q2.294074  
G1 X0.57341 Y-3.904832 G101 U0.409578 V-2.789166

- **Meso Helical Gear (MHG)**

;27. 2.2016, 05:44:51 dia=8.35mm (Helical Gear)

G71

G9

G27

G40

G47

G50

G90

G75

; Wire Compensation Definitions

D0=0

D1=0.135

;#1.0 Cavity=1 RoughCut

G0 X0 Y0 U0 V0

M21

G42 D0 ;D0=0

G1 X0 Y1.5

G42 D1 ;D1=0.135

G2 X1.5 Y0 I0 J-1.5

G2 X-1.5 Y0 I-1.5 J0

G2 X0.1 Y1.496663 I1.5 J0

M0

G42 D0 ;D0=0

G1 X0 Y0

G40

M0

;27. 2.2016, 05:46:46

; Wire Compensation Definitions

D0=0

D1=0.165

;#1.0 Cavity=1 RoughCut

G74 Z10 B0 T5.2

G42 D0 ;D0=0

G0 X0 Y-9.175 G100 U3.138035 V-8.62168

M21

G1 X0 Y-4.175 G101 U1.427934 V-3.923217

G42 D1 ;D1=0.165

G3 X0.193057 Y-4.170534 I0 J4.175 G103 U1.607821 V-3.852991 P-1.427934 Q3.923217

G3 X0.336599 Y-3.953854 I-1.278609 J1.002914 G103 U1.668597 V-3.600284 P-1.544516 Q0.505121

G3 X0.447542 Y-3.706416 I-1.42215 J0.786234 G103 U1.688221 V-3.329824 P-1.605292 Q0.252414

G3 X0.5099 Y-3.476182 I-1.533093 J0.538796 G103 U1.668074 V-3.092147 P-1.624915 Q-0.018046

G3 X0.537761 Y-3.241999 I-1.595451 J0.308562 G103 U1.614159 V-2.862558 P-1.604768 Q-0.255723

G1 X0.420306 Y-2.565803 G101 U1.272514 V-2.267313

G3 X0.803444 Y-2.472747 I-0.420306 J2.565803 G103 U1.60072 V-2.048828 P-1.272514 Q2.267313

G3 X1.168107 Y-2.322827 I-0.803444 J2.472747 G103 U1.892115 V-1.783228 P-1.60072 Q2.048828

G1 X1.470542 Y-2.938921 G101 U2.387027 V-2.258727

G3 X1.630731 Y-3.112002 I1.269568 J1.014333 G103 U2.596753 V-2.366583 P0.846082 Q1.387379

G3 X1.816508 Y-3.261612 I1.109379 J1.187415 G103 U2.822496 V-2.44363 P0.636355 Q1.495235

G3 X2.051703 Y-3.396583 I0.923602 J1.337025 G103 U3.08967 V-2.49002 P0.410613 Q1.572283

G3 X2.295192 Y-3.487509 I0.688407 J1.471996 G103 U3.349573 V-2.492185 P0.143439 Q1.618673

G3 X2.454003 Y-3.377646 I-2.295192 J3.487509 G103 U3.461232 V-2.33463 P-3.349573 Q2.492185

G3 X2.607565 Y-3.260557 I-2.454003 J3.377646 G103 U3.565486 V-2.172081 P-3.461232 Q2.33463  
G3 X2.596331 Y-3.000887 I-1.623914 J0.059827 G103 U3.466117 V-1.931914 P-1.546442 Q-0.499192  
G3 X2.540646 Y-2.735495 I-1.612681 J-0.199843 G103 U3.32302 V-1.701573 P-1.447074 Q-0.73936  
G3 X2.455766 Y-2.512579 I-1.556995 J-0.465235 G103 U3.167018 V-1.52113 P-1.303977 Q-0.969701  
G3 X2.340657 Y-2.306745 I-1.472116 J-0.688151 G103 U2.988451 V-1.367079 P-1.147975 Q-1.150143  
G1 X1.848175 Y-1.828729 G101 U2.362179 V-1.08633  
G3 X2.103444 Y-1.528242 I-1.848175 J1.828729 G103 U2.49928 V-0.716657 P-2.362179 Q1.08633  
G3 X2.310342 Y-1.192611 I-2.103444 J1.528242 G103 U2.578908 V-0.330504 P-2.49928 Q0.716657  
G1 X2.917147 Y-1.513274 G101 U3.258792 V-0.424289  
G3 X3.148478 Y-1.559143 I0.430892 J1.566846 G103 U3.49186 V-0.388272 P-0.130987 Q1.619728  
G3 X3.386713 Y-1.570983 I0.199562 J1.612715 G103 U3.719777 V-0.317917 P-0.364055 Q1.583711  
G3 X3.656324 Y-1.541933 I-0.038673 J1.624555 G103 U3.963193 V-0.198406 P-0.591972 Q1.513356  
G3 X3.906756 Y-1.472374 I-0.308284 J1.595505 G103 U4.174731 V-0.04739 P-0.835387 Q1.393845  
G3 X3.970661 Y-1.290146 I-3.906756 J1.472374 G103 U4.172457 V0.145705 P-4.174731 Q0.04739  
G3 X4.026071 Y-1.105158 I-3.970661 J1.290146 G103 U4.161256 V0.338489 P-4.172457 Q-0.145705  
G3 X3.864354 Y-0.901683 I-1.348939 J-0.906112 G103 U3.939698 V0.474381 P-0.95768 Q-1.312831  
G3 X3.663309 Y-0.719708 I-1.187221 J-1.109586 G103 U3.688539 V0.576621 P-0.736122 Q-1.448723  
G3 X3.463614 Y-0.589256 I-0.986177 J-1.291561 G103 U3.45627 V0.630906 P-0.484963 Q-1.550963  
G3 X3.249502 Y-0.490392 I-0.786482 J-1.422013 G103 U3.221257 V0.650578 P-0.252694 Q-1.605248  
G1 X2.570105 Y-0.393142 G101 U2.549571 V0.509595  
G3 X2.6 Y0 I-2.570105 J0.393142 G103 U2.443201 V0.889252 P-2.549571 Q-0.509595  
G3 X2.570105 Y0.393142 I-2.6 J0 G103 U2.280646 V1.248461 P-2.443201 Q-0.889252  
G1 X3.249502 Y0.490392 G101 U2.885809 V1.572213  
G3 X3.463614 Y0.589256 I-0.57237 J1.520877 G103 U3.053195 V1.738345 P-1.058022 Q1.233395  
G3 X3.663309 Y0.719708 I-0.786482 J1.422013 G103 U3.19623 V1.92923 P-1.225408 Q1.067263  
G3 X3.864354 Y0.901683 I-0.986177 J1.291561 G103 U3.322911 V2.168992 P-1.368443 Q0.876378  
G3 X4.026071 Y1.105158 I-1.187221 J1.109586 G103 U3.405283 V2.415506 P-1.495124 Q0.636616  
G3 X3.970661 Y1.290146 I-4.026071 J-1.105158 G103 U3.289945 V2.570387 P-3.405283 Q-2.415506  
G3 X3.906756 Y1.472374 I-3.970661 J-1.290146 G103 U3.167568 V2.719768 P-3.289945 Q-2.570387  
G3 X3.656324 Y1.541933 I-0.558716 J-1.525946 G103 U2.908449 V2.699479 P-0.003117 Q-1.625013  
G3 X3.386713 Y1.570983 I-0.308284 J-1.595505 G103 U2.645162 V2.634565 P0.256003 Q-1.604724  
G3 X3.148478 Y1.559143 I-0.038673 J-1.624555 G103 U2.425343 V2.541958 P0.51929 Q-1.53981  
G3 X2.917147 Y1.513274 I0.199562 J-1.612715 G103 U2.223652 V2.419736 P0.739108 Q-1.447203  
G1 X2.310342 Y1.192611 G101 U1.763114 V1.910871  
G3 X2.103444 Y1.528242 I-2.310342 J-1.192611 G103 U1.453902 V2.155498 P-1.763114 Q-1.910871  
G3 X1.848175 Y1.828729 I-2.103444 J-1.528242 G103 U1.111255 V2.350556 P-1.453902 Q-2.155498  
G1 X2.340657 Y2.306745 G101 U1.410545 V2.968183  
G3 X2.455766 Y2.512579 I-1.357006 J0.893985 G103 U1.448313 V3.200974 P-1.58093 Q0.375948  
G3 X2.540646 Y2.735495 I-1.472116 J0.688151 G103 U1.451831 V3.439477 P-1.618698 Q0.143157  
G3 X2.596331 Y3.000887 I-1.556995 J0.465235 G103 U1.41339 V3.707909 P-1.622216 Q-0.095346  
G3 X2.607565 Y3.260557 I-1.612681 J0.199843 G103 U1.335133 V3.955761 P-1.583774 Q-0.363779  
G3 X2.454003 Y3.377646 I-2.607565 J-3.260557 G103 U1.150786 V4.013268 P-1.335133 Q-3.955761  
G3 X2.295192 Y3.487509 I-2.454003 J-3.377646 G103 U0.963977 V4.062188 P-1.150786 Q-4.013268  
G3 X2.051703 Y3.396583 I0.444918 J-1.562921 G103 U0.76627 V3.893468 P0.952637 Q-1.316495  
G3 X1.816508 Y3.261612 I0.688407 J-1.471996 G103 U0.591422 V3.686195 P1.150343 Q-1.147774  
G3 X1.630731 Y3.112002 I0.923602 J-1.337025 G103 U0.468019 V3.482068 P1.325191 Q-0.940502  
G3 X1.470542 Y2.938921 I1.109379 J-1.187415 G103 U0.376687 V3.264637 P1.448595 Q-0.736375  
G1 X1.168107 Y2.322827 G101 U0.303207 V2.58226  
G3 X0.803444 Y2.472747 I-1.168107 J-2.322827 G103 U-0.090739 V2.598416 P-0.303207 Q-2.58226  
G3 X0.420306 Y2.565803 I-0.803444 J-2.472747 G103 U-0.482598 V2.554819 P0.090739 Q-2.598416  
G1 X0.537761 Y3.241999 G101 U-0.603499 V3.230408  
G3 X0.5099 Y3.476182 I-1.623312 J-0.074379 G103 U-0.709775 V3.440939 P-1.499976 Q-0.625099

G3 X0.447542 Y3.706416 I-1.595451 J-0.308562 G103 U-0.847117 V3.63596 P-1.393699 Q-0.83563  
G3 X0.336599 Y3.953854 I-1.533093 J-0.538796 G103 U-1.035998 V3.830531 P-1.256357 Q-1.030651  
G3 X0.193057 Y4.170534 I-1.42215 J-0.786234 G103 U-1.244992 V3.985049 P-1.067477 Q-1.225222  
G3 X0 Y4.175 I-0.193057 J-4.170534 G103 U-1.427934 V3.923217 P1.244992 Q-3.985049  
G3 X-0.193057 Y4.170534 I0 J-4.175 G103 U-1.607821 V3.852991 P1.427934 Q-3.923217  
G3 X-0.336599 Y3.953854 I1.278609 J-1.002914 G103 U-1.668597 V3.600284 P1.544516 Q-0.505121  
G3 X-0.447542 Y3.706416 I1.42215 J-0.786234 G103 U-1.688221 V3.329824 P1.605292 Q-0.252414  
G3 X-0.5099 Y3.476182 I1.533093 J-0.538796 G103 U-1.668074 V3.092147 P1.624915 Q0.018046  
G3 X-0.537761 Y3.241999 I1.595451 J-0.308562 G103 U-1.614159 V2.862558 P1.604768 Q0.255723  
G1 X-0.420306 Y2.565803 G101 U-1.272514 V2.267313  
G3 X-0.803444 Y2.472747 I0.420306 J-2.565803 G103 U-1.60072 V2.048828 P1.272514 Q-2.267313  
G3 X-1.168107 Y2.322827 I0.803444 J-2.472747 G103 U-1.892115 V1.783228 P1.60072 Q-2.048828  
G1 X-1.470542 Y2.938921 G101 U-2.387027 V2.258727  
G3 X-1.630731 Y3.112002 I-1.269568 J-1.014333 G103 U-2.596753 V2.366583 P-0.846082 Q-1.387379  
G3 X-1.816508 Y3.261612 I-1.109379 J-1.187415 G103 U-2.822496 V2.44363 P-0.636355 Q-1.495235  
G3 X-2.051703 Y3.396583 I-0.923602 J-1.337025 G103 U-3.08967 V2.49002 P-0.410613 Q-1.572283  
G3 X-2.295192 Y3.487509 I-0.688407 J-1.471996 G103 U-3.349573 V2.492185 P-0.143439 Q-1.618673  
G3 X-2.454003 Y3.377646 I2.295192 J-3.487509 G103 U-3.461232 V2.33463 P3.349573 Q-2.492185  
G3 X-2.607565 Y3.260557 I2.454003 J-3.377646 G103 U-3.565486 V2.172081 P3.461232 Q-2.33463  
G3 X-2.596331 Y3.000887 I1.623914 J-0.059827 G103 U-3.466117 V1.931914 P1.546442 Q0.499192  
G3 X-2.540646 Y2.735495 I1.612681 J0.199843 G103 U-3.32302 V1.701573 P1.447074 Q0.73936  
G3 X-2.455766 Y2.512579 I1.556995 J0.465235 G103 U-3.167018 V1.52113 P1.303977 Q0.969701  
G3 X-2.340657 Y2.306745 I1.472116 J0.688151 G103 U-2.988451 V1.367079 P1.147975 Q1.150143  
G1 X-1.848175 Y1.828729 G101 U-2.362179 V1.08633  
G3 X-2.103444 Y1.528242 I1.848175 J-1.828729 G103 U-2.49928 V0.716657 P2.362179 Q-1.08633  
G3 X-2.310342 Y1.192611 I2.103444 J-1.528242 G103 U-2.578908 V0.330504 P2.49928 Q-0.716657  
G1 X-2.917147 Y1.513274 G101 U-3.258792 V0.424289  
G3 X-3.148478 Y1.559143 I-0.430892 J-1.566846 G103 U-3.49186 V0.388272 P0.130987 Q-1.619728  
G3 X-3.386713 Y1.570983 I-0.199562 J-1.612715 G103 U-3.719777 V0.317917 P0.364055 Q-1.583711  
G3 X-3.656324 Y1.541933 I0.038673 J-1.624555 G103 U-3.963193 V0.198406 P0.591972 Q-1.513356  
G3 X-3.906756 Y1.472374 I0.308284 J-1.595505 G103 U-4.174731 V0.04739 P0.835387 Q-1.393845  
G3 X-3.970661 Y1.290146 I3.906756 J-1.472374 G103 U-4.172457 V-0.145705 P4.174731 Q-0.04739  
G3 X-4.026071 Y1.105158 I3.970661 J-1.290146 G103 U-4.161256 V-0.338489 P4.172457 Q0.145705  
G3 X-3.864354 Y0.901683 I1.348939 J0.906112 G103 U-3.939698 V-0.474381 P0.95768 Q1.312831  
G3 X-3.663309 Y0.719708 I1.187221 J1.109586 G103 U-3.688539 V-0.576621 P0.736122 Q1.448723  
G3 X-3.463614 Y0.589256 I0.986177 J1.291561 G103 U-3.45627 V-0.630906 P0.484963 Q1.550963  
G3 X-3.249502 Y0.490392 I0.786482 J1.422013 G103 U-3.221257 V-0.650578 P0.252694 Q1.605248  
G1 X-2.570105 Y0.393142 G101 U-2.549571 V-0.509595  
G3 X-2.6 Y0 I2.570105 J-0.393142 G103 U-2.443201 V-0.889252 P2.549571 Q0.509595  
G3 X-2.570105 Y-0.393142 I2.6 J0 G103 U-2.280646 V-1.248461 P2.443201 Q0.889252  
G1 X-3.249502 Y-0.490392 G101 U-2.885809 V-1.572213  
G3 X-3.463614 Y-0.589256 I0.57237 J-1.520877 G103 U-3.053195 V-1.738345 P1.058022 Q-1.233395  
G3 X-3.663309 Y-0.719708 I0.786482 J-1.422013 G103 U-3.19623 V-1.92923 P1.225408 Q-1.067263  
G3 X-3.864354 Y-0.901683 I0.986177 J-1.291561 G103 U-3.322911 V-2.168992 P1.368443 Q-0.876378  
G3 X-4.026071 Y-1.105158 I1.187221 J-1.109586 G103 U-3.405283 V-2.415506 P1.495124 Q-0.636616  
G3 X-3.970661 Y-1.290146 I4.026071 J1.105158 G103 U-3.289945 V-2.570387 P3.405283 Q2.415506  
G3 X-3.906756 Y-1.472374 I3.970661 J1.290146 G103 U-3.167568 V-2.719768 P3.289945 Q2.570387  
G3 X-3.656324 Y-1.541933 I0.558716 J1.525946 G103 U-2.908449 V-2.699479 P0.003117 Q1.625013  
G3 X-3.386713 Y-1.570983 I0.308284 J1.595505 G103 U-2.645162 V-2.634565 P-0.256003 Q1.604724  
G3 X-3.148478 Y-1.559143 I0.038673 J1.624555 G103 U-2.425343 V-2.541958 P-0.51929 Q1.53981  
G3 X-2.917147 Y-1.513274 I-0.199562 J1.612715 G103 U-2.223652 V-2.419736 P-0.739108 Q1.447203  
G1 X-2.310342 Y-1.192611 G101 U-1.763114 V-1.910871

G3 X-2.103444 Y-1.528242 I2.310342 J1.192611 G103 U-1.453902 V-2.155498 P1.763114 Q1.910871  
G3 X-1.848175 Y-1.828729 I2.103444 J1.528242 G103 U-1.111255 V-2.350556 P1.453902 Q2.155498  
G1 X-2.340657 Y-2.306745 G101 U-1.410545 V-2.968183  
G3 X-2.455766 Y-2.512579 I1.357006 J-0.893985 G103 U-1.448313 V-3.200974 P1.58093 Q-0.375948  
G3 X-2.540646 Y-2.735495 I1.472116 J-0.688151 G103 U-1.451831 V-3.439477 P1.618698 Q-0.143157  
G3 X-2.596331 Y-3.000887 I1.556995 J-0.465235 G103 U-1.41339 V-3.707909 P1.622216 Q0.095346  
G3 X-2.607565 Y-3.260557 I1.612681 J-0.199843 G103 U-1.335133 V-3.955761 P1.583774 Q0.363779  
G3 X-2.454003 Y-3.377646 I2.607565 J3.260557 G103 U-1.150786 V-4.013268 P1.335133 Q3.955761  
G3 X-2.295192 Y-3.487509 I2.454003 J3.377646 G103 U-0.963977 V-4.062188 P1.150786 Q4.013268  
G3 X-2.051703 Y-3.396583 I-0.444918 J1.562921 G103 U-0.76627 V-3.893468 P-0.952637 Q1.316495  
G3 X-1.816508 Y-3.261612 I-0.688407 J1.471996 G103 U-0.591422 V-3.686195 P-1.150343 Q1.147774  
G3 X-1.630731 Y-3.112002 I-0.923602 J1.337025 G103 U-0.468019 V-3.482068 P-1.325191 Q0.940502  
G3 X-1.470542 Y-2.938921 I-1.109379 J1.187415 G103 U-0.376687 V-3.264637 P-1.448595 Q0.736375  
G1 X-1.168107 Y-2.322827 G101 U-0.303207 V-2.58226  
G3 X-0.803444 Y-2.472747 I1.168107 J2.322827 G103 U0.090739 V-2.598416 P0.303207 Q2.58226  
G3 X-0.420306 Y-2.565803 I0.803444 J2.472747 G103 U0.482598 V-2.554819 P-0.090739 Q2.598416  
G1 X-0.537761 Y-3.241999 G101 U0.603499 V-3.230408  
G3 X-0.5099 Y-3.476182 I1.623312 J0.074379 G103 U0.709775 V-3.440939 P1.499976 Q0.625099  
G3 X-0.447542 Y-3.706416 I1.595451 J0.308562 G103 U0.847117 V-3.6

## Appendix-D

### Process Parameters and their Available Ranges on WSEM Machine Used

Process parameters	Symbol	Units	Range (M/C units)	Available increment	Range (Actual units)	Available increment
Peak current	$I_p$	A	10-12	1	10-12	1
Pulse peak voltage	$V_p$	Volts	1-2	1	60-110	50
Servo voltage	$S_v$	Volts	0-99	1	0-99	1
Pulse-on time	$T_{on}$	$\mu$ s	100-131	1	0.1-3.1	0.1
Pulse-off time	$T_{off}$	$\mu$ s	0-63	1	3.5-50.5	0.5 (3.5-19.5) 1.0 (19.5-50.5)
Wire feed rate	$W_f$	m/min	1-15	1	1-15	1
Wire tension	$W_t$	g	1-15	1	300-1980	120
Dielectric pressure	$W_p$	$\text{kg/cm}^2$	1-2	1	7-15	8
Cutting speed	$c_s$	%	1-120	1	1-120	1

## Appendix-E

**Table E1:** Results of ANOVA for considered responses of MBG.

Source	Sum of squares	DF	Mean square	F-value	P-value	Remarks
<b>For single pitch error '<math>f_{P_b}</math>'</b>						
Model	486.21	14	34.73	16.86	< 0.0001	Highly significant
$T_{on}$	80	1	80	38.83	< 0.0001	Highly significant
$T_{off}$	44	1	44	21.37	0.0004	Significant
$S_V$	139.4	1	139.4	67.68	< 0.0001	Highly significant
$W_F$	41.96	1	41.96	20.37	0.0005	Very significant
$T_{on} T_{off}$	12.22	1	12.22	5.93	0.0289	Significant
$T_{on} S_V$	10.79	1	10.79	5.24	0.0381	Significant
$T_{on} W_F$	12.25	1	12.25	5.95	0.0287	Significant
$T_{off} S_V$	12.5	1	12.5	6.07	0.0273	Significant
$T_{off} W_F$	<b>6.25</b>	<b>1</b>	<b>6.25</b>	<b>3.03</b>	<b>0.1034</b>	<b>Not significant</b>
$S_V W_F$	15.6	1	15.6	7.58	0.0156	Significant
$(T_{on}^2)$	38.92	1	38.92	18.90	0.0007	Very significant
$(T_{off}^2)$	52.39	1	52.39	25.44	0.0002	Very significant
$(S_V^2)$	38.6	1	38.6	18.74	0.0007	Very significant t
$(W_F^2)$	43.83	1	43.83	21.28	0.0004	Very significant
Residual	28.84	14	2.06			
Lack of fit	25.46	10	2.55	3.02	0.1491	Not significant
Pure error	3.37	4	0.84			
Cor Total	515.04	28				
R-Squared = 0.944, Adjusted R-Squared = 0.888, Predicted R-Squared = 0.705						
PRESS = 151.94, Adequate Precision = 14.645						
<b>For total cumulative pitch error '<math>F_{P_b}</math>'</b>						
Model	1208.86	14	86.35	15.06	< 0.0001	Highly significant
$T_{on}$	563.48	1	563.48	98.27	< 0.0001	Highly significant
$T_{off}$	101.79	1	101.79	17.75	0.0009	Very significant
$S_V$	155.74	1	155.74	27.16	0.0001	Very significant
$W_F$	101.21	1	101.21	17.65	0.0009	Very significant
$T_{on} T_{off}$	29.38	1	29.38	5.12	0.04	Significant
$T_{on} S_V$	34.99	1	34.99	6.1	0.027	Significant
$T_{on} W_F$	30.25	1	30.25	5.28	0.0376	Significant
$T_{off} S_V$	28.36	1	28.36	4.95	0.0431	Significant
$T_{off} W_F$	<b>2.4</b>	<b>1</b>	<b>2.4</b>	<b>0.42</b>	<b>0.5279</b>	<b>Not significant</b>
$S_V W_F$	32.78	1	32.78	5.72	0.0314	Significant
$(T_{on}^2)$	66.23	1	66.23	11.55	0.0043	Significant
$(T_{off}^2)$	36.29	1	36.29	6.33	0.0247	Significant
$(S_V^2)$	33.58	1	33.58	5.86	0.0297	Significant
$(W_F^2)$	61.25	1	61.25	10.68	0.0056	Significant
Residual	80.27	14	5.73			

Lack of fit	69.39	10	6.94	2.55	0.1902	Not significant
Pure error	10.88	4	2.72			
Cor Total	1289.14	28				
R-Squared = 0.9377, Adjusted R-Squared = 0.8755, Predicted R-Squared = 0.6768						
PRESS = 416.69, Adequate Precision = 13.6						
<b>For average surface roughness '<math>R_{ab}</math>'</b>						
Model	1.25	14	0.089	29.17	< 0.0001	Highly significant
$T_{on}$	0.28	1	0.28	89.99	< 0.0001	Highly significant
$T_{off}$	0.062	1	0.062	20.09	0.0005	Significant
$S_V$	0.36	1	0.36	118.67	< 0.0001	Highly significant
$W_F$	0.12	1	0.12	39.77	< 0.0001	Highly significant
$T_{on} T_{off}$	0.016	1	0.016	5.09	0.0405	Significant
$T_{on} S_V$	0.014	1	0.014	4.69	0.0480	Significant
$T_{on} W_F$	0.016	1	0.016	5.09	0.0405	Significant
$T_{off} S_V$	0.017	1	0.017	5.51	0.0341	Significant
<b><math>T_{off} W_F</math></b>	<b>0.0056</b>	<b>1</b>	<b>0.0056</b>	<b>1.83</b>	<b>0.1971</b>	<b>Not significant</b>
$S_V W_F$	0.038	1	0.038	12.40	0.0034	Significant
$(T_{on}^2)$	0.17	1	0.17	54.93	< 0.0001	Highly significant
$(T_{off}^2)$	0.066	1	0.066	21.64	0.0004	Very significant
$(S_V^2)$	0.14	1	0.14	45.95	< 0.0001	Highly significant
$(W_F^2)$	0.12	1	0.12	38.49	< 0.0001	Highly significant
Residual	0.043	14	0.003			
Lack of fit	0.03	10	0.003	0.91	0.5916	Not significant
Pure error	0.013	4	0.0033			
Cor Total	1.3	28				
R-Squared = 0.9669, Adjusted R-Squared = 0.9337, Predicted R-Squared = 0.8516						
PRESS = 0.19, Adequate Precision = 18.996						
<b>For maximum surface roughness '<math>R_{max_b}</math>'</b>						
Model	46.33	14	3.31	15.52	< 0.0001	Highly Significant
$T_{on}$	15	1	15	70.28	< 0.0001	Highly significant
$T_{off}$	6.11	1	6.11	28.64	0.0001	Significant
$S_V$	7.71	1	7.71	36.17	< 0.0001	Highly significant
$W_F$	4.33	1	4.33	20.32	0.0005	Very significant
$T_{on} T_{off}$	1.12	1	1.12	5.27	0.0377	Significant
$T_{on} S_V$	1.16	1	1.16	5.42	0.0354	Significant
$T_{on} W_F$	1.96	1	1.96	9.19	0.009	Significant
$T_{off} S_V$	1.38	1	1.38	6.47	0.0234	Significant
<b><math>T_{off} W_F</math></b>	<b>0.7</b>	<b>1</b>	<b>0.7</b>	<b>3.27</b>	<b>0.0921</b>	<b>Not significant</b>
$S_V W_F$	1.06	1	1.06	4.98	0.0426	Significant
$(T_{on}^2)$	2.33	1	2.33	10.95	0.0052	Significant
$(T_{off}^2)$	3.21	1	3.21	15.06	0.0017	Significant
$(S_V^2)$	2.19	1	2.19	10.27	0.0064	Significant

$(W_F^2)$	1.13	1	1.13	5.30	0.0372	Significant
Residual	2.99	14	0.21			
Lack of fit	2.55	10	0.26	2.37	0.2103	Not significant
Pure error	0.43	4	0.11			
Cor Total	49.32	28				
R-Squared = 0.9395, Adjusted R-Squared = 0.8789, Predicted R-Squared = 0.688						
PRESS = 15.39, Adequate Precision = 14.875						
<b>For volumetric gear cutting rate 'VGCR<sub>b</sub>'</b>						
Model	27.54	14	1.97	35.59	< 0.0001	Highly significant
$T_{on}$	13.7	1	13.7	247.75	< 0.0001	Highly significant
$T_{off}$	2.08	1	2.08	37.69	< 0.0001	Highly significant
$S_V$	6.56	1	6.56	118.60	< 0.0001	Highly significant
$W_F$	0.68	1	0.68	12.24	0.0035	Significant
$T_{on} T_{off}$	0.64	1	0.64	11.58	0.0043	Significant
$T_{on} S_V$	0.41	1	0.41	7.41	0.0165	Significant
<b><math>T_{on} W_F</math></b>	<b>0.2</b>	<b>1</b>	<b>0.2</b>	<b>3.66</b>	<b>0.0763</b>	<b>Not significant</b>
$T_{off} S_V$	0.42	1	0.42	7.64	0.0152	Significant
<b><math>T_{off} W_F</math></b>	<b>0.023</b>	<b>1</b>	<b>0.023</b>	<b>0.41</b>	<b>0.5338</b>	<b>Not significant</b>
<b><math>S_V W_F</math></b>	<b>0.0056</b>	<b>1</b>	<b>0.0056</b>	<b>0.10</b>	<b>0.7544</b>	<b>Not significant</b>
$(T_{on}^2)$	0.58	1	0.58	10.53	0.0059	Significant
$(T_{off}^2)$	0.92	1	0.92	16.68	0.0011	Significant
$(S_V^2)$	2.19	1	2.19	39.58	< 0.0001	Highly significant
$(W_F^2)$	0.28	1	0.28	5.09	0.0405	Significant
Residual	0.77	14	0.055			
Lack of fit	0.68	10	0.068	2.97	0.1532	Not significant
Pure error	0.092	4	0.023			
Cor Total	28.32	28				
R-Squared = 0.9727, Adjusted R-Squared = 0.9453, Predicted R-Squared = 0.8562						
PRESS = 4.07, Adequate Precision = 23.837						

**Table E2:** Results of ANOVA for considered responses of MHG.

Source	Sum of squares	DF	Mean square	F-value	P-value	Remarks
<b>For total profile pitch error '<math>F_{\alpha_h}</math>'</b>						
Model	103.68	14	7.41	13.49	< 0.0001	Highly significant
$T_{on}$	19.74	1	19.74	35.96	< 0.0001	Highly significant
$T_{off}$	10.29	1	10.29	18.74	0.0007	Very significant
$S_V$	11.49	1	11.49	20.92	0.0004	Very significant
$W_F$	12.16	1	12.16	22.15	0.0003	Very significant
$T_{on} T_{off}$	5.06	1	5.06	9.22	0.0089	Significant
$T_{on} S_V$	4.43	1	4.43	8.07	0.0131	Significant
$T_{on} W_F$	3.42	1	3.42	6.23	0.0256	Significant
$T_{off} S_V$	4.16	1	4.16	7.58	0.0155	Significant
$T_{off} W_F$	<b>0.95</b>	<b>1</b>	<b>0.95</b>	<b>1.73</b>	<b>0.2093</b>	<b>Not significant</b>
$S_V W_F$	6.33	1	6.33	11.52	0.0044	Significant
$(T_{on}^2)$	12.58	1	12.58	22.92	0.0003	Very significant
$(T_{off}^2)$	3.98	1	3.98	7.24	0.0176	Significant
$(S_V^2)$	11.03	1	11.03	20.1	0.0005	Very significant
$(W_F^2)$	11.20	1	11.2	20.41	0.0005	Very significant
Residual	7.68	14	0.55			
Lack of fit	5.11	10	0.51	0.79	0.6527	Not significant
Pure error	2.58	4	0.64			
Cor Total	111.36	28				
R-Squared = 0.931, Adjusted R-Squared = 0.862, Predicted R-Squared = 0.6996						
PRESS = 33.45, Adequate Precision = 12.851						
<b>For total cumulative pitch error '<math>F_{P_h}</math>'</b>						
Model	1102.66	14	78.76	18.57	< 0.0001	Highly significant
$T_{on}$	220.59	1	220.59	52.02	< 0.0001	Highly significant
$T_{off}$	152.3	1	152.3	35.91	< 0.0001	Highly significant
$S_V$	317.65	1	317.65	74.91	< 0.0001	Highly significant
$W_F$	94.64	1	94.64	22.32	0.0003	Very significant
$T_{on} T_{off}$	46.65	1	46.65	11	0.0051	Significant
$T_{on} S_V$	26.57	1	26.57	6.27	0.0253	Significant
$T_{on} W_F$	21.44	1	21.44	5.06	0.0412	Significant
$T_{off} S_V$	40.32	1	40.32	9.51	0.0081	Significant
$T_{off} W_F$	<b>2.18</b>	<b>1</b>	<b>2.18</b>	<b>0.51</b>	<b>0.4856</b>	<b>Not significant</b>
$S_V W_F$	41.93	1	41.93	9.89	0.0072	Significant
$(T_{on}^2)$	35.77	1	35.77	8.43	0.0115	Significant
$(T_{off}^2)$	54.76	1	54.76	12.91	0.0029	Significant
$(S_V^2)$	92.41	1	92.41	21.79	0.0004	Very significant
$(W_F^2)$	21.18	1	21.18	4.99	0.0423	Significant
Residual	59.37	14	4.24			
Lack of fit	41.76	10	4.18	0.95	0.5724	Not significant

Pure error	17.61	4	4.4			
Cor Total	1162.03	28				
R-Squared = 0.9489, Adjusted R-Squared = 0.8978, Predicted R-Squared = 0.7693						
PRESS = 268.07, Adequate Precision = 15.756						
<b>For average surface roughness '<math>R_{a_h}</math>'</b>						
Model	0.74	14	0.053	22.93	< 0.0001	Highly significant
$T_{on}$	0.13	1	0.13	58.63	< 0.0001	Highly significant
$T_{off}$	0.12	1	0.12	50.61	< 0.0001	Highly significant
$S_V$	0.092	1	0.092	40.08	< 0.0001	Highly significant
$W_F$	0.046	1	0.046	19.91	0.0005	Very significant
$T_{on} T_{off}$	0.076	1	0.076	32.99	< 0.0001	Highly significant
$T_{on} S_V$	0.021	1	0.021	9.17	0.009	Significant
$T_{on} W_F$	<b>0.0012</b>	<b>1</b>	<b>0.0012</b>	<b>0.53</b>	<b>0.4768</b>	<b>Not significant</b>
$T_{off} S_V$	0.013	1	0.013	5.77	0.0308	Significant
$T_{off} W_F$	<b>0.0001</b>	<b>1</b>	<b>0.0001</b>	<b>0.044</b>	<b>0.8376</b>	<b>Not significant</b>
$S_V W_F$	0.016	1	0.016	6.82	0.0205	Significant
$(T_{on}^2)$	0.11	1	0.11	49.3	< 0.0001	Highly significant
$(T_{off}^2)$	0.095	1	0.095	41.25	< 0.0001	Highly significant
$(S_V^2)$	0.097	1	0.097	42.11	< 0.0001	Highly significant
$(W_F^2)$	0.02	1	0.02	8.79	0.0102	Significant
Residual	0.032	14	0.00229			
Lack of fit	0.025	10	0.0025	1.4	0.3982	Not significant
Pure error	0.0071	4	0.0018			
Cor Total	0.77	28				
R-Squared = 0.9582, Adjusted R-Squared = 0.9164, Predicted R-Squared = 0.7982						
PRESS = 0.15, Adequate Precision = 17.678						
<b>For maximum surface roughness '<math>R_{max_h}</math>'</b>						
Model	23.43	14	1.67	11.58	< 0.0001	Highly significant
$T_{on}$	6.72	1	6.72	46.52	< 0.0001	Highly significant
$T_{off}$	0.78	1	0.78	5.4	0.0357	Significant
$S_V$	4.28	1	4.28	29.66	< 0.0001	Highly significant
$W_F$	1.24	1	1.24	8.55	0.0111	Significant
$T_{on} T_{off}$	1.24	1	1.24	8.61	0.0109	Significant
$T_{on} S_V$	1.37	1	1.37	9.48	0.0082	Significant
$T_{on} W_F$	0.8	1	0.8	5.55	0.0336	Significant
$T_{off} S_V$	1	1	1	6.92	0.0197	Significant
$T_{off} W_F$	<b>0.25</b>	<b>1</b>	<b>0.25</b>	<b>1.7</b>	<b>0.2138</b>	<b>Not significant</b>
$S_V W_F$	1.86	1	1.86	12.90	0.0029	Significant
$(T_{on}^2)$	1.57	1	1.57	10.88	0.0053	Significant
$(T_{off}^2)$	1.21	1	1.21	8.39	0.0117	Significant
$(S_V^2)$	1.79	1	1.79	12.42	0.0034	Significant
$(W_F^2)$	1.48	1	1.48	10.28	0.0063	Significant

Residual	2.02	14	0.14			
Lack of fit	1.4	10	0.14	0.9	0.597	Not significant
Pure error	0.62	4	0.16			
Cor Total	25.45	28				
R-Squared = 0.9205, Adjusted R-Squared = 0.8411, Predicted R-Squared = 0.645						
PRESS = 9.03, Adequate Precision = 12.971						
<b>For volumetric gear cutting rate 'VGCR<sub>h</sub>'</b>						
Model	22.88	14	1.63	25.17	< 0.0001	Highly significant
$T_{on}$	11.35	1	11.35	174.76	< 0.0001	Highly significant
$T_{off}$	2.07	1	2.07	31.82	< 0.0001	Highly significant
$S_V$	4.08	1	4.08	62.88	< 0.0001	Highly significant
$W_F$	0.68	1	0.68	10.42	0.0061	Significant
$T_{on} T_{off}$	0.31	1	0.31	4.74	0.0470	Significant
$T_{on} S_V$	0.3	1	0.3	4.66	0.0488	Significant
$T_{on} W_F$	<b>0.24</b>	<b>1</b>	<b>0.24</b>	<b>3.7</b>	<b>0.0751</b>	<b>Not significant</b>
$T_{off} S_V$	0.4	1	0.4	6.21	0.0259	Significant
$T_{off} W_F$	<b>0.12</b>	<b>1</b>	<b>0.12</b>	<b>1.89</b>	<b>0.1912</b>	<b>Not significant</b>
$S_V W_F$	<b>0.27</b>	<b>1</b>	<b>0.27</b>	<b>4.08</b>	<b>0.0628</b>	<b>Not significant</b>
$(T_{on}^2)$	0.4	1	0.40	6.12	0.0268	Significant
$(T_{off}^2)$	1.78	1	1.78	27.4	0.0001	Very significant
$(S_V^2)$	1.40	1	1.40	21.48	0.0004	Very significant
$(W_F^2)$	0.97	1	0.97	15.00	0.0017	Significant
Residual	0.91	14	0.065			
Lack of fit	0.76	10	0.076	1.99	0.2645	Not significant
Pure error	0.15	4	0.038			
Cor Total	23.79	28				
R-Squared = 0.9618, Adjusted R-Squared = 0.9236, Predicted R-Squared = 0.8067						
PRESS = 4.6, Adequate Precision = 19.401						